In-situ and ex-situ multi-scale physical metrologies to investigate the destructuration mechanisms of lignocellulosic matrices and release kinetics of fermentescible cellulosic carbon

Tien Cuong Nguyen

Université de Toulouse

THÈSE

En vue de l'obtention du

DOCTORAT DE L'UNIVERSITÉ DE TOULOUSE

Délivré par :
Institut National des Sciences Appliquées de Toulouse (INSA de Toulouse)

Cotutelle internationale avec :
Hanoï University of Science and Technology (HUST)

Présentée et soutenue par :
NGUYEN Tien Cuong

Le vendredi 21 novembre 2014

Titre :
In-situ and ex-situ multi-scale physical metrologies to investigate the destructuration mechanisms of lignocellulosic matrices and release kinetics of fermentable cellulosic carbon

---

École doctorale et discipline ou spécialité :
ED SEVAB : Ingénieries microbienne et enzymatique

Unité de recherche :
Laboratoire d'Ingénierie des Systèmes Biologiques et des Procédés (LISBP)

Directeur(s) de Thèse :

FILLAUDEAU Luc (CR INRA, LISBP, Toulouse)
TO Kim Anh (PR, HUST/SBFT, Hanoï, Viet-Nam)

Rapporteurs :

MORESOLI Christine (PR, Univ. Waterloo, Canada)
REMOND-ZILLIOX Caroline (PR, Univ. Reims)

Autre(s) membre(s) du jury :

ANNE-ARCHARD Dominique (IMFT, Toulouse)
COMA Véronique (PR, ENSCBP, Bordeaux)
GOMA Gérard (PR Em., INSA, Toulouse)
ROUAU Xavier (DR INRA, IATE Montpellier)

NGUYEN Tien Cuong

"In-situ and ex-situ multiscale physical metrologies to investigate the destructuration mechanism of lignocellulosic matrices and release kinetics of fermentable cellulosic carbon"

190 pages

Ingénieries microbienne et enzymatique

Institut national des Sciences Appliqués de Toulouse – 2014

N° d'ordre 1280

RESUME :

A l'heure actuelle, le manque de connaissances des mécanismes de liquéfaction et de saccharification est l'un des principaux facteurs qui pénalisent le développement des procédés de bio-raffinage. Ce travail est centré sur le développement d'analyses physiques et biochimiques in-situ (viscosimétrie, focus beam reflectance measurement) et ex-situ (rhéometrie, granulométrie laser, morphogranulométrie, sédimentation…) pour améliorer la compréhension des mécanismes de déstructuration des fibres lignocellulosiques et caractériser les cinétiques de libération de carbone fermentescible. Des substrats modèles (cellulose microcristalline, papier Whatman) et industriels (pâte à papier, bagasse de canne à sucre) ont été utilisés avec différentes conditions d'hydrolyse (1% à 30%w/v, 0.1 à 0.5mL enzyme/ g cellulose). Les résultats obtenus ont permis: (i) de proposer et de valider les mesures in-situ de la viscosité de la suspension et de la distribution des longueurs de corde des particules, ainsi que sa conversion en distribution de diamètre ; (ii) de montrer l'impact de la nature et de la concentration de substrat et des ratios enzyme/substrat sur les évolutions des paramètres physico-biochimiques lors de l'hydrolyse. Ces effets ont été quantifiés sur les limitations de transfert ; (iii) d'établir un modèle phénoménologique de comportement rhéologique des suspensions initiales ; (iv) de montrer que les cinétiques physico et bio-chimiques sont des cinétiques du second ordre ; (v) de montrer que, pour des hydrolyses à haute teneur en matière sèche, on peut réduire considérablement la limitation des transferts liée aux hautes concentrations et contrôler la cinétique de production de glucose par une stratégie d'ajouts cumulés de substrat.

MOTS CLES : *bio-raffinage, lignocellulose, pâte à papier, déstructuration des fibres, limitation de transfert, rhéométrie, viscosimétrie, morphométrie, granulométrie, taille de particule, ajouts cumulés, glucose, bioconversion*.

JURY, DATE ET LIEU DE SOUTENANCE :

MORESOLI Christine - Professeur - Université Waterloo, Canada - Rapporteur

REMOND-ZILLIOX Caroline - Professeur - Université Reims, France - Rapporteur

ANNE-ARCHARD Dominique - Chargé de recherche - IMFT, Toulouse - Examinatrice

COMA Véronique - Professeur - ENSCBP, Bordeaux - Examinatrice

GOMA Gérard - Professeur - INSA, Toulouse - Examinateur

ROUAU Xavier - Directeur de recherche - INRA, IATE, Montpellier - Examinateur

FILLAUDEAU Luc - Chargé de recherche - INRA, LISBP, Toulouse - Directeur de thèse

TO Kim Anh - Professeur - Institut Polytechnique de Hanoï, Viet-Nam - Directrice de thèse

Soutenance le 21 Novembre 2014 – Amphithéâtre Joseph Fourier – INSA Toulouse

Laboratoire d'Ingénierie des Systèmes Biologiques et des Procédés

"Wake at dawn with a winged heart
and give thanks for another day of loving."

-Khalil Gibran-

…Rắp mượn rượu vui cùng tuế nguyệt

Dở đem thân trả nợ tang bồng…"

A ma famille, mon amour, mes amis

A tous ceux qui traversent ma vie…

REMERCIEMENT

Je remercie M. Nicholas LINDLEY, directeur du Laboratoire d'Ingénierie des Systèmes Biologiques et des Procédés, d'avoir autorisé le déroulement de cette thèse au sein de son laboratoire. Une reconnaissance spéciale va en direction de M. Claude MARANGES, directeur de l'école doctorale SEVAB.

Je tiens à remercier l'Ambassade de France au Vietnam pour le soutien financier. Je remercie aussi à la fédération de recherche FERMAT (thème RheMat – Ecoulement Polyphasiques), l'unité de recherche TWB (plateau analytique physique) pour la collaboration scientifique et aussi de la mise en disposition des matériels.

J'éprouve ma gratitude envers le jury pour avoir évalué le fruit de mon travail réalisé au cours de ces années. Je remercie à Mme. Christine MORESOLI et Mme. Caroline REMOND-ZILLIOX d'avoir accepté d'être rapporteurs malgré la distance, l'éloignement des thématiques scientifiques de chacun, et surtout le court délai pour faire retourner votre réponse. Je remercie M. Xavier ROUAU, d'avoir participé dans le comité de thèse et aussi d'être un membre de jury. Je lui remercie pour tous ses apports scientifiques dans mes travaux pendant trois ans.

Je tiens à remercier M. CHU-KY Son d'avoir me faire connaissance avec l'équipe où je travaille pendant ma thèse. Il a mis dans ma main la première brique pour que je puisse construire mes travaux. Je lui remercie aussi pour ses conseils pendant les années passées et je crois encore pour les années qui suivent.

Mes remerciements vont adresser à Mme. TO Kim Anh, ma chère directrice de thèse, malgré la distance géographique, elle est toujours disponible pour discuter, donner ses avis et aussi me guider dans la vie professionnelle.

Une autre personne que je souhaiterais vivement remercier pour tous ses aides non seulement dans les échanges scientifiques mais encore pour les accueils chaleureux, Mme Véronique COMA. Merci de nous faire goûter le Cassoulet à Bordeaux !!!

Je souhaite aussi remercier chaleureusement Mme Dominique ANNE-ARCHARD pour m'avoir initié à la rhéologie. Le premier trait de pinceau est toujours le plus belle, merci bien Dominique ! Merci de toujours être disponible pour discuter avec moi, corriger mes documents et rester à côté de moi même pendant le repas…

Maintenant, vient la place toute particulière de mes remerciements à M. Luc FILLAUDEAU, mon directeur de thèse. Cette thèse n'aurait pas jamais finie sans tes aides. Je te remercie non seulement du côté scientifique mais aussi du côté humain. Merci de partager avec moi de la plus simple jusqu'à la plus dure manipulation ! Je pense que tous les remerciements ne sont pas comparables avec ce que tu as fait pour moi, mon grand.

Je remercie l'équipe de Génie microbiologique, encadrée par Mme. Carole MOLINA-JOUVE pour sa réactivité et ses connaissances à me faire partager. Je tiens à remercier M. Xavier CAMELEYRE, M. Éric LOMBARD, Mme. Carine BIDEAUX pour leurs aides pendant les manips et les traitements des données.

Un grand merci va être envoyé à tous mes collègues et mes amis qui ont partagé, pendant ces mois et années, mon quotidien dans les bureaux, dans le hall manipulé ou simplement au tour d'un taste de café. Je pense à Asma, Carlos, Elodie G, Elodie B, Estelle, Florence, Hazar, Julie M, Juile B, Jilian, Lannig, Léa, Maud, Olivier, Sandra, Sandy, Sandrine, Tuân, Xiaomin,Yannick (avec mes excuses pour les oublié(es)).

Au-delà du labo, je remercie mes amis géographiquement éloignés qui, malgré un manque de nouvelles de ma part, sont toujours restés proche de moi. Je pense à Amandine, Elodie, Julie, Hằng "A3", Hoàng, Nam (avec mes excuses pour les oublié(es)).

Pour finir, ces dernières lignes vont me permettre de témoigner de ma plus profonde gratitude et de mon amour à mes grands-parents, mes parents, ma sœur, mon frère, my lover et à toute ma grande famille. Merci de m'avoir toujours soutenu…

SCIENTIFIC VALORISATION

PUBLICATIONS

- Nguyen, T.-C., Anne-Archard, D., Coma, V., Cameleyre, X., Lombard, E., Binet, C., Nouhen, A., To, K.A., Fillaudeau, L. 2013. In situ rheometry of concentrated cellulose fibre suspensions and relationships with enzymatic hydrolysis. Bioresource Technology, 133(0), 563-572.
- Nguyen, T.-C. Anne-Archard, D., Fillaudeau, L. Rheology of lignocellulose suspensions and impact of enzymatic hydrolysis: A review. (Submitted).

INTERNATIONAL COMMUNICATIONS

- Nguyen, T. C., Anne-Archard, D., Cameleyre, X., Lombard, E., Fillaudeau, L. (2012). Production of fermentescible sugar from paper-pulp: Looking for a dynamique and multiscale integrated models based on physical parameters. 8th International Conference on Renewable Resources and Biorefineries Toulouse, France.
- Nguyen, T. C., Anne-Archard, D., Coma, V., Cameleyre, X., Lombard, E., To, K.A., Fillaudeau, L. (2013). In-situ physical analysis of cellulose fibre suspension during enzymatic hydrolysis. 9th World Congress of Chemical Engineering Seoul, Korea (oral presentation).
- Nguyen, T. C., Anne-Archard, D., Coma, V., Cameleyre, X., Lombard, E., To, K.A., Fillaudeau, L. (2014). Hydrolysis of high concentration lignocellulose suspensions with a cumulative feeding strategy: rheometry and morphogranulometry. 10th European Symposium on Biochemical Engineering Sciences Lille, France.

NATIONAL COMUNICATIONS

- Nguyen, T. C., Anne-Archard, D., Cameleyre, X., Lombard, E., Fillaudeau, L. (2012). Hydrolysis of concentrated cellulose fibre suspensions: Investigation of mechanism and limitation by physical approaches. Journée de l'ED SEVAB.
- Nguyen, T. C., Anne-Archard, D., Cameleyre, X., Lombard, E., Fillaudeau, L. (2014). Dimensionless viscosity-time curves: An in-situ snapshot of hydrolyses kinetics of complex lignocellulosic matrixes. Annual meeting – ProBio3 project – Toulouse – France.
- Nguyen, T. C., Anne-Archard, D., Cameleyre, X., Lombard, E., Fillaudeau, L. (2014) Hydrolysis of high concentration lignocellulose suspensions with a cumulative feeding strategy: rheometry and morpho-granulometry. Annual meeting – ProBio3 project – Lille – France.

ABSTRACT

In the context of biofuels and chemicals production of petroleum substitutes from renewable carbon, bioconversion of lignocellulose biomasses is currently a major challenge. The limited knowledge of liquefaction and saccharification mechanisms stands as the main factor which penalizes bio-refinery progress. The present work is centred on the development of in-situ (viscosimetry, focus beam reflectance measurement) and ex-situ (rheometry, diffraction light scattered, morphometry, decantation…) physical and biochemical analysis to expand our understanding of the destructuration mechanisms of lignocellulose fibres and to characterise the release kinetics of fermentable cellulosic carbon. Model (microcrystalline cellulose, Whatman paper) and industrial (paper-pulp, sugarcane bagasse) lignocellulose matrices under a large range of hydrolysis conditions (1% up to 30%w/v and 0.1 up to 0.5mL enzyme/g cellulose) were studied during 24h hydrolysis experiments (pertinent period to appreciate transfer limitations). Our scientific results allow:

- to propose and validate the in-situ measurements of the suspension viscosity and chord length distribution together with its conversion into particle size distribution.
- to demonstrate the impact of the substrate nature and concentration and of the enzymatic ratios on the evolution of physical- and biochemical parameters during hydrolysis. Their impacts on transfer phenomena were quantified.
- to establish phenomenological models for rheological behaviour of initial suspensions.
- to describe all physical (viscosity, particle size) and biochemical (substrate and product) kinetics by second order reaction models.
- to demonstrate that, for high dry matter concentration hydrolysis, a cumulative feeding substrate strategy allows considerably reducing the transfer limitations linked to high concentrations and to control the glucose production kinetics.

Keywords: bio-refinery, lignocellulose, paper-pulp, fibre destructuration, transfer limitation, rheometry, viscosimetry, morphometry, granulometry, particle size, cumulative feeding strategy, glucose, bioconversion

RESUME

La bioconversion des biomasses lignocellulosiques est actuellement un grand défi pour le développement de technologies de bio-raffinage. Le manque de connaissances des mécanismes de liquéfaction et de saccharification est l'un des principaux facteurs qui pénalisent le développement des procédés de bio-raffinage. Ce travail est centré sur le développement d'analyses physiques et biochimiques in-situ (viscosimétrie, focus beam reflectance measurement) et ex-situ (rhéometrie, granulométrie laser, morphogranulométrie, sédimentation…) pour améliorer la compréhension des mécanismes de déstructuration des fibres lignocellulosiques et caractériser les cinétiques de libération de carbone fermentescible. Des substrats modèles (cellulose microcristalline, papier Whatman) et industriels (pâte à papier, bagasse de canne à sucre) ont été utilisés avec différentes conditions d'hydrolyse (1% à 30%w/v, 0.1 à 0.5mL enzyme/ g cellulose). Les résultats obtenus ont permis:

- de proposer et de valider les mesures in-situ de la viscosité de la suspension et de la distribution des longueurs de corde des particules, ainsi que sa conversion en distribution de diamètre.
- de montrer l'impact de la nature et de la concentration de substrat et des ratios enzyme/substrat sur les évolutions des paramètres physico-biochimiques lors de l'hydrolyse. Ces effets ont été quantifiés sur les limitations de transfert.
- d'établir un modèle phénoménologique de comportement rhéologique des suspensions initiales
- de montrer que les cinétiques physico et bio-chimiques sont des cinétiques du second ordre
- de montrer que, pour des hydrolyses à haute teneur en matière sèche, on peut réduire considérablement la limitation des transferts liée aux hautes concentrations et contrôler la cinétique de production de glucose par une stratégie d'ajouts cumulés de substrat.

Mots-clés : bio-raffinage, lignocellulose, pâte à papier, déstructuration des fibres, limitation de transfert, rhéométrie, viscosimétrie, morphométrie, granulométrie, taille de particule, ajouts cumulés, glucose, bioconversion.

Contenu

LIST OF FIGURES

LIST OF TABLES

NOMENCLATURES

ABBREVIATION	
BAG	Sugarcane bagasse
CBP	Consolidated bioprocess
CBU	Cellobiase unit
Cellu	Cellulose
CMC	Carboxymethyl cellulose
CLD	Chord length distribution
CoSt	Corn stover
DLS	Diffraction light scattered
DM	Dry matter
DNS	3,5-Dinitrosalicylic acid
DP	Degree of polymerisation
E	Enzyme
FBRM	Focus Beam Reflectance Measurement
FPU	Filter paper unit
Glu	Glucose
Hemi	Hemicellulose
HM	Humid matter
IU	International unit
Lig	Lignin
Man	Mannose
MCC	Microcrystalline cellulose
MFC	Micro-fibril cellulose
MG	Morpho-granulometry
NCC	Nanocrystalline cellulose
NPGU	p-nitrophenyl β-D-galactopyranoside unit
PP	Paper-pulp
PSD	Particle size distribution
RVA	Rapid viscosity analyser
S	Substrate
SHF	Separate hydrolysis and fermentation
SSF	Simultaneous saccharification and fermentation
TGA	Thermogravimetry analysis
WP	Whatman paper
Xyl	Xylose

SYMBOLS

γ	Surface free energy	($N.m^{-1}$)
$\dot{\gamma}$	Shear rate	(s^{-1})
$\dot{\gamma}^*$	Complex shear rate	(s^{-1})
ϕ	Volume fraction	(/)
ϕ_c	Critical volume fraction	(/)
ϕ_m	Maxima volume fraction	(/)
ϕ_{eff}	Effective volume fraction	(/)
$[\eta]$	Intrinsic viscosity	(/)
φ	Heat flux	(W)
λ	Wavelength	(nm)
ω	Angular velocity	($rad.s^{-1}$)
ρ	Density	($kg.m^{-3}$)
ρ_s	Substrate density	($kg.m^{-3}$)
ρ_w	Water density	($kg.m^{-3}$)
μ	Viscosity	(Pa.s)
μ_0	Initial viscosity	(Pa.s)
μ_∞	Final viscosity	(Pa.s)
μ_s	Suspendant viscosity	(Pa.s)
μ_{rel}	Relative viscosity	(/)
μ^*	Dimensionless viscosity	(/)
τ	Shear stress	(Pa)
τ_0	Yield stress	(Pa)
τ^*	Complex shear stress	(Pa)
θ	Angle contact	(°)
ν	Kinetic viscosity	($m^2.s^{-1}$)
ν_s	Settling velocity	($m.s^{-1}$)
ξ	Ionisation energy	(mV)
ΔG	Gibbs free energy	($N.m^{-1}$)
BC	Bioconversion rate	(%)
BS	Back-scattering signal	(%)
C*	Critical substrate concentration	($gdm.L^{-1}$)
Cm	Mass concentration	($gdm.L^{-1}$)
Cp	Specific heat mass capacity	($J.K^{-1}.kg^{-1}$)
CrI	Crystallinity	(%)
$d_v(0.1)$	Particle diameter for 10% population	(µm)
$d_v(0.5)$	Particle diameter for 50% population	(µm)
$d_v(0.9)$	Particle diameter for 90% population	(µm)
D[4,3]	Mean volume diameter	(µm)
D_{CE}	Circle equivalent diameter	(µm)
D_{SE}	Spherical equivalent diameter	(µm)
d_s	Stocke's diameter	(µm)
F_{xy}	Force	(N)
g	Gravity	($m.s^{-2}$)
G'	Elastic modulus	(Pa)
G"	Viscous modulus	(Pa)
G*	Complex modulus	(Pa)
H	Sample height	(mm)
l_c	Chord length	(µm)
m_s	Substrate weight	(g)

N	Mixing rate	(round per second)
P	Power consumption	(W)
Qc	Critical substrate flow rate	($gdm.h^{-1}$)
Q_H	Heat flux	(J)
t	Time	(h)
t*	Dimensionless time	(/)
T	Transmission signal	(%)
Tp	Temperature	(°)
V_s	Substrate volume	(L)
V_{sup}	Supernatant volume	(L)
V_{tot}	Total volume	(L)
W	Water content	(%)
W_{SL}	Total surface energy (solid-liquid)	($N.m^{-1}$)

INTRODUCTION

In a context of climate evolution, minimising the anthropogenic greenhouse gas effect and energy and petroleum crisis, the production of biofuels and chemicals as petroleum substitutes from renewable carbon represents economic and environmental challenges. Two leading factors have to be considered: (i) fuel cost and availability and (ii) climate change.

In an effort to combat climate change, to aid energy independence, and to counteract diminishing supplies of fossil fuels, there has been a resurgence of research on renewable energy sources. All routes to biofuels start with photosynthesis and biologically produced materials, and it is at that point where they diverge. There are basically three routes to convert renewable resources into energy rich, fuel-like molecules or fuel precursors: first, direct production by photosynthetic organisms, such as plants and algae; second, fermentative or non-fermentative production by heterotrophic micro-organisms, such as bacteria, yeast, or fungi and third, chemical conversion of biomass to fuels (Grammont, 2006; Rude & Schirmer, 2009; technologies, 2009).

It is increasingly understood that 1st generation biofuels (produced primarily from food crops such as grains, sugar beet and oil seeds) are limited in their ability to achieve targets for oil-product substitution, climate change mitigation, and economic growth. Their sustainability production is under review, as is the possibility of creating undue competition for land and water used for food and fibre production. As possible exception that appears to meet many of the acceptable criteria is ethanol produced from sugar cane.

The cumulative impacts of these concerns have increased the interest in developing biofuels produced from non-food biomass. Feedstock from lignocellulosic materials includes cereal straw, bagasse, forest residue, and purpose-grown energy crops such as vegetative grasses and short rotation forest. These 2nd generation biofuels are expected to minimize many of the concerns facing 1st generation biofuels and potentially offer greater cost reduction potential in longer term (Sim et al., 2008).

Cellulosic biomass provides a low cost and abundant resource that has the potential to support large-scale production of fuels and chemicals via biotechnological routes (Gibbons & Hughes, 2009). Among the large uses of lignocelluloses resources generated through forestry and agricultural practice; the pulp and paper industry hold a strategic position.

In this aim, the promotion of bio-refineries producing multiple products, including higher-value chemicals as well as fuels and power, is a major objective of numerous consolidated programs in the world. In order to achieve economic viability, the bio-refining of lignocellulosic resources must be operated at very high feedstock dry matter content. This strict prerequisite imposes a considerable constraint particularly on the physicochemical and bio-catalytic steps, whose overall aim is to produce high quality, fermentable sugar syrups, but is essential to be compatible with industrial criteria regarding maximum reactor volumes, energy and water consumption and wastewater management. Pulp and paper industry (Vallette & De Choudens, 1987) is able to provide a tried and tested industrial model for the processing of lignocellulosic biomass into pre-treated cellulosic pulps. The pulp product of this industry is appropriate for modern bio-refining, because it displays low lignin content, is free of inhibitory compounds that can perturb fermentations and is devoid of microbial contaminants. Nevertheless the enzyme liquefaction and saccharification of paper-like pulps are subjected to the same constraints as other pulps obtained via alternative methods such as steam explosion or dilute acid hydrolysis. Therefore, the better scientific understanding and ultimately the technical mastering of these critical biocatalytic reactions, which involve complex matrices at high solids content, is currently a major challenge that must be met in order to facilitate the intensification of bio-refining operations.

There are major, global challenges to meeting humankind's needs, owing to increasing food and non-food demand, calls for reducing our environmental footprint and growing uncertainties due to climate change. The sustainable intensification of agriculture and the development of a renewable carbon-based economy will thus be major issues contributing to the emergence of a 21st century bio-economy. To meet these challenges, French government is supporting and developing integrated research that ranges from the study of genomes to the study of food, energy and chemical systems and ecosystem services, uniting numerous fields of study including social and human sciences. Progress in white biotechnology – which uses microorganisms and their enzymes to yield biofuels, biolipids, bioplastics and other chemical molecules from biomass – has fostered new advances in the development of sustainable chemistry.

My PhD work fully integrates these scientific priorities dealing with "White biotechnology". It contributed to a collaborative work based on an inter-regional partnership (LISBP, IMFT and LCPO / Midi-Pyrénées and Aquitaine) with 2 national research institutes (INRA, CNRS) and, in collaboration with 2 international structures (University of Warterloo – CAN and Hanoï University of Science and Technology –VN). My PhD research contributes to ProBio3 project. It stands in the continuity of previous research programs ending the valorisation and the diversification of pulp and paper industry including energetic and environmental constraints in addition to profitable economical and societal criteria (programs ANR-05-BIOE-007 and BIP ADEME – Prepilpat involving LCPO (ex-USBB), LISBP and Tembec SAS, Futurol OSEO).

Lignocellulosic resources issued from pulp and paper industry and annual cultures (bagasse) require a bioconversion at the highest dry matter content to be economically viable. Physicochemical and bio-catalytic treatments aim to produce high concentration of fermentable oligomers or chemical intermediates taking into account industrial constraints (ie. volume, water and wastewater management). During their treatment, the solid matrices evolve from a heterogeneous structure (solid in suspension), into a partial and macroscopic depolymerised structure (fragmentation through bio-catalytic and microbial activities) and ultimately to a solubilisation (homogeneous liquid). The dynamic of mechanisms, which is limited by coupled phenomena between flow, mass and heat transfers, need to be investigated in regards with diffusion (within solid and liquid phases), convection (mixing, homogeneity) and specific inhibitors (concentration gradient). The liquefaction mechanisms of complex cellulosic substrates require physical, chemical and biochemical characterisations with scientific and technical locks in relation with biochemical engineering. PhD scientific aims are related to the investigation of dynamic of transfer phenomena and limitation of bio-catalytic reactions with lignocelluloses resources under high concentration conditions.

The understanding of the mechanisms of liquefaction of complex cellulosic substrates at high total solids concentration is still limited and requires detailed and exhaustive characterisation; and several scientific and technical questions for bioprocess intensification and biochemical engineering also need to be investigated. **To answer to these questions, my PhD research is centred on the development of in-situ and ex-situ physical and biochemical analysis to complete the comprehension of fibre destructuration mechanism and to characterise the release kinetic of glucose (as the principal interesting compound in hydrolysis).**

These dynamics and the chosen matrices and pre-treatment processes impact the fermentation process. Based on various processes (**Figure 0-1**), fermentation required appropriated hydrolysis kinetics comparing to fermentation kinetics, the consumption of the C6 and/or C5 sugars issued from hydrolysis had to be managed in order to maximise the conversion yields into several products (bio-refinery concepts). Different strains can be selected for the process consuming C6 and C5 sugars either separately or simultaneously. Depending on the hydrolysis temperature, and the dynamics of the different transfer phenomena, the behaviour

and the performances of the microbial strains can be modified inducing different fermentation strategies to be optimized. The originality can be to develop bio-refinery approach combining two strains able to both consuming C6 and C5 sugars to obtain products of different added values to maximise the efficiency of the integrated process and its economic rentability.

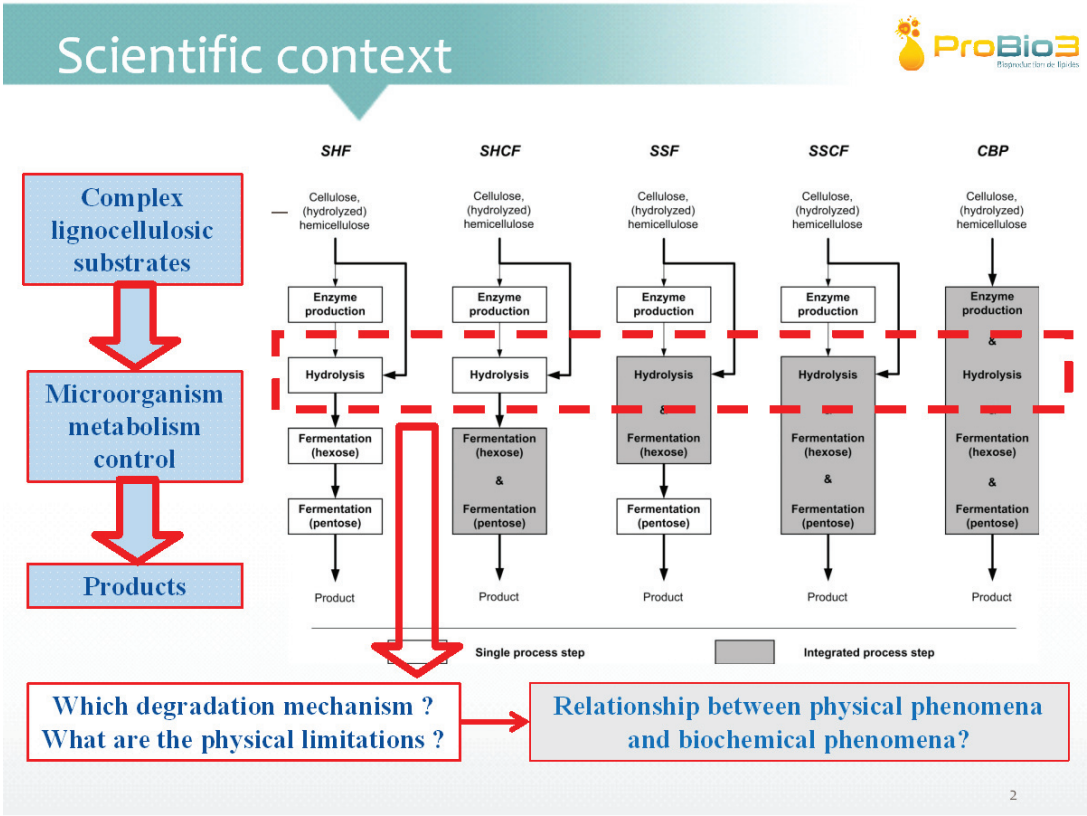

Figure 0-1: Technological and scientific positioning of research. Abbreviations: separate hydrolysis and fermentation (SHF), separate hydrolysis and co-fermentation (SHCF), simultaneous saccharification and fermentation (SSF), simultaneous saccharification and co-fermentation (SSCF), consolidated bioprocessing (CBP). (Jäger & Büchs, 2012) Adapted from (Lynd et al., 2002).

Table 0-1 summarizes the aims, challenges and proposed strategy and methodology. Scientific complexity of the project corresponds to three degrees of freedom of the study respectively related to (i) matrices (nature, structure and composition), (ii) multi-scale approach associated with in-situ and ex-situ metrologies and (iii) operating conditions (high dry matter content, transfers and inhibition). The originality of the approach is based on:

1. Considered matrices constitute a realistic issue from economic and technological standpoints,
2. Study carries out under diluted up to high substrate concentration,
3. Multi-scale investigation using state of the art analytical technologies under a multidisciplinary approach (process engineering, bioengineering, fluid mechanics, chemical analysis and biochemistry),

Table 0-1: Overview of scientific stakes.

Overarching aim :	- To improve biocatalytic destructuration of lignocellulosic biomass to produce concentrated fermentable substrates - To alleviate scientific bottlenecks and lead to the development of new intensified bioprocesses.
Critical challenges :	- Related to the development of phenomenological descriptions of the bio-catalytic processes that occur in industrial conditions.
Strategy :	- Investigate the degradation of selected model lignocellulosic matrices exhibiting a growing chemical and structural complexity with multi-scale and in-situ/ex-situ physical and/or biochemical metrologies.
Approach :	- State of the art analytical technologies, coupled to significant methodological developments, and a multidisciplinary approach - To involve scientists possessing expertise in process engineering, bioengineering, fluid mechanics, chemical analysis and biochemistry.

In this work, five different substrates are considered: microcrystalline cellulose (MCC), dried and milled Whatman paper (WP), extruded softwood and hardwood paper-pulps (PP) and dried and milled sugarcane bagasse. The substrate concentrations range from dilute (1%w/v) to concentrated (up to 10%w/v) regime with the enzymatic activities (Industrial cocktail Accellerase 1500) varying between 5 and 25FPU/g cellulose. All experiments are conducted at 40°C, pH=4.8 (compatibility with microorganism culture conditions and representative of substrate adds in agro-industrial process) and during 24h (pertinent period to appreciate transfer limitations). To investigate the evolution of physical-biochemical parameters and determine the transfer limitations linked to physical (mass/heat)-biochemical (conversion efficiency) phenomena, multi-scale characterisation was implemented in using numerous analysis techniques. The knowledge of enzymatic hydrolysis could be developed into three blocks: rheometry (macro-scale), morpho-granulometry (micro-scale) and biochemistry (molecular scale). Each block is characterised by in-situ and ex-situ measurements. The monitoring in-situ suspension viscosity and particle size give us the significant advantages, especially for the complex matrices like lignocellulose biomasses.

Our work operated into three principal steps. The first corresponded to the physical-thermal-biochemical characterisations of substrates and to the study of suspension rheology before hydrolysis. The second was hydrolysis of substrate suspensions at batch mode and dilute concentration (1-3%w/v) to understand the fibre degradation mechanism. The last step used the results of second step to hydrolyse in semi-continuous mode with cumulative feeding substrate strategy in order to increase dry matter content and maintain the favourable condition of enzymatic hydrolysis.

This manuscript is structured around five parts:

- A short introduction which gives economical and industrial context and defines our scientific objectives.
- A bibliographic overview focussing on two major items: (i) Overview of second generation biofuels and (ii) Rheology of lignocellulose suspensions and impact of hydrolysis, will end with the objective of study.
- Materials & Methods will detail the experimental set-up and analyses. A specific description is conducted for original instruments related to physical measurements. This part ends with the description of our strategy of investigation.
- Results constitute the most important part of this document. It integrates (i) an overview of substrates and experiments presentation, (ii) a full description of experimental results and (iii) discussion and modelling.
- Finally a short conclusion will resume main results and draw-up perspectives.

1 BIBLIOGRAPHY SYNTHESIS

1.1 Overview of second generation biofuels

Since several years, the environment preoccupation and energy control are in the heart of scientific and social debate. Behind the increase of energy consumption, the depletion of fossil resources; the development of biofuels presents like an important solution to solve these problems beside the approaches of wind energy, solar energy…

It is increasingly understood that the 1st generation biofuels (produced primarily from food crops such as grains, sugar beet and oil seeds) are limited in their ability to achieve targets for oil-product substitution, climate change mitigation, and economic growth. Their sustainability production is under review, as is the possibility of creating undue competition for land and water used for food and fibre production.

The cumulative impacts of these concerns have increased the interest in developing biofuels produced from non-food biomass. Feedstock from lignocellulosic materials includes cereal straw, bagasse, forest residue, and purpose-grown energy crops such as vegetative grasses and short rotation forest. These 2nd generation biofuels are expected to minimize many of the concerns facing 1st generation biofuels and potentially offer greater cost reduction potential in longer term (Sim et al., 2008).

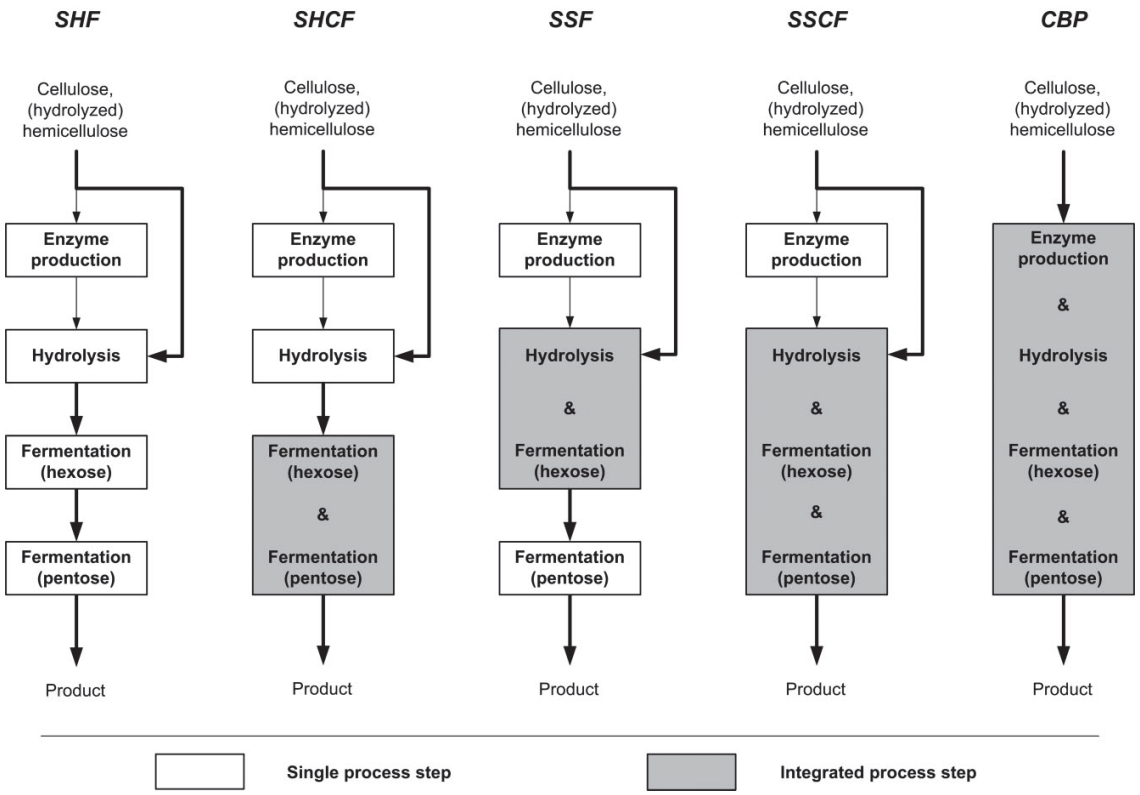

Figure 1-1: Various (integrated) configurations of biologically mediated processing steps during the biocatalytic conversion of lignocellulose. Abbreviations: separate hydrolysis and fermentation (SHF), separate hydrolysis and co-fermentation (SHCF), simultaneous saccharification and fermentation (SSF), simultaneous saccharification and co-fermentation (SSCF), consolidated bioprocessing (CBP) (Jäger & Büchs, 2012) adapted from (Lynd et al., 2002).

Cellulosic biomass provides a low cost and abundant resource that has the potential to support large-scale production of fuels and chemicals via biotechnological routes (Gibbons & Hughes, 2009). For example with the conversion into ethanol fuel is eventually expected to provide a significant portion of the world's energy requirements. In 2030, about 10% of global lignocellulosic residues could be converted in around 155 billion lge (5.2 EJ) lignocellulosic ethanol or roughly 4.1% of the projected transport fuel demand (Menon & Rao, 2012).
The first hydrolysis methods used were chemicals, but they are less competitive at the moment, because of the cost of the reagents and the formation of many secondary products and inhibitory compounds. They are now competitive by enzymatic methods, which allow more specific and better yields of hydrolysis in less severe conditions (Ogier et al., 1999). An enzyme-based process can be divided into four principal steps: (1) Pre-treatment: due to the recalcitrant nature of native lignocelluloses, physical/chemical methods are needed to generate an enzymatically convertible material; (2) Enzymatic hydrolysis: where the cellulose and hemicelluloses are enzymatically degraded to sugar monomers; (3) Fermentation: sugar monomers are converted into interest molecules, often by yeast; (4) Distillation to recover products (Bommarius et al., 2008; Lee, 1997; Zhang et al., 2009) (**Figure 1-1**). In order to produce sugars from the biomass, the biomass is pre-treated with physical or/and thermo-chemical, possible biological in order to reduce the size of the feedstock and to open up the plant structure. The cellulose and the hemicellulose portions are broken down (hydrolysed) by enzymes simple sugars that are then fermented into interest products by specific varieties of microorganisms. Currently this biochemical route is the most commonly used process (Karunanithy et al., 2013).

1.1.1 Structure of lignocellulose biomass

Lignocellulose biomass is one of the most abundant renewable resources and certainly one of the least expensive. The structural materials that plants produce to form the cell walls, leaves, stems, stalks, and woody portions of biomass are composed mainly of cellulose, hemicellulose, and lignin (Fan et al., 1987). In general, biomass consists of 40-50% cellulose, 25-30% hemicellulose, 15-20% lignin and other extractable components (Knauf & Moniruzzaman, 2004).

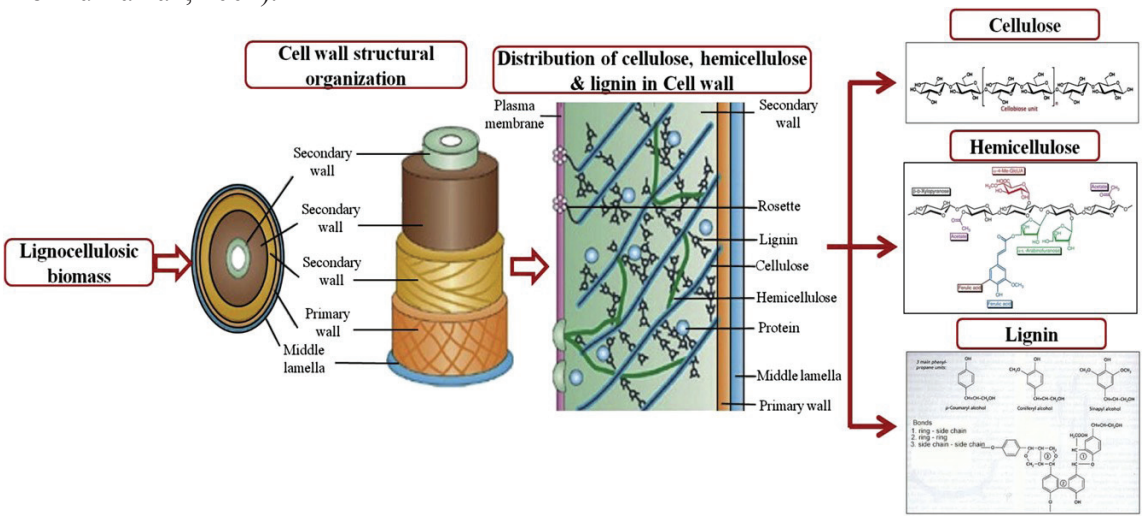

Figure 1-2: Diagrammatic illustration of the framework of lignocellulose (Menon & Rao, 2012).

A representative diagrammatic framework of lignocellulosic biomass is illustrated in **Figure 1-2**. The cellulose chains are packed into micro-fibrils which are stabilised by hydrogen

bonds. These fibrils are attached to each other by hemicelluloses and amorphous polymers of different sugars as well as other polymers such as pectin and covered by lignin. The cellulose micro-fibrils which are present in the hemicellulose-lignin matrice are often associated in the form of bundles or macro-fibrils.

Cellulose is a high molecular weight, linear chain, polymer of D-glucose linked together by β-(1-4)-glucosidic bonds. In native cellulose, each cellulose molecule is a long unbranched chain of D-glucose subunits with a molecular weight ranging from 50,000 to over 1 million Danton. The extensive hydrogen linkages among molecules lead to a crystalline and strong matrice structure (Ebringerova et al., 2005). Cellulose is the most prevalent organic polymer and is approximately 30% of the plant composition (Demirbas, 2005). Cotton, flax and chemical pulps represent the purest sources of cellulose (80-95% and 60-80%, respectively) while soft and hardwoods contain approximately 45% cellulose (**Table 1-1**).

Hemicelluloses are amorphous and variable structure formed of hetero-polymers including hexoses (D-glucose, D-galactose and D-mannose) and pentose (D-xylose and L-arabinose) and may contain sugar acids (uronic acids) such as: D-glucuronic, D-galacturonic and methylgalacturonic acids (McMillan James, 1994; Saha, 2003). Its backbone chain is primarily composed of xylan β-(1-4)-linkages that include D-xylose (nearly 90%) and L-arabinose (approximately 10%) (Gírio et al., 2010). The hemicelluloses of softwood are typically glucomannans while hardwood hemicellulose is more frequently composed of xylans (McMillan James, 1994).

Lignin is composed of polymerised phenylpropanoic alcohol in a complex three dimensional structure. It is composed of three phenolic monomers: coumaryl, coniferyl and sinapyl alcohol. Lignin is a complex hydrophobic, cross-linked aromatic polymer that interferes with the hydrolysis process. In the agriculture sub-product, his contents are lower than those of wood (**Table 1-1**).

Table 1-1: Composition of several lignocellulose feedstocks.

Feedstocks	Carbohydrate compositions (% dm)			References
	Cellulose	Hemicellulose	Lignin	
Barley straw	36-43	24-33	6-10	(García-Aparicio et al., 2006)
Bamboo	49-50	18-20	23	(Alves et al., 2010)
Banana waste	13	15	14	(Monsalve et al., 2006)
Corn stover	35-40	21-25	11-19	(Mosier et al., 2005)
Cotton	85-95	5-15	0	(Kadolph & Langford, 1998)
Eucalyptus	45-51	11-18	29	(Alves et al., 2010; Pereira, 1988)
Hardwood	10-55	24-40	18-25	(Malherbe & Cloete, 2002)
Hard wood-Populus	51	21	23	(Vallette & De Choudens, 1987)
Rice straw	29-35	23-26	17-19	(Prasad et al., 2007)
Wheat straw	35-39	22-30	12-16	(Prasad et al., 2007)
Grasses	25-40	25-50	10-30	(Stewart et al., 1997)
Sugarcane bagasse	25-45	28-32	15-25	(Singh et al., 2009)
Olive tree	25	16	19	(Cara et al., 2008)
Soft wood	45-50	24-40	18-25	(Malherbe & Cloete, 2002)
Soft wood	48	21	27	(Vallette & De Choudens, 1987)
Sorghum straw	32-35	24-27	15-21	(Herrera et al., 2003; Vázquez et al., 2007)

1.1.2 Pre-treatment of lignocellulose biomass

The structure of lignocellulosics in the cell wall resembles that of a concrete pillar with cellulose fibres being the metal rods and lignin the natural cement. Biodegradation of untreated native lignocellulosics is slow, giving a very low extent of degradation (Chang et al., 1981; Kaar & Holtzapple, 1998). The resistance of biomass to enzymatic attack can be contributed to three major factors: lignin content, cellulose accessibility and cellulose crystallinity (Agbor et al., 2011; Ladisch et al., 1979). To increase the susceptibility of cellulosic material, structural modification by means of various pre-treatment strategies is indispensable (Wyman, 2007). In theory, the ideal pre-treatment process produces a disrupted, hydrated substrate that is easily hydrolysed without the formation of sugar degradation products and fermentation inhibitors (Agbor et al., 2011). Many pre-treatment methods were studied and reported in literature. They can be classified into biological, physical, chemical and physico-chemical pre-treatments.

1.1.2.1 Biological pre-treatments

Biological pre-treatment employ microorganisms mainly brown, white and soft-rot fungi which degrade lignin and hemicellulose and very little of cellulose, more resistant than the other components (Sánchez, 2009). Lignin degradation by white-rot fungi, the most effective for biological pre-treatment of lignocellulosic materials, occurs through the action of lignin-degrading enzymes such as peroxidases and laccases (Kumar et al., 2009). In general, such processes offer advantages such as low-capital cost, low energy, no chemicals requirement, and mild environmental conditions. However, the main drawback to develop biological methods is the low hydrolysis rate obtained in most biological materials compared to other technologies (Sun & Cheng, 2002).

1.1.2.2 Physical pre-treatments

Physical pre-treatments consist generally two methods: mechanical pre-treatment and extrusion pre-treatment. The objective of the mechanical pre-treatment is a reduction of particle size and crystallinity of lignocellulosic in order to increase the specific surface and reduce the degree of polymerisation. It can be produced by a combination of chipping, grinding or milling depending on the final particle size of the material (10–30 mm after chipping and 0.2–2 mm after milling or grinding) (Sun & Cheng, 2002). Different milling processes (ball milling, two-roll milling, hammer milling, colloid milling and vibrio energy milling) can be used to improve the enzymatic hydrolysis of lignocelullosic materials (Taherzadeh & Karimi, 2008). Power consumption requirements of this method are taken into account that this pre-treatment is not likely an economic process. For extrusion, the materials are subjected to heating, mixing and shearing, resulting in physical and chemical modifications during the passage through the extruder. Screw speed and barrel temperature are believed to disrupt the lignocellulose structure causing defibrillation, fibrillation and shortening of the fibres, and, in the end, increasing accessibility of carbohydrates to enzymatic attack (Karunanithy et al., 2013).

1.1.2.3 Chemical pre-treatments

These pre-treatments methods could be classified by chemical nature of reagents and consist four main groups: alkaline, acid, ozone, Organosolv and ionic liquids pre-treatment.
Alkali pre-treatments increase cellulose digestibility and they are more effective for lignin solubilisation, exhibiting minor cellulose and hemicellulose solubilisation than acid or hydrothermal processes (Carvalheiro et al., 2008). Sodium, potassium, calcium and ammonium hydroxides are used for this pre-treatment.

The main objective of the acid pre-treatments is to solubilize the hemicellulose fraction of the biomass and to make the cellulose more accessible to enzymes. High hydrolysis yields have been reported when pre-treating lignocellulosic materials with diluted H_2SO_4 which is the most studied acid. Hydrochloric acid, phosphoric acid and nitric acid have also been tested (Mosier et al., 2005). Organic acids such as fumaric or maleic acids are appearing as alternatives to enhance cellulose hydrolysis for ethanol production.
Ozone is a powerful oxidant that shows high delignification efficiency (Sun & Cheng, 2002). Ozonolysis has been applied on several agricultural residues such as wheat straw and rye straw (García-Cubero et al., 2009).
For Organosolv method, numerous organic or aqueous solvent mixtures can be utilized, including methanol, ethanol, acetone, ethylene glycol and tetrahydrofurfuryl alcohol, in order to solubilize lignin and provide treated cellulose suitable for enzymatic hydrolysis. Comparing to other chemical pre-treatments the main advantage of Organosolv process is the recovery of relatively pure lignin as a by-product (Zhao et al., 2009).
The ionic liquids are used for dissolving simultaneously carbohydrates and lignin. As a result, the intricate network of non-covalent interactions among biomass polymers of cellulose, hemicellulose, and lignin is effectively disrupted while minimizing formation of degradation products. Ionic liquids are salts, typically composed of large organic cations and small inorganic anions.

1.1.2.4 Physico-chemical pre-treatments

There are several methods in combining the physical technique and chemical reagent to treat lignocellulose biomass. We present here seven main techniques: steam explosion, liquid hot water, ammonia fibre explosion, wet oxidation, microwave pre-treatment, ultrasound pre-treatment and CO_2 explosion.
Steam explosion (SO_2 steam explosion) is the most widely employed physico-chemical pre-treatment for lignocellulosic biomass. It is a hydrothermal pre-treatment in which the biomass is subjected to pressurised steam for a period of time ranging from seconds to several minutes, and then suddenly depressurised. This pre-treatment combines mechanical forces and chemical effects due to the hydrolysis (auto-hydrolysis) of acetyl groups present in hemicellulose.
The objective of the liquid hot water is to solubilise mainly the hemicellulose, to make the cellulose more accessible and to avoid the formation of inhibitors. Pressure is applied to maintain water in the liquid state at elevated temperatures (160–240°C) and provoke alterations in the structure of the lignocellulose.
In the ammonia fibre explosion process, biomass is treated with liquid anhydrous ammonia at temperatures between 60 and 100°C and high pressure for a variable period of time. The pressure is then released, resulting in a rapid expansion of the ammonia gas that causes swelling and physical disruption of biomass fibres and partial decrystallisation of cellulose. This technique has been reported to decrease cellulose crystallinity and disrupt lignin–carbohydrates linkages (Laureano-Perez et al., 2005).
Wet oxidation is an oxidative pre-treatment method which employs oxygen or air as catalyst. It has been proven to be an efficient method for solubilisation of hemicelluloses and lignin and to increase digestibility of cellulose (Martín et al., 2008).
Pre-treatment by microwave were carried out by immersing the biomass in dilute chemical reagents and exposing the slurry to microwave radiation for given times (Keshwani & Cheng, 2010).
Ultrasound effects on lignocellulosic biomass have been employed for extracting hemicelluloses, cellulose and lignin but less research has been addressed to study the susceptibility of lignocellulosic materials to hydrolysis (Sun & Tomkinson, 2002).

The method of carbonic gas explosion is based on the utilisation of CO_2 as a supercritical fluid, which refers to a fluid that is in a gaseous form but is compressed at temperatures above its critical point to a liquid like density. It can effectively remove lignin increasing substrate digestibility (Schacht et al., 2008).
Table 1-2 presents the effect of different pre-treatment technologies on the structure of lignocellulose. Among these methods, chemical and physic-chemical techniques present like the most interesting method to pre-treat the biomass. A combination of different methods could be effectively interesting approaches for pre-treating complex matrices.

Table 1-2: Summarise of effects of different pre-treatment technologies on lignocellulose structure (Alvira et al., 2010) (H: high effect; M: moderate effect; L: low effect).

	Physical pre-treatment	Chemical pre-treatment		Physical-chemical pre-treatment			
	Milling	Acid	Alkaline	Steam explosion	Wet oxidation	Ammonia fibre explosion	CO_2 explosion
Increases accessible surface area	H	H	H	H	H	H	H
Cellulose decrystallisation	H	-	-	-	-	H	-
Hemicellulose solubilisation	-	H	L	H	H	M	H
Lignin removal	-	M	M	M	L	H	-
Generation of toxic compounds	-	H	L	H	L	L	-

1.1.3 Saccharification of lignocellulose

The lignocellulose biomass are degraded naturally by microorganism, predominately by fungi and most rapid by basidiomycetes group (Rabinovich et al., 2002). In bioethanol production process, the degradation of lignocellulose substrates are promoted and realised by specific enzymes which are extracted from microorganism cultures.

1.1.3.1 Saccharification of cellulose

Enzymatic hydrolysis of cellulose is carried out by cellulase enzymes. The products of the hydrolysis are usually reducing sugars, including glucose. Cellulases are composed of a complex mixture of enzyme proteins with different specificities to hydrolyse the β-(1-4)-glycosidic linkages bonds. They are divided into three major enzyme activity classes: endoglucanases or endo-1-4-β-glucanase; exoglucanases including 1,4-β-D-glucanohydrolases (also known as cellodextrinases) and 1,4-β-D-glucan cellobiohydrolases (cellobiohydrolases); β-glucosidases (Goyal et al., 1991; Lynd et al., 2002; Rabinovich et al., 2002).
Endoglucanases are thought to initiate attack randomly at multiple internal sites in the amorphous regions of the cellulose fibre which opens-up sites for subsequent attack by the cellobiohydrolases (Lynd et al., 1991). Exoglucanase is the major component of the fungal cellulase system accounting for 40–70% of the total cellulase proteins, and can hydrolyse highly crystalline cellulose (Esterbauer et al., 1991). They remove monomers and dimers from

the end of the glucan chain. Cellobiose dimers are cleaved by β-glucosidases to yield glucose monomers. **Figure 1-3** summarises the enzymatic degradation of cellulose. Ideally, if the cellulose hydrolysis has totally finished, the cellulose is converted into glucose as presents as **Eq.1-1**:
For cellulose:

$$(C_6H_{10}O_5)_n + nH_2O \rightarrow nC_6H_{12}O_6 \quad \textit{(Eq. 1-1)}$$

For cellobiose:

$$C_{12}H_{22}O_{11} + H_2O \rightarrow 2\,C_6H_{12}O_6 \quad \textit{(Eq. 1-2)}$$

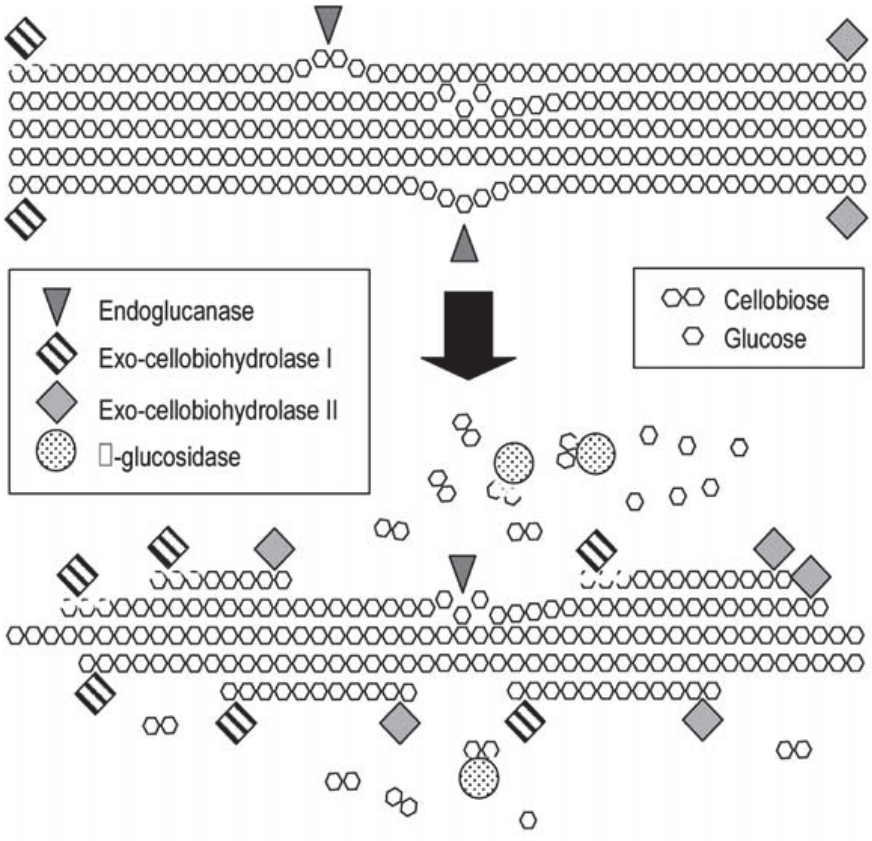

Figure 1-3: A simplified schematic representation of the process involved in complete enzymatic hydrolysis of a cellulose micro-fibril (Malherbe & Cloete, 2002).

1.1.3.2 Hemicellulose biodegradation

Due to the complexity of hemicellulose and the large number of enzymes required for its total hydrolysis, synergy studies have only identified some of the interactions that take place between different hemicellulases on different substrates (Malherbe & Cloete, 2002). Hemicellulases are frequently classified according to their action on distinct substrates, endo-1,4-β-D-xylanases and endo-1,4-β-D-mananases.
Endo-1,4-β-D-xylanases generate oligosaccharides from the cleavage of xylan and xylan 1,4-β-xylosidases produce xylose from oligosaccharides. In addition, hemicellulose degradation needs accessory enzymes such as xylan esterases, ferulic and p-coumaric esterases, α-1-

arabinofuranosidases, and α-4-O-methyl glucuronosidases, acting synergistically to efficiently hydrolyse wood xylans and mannans.
Endo-1,4-β-mannanases and exo-β-mannosidases are required to convert mannans into simple sugar. Additional enzymes, such as β-glucosidases, α-galactosidases and acetyl mannan esterases are required to remove side chain sugars that are attached at various points on mannans (Dhawan & Kaur, 2007).
Eq.1-3 to **1-7** described the hydrolysis of five main components of hemicellulose: xylan, glucuronoxylan, arabinoxylan, glucomannan and xyloglucan.

$$(C_5H_8O_4)_n + nH_2O \rightarrow nC_5H_{10}O_5 \quad \textit{(Eq. 1-3)}$$
$$xylan + H_2O \rightarrow xylose$$

$$(C_5H_7O_3 - OOC - C_5H_9O_5)_n + 2nH_2O \rightarrow nC_5H_{10}O_5 + nC_5H_9O_5 - COOH \quad \textit{(Eq. 1-4)}$$
$$glucuronoxylan + H_2O \rightarrow xylose + gluconic\,acid$$

$$(C_{10}H_{18}O_9)_n + nH_2O \rightarrow nC_5H_{10}O_5 + nC_5H_{10}O_5 \quad \textit{(Eq. 1-5)}$$
$$arabinoxylan + H_2O \rightarrow xylose + arabinose$$

$$((C_6H_{10}O_5)_{16} - (C_6H_{10}O_5)_{10})_n + 26nH_2O \rightarrow 16nC_6H_{12}O_6 + 10nC_6H_{12}O_6 \quad \textit{(Eq. 1-6)}$$
$$glucomannan + H_2O \rightarrow mannose + glu\cos e$$

$$(C_6H_{10}O_5 - C_5H_8O_4)_n + 2nH_2O \rightarrow nC_6H_{12}O_6 + nC_5H_{10}O_5 \quad \textit{(Eq. 1-7)}$$
$$xy\log lucan + H_2O \rightarrow glu\cos e + xylose$$

Xylose, mannose, arabinose, galactose, rhamnose and also glucose present like the simple sugars the most commonly released during hemicellulose hydrolysis. Generally, for hardwood biomass, xylose presents in the largest amount (could be present until 90%) and for softwood, mannose and xylose take the equal part (Vallette & De Choudens, 1987).

1.1.3.3 Lignin biodegradation

Lignin degradation is an oxidative process and phenol oxidases are the key enzymes composed lignin peroxidases, manganese peroxidases and laccases (Kuhad et al., 1997; Leonowicz et al., 1999). Lignin peroxidases and manganese peroxidases oxidise the substrate by two consecutive one-electron oxidation steps with intermediate cation radical formation. Laccase has broad substrate specificity and oxidises phenols and lignin substructures with the formation of oxygen radicals.
The pathways of lignocellulose degradation by enzymes are so complex and partially understood. It is really a challenge to develop the knowledge of this domain.

1.1.4 Enzymatic saccharification strategies

In order to produce bioethanol, the pre-treated lignocellulose biomass would be hydrolysed and then be fermented to convert the simple sugars (hexose also pentose) into ethanol.
Conventionally, this process could be realised in two separate steps: hydrolysis and fermentation (SHF). In addition, it could be realised in simultaneous saccharification and fermentation (SSF) or more recently consolidated bioprocessing (CBP) which integrates enzyme production, saccharification and fermentation into a single process.

1.1.4.1 Separate hydrolysis and fermentation

SHF is a conventional two-step process where cellulose is enzymatically hydrolysed by cellulase to form simple sugars like glucose in the first step and these sugars are fermented to obtain the product in the second step by using *Saccharomyces, Zymomonas* or other

microorganisms (Fan et al., 2003; Herrera et al., 2003; Ingram & Doran, 1995; Zhao et al., 2009). The main advantage of SHF is the ability to carry out each step at its optimum conditions: temperature, pH…Typically, separate hydrolysis and fermentation processes involve the inhibition of the hydrolytic enzymes (cellulases) by saccharide products such as glucose and cellobiose.

Considering economy conditions, the ethanol concentration in the broth entering distillation should be above 4% w/w to make and economically feasible process (Fan et al., 2003; Laureano-Perez et al., 2005). This ethanol concentration would require an initial substrate concentration above 15% w/w (dry basis) assuming a substrate with a cellulose content of 60%, conversion 90%, and ethanol yield of 0.5 g/g-glucose (Jorgensen et al., 2007). This substrate condition could require very high forces for agitation and mixing; also provoke the ‘‘solids effect’’ (Kristensen et al., 2009) in which expected glucose yields become reduced as substrate concentration is increased. One approach to addressing this problem involves the use of fed batch additions of substrate. Operating enzymatic hydrolysis of lignocellulosic biomass in fed-batch mode, where fresh substrate and enzyme are added at different times when the apparent viscosity of the material has decreased, allows to significantly increasing the initial concentration of substrate. The substrate concentration could be up to 30%w/w (Lu et al., 2010). The ethanol concentration could be obtained about 6%w/v for Kraft paper mill sludge (Martín et al., 2008). Some reported studies of enzymatic hydrolysis of lignocellulosic biomass in fed-batch mode are summarised in **Table 1-3**. In fed-batch enzymatic hydrolysis, two or three additions of substrate are commonly used, and that enzymes can be supplemented at each substrate addition to maintain the initial loading or fed at the beginning of the reaction based on the final cumulative concentration of substrate.

Table 1-3: Fed-batch hydrolysis: literature synthesis.

Author	Substrate	Strategy: substrate (%) + enzyme (time)
(Herrera et al., 2003)	Olive pulp	15 + E (0h); 5 + E (24h); 5 + E (48h)
	Olive pulp	15 + E (0h); 7.5 + E (24h); 7.5 + E (48h)
	Olive pulp + Olive stones	15 + E (0h); 10 + E (24h); 5 + E (48h)
	Olive pulp + Olive stones	10 + E (0h); 15 + E (24h); 5 + E (48h)
(Ballesteros et al., 2002)	Recycled paper	5 + E (0h); 3 + E (24h); 2 + E (48h)
(Rosgaard et al., 2007)	Barley straw	5 + E (0h); 5 (6h); 5 (24h)
	Barley straw	5 + E (0h); 10 (24h)
	Barley straw	5 + E (0h); 5 + E (6h); 5 + E (24h)
	Barley straw	5 + E (0h); 10 + E (24h)
(Hodge et al., 2009)	Corn stover	15 + E (0h); 2.5 + E (12h); 2.5 x 4 + E (24h, 4x24h)
(Lu et al., 2010)	Corn stover	15 + E (0h); 5 (2h)
	Corn stover	15 + E (0h); 10 (2h)
	Corn stover	15 + E (0h); 7.5 (2h); 7.5 (4h)
(Elliston et al., 2013)	Shredded copier paper	5 + E (0h); 5 + E (6h); 2.5 x 4 + E (12h, 4x18h)

1.1.4.2 Simultaneous Saccharification and Fermentation

SSF is the most promising process for ethanol production from lignocellulosic materials with multiple researchers focusing on the process (Du et al., 2014; Rabinovich et al., 2002; Schacht

et al., 2008; Sun & Tomkinson, 2002). The simple sugars released from enzymatic hydrolysis could be directly converted into interest products throughout microorganism like *Saccharomyces, Yarrowia*. Therefore, SSF process keeps the concentration of saccharides too low to cause any considerable cellulase inhibition (Keshwani & Cheng, 2010). For example, ethanol production by SSF at high dry matter content has been studied extensively and dry matter levels of up to 17% have resulted in production of 52.3 $g.L^{-1}$ ethanol (Sun & Tomkinson, 2002). The SSF process could be also realised in batch or/and fed-batch mode.

1.1.5 Hydrolysis yield

There are many different ways and methods to estimate the efficiency of enzymatic hydrolysis. This depends clearly on the objective of each study. Effectively, for a bioprocess in converting lignocellulose, the main goal keeps always monosaccharides productions. Most commonly, the yield of glucose released is taken like the first quantity to evaluate the efficiency of enzymatic hydrolysis. In several cases, the other monomers such as xylose could be noticed. For the studies of effect of single or two separate enzyme activities which have not capacity to hydrolyse lignocellulose into simple sugars, the quantification has to take place another component like cellobiose…

Therefore, to quantify these products of hydrolysis, a number of methods were proposed in the literature. Hydrolysis yield could be based on reducing sugars which are determined by DNS (dinitrosalicylic acid) method (Goyal et al., 1991). Yield should be also determined based on the monomer sugars that are formed during enzymatic degradation: glucose, xylose, mannose, arabinose. This is generally carried out by HPLC analysis and various columns and methods can be used (Lynd et al., 2002). Or simplest, the calculation is based on glucose concentration.

The standard calculation for yield as proposed by the NREL (National Renewable Energy Laboratory of US) is:

$$Hydrolysis(\%) = \frac{\text{Amount of released Glucose}}{\text{Potential quantity of Glucose}} = \frac{[Glu] + 1.0526 \cdot [Cellobiose]}{1.111 \cdot F_{cellulose} \cdot [Ini.Sol]} \cdot 100 \quad \textit{(Eq. 1-8)}$$

with [Glu]: glucose concentration in the supernatant ($g.L^{-1}$); [Cellobiose]: cellobiose concentration in the supernatant ($g.L^{-1}$); $F_{cellulose}$: concentration of cellulose in the substrate (g cellulose/g dry matter); [IniSol]: concentration of initial solid in total volume ($g.L^{-1}$). Coefficients (1.111 and 1.0526) are related to stoichiometric equation regarding respectively hydrolysis of cellulose and cellobiose (**Eq. 1-1** and **1-2**). This calculation (**Eq. 1-8**) is realistic only if the solid fraction is negligible in front of total volume (Vtot~ Vsup) (often for substrate concentration inferior to 5%w/v (García-Aparicio et al., 2007)). For the concentrated, **Eq. 1-8** becomes as follow:

$$Hydrolysis\ (\%) = \frac{([Glu] + 1.0526 \cdot [Cellobiose]) \cdot V_{sup}}{(1.111 \cdot F_{cellulose} \cdot [Ini.Sol]) \cdot V_{Tot}} \cdot 100$$

$$Hydrolysis\ (\%) = \frac{[Glu] + 1.0526 \cdot [Cellobiose]}{1.111 \cdot F_{cellulose} \cdot [Ini.Sol]} \cdot (1 - \phi) \cdot 100 \quad \textit{(Eq. 1-9)}$$

With Vsup: volume of supernatant (L), Vtot: total volume (solid and liquid fractions) (L) and ϕ volume solid fraction (/).

Taking only the criteria of glucose production, **Eq. 1-9** becomes the simplest calculation presented as below:

$$Hydrolysis\ (\%) = \frac{\text{Glucose}_{\ produced}(g)}{1.111 \cdot Cellulose_{\ initial}(g)} \cdot 100 \quad \textit{(Eq. 1-10)}$$

Peng and Chen (2011) reported a calculation of degree of saccharification basing on reducing sugars which presented in **Eq. 1-11**:

$$Hydrolysis(\%) = \frac{\text{Reducing sugar concentration obtained}}{\text{Potential sugar concentration in the substrate}} \cdot 100 \quad \textit{(Eq. 1-11)}$$

For hemicellulose, because of the complexity of hemicellulose compositions, it is difficult to propose a unique equation which translates the hemicellulose conversion. However, if we consider that the main components of hemicellulose are xylan and mannan, the hydrolysis yield could be calculated as below:

$$Hydrolysis_{hemicellulose} = \frac{Xyl(g) \cdot 0.88 + Man(g) \cdot 0.9}{Hemicellulose_{initial}(g)} \cdot 100 \quad \textit{(Eq. 1-12)}$$

where Xyl, quantity of obtained xylose (g); Man, quantity of obtained mannose (g), $Hemicellulose_{initial}$, quantity of initial hemicellulose (g). Coefficients (0.88 and 0.9) are related to stoichiometric equation regarding respectively hydrolysis of xylan and glucomannan (**Eq. 1-3** and **1-6**).

The hydrolysis efficiency depends on such of factors. We can cite here like biomass nature, pre-treatment technique, quantity and composition of enzyme, operation conditions. **Table 1-4** summarises the hydrolysis yield for different substrates reported in literature. In this table, we divided biomass into three groups: woody biomass, agricultural residues and other biomass. Each type of substrate underwent different pre-treatments but physical-chemical pre-treatments present like the most commonly. The hydrolysis conditions were probably found at 50°C during at least 48h. The high different between these studies was in the used enzyme concentration which varied not only in enzyme quantity but also in enzyme compositions. Therefore, a few studies reported a total conversion into simple sugars (>90%) beside the results of partly conversion (<50%). These hydrolysis conditions can give us the ideals to realise our hydrolysis in saving energy consumption and decreasing the product cost.

1.1.6 Position of paper-pulp and paper industry

As mentioned above, lignocellulose feedstocks present like the most interesting raw material to produce biofuel in second generation. These substrates include woody substrates (hardwood and softwood), products from agriculture (straw) or those of lignocellulosic waste industries (food processing, paper). Among these large uses of lignocelluloses resources, the pulp and paper industry hold a strategic position.

In this aim, the promotion of bio-refineries producing multiple products, including higher-value chemicals as well as fuels and power, is a major objective of numerous consolidated programs in the world. In order to achieve economic viability, the biorefining of lignocellulosic resources must be operated at very high feedstock dry matter content. This strict prerequisite imposes a considerable constraint particularly on the physicochemical and bio-catalytic steps, whose overall aim is to produce high quality, fermentable sugar syrups, but is essential to be compatible with industrial criteria regarding maximum reactor volumes, energy and water consumption and wastewater management. Pulp and paper industry (Vallette & De Choudens, 1987) is able to provide a tried and tested industrial model for the processing of lignocellulosic biomass into pre-treated cellulosic pulps. The pulp product of this industry is appropriate for modern bio-refining, because it displays low lignin content, is free of inhibitory compounds that can perturb fermentations and is devoid of microbial contaminants (biochemical properties of different paper-pulp and also of wood were localised in **Annexe 1**)

Figure 1-4 presents the process of biofuel production in coupling with paper and paper pulp industry. Green part schematises the paper-pulp production whereas the orange part shows

different steps to produce the biofuels. Two main advantages are highlighted here for this process. The first is the perfect control of paper-pulp quality in the efficiency of woody substrate pre-treatment and the elimination of lignin content in biomass. The second presents in the energy independence of paper industry which could reduce the final biofuel costs.
In summary, the paper-pulp coming from pulp industry exhibits a favourable substrate to produce biofuel and an ability to support large-scale production.

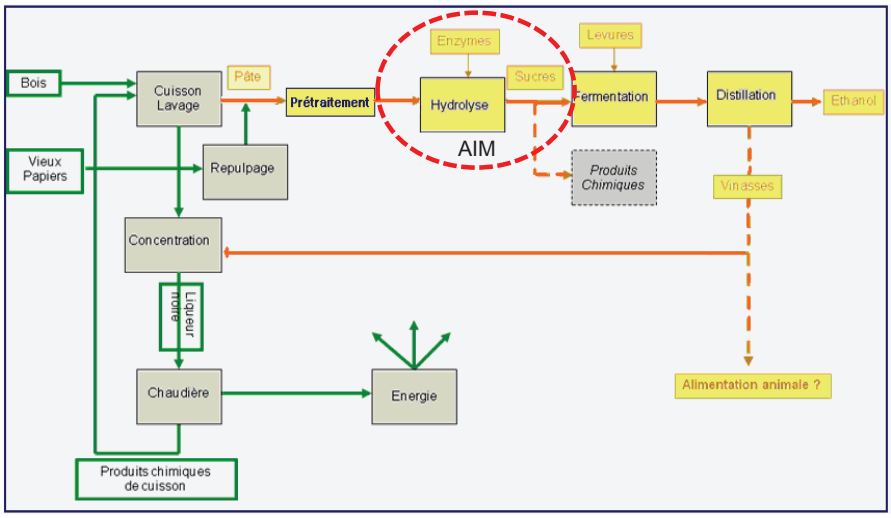

Figure 1-4: Coupling of biofuel production and pulp and paper process- Focus on our point of interest.

1.1.7 Current technology in bio-refinery

The development of bio-refinery process is of the most importance to place the vision of suitable economic based on bio-resources. In general, the bio-refinery or green biotechnology was defined as "The complex (to fully integrated) systems of sustainable, environmentally and resource- friendly technologies for the comprehensive (holistic) material and energetic utilization as well as exploitation of biological raw materials in the form of green and residue biomass from a targeted sustainable regional land utilization" (Kamm et al., 1997). More detail, bio-refinery concept presents the utilisation of lignocellulose biomass to produce biofuels, cellulose, hemicellulose, lignin and by-products. The important role of green biotechnology is to replace the petro-derived chemicals by those from biomass in which determine the suitability of chemical industry. The main biomass resources include short rotation forestry (willow, poplar, *eucalyptus*), wood wastes (forest residues, sawmill and construction/industrial residues, etc.), sugar crops (sugar beet, sweet sorghum, jerusalem artichoke), starch crops (maize, wheat), herbaceous lignocellulosic crops (*miscanthus*), oil crops (rapeseed, sunflower), agricultural wastes (straw, slurry), municipal solid waste and refuse, and industrial wastes (residues from the food industry). These fractions can be used directly as desired biochemical or can be converted by chemical, enzymatic, and/or microbial approaches. Conversion of these by-products to high-value co-products will offset the cost of biofuel, improve the economy of lignocellulose biorefinery, minimize the waste discharge, and reduce the dependence of petroleum-based products. The bio refinery will offer new economic opportunities for agriculture and chemical industries by the production of a tremendous variety of chemicals, transportation fuels, and energy (FitzPatrick et al., 2010).
In Europe, there are about 34 bio-refineries (in service and planned) and they could be classified into four groups: (i) the “Green Bio-refineries” using “nature-wet” biomasses such as green grass, alfalfa, clover, or immature cereal; (ii) the “Lignocellulosic Feedstock Bio-

refinery" using "nature-dry" raw material such as cellulose-containing biomass and wastes; (iii) the "Whole Crop Bio-refinery" uses raw material such as cereals or maize; (iv) the "Bio-refinery Two Platforms Concept" includes the sugar platform and the syngas platform (Kamm et al., 2006).

It has a numerous bio-refineries which convert biomass into mainly traditional products like starch, sugar, oleochemicals…In the other hand, it evokes really a challenge for the application of innovative bio-refinery concepts (in the mean of conversion from biomass feedstocks into production of various products liked to fuels, power, heat, chemicals and materials). The instability of raw material supplies (agriculture and forestry-based product), the importance of capital investigations, and the low demand of these bio-products are the main barriers to slow down the bio-refinery progress.

Nevertheless, face with the exhaustion of fossil resources, bio-refinery gives us an important solution in using the renewable materials to convert into interest products. The problem is only that these products came from bio-refinery process can compete economically and qualitatively with the conventional products. However, it can be concluded that there exist additional opportunities to adopt bio-refinery concepts economically successful in Europe in the four analysed industry branches in the medium to long-term.

Table 1-4: Hydrolysis yield reported in literature.

Substrate	Pre-treatment	Enzymes	Hydrolysis conditions	Yield (sugar based)	References
Woody biomass					
Hardwood chips 20%	Green liquor	20FPU/g + β-glucosidase + xylanase	48h at 50°C	63% (total sugar)	(Xue et al., 2012)
Hardwood pulp 20%	-	20FPU/g + 80CBU/g	96h at 50°C	80% (glucose)	(Zhang et al., 2009)
Softwood 10%	Diluted acid	20FPU/g + β-glucosidase	24h at 40°C	40% (glucose)	(Wiman et al., 2010)
Softwood 1%	Ethanol	10FPU/g	24h at 50°C	95% (glucose)	(Tu et al., 2009)
Softwood chips 1%	Organosolv	45FPU/g + 30CBU/g	72h at 50°C	80% (glucose+xylose)	(Koo et al., 2011)
Poplar 20%	Steam explosion	Not reported	48h at 50°C	44% (glucose)	(Di Risio et al., 2011)
Agricultural residues					
Barley straw 5%	Steam explosion	15FPU/g + 15IU/g	168h at 50°C	80% (total sugar)	(García-Aparicio et al., 2006)
Barley straw 10%	Steam explosion	7.5FPU/g + 15CBU/g	72h at 50°C	73% (total sugar)	(Rosgaard et al., 2007)
Sugarcane bagasse 10%	Steam explosion	10FPU/g	36h at 50°C	48% (glucose)	(Pereira et al., 2011)
Corn stover 2%	Liquid hot water	15FPU/g + 65IU/g	168h at 50°C	60% (glucose)	(Zeng et al., 2007)
Corn stover 10%	Ethanol	5FPU/g + 5CBU/g	72h at 50°C	51% (total sugar)	(Chandra et al., 2011)
Corn stover 15%	Steam explosion	20FPU/g	96h at 50°C	75% (glucose + cellobiose)	(Lu et al., 2010)
Rice straw 17%	Liquid hot water	13FPU/g + 35CBU/g	48h at 45°C	65% (glucose)	(Ingram et al., 2011)
Wheat straw 20%	Steam explosion	7FPU/g + β-glucosidase	96h at 50°C	60% (glucose)	(Jorgensen et al., 2007)
Other biomass					
Recycled paper 7.5%	Milling	45FPU/g	72h at 50°C	48% (glucose)	(Ballesteros et al., 2002)
Paper sludge 5%	-	30FPU/g	72h at 50°C	80% (reducing sugars)	(Peng & Chen, 2011)
Filter paper 15%	-	10FPU/g + β-glucosidase	96h at 50°C	48% (total sugar)	(Kristensen et al., 2009)

1.1.8 Conclusion

The second bioethanol give us an interesting opportunity to minimise the greenhouse gas effect and energy and petroleum crisis. To convert lignocellulose biomass into ethanol, the key steps focus in pre-treatment technique and in conversion into fermentable sugars. The major challenges in cellulosic ethanol are linked to reducing the costs associated with production, harvest, transportation, and up-front processing in order to make cellulosic ethanol competitive with grain-based fuel ethanol (Eggeman and Elander, 2005). Therefore, the better scientific understanding and ultimately the technical mastering of these critical bio-catalytic reactions, which involve complex matrices at high solids content, is currently a major challenge that must be met in order to facilitate the intensification of bio-refining operations. Amongst the main parameters to be studied, the rheological behaviour of the hydrolysis suspension and the fibre particle size of, stand out as a major determinants of process efficiency and determine equipment to be used and the strategies applied (Wiman et al., 2010). The choice of agitation system, fundamental to heat and/or mass transfer, and to disruption of agglomerated particles, influences the bioconversion of cellulose into simple sugar (Um, 2007). It requires detailed knowledge of the rheological behaviour of the substrate suspensions.

The second part of this chapter will focus on rheological characterisation of lignocellulose suspensions and impact of hydrolysis on these parameters.

1.2 Rheology of lignocellulose suspensions and impact of hydrolysis

Synthetizing the reported results in literature, this chapter will be structured into three parts which present (i) Classical rheological models for non-Newtonian fluids; (ii) Rheometry device and set-up for rheological characterisation of lignocellulose suspensions; (iii) Rheological behaviour analysis.

1.2.1 Rheological behaviour: overview of classical models

Lignocellulose suspensions are complex medium with tri-phases properties (solid-liquid-gas) where gas issued from the agitation. These suspensions exhibit various rheological behaviours which could be modelled by different models.

1.2.1.1 Rheological characterisation and classical rheological models

The two main parameters used in rheology are the shear rate $\dot{\gamma}$ (s^{-1}) which characterises the kinematics, and the shear stress, τ (Pa or $N.m^{-2}$) which characterises the forces. The shear stress is defined as a tangential force per unit area and the shear rate as the velocity gradient.

$$\tau_{xy} = \frac{F_{xy}}{S} \text{ and } \dot{\gamma} = \frac{d\upsilon_x}{dy} \quad \textit{(Eq. 1-13)}$$

The main rheological characteristic is the viscosity or dynamic viscosity μ, which is the ratio of shear stress τ_{xy} to shear rate $\dot{\gamma}$ in a permanent pure shear flow:

$$\mu = \frac{\tau_{xy}}{\dot{\gamma}} \quad \textit{(Eq. 1-14)}$$

The kinetic viscosity ν is defined as the ratio of dynamic viscosity to density, ρ:

$$\nu = \frac{\mu}{\rho} \quad \textit{(Eq. 1-15)}$$

The dynamic viscosity could vary with shear rate: the fluid is then called a non-Newtonian fluid.

The flow curve $\tau_p = f(\dot{\gamma})$, or equivalently the rheogram $\mu = f(\dot{\gamma})$, is a complete characterisation of the rheological behaviour if the fluid is not elastic or thixotropic (time-dependent viscosity). **Table 1-5** shows the main rheological behaviour and modelling.

Table 1-5: Fluid classification and usual models for rheological behaviour.

Fluids		Behaviour laws
Perfect fluid (or Pascal's fluid)		$\mu = 0$
Newtonian fluids		$\tau_p = \mu \cdot \dot{\gamma}$ *with* $\mu = Cte$
Non-Newtonian time-independent viscous fluids	Shear-thinning : $\mu(\dot{\gamma}) \downarrow$ $(0 < n < 1)$ Shear-thickening : $\mu(\dot{\gamma}) \uparrow$ $(n > 1)$	Ostwald-de Waele's model: $\tau = k \cdot \dot{\gamma}^n$
	Viscoplastic (Yield stress fluid, no flow if $\tau < \tau_S$)	Bingham : $\tau = \tau_S + \mu \cdot \dot{\gamma}$ Herschel-Bulkley : $\tau = \tau_s + k\dot{\gamma}^n$ Casson : $\tau^{1/2} = \tau_s^{1/2} + k_C \cdot \dot{\gamma}^{1/2}$
Time-dependent non-Newtonian fluids.	Thixotropic	$For\ \dot{\gamma} = Cte \Rightarrow \mu(t) \downarrow$
	Anti-thixotropic	$For\ \dot{\gamma} = Cte \Rightarrow \mu(t) \uparrow$
Viscoelastic fluids		Complex rheological models For oscillatory shear flows: $\tau^* = G^* \cdot \dot{\gamma}^*$ $\tau = G'(\omega)\sin(\omega t) + G''(\omega)\cos(\omega t)$ $G^* = \frac{\tau_0}{\dot{\gamma}_0} \cdot (\cos(\delta) + i \cdot \sin(\delta)) = G' + i \cdot G''$

The shear-thinning fluids (also called pseudoplastic) generally have, for the low and high shear rates, a Newtonian plateau (μ_0 and μ_∞ resp.). This can be modelled by using three or four parameters models as listed in **Table 1-6**:

Table 1-6: Extended models from the power law model.

Sisko	$\mu = \mu_\infty + k\dot{\gamma}^{n-1}$
Cross	$\frac{\mu - \mu_\infty}{\mu_0 - \mu_\infty} = \frac{1}{1 + (\dot{\gamma} \cdot t)^m}$
Powell-Eyring	$\mu = \mu_\infty + (\mu_0 - \mu_\infty) \cdot \frac{Argsh(\beta \cdot \dot{\gamma})}{\beta \cdot \dot{\gamma}}$
Carreau	$\mu = \mu_\infty + (\mu_0 - \mu_\infty) \cdot (1 + \beta \cdot \dot{\gamma}^2)^{n-1/2}$
"Local" power-law	$\mu = k(\dot{\gamma}) \cdot \dot{\gamma}^{n(\dot{\gamma})-1}$

1.2.1.2 Suspension rheology modelling

The simplest method used to describe the suspension consists in modelling the behaviour of solid particles in a Newtonian medium. These viscosity models are expressed as a function of numerous parameters linked to the solid phase (particle size, shape, concentration, spatial orientation of the particles in the fluid, ...) but also as a function of parameters related to the suspending fluid (generally Newtonian fluid).

The most commonly used models describing the relationship between the suspension viscosity and substrate volume fraction can be written as follow (Quemada, 2006):

$$\frac{\mu}{\mu_S} = \left(1 - \frac{\phi}{\phi_m}\right)^{-q} \quad with \; -1 \geq q \geq -2 \quad \textit{(Eq. 1-16)}$$

with μ_s, suspending fluid viscosity; ϕ, substrate volume fraction; ϕ_m, maximum substrate volume fraction. We consider in general three concentration regimes: dilute, semi-dilute and concentrated. The first one corresponds to very small values of volume fractions, $\phi \to 0^+$: the average distance between particles is large compared to their radius. The particles can move freely through the suspension under the action of Brownian forces without perturbation induced by neighbouring particles. In semi-dilute suspensions the flow perturbations created by the presence of particles will influence the movement of close particles. Hydrodynamic interactions between particles become important. The last regime corresponds to concentrated suspensions with a lot of contacts between the particles. The viscosity of the suspension increases rapidly with volume fraction. When ϕ reaches a critical value ($\phi_G \approx 0.58$ for spherical monodisperse particle **Figure 1-5**), each particle is confined in a cage formed by its nearest neighbours. For volume fractions above this value, only a vibration of the particles inside the cage remains possible, and this possibility completely disappears when ϕ reaches the value of dense packing ($\phi_{RCP}=0.637$ for monodisperse spheres).

Table 1-7: Rheological models for solid-liquid suspensions (Quemada, 2006).

Suspension	Hard sphere	Soft sphere
Dilute to semi-dilute ($\boldsymbol{\phi \leq 0,01}$)	1-Einstein : $\mu_{rel} = \frac{\mu}{\mu_S} = (1 + [\mu] \cdot \phi)$ $[\mu]$ Intrinsic viscosity ($L.g^{-1}$) 2- Batchelor : $\mu_{rel} = \frac{\mu}{\mu_S} = \left(1 + 2.5 \cdot \phi + K_H \cdot 2.5^2 \cdot \phi^2\right)$ with k_H, Hyggins's coeffient (thermodynamic interactions particle-particle) and $\phi = \frac{c \cdot [\eta]}{2.5}$. C : mass concentration. 3-Krieger-Dougherty : $\mu_{rel} = \frac{\mu}{\mu_S} = \left(1 - \frac{\phi}{\phi_m}\right)^{-[\mu]\phi_m}$ with ϕ_m, the maximum solid volume fraction and $0.2<\phi<0.6$.	Introduction of ϕ_{eff}, effective volume fraction. 5- Batchelor adapted $\mu_{rel} = \frac{\mu}{\mu_S} = \left(1 + 2.5 \cdot \phi_{eff} + 5.9 \cdot \phi_{eff}^2\right)$ $with \; \phi_{eff} = k \cdot c$ C : mass concentration ($g.ml^{-1}$) k : specific volume ($mL.g^{-1}$) for $\phi_{eff} < 0.1$ 3-Krieger-Dougherty adapted : $\mu_{rel} = \frac{\mu}{\mu_S} = \left(1 - \frac{\phi_{eff}}{\phi_m}\right)^{-[\mu]\phi_m}$ $with \; \phi_{eff} = k \cdot c$
Concentrated	4- Douglas-Garboczy : $\mu_{rel} = \frac{\mu}{\mu_S} = K \cdot \left(1 - \frac{\phi}{\phi^*}\right)$ with ϕ^* critical volume fraction (percolation threshold) and K, proportionality constant ($\to 1$)	

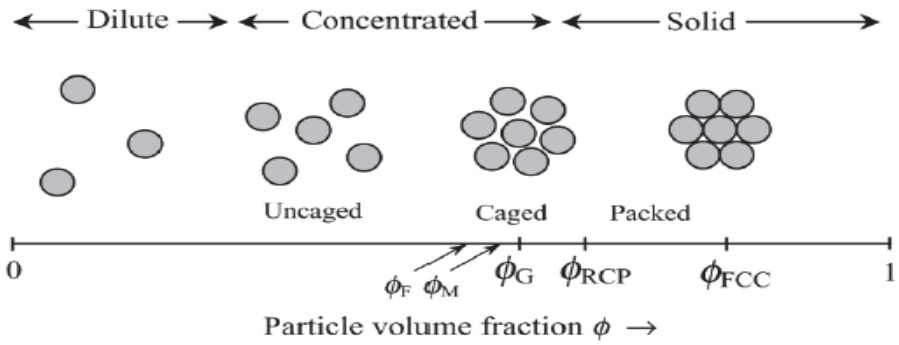

Figure 1-5: Schematic representation of the concentration-structure in a dispersion of hard spheres (freezing, ϕ_F =0.494; melting, ϕ_M=0.545 et glassy, ϕ_G =0.58).

The frontier between the different concentration domains strongly depends on the nature and on the intensity of interaction between the particles. As an example: a 5%vol suspension of neutral monodisperse spheres behaves as a dilute and Newtonian suspension while a 1% vol or less clay suspension are viscoplastic with a very high yield stress together and a thixotropic behaviour.

Figure 1-6 illustrates not only the dependence of viscosity on concentration but also on the particle shape. An increase of aspect ratio implicates a magnification of suspension viscosity (Marti et al., 2005; Santamaria-Holek & Mendoza, 2010). Particles with the more complex shape show the larger viscosity dependence with concentration. For example, at the same concentration 20%v/v, the viscosity of spherical particle suspension is about 7 times less than those of rods particle suspension. So it requires detailed knowledge of this effect and if possible, proposes a critical diameter of particle to characterise this relationship.

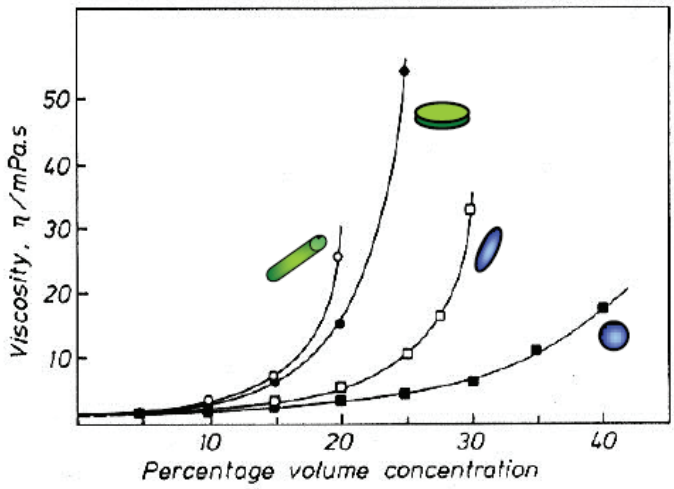

Figure 1-6: Shape dependence of the viscosity of aqueous suspensions for a shear rate equal to 300s^{-1} (Barnes et al., 1989).

1.2.2 Lignocellulose: nature and characterisation

To investigate the current state of scientific research in this domain and its development since 40 years, we realised automatic search on four profiles:

- Profile 1: (Rheo* OR visco* OR newt*) AND (suspension* OR dissolution*) AND cellulose*;
- Profile 2: (Rheol* OR visco*) AND fiber* AND cellulose*;

- Profile 3: (Rheol* OR visco*) AND (paper pulp* OR pulp suspension*);
- Profile 4: Bioproce*

to obtain the publication number for the last 35 years. The results are presented in **Figure 1-7**. Profile 1 and 2 focus on rheological aspects of cellulose suspensions, with a special focus on the fibre influence for profile 2. Profile 3 checks for rheology concerning paper pulp while profile 4 describes the general evolution in biotechnology process. We observed a regular and remarkable increase since 1990 – the petroleum crisis- for all profiles. This evolution translates the same tendency of rheology researches with the interest general of biotechnology domain.

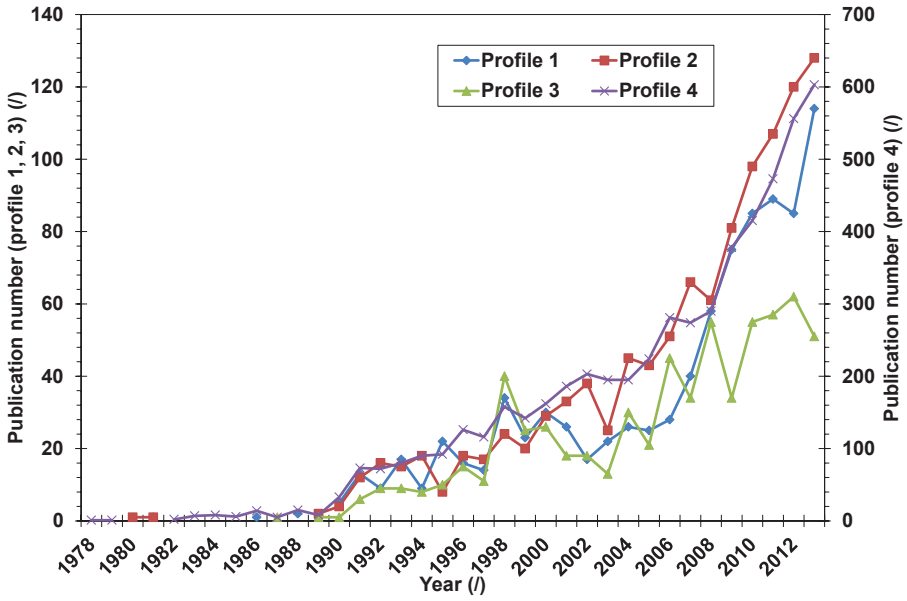

Figure 1-7: Publications per year since 1978 (Profil 1 : (Rheo* OR visco* OR newt*) AND (suspension* OR dissolution*) AND cellulose*; Profil 2 : (Rheol* OR visco*) AND fiber* AND cellulose*; Profil 3 : (Rheol* OR visco*) AND (paper pulp* OR pulp suspension*); Profil 4 : Bioproce*).

1.2.2.1 Physical characterisation of fibres

Table 1-8 presents the scientific publications linked to rheology, characterisation of lignocellulosic matrices and enzymatic hydrolysis. We can observe that there is not a great quantity of publications investigating all of the three domains above. The studied substrates are very different between these studies. They could be classified into two groups: cellulose (simple matrices) and lignocellulose (complex matrices). The cellulose matrices mainly include micro and nano crystalline cellulose, whereas we can find a numerous of lignocellulose substrates: woody materials, by-products of agriculture…

For the characterisation of substrates, we focussed on physical and biochemical properties such as: particle diameter, aspect ratio, density, crystallinity, biochemical compositions. Surprisingly, there is no publication presenting all of these properties. In other words it is missing a global view of raw material characteristics. Predominately, the physical properties were reported not equally with their important influences on rheological behaviour. Biochemical characterisations (content of cellulose, hemicellulose, lignin…) were presented only in the publications in which studied the enzymatic hydrolysis.

Table 1-8: Scientific publications linked to rheology, physico-chemical characterisations of lignocellulosic materials and enzymatic hydrolysis (NCC, nano-crystalline cellulose; MCC, micro-crystalline cellulose; MFC, micro-fibril cellulose; PP, paper-pulp; BAG, sugarcane bagasse; CoSt, corn stover; WhSt, wheat stover).

	Matrices	Publication	Study operations		Physical properties					Biochemical compositions				
			Suspension	Hydrolysis	$d_{m\ (\mu m)}$	A. ratio	ρ (kg/m3)	ζ (mV)	CrI	% DM	Cellu.	Hemi.	Lig.	Ash
Cellulose	NCC	(Araki et al., 1998)	x	-	0.18±0.075	51±21	-	-	-	-	-	-	-	-
	NCC	(Boluk et al., 2011)	x	-	0.18±0.06	30±14	-	-62.8	-	-	-	-	-	-
	NCC	(Gonzalez-Labrada & Gray, 2012)	x	-	0.117	29	-	-47	-	-	-	-	-	-
	NCC	(Lu et al., 2014)	x	-	0.87	5.4	1560	-58	-	-	-	-	-	-
	MCC	(Luukkonen et al., 2001)	x	-	60	-	-	-	-	-	98	0	0	2
	MCC	(Tatsumi et al., 2001)	x	-	0.72-350	21-450	-	-	-	-	-	-	-	-
	MCC	(Bayod et al., 2005)	x	-	30-35	1.5-7	-	-	-	-	-	-	-	-
	MCC	(Horvath & Lindstrom, 2007)	x	-	20-30	-	-	-	-	-	-	-	-	-
	MCC	(Um & Hanley, 2008)	x	x	91	-	-	-	-	-	88	-	-	-
	MCC	(Tatsumi et al., 2008)	x	-	1.7	22	-	-	-	-	-	-	-	-
	MCC	(Tozzi et al., 2014)	x	-	24-27	-	-	-	-	90-92	68-72	7-7.8	4-5	0.15
	MFC	(Lowys et al., 2000)	x	-	-	-	-	-20	-	-	85	11	0	4
	MFC	(Agoda-Tandjawa et al., 2010)	x	-	10	80-500	-	-	11-13	-	93	-	-	3.6
	MFC	(Saarikoski et al., 2012)	x	-	-	-	-	-	-	-	-	-	-	-
Lignocellulose materials	BAG	(Geddes et al., 2010)	x	x	$(25\text{-}50).10^3$	-	-	-	-	-	38	28	-	-
	BAG	(Pereira et al., 2011)	-	x	<2000	-	1420	-	-	-	43.6	8.75	33.75	-
	CoSt	(Pimenova & Hanley, 2004)	x	-	120	-	-	-	-	-	-	-	-	-
	CoSt	(Stickel et al., 2009)	x	-	100	1-20	-	-	-	-	-	-	-	-
	CoSt	(Viamajala et al., 2009)	x	-	-	-	-	-	-	93.5	33.2	21.6	-	-
	CoSt	(Dunaway et al., 2010)	x	x	-	-	-	-	-	-	60	5	32	3
	CoSt	(Dibble et al., 2011)	x	x	80-680	-	-	-	-	-	42-60	4.0-24	18-26	-
	WP	(Samaniuk et al., 2011)	x	x	600	-	-	-	-	100	99	-	-	-
	CoSt		x	x	3000	-	-	-	-	100	50	-	-	-
	PP	(Damani et al., 1993)	x	-	1180/1290	-	356/538	-	-	-	-	-	-	-
	PP	(Chen et al., 2003)	x	-	30/15	107/73	-	-	-	-	-	-	-	-
	PP	(Blanco et al., 2006)	x	-	1000	-	-	-	-	-	-	-	-	-
	PP	(Derakhshandeh et al., 2010)	x	-	670-2960	-	-	-	-	-	-	-	-	-
	PP	(Le Moigne et al., 2010)	-	x	-	-	-	-	46-49	-	90-94.7	2-3.5	1.1-1.8	-
	PP	(Chaussy et al., 2011)	x	-	1280	-	-	-	-	-	-	-	-	-
	PP	(Wiman et al., 2010)	x	x	188	-	-	-	-	13	48	3.2	45	-
	WhSt	(Szijarto et al., 2011)	-	x	-	-	-	-	-	34	58.9	-	-	-
	Wood	(Dasari & Berson, 2007)	x	x	33-850	-	-	-	-	-	39.7	19.8	-	-
	Wood	(Palmqvist & Liden, 2012)	-	x	<10000	-	-	-	-	36.5/12.7	50.2/42.9	-	36.8/46	-

1.2.2.2 Rheometric device and set-up

Suspensions exhibit a very wide range of rheological behaviour and numerous examples can be found to illustrate shear-thinning/shear-thickening behaviour, viscoplasticity with observation of a yield stress, elasticity, or thixotropy. Many parameters influence the nature and the intensity of these non-Newtonian characters: the concentration, the granulometry and the morphology of the objects, the nature and the magnitude of the particle interactions …etc. Many industries, and especially when bioprocesses are involved, are confronted with these behaviours which can affect, sometimes in a drastic way, hydrodynamics and transfer efficiency (mass or/and heat). It is then of crucial interest to explore the rheology of the suspension to ensure the better implementation of a process and the right choice of equipment. The cheapest and easy-to-use viscometers that are the capillary viscometer and the falling (or rolling) ball viscometer are well-adapted for Newtonian fluids but are somewhat difficult to use with unknown non-Newtonian fluids. Their use is much reduced in the domain studied here. The works of Luukkonen et al. (2001) (Luukkonen et al., 2001) and of Gonzalez-Labrada and Gray (2012) on nano- and microcrystalline cellulose can be quoted. A sharp rheometry analysis was made by Tozzi et al (2014) by using MRI (Magnetic Resonance Imaging) to determine the velocity field in a portion of a cylindrical duct. Completed by the measure of the pressure drop, the velocity profile brings information on the nature and the characteristics of the fluid. However this technique is still rare.

The very classical and better way to obtain a rheological characterization (mostly viscosity, but not only) is the use of rheometers or viscometers equipped with cone and plate (CoPl), narrow-gap coaxial cylinders (CoCy) or parallel plates (PaPl). The generated flow is then a simple shearing flow with, except for the parallel plates, a constant shear rate all over the fluid. The large-gap coaxial cylinders, which are frequently used in industry, can be considered separately among viscometers as, in this case of large gap, no assumption on the velocity profile can be done (the knowledge of the fluids rheological characteristics are necessary for that). The raw data cannot then be exploited as simply as in the Newtonian case (Swerin, 1998). Coming back to the usual geometries for rheometers and viscometers, they usually require a small volume of fluid but this advantage turns into a drawback when the size of the objects in suspension are not negligible when compared to a characteristic dimension of the geometry (for instance a usual gap for parallel plates or concentric cylinders is around 1mm, and is lower for cone and plate geometries). To extract viscosity from the global measurements realized on a rheometer (torque and angular velocity), it is indeed necessary to consider the fluid as a homogeneous media. This assumption can become hazardous when suspensions are studied and this has to be kept in mind.

To overcome this difficulty, a current way is to use the mixing system (MixS) of a process, when it exists, as a rheometer. As for this last one, the measurements are the torque and the rotation rate (or equivalently the power consumption and the rotation rate), but the difficulty here lies in the complex flow field generated. Determination of viscosity then relies on a previous determination of the power number-Reynolds number characteristic curve of the MixS, where the power number Np is a dimensionless number linked to the power consumption. The knowledge of Np gives a value of the Reynolds number and then estimation of the viscosity if the fluid is a Newtonian one, and of an equivalent viscosity if the fluid is non-Newtonian. In this last case, interpretation of the frequency rotation, power consumption measurements requires an additional hypothesis that was first proposed by Metzner and Otto (1957). These authors showed that, for a large range of shear-thinning fluids represented by a power-law model ($\tau = k \cdot \dot{\gamma}^n$), the equivalent shear rate corresponding to the equivalent viscosity is proportional to the frequency rotation via a Ks coefficient (known as Metzner-Otto coefficient). In addition Ks depends only on the mixing system

characteristics. It is thus enough to determine it in a preliminary stage. This on-line viscosimetry method was largely used (Rao, 1975; Samaniuk et al., 2011). Note that such a device gives access only to viscosity that is to say to shear-thinning/shear-thickening character of the fluid.

One can also point out that geometries such as anchor or helical ribbon are proposed for rheometers which are then used as well-characterized mixing systems and have to be used with the same precautions as for mixing systems. More simply, but also less rich in information, such geometries can also be used in a relative way to follow the time evolution of some global viscosity in a process (Geddes et al., 2010). A special geometry proposed for rheometers is the four-bladed vane (or six-bladed). Never used as a mixing system, its use on rheometers is especially interesting for yield stress fluids to avoid wall slip effects which are currently observed for suspensions (formation of a depletion layer caused by migration of fibres away from the wall). This geometry allows a precise determination of the fluid behaviour for small shear rate and is then of a special interest for determination of the yield stress. Its use for intermediate and high shear rates requires a careful analysis as; in that case, it is assimilated to large-gap coaxial cylinders geometry. Such geometry was used by Knutsen et al. (2010) for fibrillated cellulose suspensions and by Derakhshandeh et al. (2010). These last authors examined in more detail the validity of such a geometry for fibre suspension by analysing the velocity profile determined by ultrasonic Doppler velocimetry.

Focusing now on the data extracted from these measurements, the main and most known characteristic is the viscosity. Suspensions are generally shear-thinning and this behaviour is quantified by the power-law index n and the consistency k (fit of a power-law on the concerned region of the rheogram). This is, in practice, the only characteristic that can be obtained using a viscometer or a mixing system, together with the yield stress. This last one is evaluated from the low shear rate region of the rheogram and several methods are used: shear stress limit when the shear rate tends to zero, adjustment of a Herschel-Bulkley type model ($\tau = \tau_0 + k \cdot \dot{\gamma}^n$) (Lowys et al., 2000; Um & Hanley, 2008), peak torque (or shear stress) during a transient flow experiments at a slow, steady rate (Knutsen & Liberatore, 2010a), stress ramp analysed in terms of deformation vs shear stress curve.

With rheometers, additional rheological characterizations can be obtained and oscillatory stress sweeps and oscillatory frequency sweeps are the most largely used. Sinusoidal shear stress (or strain) give information on elasticity (part of the strain which is phased with the shear stress) and viscosity (part of the shear rate which is phased with the shear stress). The complex modulus G* that is defined as the ratio of shear stress to strain has a real part G' (the storage modulus) and an imaginary out-phase component G'' (the loss modulus). It is used to characterize viscoelasticity of materials as well as viscoplasticity.

The choice of rheometer type depends on nature of the fluid measured. Irregular geometries are commonly used to study fluids displaying complex characteristics including large particles, settling problems, slip and time dependency. Geometries which facilitate mixing, such as helical ribbons, anchors and paddles, can overcome settling out problems and errors due to slip. The vane geometry has proven popular for yield stress determination and slip analysis (Cullen et al., 2003). For lignocellulose suspension, the common problems in measurement are heterogeneous suspension, floc forming and particle decantation (Barnes, 1997; Nguyen & Boger, 1992).

Two modes of viscosity measurement were found: ex and in-situ. Ex-situ measurement was presented like the most usually method. This approach is limited by the number of samples and affected by the substrate properties, predominately decantation and flocculation of material. To solve these problems, a method allowing the suspension viscosity to be followed in-situ was proposed: with RVA rheometer (Szijarto et al., 2011), with a four pitched-blade

turbine connected with a torquemeter, with disk refiner as a rotational rheometer (Chaussy et al., 2011).

Table 1-9: Synthesys of measured systems and quantities.

Author	Measured system	Measured quantities
(Bennington et al., 1990)	Concentric cylinder rheometer	G', G"
(Damani et al., 1993)	Weissenberg Rheometer – parallel plate	G', G"
(Araki et al., 1998)	Double cylinder – Brookfield	μ
(Tatsumi et al., 1999)	Weissenberg Rheometer – cone plate	τ and G', G"
(Lowys et al., 2000)	AR1000, TA Inst. Cone plate and parallel plate	τ and G', G"
(Luukkonen et al., 2001)	Capillary rheometer	τ
(Pimenova & Hanley, 2004)	Double helical ribbon-Brookfield	μ and G', G"
(Bayod et al., 2005)	Concentric cylinder rheometer	μ
(Dasari & Berson, 2007)	Physica MCR 300-six-bladed vane	μ
(Stickel et al., 2009)	Parallel plate-Bohlin	μ and G', G"
(Agoda-Tandjawa et al., 2010)	Controlled strain rheometer-parallel plate	μ and G', G"
(Derakhshandeh et al., 2010)	Couette rheometer: four-blade vane	τ
(Chaussy et al., 2011)	Disk refiner as a rotational rheometer	μ
(Samaniuk et al., 2011)	Magnetoelastic sleeve torque transducer	Torque
(Szijarto et al., 2011)	RVA-rotational viscometer	μ
(Gonzalez-Labrada & Gray, 2012)	Rolling ball viscometer	μ
(Saarikoski et al., 2012)	Concentric cylinder rheometer	G', G"
(Tozzi et al., 2014)	Magnetic resonance based rheometer	μ

1.2.2.3 Experimental conditions

The lignocellulose suspensions were processed in various ranges of mass concentrations (**Figure 1-8**) varying between 0.1 and 1000gdm/L and for a large range of characteristic dimension (from 0.1μm up to few millimetres). However, the great part of studies focuses on low and medium concentration (1-200 gdm/L). Common temperature used was between 20 and 30°C. The pH keeps the natural pH of suspensions (around 7) excluding few of articles which investigated the effect of pH to the rheological behaviour (Agoda-Tandjawa et al., 2010; Derakhshandeh et al., 2010) (pH varies from 4 to 10).

Articles scrutinising hydrolysis mechanism were mainly realised between 40-55°C for temperature, 4.8-5.0 for pH, 10-200gdm/L for substrate concentration and 0.25-50 FPU/g cellulose for cellulase activity. The main goals for these studies were exploration of (i) hydrolysis enzymatic kinetics and (ii) rheological behaviour (Dasari & Berson, 2007; Dibble et al., 2011; Dunaway et al., 2010; Geddes et al., 2010; Le Moigne et al., 2010; Palmqvist & Liden, 2012; Pereira et al., 2011; Samaniuk et al., 2011; Szijarto et al., 2011; Um & Hanley, 2008; Wiman et al., 2010); (i) and (ii) and (iii) particle size evolution (Dibble et al., 2011; Wiman et al., 2010). The articles investigating flow properties of suspension together with hydrolysis kinetics represent 50% of total articles. This point reveals the interest for application concerning the lignocellulose matrices valorisation by enzymatic method especially from 2010. However, simultaneous study of particle size and rheological behaviour during hydrolysis presents a minor part. This approach could be developed to better understand the relationship between two quantities.

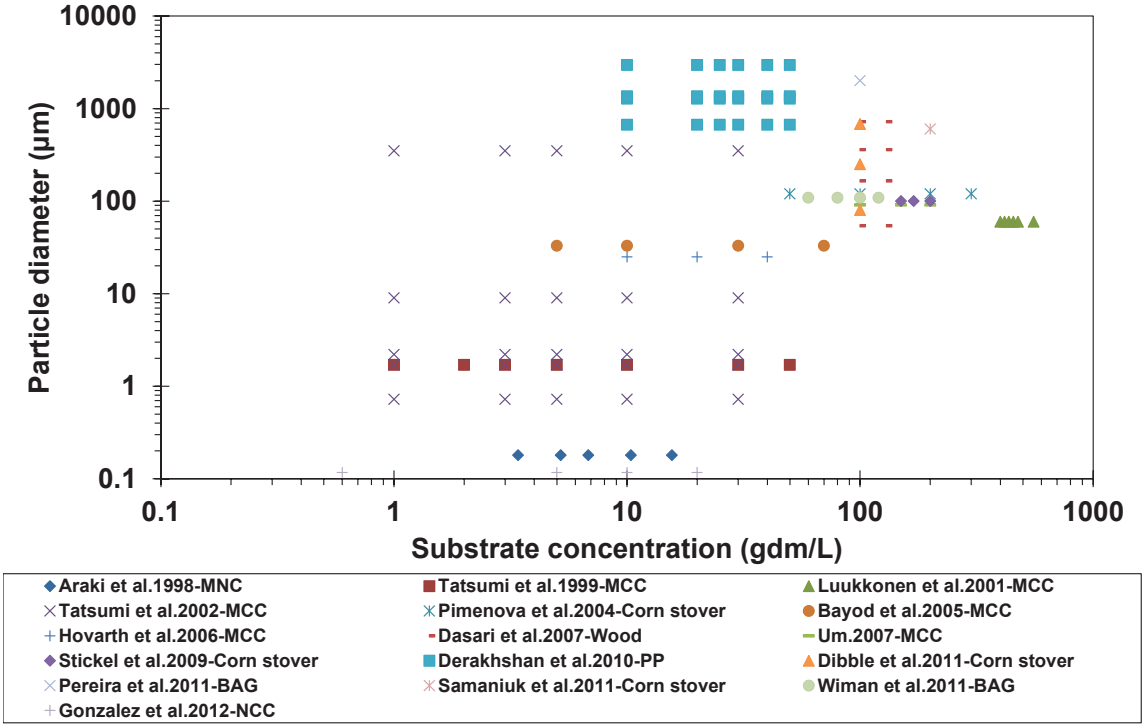

Figure 1-8: Publication synthesys: particle diameters versus substrate concentrations studied (MNC, micro-fibril cellulose; MCC, micro-crystalline cellulose; NCC, nano-crystalline cellulose; BAG, sugarcane bagasse; PP, paper-pulp).

1.2.3 Rheological behaviour of lignocellulose suspension

The different physical properties described above make the rheology of lignocellulose suspensions complex. Various approaches for the characterization of rheological behaviour were proposed. The first one is the determination of the flow curve $\tau = f(\dot{\gamma})$ which gives the viscosity of the suspension. Secondly, the rheological properties of a suspension can be completed by the yield stress or by viscous and elastic modulus determined in a dynamic mode. All these rheological characteritics are function of physical parameters such as volume fraction, mass concentration, aspect ratio…

One critical physical parameter for lignocellulose materials is the large aspect ratio. This induces significant contacts among particles (fibres) at all concentrations and this has a strong effect on suspension rheology. An increase of aspect ratio implicates a magnification of suspension viscosity (Marti et al., 2005; Santamaria-Holek & Mendoza, 2010). Not only has the aspect ratio influenced on the viscosity, but also an impact of the particle shape was found (Clacke et al., 1967 cited by Barnes et al., 1989; Santamaria-Holek & Mendoza, 2010).

1.2.3.1 Observed rheological behaviour

A Newtonian behaviour was found for substrate concentration less than 0.1% which then corresponds to a dilute regime. A critical concentration (C=0.1%) was confirmed for both NCC (Boluk et al., 2011) and MCC (Tatsumi et al., 2001; Tatsumi et al., 1999). Wu et al. 2014 demonstrated a little bit superior value (C=0.4%) for NCC. No substrate critical concentration was presented or proposed for complex matrices. This point could be explained by the study in very low concentration which is not interesting in condition of lignocellulose valorisation.

For substrate concentration larger than 0.1%, all studies demonstrated non-Newtonian behaviour of shear-thinning or pseudoplastic type (**Figure 1-9**). The suspension viscosity decreases with the increase of shear rate and this viscosity could be described by power law model with presence or not of a yield stress.

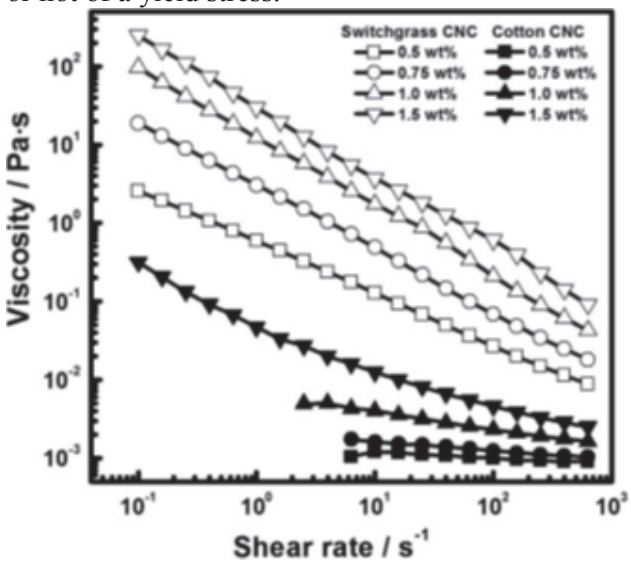

Figure 1-9: Apparent viscosity versus shear rate for swichgrass NCC (open symbol) and cotton NCC suspensions (solid symbol) at same concentrations (Wu et al., 2014).

Table 1-10: Example of viscosity for corn stover suspensions.

Author	Substrate	Concentration	Shear rate (s^{-1})	Viscosity (Pa.s)
(Pimenova & Hanley, 2004)	CoSt	15%	10	15
(Stickel et al., 2009)	CoSt	15%	10	25
(Viamajala et al., 2009)	CoSt	15%	10	20
(Dunaway et al., 2010)	CoSt	15%	10	10

Table 1-10 illustrates the viscosity of corn stover suspensions for a given concentration and a given shear rate. These results demonstrated the homogeneous value (in general) measured by different author and methods. This identical value magnitude could originate from the same substrate type, the same pre-treatment method (diluted-acid with H_2SO_4- standard protocol from NREL) and the same rang of particle diameter (100-120µm for volume mean diameter).

1.2.3.2 Structure and consistency index

As mentioned before, the suspensions are generally shear-thinning and viscosity is correctly represented by a power law model $\mu = k \cdot \dot{\gamma}^{n-1}$ with n: flow behaviour index or power law index and k: consistency index. **Figures 1-10** and **1-11** present on 3-D graphs the relationship between respectively the consistency index and the power law index and the particle diameter the concentration of the various substrates picked out in literature. Among all the cited publications, only 25% present these two indexes. This point evokes the difficulty for data treatment and general tendencies observation. Furthermore, there is no result presented for particle diameter less than 30µm or greater than 600µm, just one result for substrate concentration greater than 150gdm.L^{-1} (Pimenova & Hanley, 2004). Bayod et al. 2005 and Pimenova & Hanley, 2004, studied MCC and corn stover suspension respectively, report results that strongly differ from other authors. So these results are not presented in these two figures.

Concerning the consistency index **(Figure 1-10)**, it is always found to increase with the substrate concentration and/or the particle diameter. For example, with PP: k increased 6 folds (from 3.3 to 17.1 $Pa.s^n$) for concentration varying from 28 to 42gdm/L ; at the same concentration of 50gdm/L, k increased 2 folds (from 62 to 112 $Pa.s^n$) for particle mean diameter varying from 670 to 2960µm (Derakhshandeh et al., 2010). So the effects of concentration and particle size on consistency index are of the same magnitude. The relationship can be modelled by linear equation or quadratic model. This tendency is observed visually on graphic but also validated by (Bayod et al., 2005).
Concerning now the power law index **(Figure 1-11),** it decreases from 1 (Newtonian behaviour) to values as weak as 0.1 when the substrate concentrations increase. That strengthens the non-Newtonian behaviour occurrence. For example, with NCC: n decreases from 0.962 to 0.75 for concentration varying from 0.6 to 20gdm.L^{-1} (Gonzalez-Labrada & Gray, 2012); with corn stover n decreases from 0.91 to 0.5 for concentration varying from 50 to 300gdm.L^{-1}. For particle diameter less than 1000µm, when substrate concentration comes to 0, n comes to 1; the suspension behaves as water (Gonzalez-Labrada & Gray, 2012; Pimenova & Hanley, 2004; Um & Hanley, 2008). For particle diameter superior to 1000µm, there is no study on sufficiently low concentrations to observe a tendency for n when concentration comes to 0. This point could be explained by fibre shape and aspect ratio…For particle diameter superior to 1000µm and concentration superior to 10gdm.L^{-1}, the power law index comes to 0.2 whatever concentration and diameter (Derakhshandeh et al., 2010). This observation could be considered like one critical value of power law index or simply due to model choice (power law model or Herschel-Bulkley model) and adjustment zone.

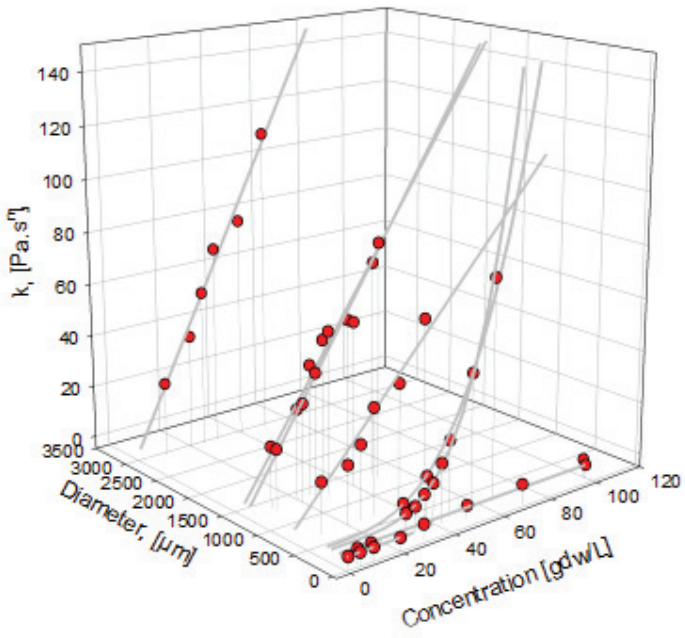

Figure 1-10: Evolution of consistency index as a function of particle diameter and concentration.

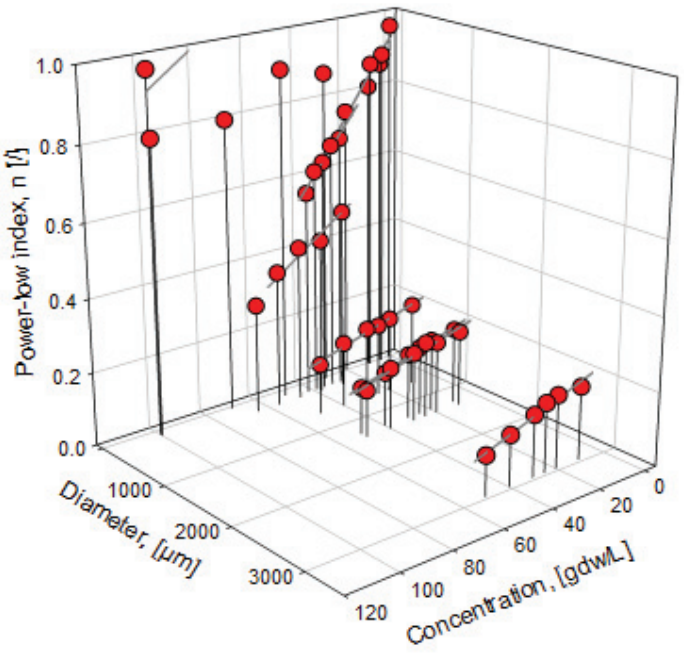

Figure 1-11: Evolution of power-low index as a function of particle diameter and concentration.

1.2.4 Physical properties of fibre and suspension during the enzymatic hydrolysis

Concerning the general evolution of viscosity: all studies conclude that the viscosity of suspension decrease during enzymatic hydrolysis. This reduction depends strongly on the nature of matrices, nature and activity of enzyme, concentration of substrates and experimental conditions such as temperature, rotation speed… During the hydrolysis, two phrases of viscosity could be observed. During a first stage, viscosity decreases rapidly andthen, reaches a steady value in a second phrse (i.e. **Figure 1-12).** Dasari et al. (2007) studied the hydrolysis of red-oak sawdust and demonstrated that viscosity decreased 10 times after 24h hydrolysis. For acid-pretreated sugarcane bagasse, viscosity was reduced by 77% to 95% after 6h (Geddes et al., 2010) and by 75 to 82% within 10h (Pereira et al., 2011). This decrease and the final plateau value depend on the enzyme loading (Geddes et al., 2010). For spruce pulp, initial and final viscosities (µinitial/µfinal) were 0.24/0.028, 0.4/0.058 and 0.84/0.087µm for concentrations of 10, 15 and 20% (w/w), respectively (Um, 2007). This decrease of viscosity is due to mainly (i) substrate solubilisation and (ii) particle size diameter reduction. However, there were not a lot of articles exploring the relationship between particle size and viscosity evolution. Some publications can be cited like (Um & Hanley, 2008; Wiman et al., 2010). Both of these authors concluded to a reduction around 2 folds of particle mean diameter for 24h or 48h hydrolysis.

In the goal of easier comparison of viscosity evolution during enzymatic hydrolysis, author proposes the use of a quantity $t(\mu/\mu_0=0.1)$ defined as the necessary time for 90% viscosity reduction. A summary of all past works at different experimental conditions is presented in **Figure 1-13**. Observing only one data series (one publication), the relationship between $t(\mu/\mu_0=0.1)$ and cellulase activity is clearly demonstrated: the more important the enzyme quantity is, the less the time $t(\mu/\mu_0=0.1)$ is. However, if we want to have a tendency for all of lignocellulose substrates in all of experimental conditions, we only obtain a large dispersion

of points. This illustrates lively the complexity of rheology study in hydrolysis condition which not only depends on enzymatic activity but also on substrate nature, substrate bio-chemical-physical properties and on experimental conditions.

Szijarto et al. 2011 explored hydrolysis experiments of hydrothermally pretreated wheat straw with purified enzymes from *Trichoderma reesei*. Results obtained at 15% (w/w) solids revealed that endo-glucanases are the key enzymes to rapidly reduce the viscosity of lignocellulose substrate. Cellobiohydrolases had only minor action and the xylanase has practically no effect on the viscosity.

Palmqvist & Liden, 2012 monitored the impeller torque (and hence power input) in a stirred tank reactor throughout high solid enzymatic hydrolysis (< 20% w/w) of steam-pre-treated *Arundo donax* and spruce. The decrease in torque during spruce hydrolysis was much slower than *Arundo donax* hydrolysis because of a higher amount of lignin compared to the arundo (46% and 37% respectively). The lignin structure is not broken down during the hydrolysis and might therefore contribute to maintain high viscosities of the spruce material.

For rheological behaviour: a typical pseudo-plastic behaviour was confirmed during hydrolysis (Dunaway et al., 2010; Pereira et al., 2011; Rosgaard et al., 2007). The consistency index decreased and the power-low index increased as hydrolysis proceeded (Dunaway et al., 2010; Rosgaard et al., 2007; Um & Hanley, 2008; Wiman et al., 2010). Rosgaard et al. 2007 studied the hydrolysis of steam-pre-treated barley straw and demonstrated that for 15% dry matter concentration, consistency index decreased from 16536 to 185 $Pa.s^n$ while the power law index increased from 0.07 to 0.47 for 6h and 72h hydrolysis respectively. Dunaway et al. 2010 surveyed the hydrolysis of pre-treated corn stover in range of concentration of 10-25%. They concluded that the consistency index, k, decreases rapidly with time, with the largest rate of decrease (around 10 times) occurring in the first 8 h.

One of the rheological parameters which was followed during enzymatic hydrolysis was the elasticity of the suspension through oscillations measurements. However, few articles were found (Fillaudeau et al., 2011; Wiman et al., 2010). Wiman et al. 2010 carried out a comprehensive rheological characterization of dilute acid pre-treated spruce during hydrolysis. Fillaudeau et al. 2011 explored the enzymatic liquefaction and saccharification of paper-pulp. Both authors confirmed that elastic modulus was always superior to viscous modulus in the initial step and during hydrolysis, confirming a viscoplastic behaviour. These two modules decreased as a function of hydrolysis time: around 100 times for 48h and 100h for spruce and paper pulp respectively. Wiman et al. 2010 demonstrated that the yield stress decreased dramatically with time and typically power law depends on substrate volume fraction.

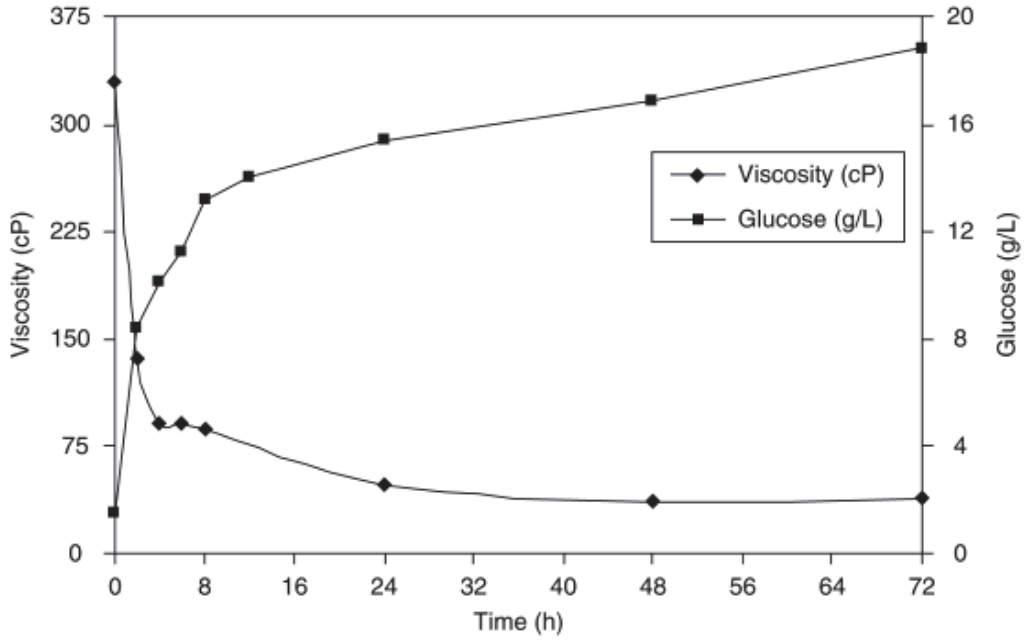

Figure 1-12: Evolution of suspension viscosity as a function of hydrolysis time –13%w/w red-oak sawdust suspension (Dasari & Berson, 2007).

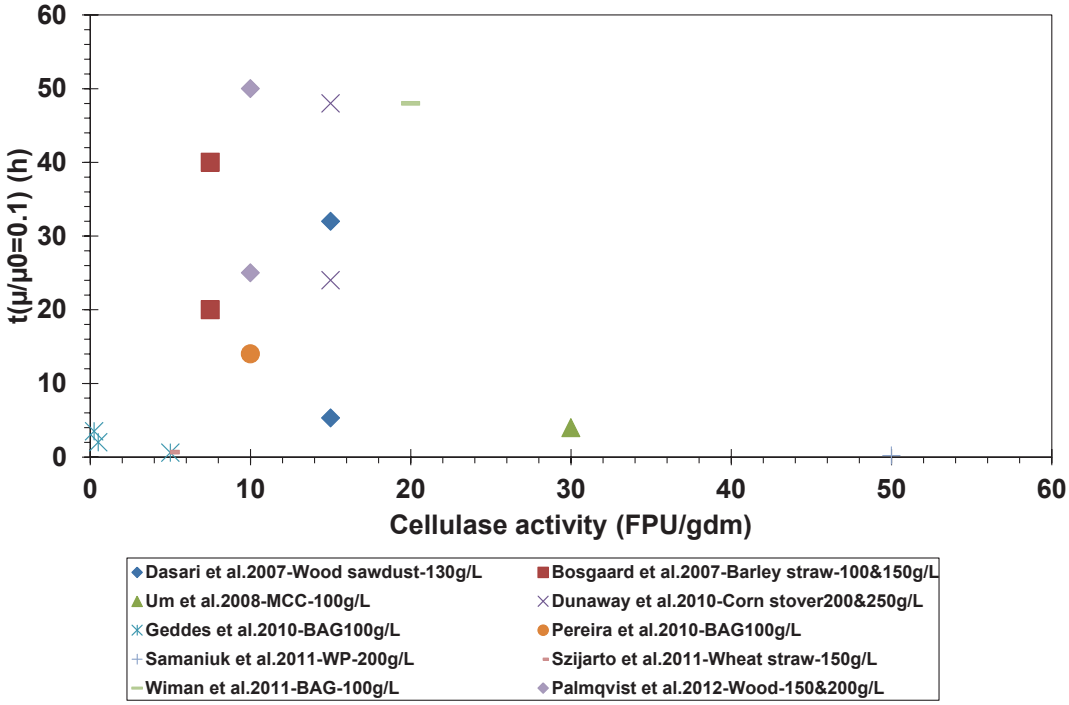

Figure 1-13: Synthesys of $t(\mu/\mu_0=0.1)$ as a function of cellulase activity per mass of cellulose.

1.3 Objective of study

In an effort to combat climate change, to aid energy independence, and to counteract diminishing supplies of fossil fuels, there has been a resurgence of research on renewable energy sources. The biochemical conversion of biomass to fuels presents as an interesting route. Cellulosic biomass provides a low cost and abundant resource that has the potential to support large-scale production of fuels and chemicals via biotechnological routes. This conversion has been studied since few decades and many parameters were explored. The treatment from lignocellulose biomass to fermentable sugars could be translated by a partly depolymerisation of fibre and solubilisation of solid fraction. The dynamic of these mechanisms, which are limited by coupled phenomena between flow, mass and heat transfers, need to be investigated in regards with diffusion (within solid and liquid phases), convection (mixing, homogeneity) and specific inhibitors (concentration gradient). The liquefaction mechanisms of complex cellulosic substrates require physical, chemical and biochemical characterisations with scientific and technical locks in relation with biochemical engineering. In addition, the implementation of concentrated suspensions is required to release a carbon substrate to a concentration compatible with industrial bioprocessing. The relationship between particle concentration and morphology with the rheological behaviour directly affects the kinetics of sugar release and process control. In these domains, analysing the results reported in literature, we can see:

- For rheometry: Conventional models clearly describe the rheological behaviour of a given suspension. However, the construction of rheological model based on physical properties of the substrat is complex. Beyond models taking into account the volume fraction, the variables such as particle dimensions are sometimes included, rarely the particle size or size distribution and morphology. The integration of population changes during hydrolysis in the model was not found for any publication.
- For morpho-granulometry: a limited quantity of publications reported the evolution of these parameters in bioprocess.

In this thesis study, our purpose was to investigate the destructuration of fibre during attack enzymatic under multi-scale approach using different techniques of analysis: macro-scale (rheometry); micro-scale (morpho-granulometry) and molecular scale (biochemistry). This tripod frame leads to analyse and to compare the in- and ex-situ methods (excluded biochemical analysis). Then phenomenological models could be established and discussed in light of theory before to embrace all results and to provide a full overview of mechanism.
Our aim will focus on “In-situ and ex-situ multi-scale physical metrology to understand the destructuration mechanism of lignocellulosic matrices and release kinetics of fermentable carbon substrates for industrial biotechnology”.

2 MATERIALS & METHODS

2.1 Experimental set-up

An experimental set-up was specifically developed, it consists of a bioreactor (double jacket tank) and a home-designed impeller system associated with several in-situ sensors (temperature, pH, RPM, torque, FBRM).

The bioreactor was a homemade glass tank (diameter: 130mm, Hmax: 244mm, V: 2.0L) with a water double-jacket for thermal regulation (**Annexe 2**). A specific agitator (**Annex 3**) includes a double impeller (TC1) to minimize the difficulty in substrate mixing and to ensure the suspension homogeneity. The first impeller consists of three inclined blades (diameter: 73.5mm, angle: 45°, h=38mm) located at 75mm height from the bottom to ensure mixing. The second is a close bottom mixer including 2 large blades (diameter: 120mm, h=22mm) to avoid substrate decantation. The impeller shaft is connected to a viscometer working at imposed speed (Viscotester HaakeVT550, Thermo Fisher Scientific, ref: 002-7026) (**Figure 2-1**). This allows on-line torque measurements. The rotational speed may range between 0.5 and 800 rpm and torque between 0.1 and 30mN.m (< 400rpm) and 20mN.m (> 400 rpm) (accuracy ±0.5%). Temperature was controlled by circulation (cryostat Haake DC30, -50-200°C±0.01, Thermo Scientific) through the water jacket. Suspension pH was controlled by a pHmeter (Mettler Toledo Seveneasy S20, 0-14±0.01, -5-105°C). The pH adjustment was achieved with NaOH 10N and H_3PO_4 85%. The viscometer and the cryostat were controlled by software from HaakeRheoWin Job Manager (Thermo Fisher Scientific) which also ensured data recording (temperature, torque, mixing rate). A focused beam reflectance sensor (FBRM-G400-Mettler Toledo, range from 0.1 to 1000µm) was located in bulk in order to measure the distribution of particle chords.

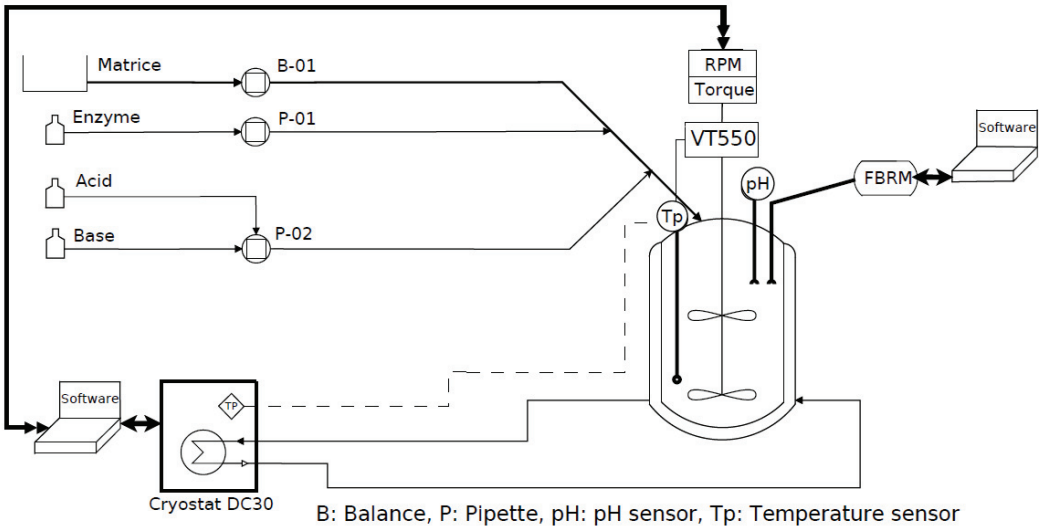

Figure 2-1: PID of experimental set-up.

2.2 Substrates and enzymes

2.2.1 Lignocellulose matrices

Five cellulose matrices were selected and studied in order to investigate different fibre morphologies, biochemical composition and structure and particle size distributions:

- MCC: microcrystalline cellulose (ACROS Organics, ref: 382310010),
- WP: a dried and milled (Bosch MKM6003 mill, 720 rpm, 60s) Whatman paper (Whatman International Ltd., Maidstone, England, Cat No 1001 090)
- PP-27: a paper-pulp from coniferous (soft) wood (Tembec Co., Saint-Gaudens, France, type FPP27) after extrusion (Extruder Eurolab 16, 400mm failure, extrusion line: 25 L/D 18/25 conveying, 7/25 shear stress).
- PP-31: a paper-pulp from deciduous (hard) wood (Tembec Co., Saint-Gaudens, France, type FPP31) after extrusion (Extruder Prism TSE24MC, 400mm failure, Thermo Electron Corp, extrusion line: 7/8 mixing, 1/8 shear stress,).
- BAG: a dried milled (hammer mill, screen pore 0.25mm) sugar cane bagasse (by-product of Lam Son cane sugar factory, Vietnam)

The five model and industrial substrates are henceforth referred as MCC, for microcrystalline cellulose, WP for Whatman paper, PP-27 and PP-31 for extruded paper pulp and BAG for sugar cane bagasse. The academic substrates, MCC and WP were considered as reference matrices for rheological analysis (MCC) and hydrolysis (WP). The industrial substrates, PP-27 and PP-31 were selected because of the need of pre-treated substrate, which are supposed to be easy to hydrolyse and applicable for industry (under high dry matter content).The last and raw substrate, BAG, selected with recommendation of our partner EBTA (Hanoi, Vietnam), exhibits the highest biochemical and structural complexity . The influence of this complexity on hydrolysis efficiency has interest to be observed during enzymatic attack.

All these matrices were characterised by physic-chemical analyses: water and ash contents, biochemical composition, crystallinity/amorphous ratio, morpho-granulometry (size distribution), density, surface tension, specific heat, thermo-gravimetric analyse, decantation kinetics and suspension rheometry.

2.2.2 Enzyme cocktail

An enzyme cocktail (Enzyme ACCELLERASE® 1500 Genencor, ref. 3015155108) containing exoglucanases, endoglucanases (2200 to 2800 CMC U/g), hemicellulases and β-glucosidases (525 to 775 pNPG U/g) was used. This cocktail is an enzyme complex intended specifically for the lignocellulosic biomass processing industries, including renewable fuels and chemicals. Its optimal temperature and pH were 50°C (range 50 to 65°C) and pH 4.8 (range 4 to 5). An ACCELLERASE® 1500 dosage rate (none standard) of 0.1 to 0.5 mL per gram of cellulose or roughly 0.05 to 0.25 mL per gram of biomass (depending on biomass composition) is recommended by the manufacturers (**Annexe 4**). Cocktail is kept cold at 4°C (±2) to avoid degradation. Inactivation may occur for temperature superior to 70°C and pH<4 or pH>7. Enzymatic activities were characterized at the same value range in the bibliography between 50 and 60 FPU/mL: 52 (Govumoni et al., 2013), 57±2.8 (Alvira et al., 2011), 61.9 (Wilson, 2013), 62.2 (Pessani, 2011). The FPU (filter paper unit) (characterise all of cellulase activities) was calculated from enzyme dilutions producing 2.0 mg glucose per assay: FPU = 0.37/enzyme concentration to release 2.0 mg glucose units/ml. The protocol was presented by IUPAC (Ghose, 1987).

2.3 Biochemical analysis

2.3.1 Water content

The water content of substrate and hydrolysed suspension were determined by drying at low temperature and pressure. The mass differences before and after drying is the water content in the sample. Empty eppendorfs (Sorenson ^{TM} Bioscience, Inc.) were numbered, drilled (4-5 pores on the cover) and placed during 24h in an oven at 60°C, 200mbar (Heraeus, Thermo Scientific, 0-760mmHg, 50-150°C). After 24h, these eppendorfs were taken out, placed at

least 1h in a dessicator (ambient temperature) with silica gel. Mass were after quantified with a precision balance (Sartorius ED224S, 0.005-230g ± 0.1mg). These masses were noted m_{epp}. During enzymatic hydrolysis, a volume of sample (≈1mL) was put in the eppendorf (with a pipette, Mettler Toledo, 500-5000µL ± 5µL). This eppendorf was replaced in the oven (ambient temperature) with silicagel during 1h and quantified with a balance (accuracy 10^{-4}g). This mass was noted m_{ini}. These eppendorf were placed in the oven at 60°C, 200mbar during 5 days and quantified. This final weight was noted m_{fin}. Water content (W) and dry matter (DM) were calculated following **Eq.2-1** (accuracy ±0.5%):

$$W(\%) = \frac{m_{ini} - m_{fin}}{m_{ini} - m_{epp}} \cdot 100 \qquad \textit{(Eq. 2-1)}$$
$$DM(\%) = 100 - W$$

However, the lignocellulose suspensions presented a high heterogeneity so a good sampling was difficult to realise. The taken total volume of samples must remain low compared to the total volume in the reactor (namely to preserve validity of in-situ viscosity measurements). This was a constraint and we chose to take small volume (1mL) although that does not insure to obtain a representative sample, due to heterogeneity of suspensions. Therefore, an error more important could be found for samples during hydrolysis.

2.3.2 Glucose (YSI)

Glucose concentration was checked in the supernatant along enzymatic hydrolysis by Analyser YSI model 27A (Yellow Springs Instruments, Yellow Springs, Ohio, sample volume=25µL) (Dunaway et al., 2010; Pereira et al., 2011; Samaniuk et al., 2011). This machine uses an immobile enzyme (glucose-oxidase) fixed on a membrane to produce peroxide from glucose in the sample:

$$C_6H_{12}O_6 + O_2 \xrightarrow{glucose-oxydase,H_2O} HOCH_2(CHOH)_4COOH + H_2O_2 \qquad \textit{(Eq. 2-2)}$$

The oxidation of peroxide on a platinum electrode liberates these electrons which induce an electric current proportional to glucose concentration. The machine will measure this electric current and bring the glucose concentration in $g.L^{-1}$. The range of result varies between 0-2.5 $g.L^{-1}$ ± 2% and between 2.5-9.0 $g.L^{-1}$ ± 5%.

2.3.3 Monomers and Oligosaccharides with DP<6 (HPLC)

The reactor samples were centrifuged at 13000 rpm for 5 min. Glucose and soluble cello-oligosaccharide, with degree of polymerization DP<6, in the supernatants were quantified by an AMINEX HPX-87P carbohydrate analysis column (Bio-Rad Laboratories, Richmond, CA) using a high performance liquid chromatography system (separations module: Waters Alliance 2690, refractometer detector: Waters 2414, Milford, MA). This column was usually found in literature to quantify glucose concentration (Elliston et al., 2013; Gupta et al., 2008; Kadic et al., 2014; Tozzi et al., 2014) but in our study, we optimised the working conditions to capacitate detect the different cello-saccharides. Analysis was operated at 60°C with deionised water and $Pb(NO_2)_2$ 0.1M as mobile-phase (ratio 80/20v/v) at a flow rate of 0.5 mL/min for 30 min. Glucose and cello-oligosaccharide standards with a DP of 2 to 5 were from Sigma Chemical Co., St. Louis, Mo. The retention time of these composes is presented in **Table 2-1**:

Table 2-1: Retention time of composes may be present in hydrolysed suspension.

Compound	Retention time (±0.03 min)
Xylose	17.74
Glucose	16.22
Cellobiose	13.29
Cellotriose	11.67
Cellotetraose	10.72
Cellopentaose	10.23

2.3.4 Ash content

Ash content was determined by weighting before and after calcinations. Empty hemolysis tubes were placed in a metal support and calcined in an oven at 550°C (Controller B170, Nabertherm, 30-3000°C) during 12h (temperature ascendant step: 2h). In the end of 12h, these tubes were placed in a desiccators (with silica gel) for return to ambient temperature before quantify their weights, m_{tub} (Satorius ED224S, max 230g±0.1mg). Secondly, about 1g of dried matter (substrate) was placed in the tube. The total mass (tube + substrate) was determined and noted m_{ini}. The programme was repeated and the weight after calcination was quantified ensuring the different between two measurement < 0.05mg. This mass was noted m_{fin}. The ash content was deduced like equation below (±2%):

$$Ash(\%) = \frac{m_{ini} - m_{fin}}{m_{ini} - m_{tub}} \cdot 100 \quad \textit{(Eq. 2-3)}$$

2.4 Physical and physico-chemical analysis

2.4.1 Densimetry

2.4.1.1 Densimetry of fluids

The density of fluids was determined by a densimeter Mettler Toledo DE40 (10^{-4} to 3 g.cm^{-3} ±10^{-4}g.cm^{-3}; 4-90°C±0.05°C). This device is based on the measurement of an induced mechanical oscillation on a "U" tube. A magnet is fixed on the tube "U" vibrating at different frequencies depending on the density range of the fluid contained in the tube. The oscillation period T of the system changes as a function of the total mass of the system ("U" tube + fluid within the tube). The internal volume of the tube is constant and defined for a given temperature; the period of oscillation of the system is directly related to the density of the fluid contained in the tube. The relationship between density and oscillation period is given by **Eq.2-4**:

$$\rho_{sam} = \left(\frac{K}{4\pi^2 V_{cell}} \right) \times T^2 + \left(-\frac{m_{cell}}{V_{cell}} \right) \quad \textit{(Eq. 2-4)}$$

In **Eq.2-4**, K (g.s^{-2}) is a constant of the cell, m_{cell} (g) and V_{cell} (mL) are the weight and the volume of the cell, T (s) is the oscillation period and ρ_{sam} (g.mL^{-1}) the sample density.

Before sample measurement, the machine was calibrated with air and distilled water at desired temperature (20, 30 and 40°C). The sample was injected slowly in tube U with a syringe. Sample volume necessary is approximately 1mL. The tube is rinsed with 3-5mL of sample before measurement.

2.4.1.2 Densimetry of substrates

The density of substrates was determined by gravimetry-volume method (proportion of substrate volume and added water volume in a volumetric flask). This density corresponds to

the suspended matric, including its initial water content (if applicable). It was used to calculate the volume fraction, even though other definitions can be proposed. It characterizes raw matter and emanates directly from the industrial process.
Firstly, the empty and dry flask (Flask Duran, type A, 100±0.1mL, 20°C) was weighted (Sartorius ED822CW, 0.5-820g±0.01g). A quantity of substrate (7 different quantities ranging from 5 to 30g) was added in each flask. Secondly, distilled water was injected slowly in the flask. Before the flask volume was reached, it was gently manually shacked to avoid air bubbles and ensure the water distribution in substrate. All measurements were realised at ambient temperature (20°C±2). The substrate density (±5%) was calculated with **Eq. 2-5**:

$$\rho_s = \frac{m_s}{V_s} = \frac{m_1 - m_0}{V_{tot} - V_w} \quad \textit{(Eq. 2-5)}$$
$$V_w = \frac{m_2 - m_1}{\rho_w^{20}}$$

with ρ_s, ρ_w^{20}: substrate density and water density at 20°C respectively ($g.mL^{-3}$).
m_s, m_0, m_1, m_2: mass of substrate, empty flask, flask before and after water added respectively (g).
V_s, V_{tot}, V_w: volume of substrate, flask and water added respectively (mL).
ρ_s here is the apparent density or density for substrate humid matter. It is necessary to calculate the intrinsic density or density for substrate dry matter ρ_{DM}. We have:

$$m_s = m_{water} + m_{DM}$$
$$\Leftrightarrow \rho_s \cdot V_s = \rho_w \cdot V_w + \rho_{DM} \cdot V_{DM}$$
$$\Leftrightarrow \rho_s = \frac{V_w}{V_s} \cdot \rho_w + \frac{V_{DM}}{V_s} \cdot \rho_{DM}$$
$$\Leftrightarrow \rho_s = \frac{1}{\frac{m_w}{\rho_w} + \frac{m_{DM}}{\rho_{DM}}} \cdot m_s$$
$$\Leftrightarrow \rho_s = \frac{1}{\frac{W}{\rho_w} + \frac{DM}{\rho_{DM}}}$$

So $$\frac{1}{\rho_{DM}} = \frac{1}{DM} \cdot \left(\frac{1}{\rho_s} - \frac{W}{\rho_w} \right) \quad \textit{(Eq. 2-6)}$$

2.4.2 Surface free energy (Contact angle measurement – Partnership with UW)

Adhesive forces between a liquid and a solid cause a liquid drop to spread across the surface. Cohesive forces within the liquid cause the drop to ball up and avoid contact with the surface. The contact angle (θ) is the angle at which the liquid–vapour interface meets the solid–liquid interface. The contact angle is determined by the resultant between adhesive and cohesive forces. As the tendency of a drop to spread out over a flat, solid surface increases, the contact angle decreases. Thus, the contact angle provides an inverse measure of wettability. The mechanical equilibrium of a liquid drop on a solid surface is determined by the balance of the three surface tension forces acting at the liquid-solid-vapour contact line. The mechanical equilibrium is represented by the well-known Young's equation.

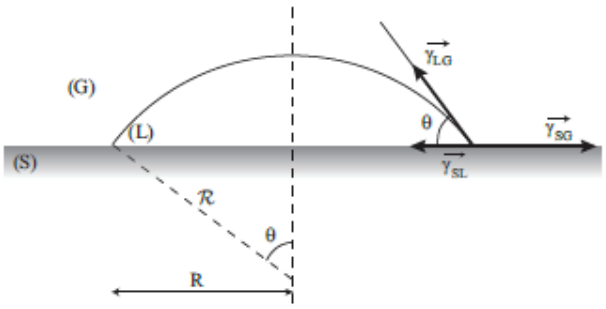

Figure 2-2: Three phases system assuming a spherical drop interface (Poulard, 2005).

$$\gamma_{SG} + \gamma_{SL} \cdot \cos(\pi) + \gamma_{LG} \cdot \cos(\pi - \theta) = 0$$
$$\gamma_{LG} \cdot \cos(\theta) = \gamma_{SG} - \gamma_{SL} = \gamma_S - \gamma_{SL} - \pi_E \quad \textit{(Eq. 2-7)}$$

With γ_S, γ_L, γ_G: surface free energy of solid, liquid and gas, γ_{SG}, γ_{LG}, γ_{SL}: surface free energy of interfaces (solid-gas, solid-liquid and liquid-gas) ($N.m^{-1}$), θ: contact angle (°), π_E: equilibrium spreading pressure (adsorbed vapour of liquid on solid) ($N.m^{-1}$).
The Dupré's equation amounts to a conservation of total energy in a reversible process of adhesion and cohesion of two phases. The work of adhesion is expressed by:

$$W_{SL} = \gamma_{SG} + \gamma_{LG} - \gamma_{SL} \quad \textit{(Eq. 2-8)}$$

The combination of the Young and Dupré's equations results in:

$$W_{SL} = \gamma_{LG} \cdot (1 - \cos(\theta)) \quad \textit{(Eq. 2-9)}$$

In this way, the two unknowns (γ_{SG} and γ_{SL}) of the original Young's equation can be reduced to only one, W_{SL}.
Fowkes (1964) provided a method of analysing the energies of surfaces from contact angles which does not require detailed knowledge of the surface compositions of solids. Fowkes (1964) considered that the total surface tension of a solid or a liquid can be decomposed into components corresponding to the specific types of intermolecular interactions.

$$\gamma = \gamma^d + \gamma^p + \gamma^i + \ldots \quad \textit{(Eq. 2-10)}$$

where d, p, and i stand for the dispersion, polar and induction interactions. A large number of terms can follow afterwards as indicated by the dots. This division of the surface tension into components allowed the work of adhesion to be expressed as follows:

$$W_{SL} = 2 \cdot \sqrt{\gamma_S^d \cdot \gamma_L^d} + 2 \cdot \sqrt{\gamma_S^p \cdot \gamma_L^p} + 2 \cdot \sqrt{\gamma_S^i \cdot \gamma_L^i} + \ldots \quad \textit{(Eq. 2-11)}$$

In order to estimate the surface free energy components of solid surface, contact angles of several liquids are measured (liquids whose surface tension components have already been determined). The surface tension components of the solid are determined by combining **Eq. 2-9** and **2-11** as follows:

$$W_{SL} = \gamma_{LG} \cdot (1 - \cos(\theta)) = 2 \cdot \sqrt{\gamma_S^d \cdot \gamma_L^d} + 2 \cdot \sqrt{\gamma_S^p \cdot \gamma_L^p} + 2 \cdot \sqrt{\gamma_S^i \cdot \gamma_L^i} + \ldots \quad \textit{(Eq. 2-12)}$$

The induction components of the surface free energies of solids and liquids are generally negligible in comparison with the two other terms. Thus, for all practical purposes, it is sufficient to account for the dispersion and polar terms only.

In our conditions, dispersive and polar contributions are considered. Gibbs (or total) energy is then given by the relation:

$$\Delta G_{TOT} = \Delta G^{d} + \Delta G^{p} \quad \textit{(Eq. 2-13)}$$

$$\textit{With } \Delta G^{d} = -W_{SL}^{d} = \gamma_{SL}^{d} - \gamma_{S}^{d} - \gamma_{L}^{d} \textit{ and } \Delta G^{p} = -W_{SL}^{p} = \gamma_{SL}^{p} - \gamma_{S}^{p} - \gamma_{L}^{p} \quad \textit{(Eq. 2-14)}$$

Thermodynamically, if ΔG_{TOT} is positive, the adhesion is disadvantaged (repulsion) and reciprocally, if ΔG_{TOT} is negative, the adhesion is advantaged (attraction). The total free energy of interaction is the sum of the electrostatic free energy, ΔG_{TOT} and non-electrostatic.
Contact angle measurements enable to measure surface free energy of materials and consequently to determine the total surface energy. A Drop shape, analyser DSA100 (Krüss GmbH, Germany) was used at room temperature in a static mode. The measurement was digitally recorded and the videos analysed with the software DSA1 V1.9-03 9 (Krüss GmbH, Germany). Two analysis methods were considered for low contact angle values: Tangent method 1 and Young-Laplace method (sessile drop) (Krüss GmbH, 2004). The initial contact angle and the change over time (at least ten seconds) were recorded for a drop of liquid deposited on the compact of a given material. The mean contact angle and the standard deviation were then obtained by summarizing values issued from 12 liquid drops per specimen (aberrant data were removed); depending on how well the drop shape is fitted by the method. With Tangent 1 method, the complete profile of a sessile drop was fitted to a general conic section equation. The derivative of the equation at the baseline gives the slope at the three-phase contact point and thus the contact angle. With Laplace Young method, the profile of a sessile drop in the region of the baseline was fitted to the rational function ($y=a+bx+cx^{0.5}+d/\ln(x)+e/x^{2}$). From the fitted parameters the slope of the three-phase contact point at the baseline was first determined and used to determine the contact angle. This function has been selected from numerous theoretical simulations.
Contact angle measurements were conducted with milled and compacted materials and using two liquids: water and diiodomethane (**Table 2-2**). For each given material, three experiments were realised: water contact angle on milled and unmilled material, diiodomethane contact angle on unmilled material. Each experiment was carried out on 12 samples in order to estimate the error associated with the measurement. The surface energy properties of the liquids are summarised in **Table 2-2**.

Table 2-2: Surface energy properties of water and di-iodomethane.

Liquid	Total surface energy (σ_{tot}, mN/m)	Dispersive component (σ_{tot}, mN/m)	Polar component (σ_{tot}, mN/m)
Water (W)	72.8	21.8	51.0
Diiodomethane (D)	50.8	50.8	0.0

A preliminary preparation of the samples involved a milling and compaction steps. An ultra-centrifugal mill ZM200 (Retsch GmbH, Germany) and 0.08 mm sieve with trapezoid shaped holes (part # 03.647.0231) were used to mill the materials. A dischargeable KBr pellet die (International Crystal Laboratories, USA) at room temperature was used to compact 0.2g of substance as suggested for pigment specimens in ASTM D7490–08 (American Society for Testing and Materials, 2008). The KBr mould is 13mm in diameter and a 4 ton pressure was applied for 30s, followed by a 60s 7ton load (7000 kg/132.73 mm^2= 517.19 MPa) in a press Model #3925 (Carver Inc., USA). The compacts are then fixed onto a microscope object slide (Pearl 7101, T& Q Industries, China) with double sided tape (137-2C, Scotch, Canada) and stored in a desiccator (Nalgene, Sybron Corporation, USA) until testing. In order to minimize

the potential humidity absorbed by the samples, the compaction and the contact angle measurement were always carried out the same day.

2.4.3 Thermal properties analysis

The physical and chemical properties of any material change under the influence of temperature. Techniques dedicated to thermal analyses (thermogravimetry, dilatometry, thermo-mechanic, thermo-optic or calorimetry) are adapted to characterize the behaviour of liquid, amorphous or crystalline material submitted to thermal variation under controlled conditions. Principle of these techniques is based on the determination of mass, volume, specific heat capacity, spectro-mechanical or structural properties, as a function of temperature.

2.4.3.1 Specific heat capacity

Differential Scanning Calorimeters (DSC) quantitatively determines conversion temperatures and enthalpies for solids and liquids by measuring the heat fluxes to both the sample and to a reference as a function of temperature and time. This technique is used to characterize state and/or structure change. It enables to measure various physical data: specific heat capacity, enthalpy variation due to phase transition or chemical reaction, purity degree of substance and reaction kinetics as example. Considering instrument and experimental base lines previously characterized with differential scanning calorimeter, the heat flux associated to an inert sample is expressed by:

$$\varphi = \frac{dQ_H}{dt} = m \cdot Cp \cdot \frac{dTp}{dt} \quad \textit{(Eq. 2-15)}$$

With m: sample mass (determined at ± 0,01 mg) (g), Cp : specific heat mass capacity ($J.K^{-1}.kg^{-1}$), Q_H: heat quantity (J), φ: heat flux (W) and Tp: temperature (K).
A differential scanning calorimeter (Micro DSC III, SETARAM Instrumentation-SN: 60/50287.06.102- associated with CS 32 controller –SN: 06 102 and SETSOFT 2000 software for data acquisition and treatment) was used. Its technical specifications are for temperature: -20°C to + 120 °C, thermal kinetics: 0.001 to 1.2°C.min^{-1} and flux meter range: 0.2µW to 20mW (LOD: 0.2 to 2 µW, resolution: 40 nW). In our conditions, specific heat of each matrices were determined between 15 and 65°C (thermal kinetics: 0.1°C.min^{-1}) with dried matter (0.1 to 0.5g) placed in measurement cells (Hastelloy C276 ref 31/1528).

2.4.3.2 Heat degradation (Thermo-Gravimetric Analysis - Partnership with UW)

Thermogravimetric Analysis (TGA) determines the temperature- and time-dependent changes in the mass of a sample that occur during a specific temperature program and in a defined atmosphere. A quantity of about 5mg sample was analysed by TGA (Q500 V20-TA instruments, USA). The nitrogen was added with flow rate 50mL.min^{-1}. The temperature varied between 40°C and 800°C. Heating rate was 50°K.min^{-1} unless weight change was detected at which point the heating rate would be 1°K.min^{-1}.

2.4.4 Decantation kinetics and hydrodynamic diameters

The Turbiscan LAB ™ (Formulation, France, 0-95%v/v, 0.1-1000µm, room temperature to 60°C) can identify and follow the destabilization phenomena (migration or particle size change) of complex systems. The LAB Turbiscan™ technology is based on the multiple lights scattering (MLS). This technique consists in sending photons (light) into the sample. These photons, after being scattered many times by objects in suspension (droplets, solid particles, gas bubbles…) emerge from the sample and are detected by the measurement device of the Turbiscan. The interest is to analyse concentrated samples without dilution. A sample (substrate and hydrolysed suspension) is placed in a test tube (V≈20mL). The device sends a

beam of light (λ=880nm) and collects the transmitted (180°) or the backscattered (45°) stream by scanning the height of the tube (2-55mm, resolution 40µm) at intervals of time defined (2 scans/minute). The measurement enables the quantification of several parameters, as BS (backscattering) and T (transmission) signals, which are linked to particles average diameter (d) and volume fraction (ϕ) (**Figure 2-3**).

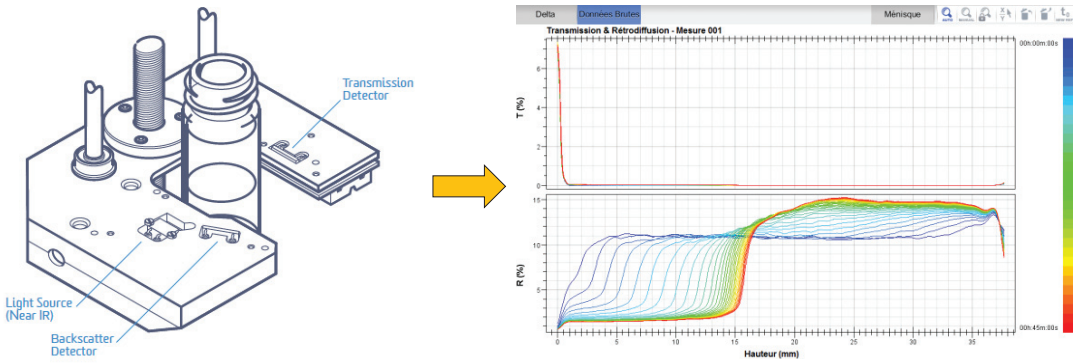

Figure 2-3: View of measurement cell of Turbiscan Lab and example of results showing Transmitted and Backscattered signals.

Considering a suspension of non-absorbing spheres randomly dispersed in a transparent fluid (distilled water), the mean free path of the light, l, can be estimated through the particle surface density (derived from particle mean diameter d and particle volume fraction ϕ) and the scattering efficiency factor Qs:

$$l(\phi,d) = \frac{1}{n\cdot(\pi\cdot d^2/4)\cdot Q_s} = \frac{2\cdot d}{3\cdot\phi\cdot Q_s} \qquad \textit{(Eq. 2-16)}$$

$$\phi = n\cdot\frac{\pi\cdot d^3}{6}$$

where n is the particle density.
For Mie scatterers and larger ones (λ/10 up to 10xλ, λ being the wavelength of the incident light), light scattering becomes anisotropic. This anisotropy can be characterised by the asymmetry factor g, which is the average cosine of the scattering angles weighted by the phase function or scattering diagram of the scatterer (g' = 0 for isotropic Rayleigh scatterers and 0 < g' < 1 for Mie scatterers) (Kerker, 1969; Snabre & Arhaliass, 1998). For non-isotropic scatterers, we further define the photon transport mean free path l* = l / (1-g') representing a decorrelation length above which the photon "forgets" the direction of the incident beam (Gandjbakhche et al., 1994; Ishimaru & Kuga, 1982; Snabre & Arhaliass, 1998). The characteristic size of the backscattered spot light is representative of the photon transport mean free path l*. The backscattered light flux BS measured through a thin detection area of thickness dh is calculated by the **Eq. 2-17**:

$$BS = \left(\frac{dh}{l^*}\right)^{1/2} \qquad \textit{(Eq. 2-17)}$$

Using the Mie theory corrected for high volume fraction with the approximation of Percus Yevik (Ishimaru & Kuga, 1982), the transport mean free path l* scales as particle mean diameter and the inverse of particle volume fraction:

$$l^*(d,\phi) = \frac{2 \cdot d}{3 \cdot \phi \cdot (1 - g') \cdot Q_s} \quad \textit{(Eq. 2-18)}$$

From **Eq. 2-17** and **2-18**, back-scattered signal is proportionally with the square root of volume fraction ϕ.

The photon mean free path l represents the mean distance travelled by photons before undergoing a scattering phenomenon. The Lambert - Beer law gives an analytical expression of the transmission T, measured by the optical analyser as a function of the photon mean free path l:

$$T(l, r_i) = T_0 \cdot e^{\frac{-2 \cdot r_i}{l}} = T_0 \cdot e^{\frac{-3 \cdot r_i \cdot \phi \cdot Q_s}{d}} \quad \textit{(Eq. 2-19)}$$

where r_i is the measurement cell internal radius and T_0 the transmission for the suspending phase. Therefore, the transmission T directly depends on the particle mean diameter d and varies linearly with e^{ϕ}.

Figure 2-4 shows, as an example, the backscattering (BS) and the transmission (T) versus the particle volume fraction, ϕ for a latex beads suspension in water. In the concentrated regime ($\phi > \phi_c$), the figure shows an increase of the backscattering level BS with particle volume fraction before reaching a maximum for a volume fraction ϕ_L. The critical volume fraction ϕ_c between dilute and concentrated regimes corresponds to a photon transport mean free path $l^*(\phi_c)$ equals to the measurement cell diameter $2r_i$ (Bru et al., 2004). In the diluted regime ($\phi < \phi_c$), the transmission T decreases exponentially with particle volume fraction in good accordance with the physical model and reaches a zero value in the concentrated regime ($\phi > \phi_c$).

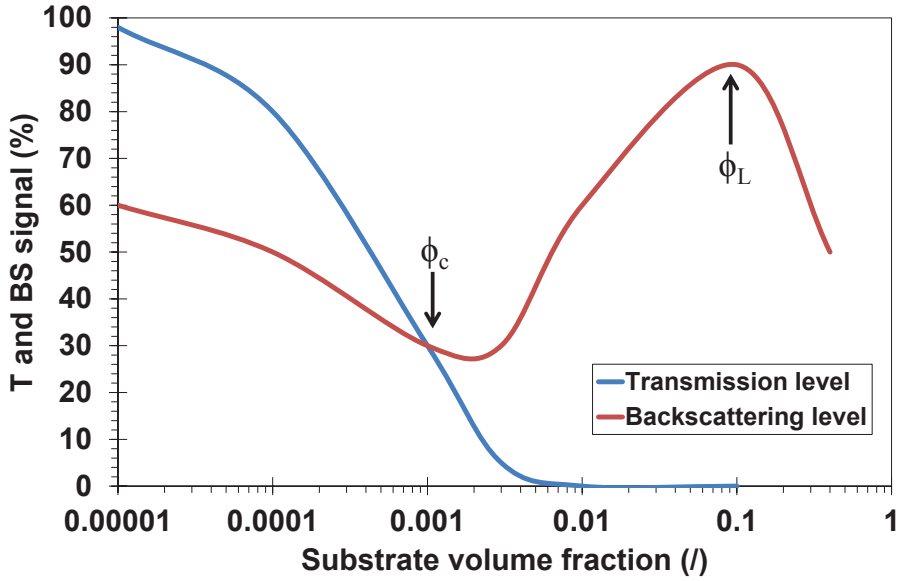

Figure 2-4: Transmission level, T, and backscattering level, BS, versus particle volume fraction for 0.17µm latex spheres in water (Snabre et al., 2004).

For diameter particle calculation, the Stockes's law is applied. In these conditions of laminar flow, for spherical and smooth surface particles, homogeneous suspension and no interaction between the particles, we have, in the dilute regime (ϕ <0.5%):

$$F_d = 6\pi \cdot r \cdot v \textit{ and } v_s = \frac{(\rho_s - \rho_w) \cdot d_s^2 \cdot g}{18 \cdot \mu} \quad \textit{(Eq. 2-20)}$$

where F_d is the frictional force – known as Stokes' drag – acting on the interface between the fluid and the particle (N), μ is the dynamic viscosity ($kg.ms^{-1}$), r is the radius of the spherical object (mv is the particle's velocity (ms^{-1}), v_s is the particle's settling velocity (ms^{-1}), g is the gravitational acceleration ($m.s^{-2}$), ρ_s is the mass density of the particles ($kg.m^{-3}$) and ρ_w is the mass density of the fluid (water) ($kg.m^{-3}$).
In the case of non-spherical particles, d_s=2r is known as the Stokes diameter, i.e. the diameter of the spherical particle that diffuses at the same rate.
In concentrated suspension (ϕ >0.5%), the modified Stockes's law is used:

$$v_s = \frac{(\rho_s - \rho_m)\cdot d_s^2 \cdot g}{18\cdot \mu_m} \quad \textit{(Eq. 2-21)}$$

With $\rho_m = (D\cdot\rho_w + 1)/(D + 1/\rho_s); \mu_m = \mu_w \cdot (D + 1/\rho_s)/(D - D_{\lim})$
Where D = dilution (m_{fluid}/m_{solid})
D_{lim} = dilution minima (m_{fluid}/m_{solid})
In road book of Turbiscal Lab apparatus, another model was proposed (Mills & Snabre, 1994):

$$v_s = \frac{(\rho_s - \rho_m)\cdot d_s^2 \cdot g}{18\cdot \mu_m} \cdot \frac{1-\phi}{1+\frac{4.6\cdot\phi}{(1-\phi)^3}} \quad \textit{(Eq. 2-22)}$$

In present work, the decantation analysis using Turbiscan Lab was performed with two principal goals: (i) substrate concentration estimation for initial and hydrolysed suspensions, (ii) particle's settling velocity determination and particle diameter distribution.
First of all, a step consisted in a calibration of T and BS with substrate suspension for different concentrations was realised. Six (four for WP) substrate volume fractions varying between 0.01 to 20%v/v were examined for raw materials. The mean values of T and BS signals for homogeneous suspensions as a function of substrate concentration enable to determine the validity of **Eq. 2-18** and **2-19**. The two curves T(ϕ) and BS(ϕ) intercept for a critical volume fraction ϕ_c which could characterise each substrate. If it is considered that the optical parameters of fibre and the suspension density remain stable during enzymatic attack, a profile of substrate concentration in sample measured as a function of sample height and analysis time could be established. Then, the overall mass balance of suspensions before and after hydrolysis would be calculated (by integrating concentration profile) and compared with those determined by other methods. Beside it, the critical height h* of the settled suspension could be discussed.
In a second step the decantation kinetics are analysed and compared for different hydrolysis times and for different matrices. The particle's settling velocity, v_s, together with the falling particle diameter, d_s, could be deduced as follow.

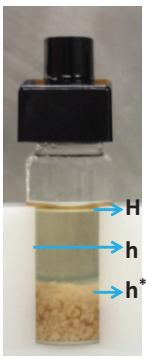

For a given ϕ, the variation of sample height during a period dt is monitored. This variation was dh; so we have:

$$v_s(\phi, t) = \frac{dh}{dt} \quad \textit{(Eq. 2-23)}$$

For the supernatant, h varied between h^* and H, we have ϕ varied between ϕ_{min} and ϕ*.

$$d\bar{h} = \frac{1}{\phi_{\min} - \phi^*} \cdot \int_{\phi_{\min}}^{\phi^*} dh \cdot d\phi \quad \textit{(Eq. 2-24)}$$

From **Eq. 2-23** and **Eq. 2-24**, $v_s(t) = \frac{d\bar{h}}{dt}$, this quantity illustrates the average particle's settling velocity in the supernatant during a period dt. After that, the particle diameter could be determined from **Eq. 2-20** or **Eq. 2-21**. It is possible to build the cumulative distribution in volume of hydrodynamic diameter.

2.4.5 Crystallinity index (Partnership with LCPO)

X-ray diffraction (XRD) patterns were collected on a PANalitycal X'pert MPD Bragg-Brentano θ-θ geometry diffractometer equipped with a secondary monochromator over an angular range of 2θ = 8-80°. Each acquisition lasted for 74 minutes. The Cu-Kα radiation was generated at 40 KV and 40 mA (λ = 0.15418 nm).
The samples were put on sample holders made of aluminum alloy and flattened with a piece of glass. The X-ray apparent crystallinity of cellulose was calculated from the height ratio between the intensity of the crystalline peak and the total intensity without subtraction of the background signal (non-crystalline) measured without cellulose (verified as negligible).
The crystalline portion of the total contribution at 22.5° was determined by the Segal method (Segal et al., 1959). Thus, apparent crystallinity (Cr) was calculated by using the following formula:

$$CrI(\%) = \frac{I_{002} - I_{am}}{I_{002}} \cdot 100 \quad \textit{(Eq. 2-25)}$$

where I_{002} is the intensity for the crystalline portion of cellulose at about 2θ = 22.5° and I_{am} represents the amorphous portion at about 2θ = 18°.

2.4.6 Rheometry

Lignocellulose suspensions present complex rheological behaviour and that there are no standard method for studying their flow behaviour. These suspensions usually show an apparent yield stress, a shear-thinning behaviour (decrease of viscosity with increasing shear rate) and elasticity. The most useful models for these behaviours are the Bingham and the Herschel-Bulkley models. To characterise these rheological properties as finely as possible, we combined two measurement strategies: (i) ex-situ rheometry (oscillation mode) will bring to us the information of yield stress and elasticity, (ii) in-situ viscometry allows following in real time the suspension viscosity during enzymatic attack.

2.4.6.1 Ex-situ rheometry

Flowing curves were measured with a Mars III rheometer (Thermo Scientific, torque measured range: 10^{-8} – 0.2 N.m, with oscillation: 3.10^{-8} < C < 0.2 N.m, rotation speed range: 10^{-7} – 4500 RPM, frequency: 10^{-6} – 10^{2} Hz,). The experimental strategy and the data acquisition were performed using the software RheoWin Job Manager.
For hydrodynamic identification of the reactor, Newtonian (water, Marcol oil, glycerol) and non-Newtonian homogeneous fluids (glucose-xanthan and sucrose-xanthan: 640g.L^{-1} glucose and 947g.L^{-1} sucrose) were used. Viscosity and rheological behaviour for all these test fluids were measured with a cone and plate system (60mm diameter, angle 2°) and for shear rate varying from 10^{-2} to 10^{3} s^{-1} at two different temperatures, 20°C and 40°C. The characteristics of these fluids are presented in **Table 2-3**.
Rheometry of the suspension during hydrolysis was realised with serrated plates (35mm) (gap size: 1.5 mm). To avoid the evaporation during the measurements, the samples are enclosed by a film of Vaseline. Two successive protocols were performed. First, an oscillatory shear flow at a fixed frequency (1Hz) is realized with increasing shear stress amplitude from 0.1 to 20 Pa. This first measurement is used to determine the linear domain of the suspension. After

these measurements, a scan is carried out in the linear domain at frequencies from 0.5 Hz to 20 Hz and fixed constraint. Analysis of samples is done at 20°C.

Table 2-3: Characteristics of used fluids.

Fluid	Newtonian	Non-Newtonian		Density ($kg.m^{-3}$) (20/40°C)
	μ (Pa.s) (20/40°C)	n (/) (20/40°C)	K ($Pa.s^n$) (20/40°C)	
Distilled water	10^{-3}/$6.5.10^{-4}$	-	-	998.2/992.2
Marcol oil	0.01/$5.4.10^{-3}$	-	-	827.6/811.9
Glycerol	1.20/0.25	-	-	1261.1/1255.0
Glucose-Xanthan 0.04%	-	0.65/0.69	0.12/0.07	1237.3/1229.5
Glucose-Xanthan 0.1%	-	0.45/0.50	0.51/0.34	1237.7/1229.7
Sucrose-Xanthan 0.04%	-	0.74/0.75	0.70/0.36	1236.5/1226.5

2.4.6.2 In-situ rheometry

The approach of ex-situ measurement was limited by the number of samples and the substrate properties, predominately decantation and flocculation of material. To solve these problems, a method allowing to follow the suspension viscosity was set up. This method is based on the determination of power consumption (or the power number Np in its dimensionless form) versus the Reynold number during suspension mixing. The viscosity is calculated from standard curve of power consumption for the mixing system under consideration.
The dimensionless power number Np and the mixing Reynold number Re was are evaluated for Newtonian fluids, by:

$$Np = \frac{P}{d^5 \cdot \rho \cdot N^3}; P = 2\pi \cdot N \cdot C \qquad \textit{(Eq. 2-26)}$$

$$\mathrm{Re} = \frac{\rho \cdot N \cdot d^2}{\mu}$$

This single master curve depends only on impeller/reactor shape and geometry. In the laminar regime (Re<10-100), the product Np.Re is a constant, named Kp, which is then defined as follows:

$$Np \cdot \mathrm{Re} = Kp \qquad \textit{(Eq. 2-27)}$$

Kp is a function of impeller shape and geometry for any Newtonian fluid. A deviation from Eq. 2-26 indicates the end of laminar regime. In fully turbulent flow (Re $>10^4 - 10^5$) and for Newtonian fluids, the dimensionless power number Np is assumed to be independent of mixing Reynolds number and equal to a constant, Np_0. In our study, three Newtonian fluids (distilled water, Marcol 52 oil and glycerol) were used to cover a large range of mixing Reynolds numbers. The torque and mixing rate (ascent / descent cycles, 0.5/800/0.5 RPM) were measured for each fluid at 20 and 40°C. Calculating Np and Re, the power consumption curve was then established.
The Kp value obtained was 97.9 which is higher than values from the literature ((Rushton et al., 1950): for propeller Kp: 40-50, for flat-blade turbine Kp: 66-76). Experimental results confirm that the laminar regime prevailed up to Re ≈ 50 **(Figure 2-5)**
A semi-empirical model including laminar and transition regions was considered for the reference curve with a one-to-one relationship between Np and Re:

$$Np = \left(\left(\frac{Kp}{\mathrm{Re}_{Ag}} \right)^{q} + N_{p0}^{q} \right)^{1/q} \quad with: N_{p0} = 0.128; q = 0.782 \quad \textit{(Eq. 2-28)}$$

In the non-Newtonian case, a generalised mixing Reynolds number has to be defined as the viscosity is not a constant. The well-known Metzner and Otto concept (1957) was used: an equivalent viscosity μ_{eq} is defined as the Newtonian viscosity leading to the same power number. Metzner and Otto (1957) showed that the equivalent shear rate $\dot{\gamma}_{eq}$ associated to this viscosity (through the rheological behaviour of the fluid) is proportional to the rotation frequency, then introducing the Metzner-Otto parameter Ks:

$$\dot{\gamma}_{eq} = K_s \cdot N \quad \textit{(Eq. 2-29)}$$

This leads, for the shear-thinning fluid modelled by a power-law $\mu = k \cdot \dot{\gamma}^{n-1}$, to the generalized Reynolds number:

$$\mathrm{Re}_g = \frac{\rho \cdot N^{2-n} \cdot d^2}{k \cdot K_s^{n-1}} \quad \textit{(Eq. 2-30)}$$

Ks is a constant depending only on the geometry of the stirring system. **Eq.2-29** can be extended to the transition region using a power equation (Jahangiri et al., 2001). Xanthan solutions (0.04%; 0.1%; 0.4%) in glucose solution (650g.L^{-1}) and in sucrose solution (943g.L^{-1}) were used to determine the proportionality constant Ks. Using the power consumption curve established with Newtonian fluids, the apparent viscosity μ was calculated from torque and mixing rate measurements. The corresponding value of the shear rate, $\dot{\gamma}_{eq}$, was extracted from the rheograms of the Xanthan solutions. Rieger and Novak's approach (Rieger & Novak, 1973) was used to determine the value of Ks: **Eq. 2-30** with the generalized Reynolds number Re^* is written in a similar form:

$$Np \cdot \mathrm{Re}^* = Kp(n) \quad \textit{(Eq. 2-31)}$$

With $\mathrm{Re}^* = \frac{\rho \cdot N^{2-n} \cdot d^2}{k}$ and $Kp(n) = Kp \cdot Ks^{n-1}$

The value of Ks is directly deduced from the curve $Kp(n) = f(n-1)$ using the previously determined Kp value. This leads to Ks ≈ 32±2. In the case studied, the extension to the transition region using a power equation (Jahangiri et al., 2001) is not relevant. Once the experimental set-up was characterised by its power consumption curve Np(Re) and the Ks value, in-situ viscometry of the suspension was performed before and along the bio catalytic reaction.

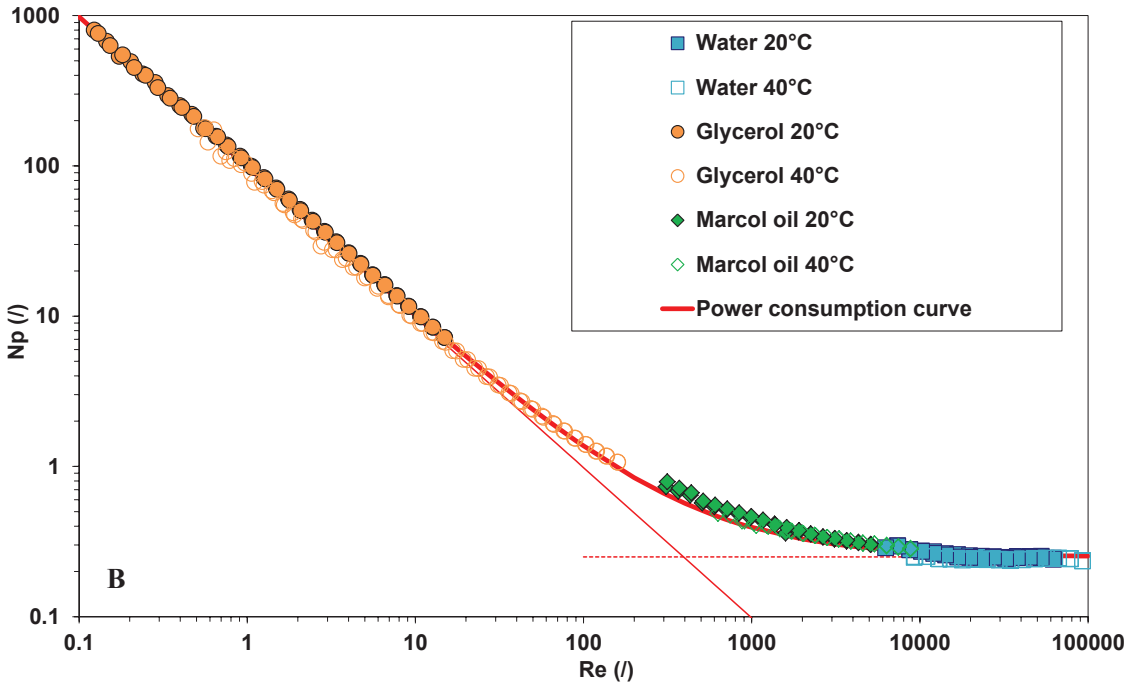

Figure 2-5: Power consumption curve established for bioreactor (V=1.3L; impeller TC1).

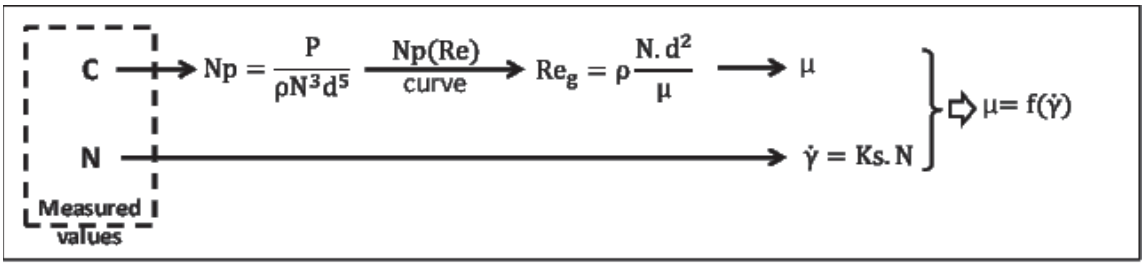

Figure 2-6: In-situ viscometry.

2.4.7 Particle size and morphology analysis

Amongst the main parameters to be studied, the rheological behaviour of the hydrolysis suspension and the fibre particle size and morphology stand out as the major determinants of the process efficiency. They are the principal elements for the choice of the equipment and the strategy. This section will detail the different methods used to characterise particle size and shape. Two types of measurements were used: in-situ chord length measurement (FBRM) and ex-situ particle size analysis which consist in two methods: laser granulometry and morpho-granulometry.

2.4.7.1 Theoretical review

To compare the particle sizes of the various matrices and also to monitor their changes during enzymatic attack, the analysis of distribution profile is used. These distribution profiles can be compared via distribution functions E(x) and cumulative distributions F(x) (**Eq.2-32**). They can be represented as discrete or continuous functions (p_i is the probability corresponding to class i).

$$E(x)\cdot dx = \frac{dn}{n} = p_i \Rightarrow \int_0^{\infty} E(x)\cdot dx = 1 \quad \textit{and} \quad F(x) = \int_0^{\infty} E(x)\cdot dx = \sum_{i=0}^{\infty} p_i = 1 \quad \textit{(Eq. 2-32)}$$

Each distribution function can be characterized by a range of moment and centred moments of order j (**Eq. 2-33**) (Ham & Platzer, 2004; Morice, 1972; Villermaux, 1993)

$$\Gamma^i = \int_0^\infty x^i \cdot E(x) \cdot dx \quad and \; \Gamma^{i'} = \int_0^\infty (x - \bar{x})^i \cdot E(x) \cdot dx \quad \textit{(Eq. 2-33)}$$

The function E(x) is characterised by his average value, $\bar{x}$ which corresponds with moment of order 1, Γ^1. The variance σ^2 and the reduced variance $\beta^2 = \frac{\sigma_x^2}{\bar{x}^2}$ correspond respectively with centred moments of order 2; $\Gamma^{2'}$ and $\frac{\Gamma^{2'}}{\bar{x}}$ characterise the dispersion of distribution curve. The centred moments of order 3, $\Gamma^{3'}$ or $\frac{\Gamma^{3'}}{\sigma^3}$ provides information on the asymmetry of the curve (Skewness). An asymmetric distribution is left when S<0 and is right when S>0. The centred moments of order 4, $\Gamma^{4'}$ or $\frac{\Gamma^{4'}}{\sigma^4}$ allows evaluate the spread of the distribution curve (Kurtosis).

There are various ways to define the size of a particle as the "diameter" (**Table 2-4**). Allen (1968) listed thirteen possible ways to define a equivalent diameter of a given particle using sphere as reference. The sphere is chosen as reference because of its unambiguous definition of the diameter. However, most of the particles are not spherical; the knowledge of more than one dimension is required to describe the shape of a particle. The most useful diameter is the diameter of the volume equivalent sphere, d_v, which corresponds to the diameter of the sphere having the same volume as the particle.

Each measurement technique for spherical geometry should give the same result. For irregular shapes, there is an influence of the measurement method, which must then be selected with a particular care.

Table 2-4: Diversity of particle equivalent diameter definitions.

Symbol	Appellation	Definition
d_v	Volume diameter	Diameter of the sphere that has the same volume as the particle: $v_i = \frac{\pi}{6} \cdot d_v^3$
d_s	Surface diameter	Diameter of the sphere that has the same area as the particle: $s_i = \frac{\pi}{4} \cdot d_s^2$
d_p	Perimeter diameter	Diameter of the sphere that has the same perimeter as the projected area of the particle: $p_i = \pi \cdot d_p$
d_c	Falling diameter	Diameter of the sphere that has the same density and the same free-fall velocity of the particle in a fluid at the same density and same viscosity.
d_{St}	Stockes's diameter	Diameter of a sphere freely falling at the same velocity as the particle in a laminar flow (Rep<0,2).
d_t	Sieving diameter	Side of the smallest square mesh through which the particle can move.
d_F	Feret diameter	The distance between the two parallel planes restricting the object perpendicular to that direction.
d_d	Diffraction diameter	Diameter of the circle that generates the same beam deflection that the particle due to the wave nature of the radiation.

Because of the non uniforme size of particles, the variation of population size is presented as a size distribution. In this work, the frequency distributions or cumulative distributions are used.

Most existing techniques give the characterization of distributions based on the number, length, surface or volume of the particles.
Depending on the definition of the classes of particle, four types of distributions are defined (**Table 2-5**). Considering the complexity of particle shapes and according to the highlighted properties, it is important to define a mean diameter (and standard deviation describing the width of the distribution around this average trend) for a given particle population. The average diameter is defined as follows:

$$d_{p,q} = \left[\frac{\sum n_i \cdot d_i^p}{\sum n_i \cdot d_i^q} \right]^{1/p-q}$$ with n_i: the number of particles of diameter d_i. (Brittain, 2001).

We note $d_{1,0}$ the number-average diameter, $d_{2,0}$ the quadratic mean diameter, $d_{3,0}$ the cube average diameter, $d_{4,3}$ the mass or volume mean diameter, $d_{3,2}$ the area-average diameter or Sauter diameter...

Table 2-5: Definitions of distributions in number, dimension, surface and volume.

Distribution	Signification	Formula
Distribution in number	Percentage in number associated with each class	$p_{n_i} = \frac{n_i}{\sum n_i}$
Distribution in dimension	Percentage in dimension associated with each class	$p_{d_i} = \frac{n_i \cdot d_i}{\sum n_i \cdot d_i}$
Distribution in surface	Percentage in surface associated with each class	$p_{s_i} = \frac{n_i \cdot d_i^2}{\sum n_i \cdot d_i^2}$
Distribution in volume	Percentage in volume associated with each class	$p_{v_i} = \frac{n_i \cdot d_i^3}{\sum n_i \cdot d_i^3}$

2.4.7.2 Diffraction Light Scattering (DLS)

Particle size distribution was determined through laser diffraction analyses (Mastersizer 2000 Hydro, Malvern Instruments Ltd. SN: 34205-69, range from 0.02 to 2000µm). A suspension (at three concentrations) was added drop by drop to the circulation loop (100-150mL). Analysis are conducted at room temperature (20°C) with obscuration rates (red λ=632.8nm and blue λ=470.0nm lights) ranging between 10 and 40%. Particle volume distribution and the associated cumulative curve versus particle diameter were determined (**Figure 2-7**). Laser diffraction analysis converts the detected scattered light into a particle size distribution. Successful deconvolution relies on an appropriate description of light behaviour: either Mie theory or the Fraunhofer approximation (of Mie theory). Historically, the use of Mie theory was limited by computing power, which was eliminated in the last decade by dramatic increases in processing power. This method was designed for spherical particles, so relative measurements were made in order to take complex particle shape, refractive index and measurement repeatability into consideration.

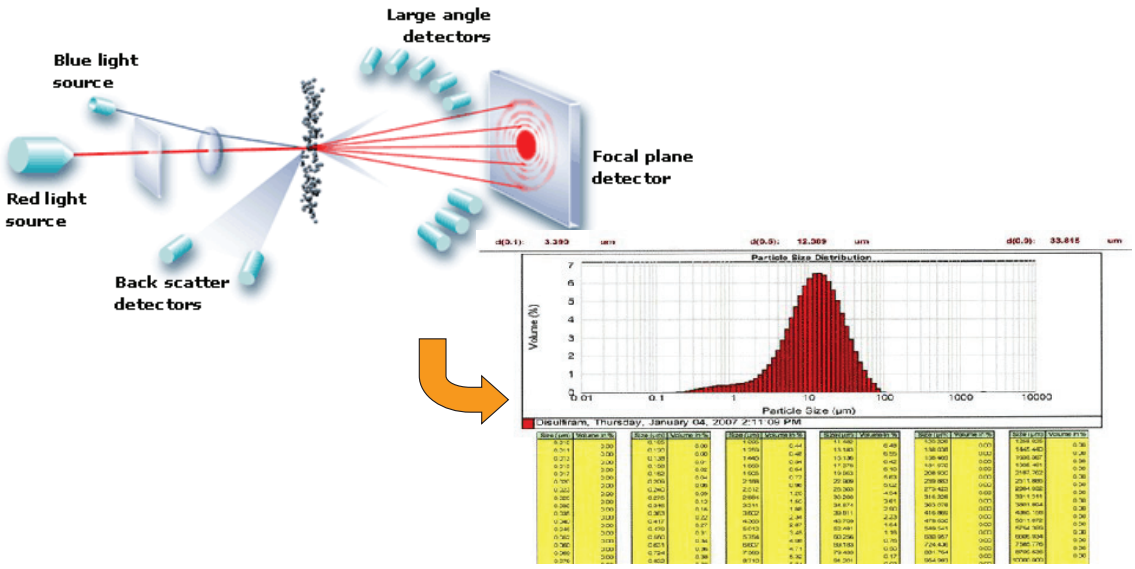

Figure 2-7: Operational principal of laser granulometer – Example of result presentation.

2.4.7.3 Morpho-granulometry (MG)

Fibre morphology was observed using a mopho-granulometer (Mastersizer G3S, Malvern Instruments Ltd. SN: MAL1033756, software Morphologi v7.21). This optical device includes a lens (magnification: from x1 to x50, dimension min/max: 0.2/3000µm), an optical system (Nikon CFI60 Brightfield/Darfield) and a camera (IEEE1394a, FireWireTM, 2592x1544pixels). This instrument allows:

- Capture of automatic and standard image
- On-line image treatment
- Analyse under "dry" or "wet" way

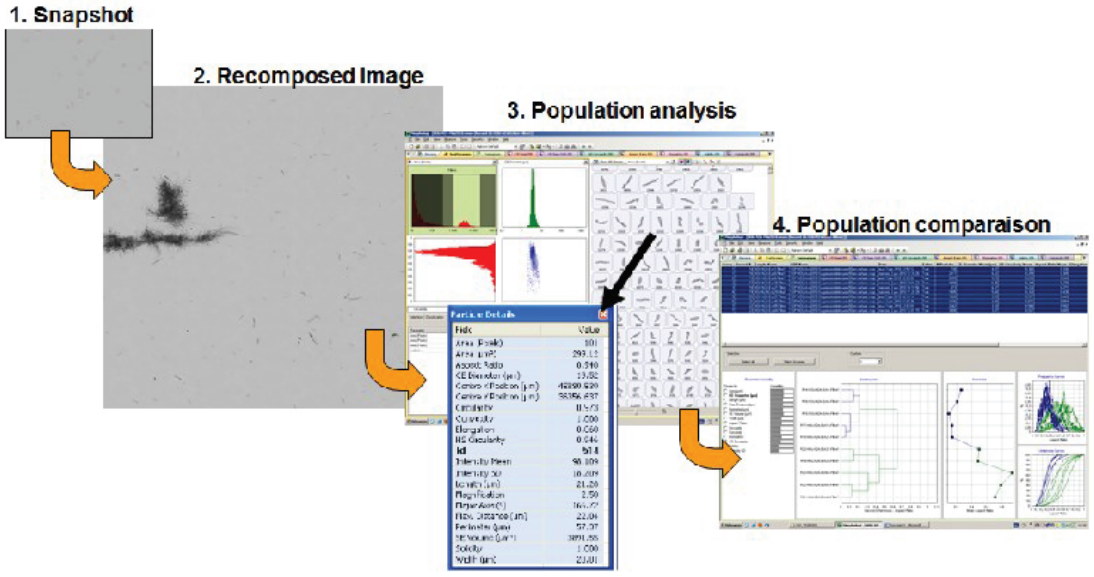

Figure 2-8: Principe and working step with Morphology G3S apparatus.

After image acquisition on a defined area, individual objects are identified and each of them analysed. Multiple dimensional and morphometric parameters are calculated for each particle and associated distributions are generated for each parameter. These parameters are: Circle Equivalent diameter, Mean diameter, Length, Width, Perimeter, Area, Aspect ratio

(width/length), Circularity, HS Circularity, Convexity, Solidity, Elongation, Major Axis, Max. Distance, SE Volume, Mean Intensity, Intensity Standard Deviation.

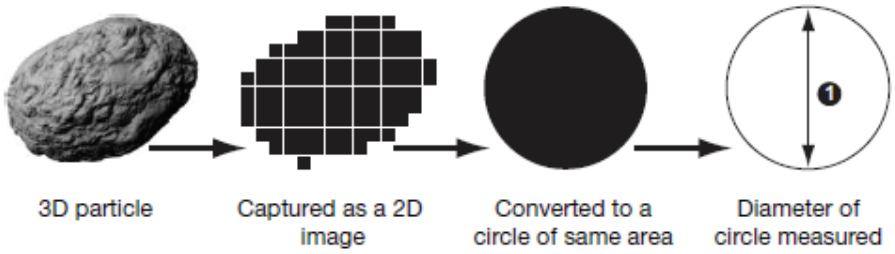

Figure 2-9: Data acquisition and image analysis of Morphology G3S.

Samples were analysed under "dry" and "wet" way. For "dry" analysis, the powder was dispersed using a specific dispersion unit (0.25mg substrate, 1.8bar). For "wet" analysis, the suspensions (approximately 5g.L^{-1}) were observed between cover glasses and slides. A 10mmx10mm surface was observed under standardized conditions (light intensity: 80±0.2; magnification: x2.5 and x10). The images were filtered and analysed to determine the number of particles and their geometric properties (diameter, aspect ratio, etc.).

Table 2-6: Main steps in SOP.

Sample carrier	Plate glass Compensate for plate tilt
Illumination	Diascopic light source Automatic light calibration with a calibration intensity: 80 ±0.2
Optic selection	Magnification x2.5 Measurement overlap 50% (between 2 pictures) Manual focus, no z stacking
Threshold	Threshold for particle detection (ranging 0-255): Threshold: 170, background around 180.
Scan area	Square area: 10x10mm² Enabling refine position before measurement.
Analysis setting	Soft analysis ID : 3.00 Trash size : 2 pixels (equivalent to 2.5µm²) Segmentation method: none No fill holes.
Filters	None

2.4.7.4 Focus Beam Reflectance measurement (FBRM)

Focus beam reflectance measurement enable in-situ quantification and characterisation of chord length distribution. The FBRM sensor (FBRM G400, Mettler-Toledo, range: 0.1 to 1000µm) is set up in the bioreactor for detect and monitor the changes of particle dimensions during enzymatic hydrolysis in real time. The FBRM measurement is a laser based technique. A solid-state laser light source (λ=795nm) provides a continuous beam of monochromatic light that is launched down FBRM® probe. An intricate set of lenses focuses the laser light to a small spot. This focal spot is carefully calibrated to be positioned at the interface between the probe window and the actual process. Tightly controlling the position of the focal spot is necessary for a sensitive and repeatable measurement. A precision motor - pneumatic or electric - is used to rotate the precision optics at a constant speed. The scan speed is fixed at 2 ms^{-1}. The focused beam scans a circular path at the interface between the probe window and

the particle system. As the scanning focused beam sweeps across the face of the probe window, individual particles or particle structures (agglomerated or floc) will backscatter the laser light back to the probe. Particles and droplets closest to the probe window will be located in the scanning focused spot and backscatter distinct pulses of reflected light. These pulses of backscattered light are detected by the probe and translated into Chord Lengths, based on the simple calculation of the scan speed (velocity) multiplied by the pulse width (time); a chord length is simply defined as the straight-line distance from one edge of a particle or particle structure to another edge. Thousands of individual chord lengths are typically measured each second to produce the Chord Length Distribution which is the fundamental measurement provided by FBRM®.

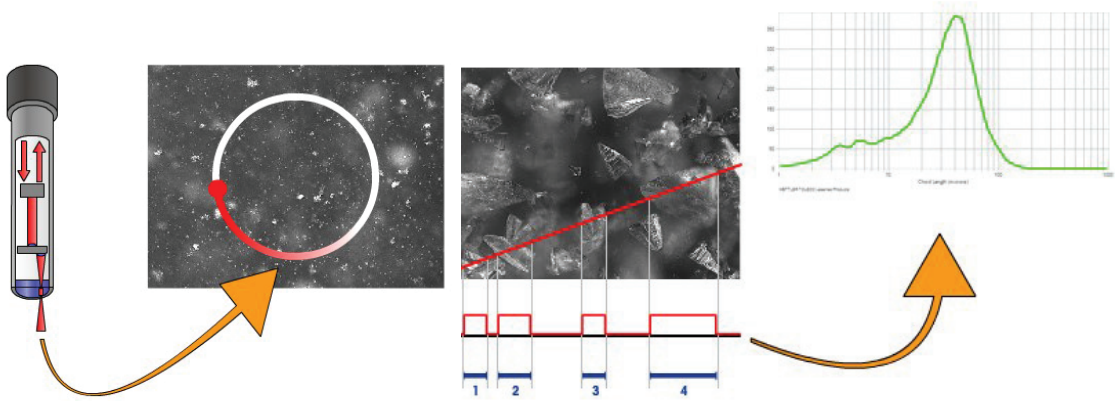

Figure 2-10: Operational principle of FBRM sensor from light signal up to CLD.

Differently from others methodologies (diffraction light scattering, morpho-granulometry), the focus beam reflectance measurement provides the chord length distribution (CLD). For easier comparison between the three methods, CLD should be converted into particle size distribution (PSD) based on theoretical consideration. Some modelling approaches for the generation of CLD from known PSD can be found in the literature (Barrett & Glennon, 1999; Ruf et al., 2000). Furthermore, solutions for the inverse problem of reconstructing a PSD from a CLD using these models have been addressed (Hukkanen & Braatz, 2003; Li & Wilkinson, 2005; Worlitschek & Mazzotti, 2004; Wynn, 2003). Many restrictive assumptions are necessary to obtain these models. They can be summarized as follows (Kail et al., 2007):

- All particles are identical in their shape and have a random orientation with respect to the laser beam.
- The time-averaged PSD in the scanning zone is equivalent to the actual PSD.
- If the laser beam crosses a particle at a distance less than a maximum detection depth, a chord is measured. Otherwise, no reflection is detected. The maximum detection depth is independent of particle size.
- The particle velocity relative to the probe is negligible compared to the velocity of the laser beam.
- The extension of the laser beam is negligible compared to the particle size.
- The three-dimensional particle field is reduced to a two-dimensional projection of particle silhouettes for further computation.
- The circular path of the laser beam in the medium is simplified to a straight line.
- Particle silhouettes do not overlap. Therefore, the chord length distribution of a particle size distribution can be generated from the chord length distributions of single particles.

- When a chord is traced across a particle's silhouette, the detected length is the entire length of the chord.
- The chord length is calculated from the time taken for the beam to cross the particle, divided by the laser beam velocity in the focus plane.

By considering spherical particles and applying above assumptions, it is possible to derive an analytical solution for transforming a known PSD into a CLD.
Considering a sphere of diameter D=2R, a chord l_c (**Figure 2-11**) could be formulated by **Eq: 2-34**:

$$\left(\frac{l_c}{2}\right)^2 + r^2 = R^2 \quad \textit{(Eq. 2-34)}$$

The radius distribution, $E_D(r)$ and cumulative distribution, $F_D(r)$ functions in number are for a sphere of diameter D:

$$E_D(+r) = E_D(-r) = \alpha = const \quad \textit{(Eq. 2-35)}$$

$$F_D(r) = \int_{-r}^{+r} E_D(r)\cdot dr = 2\cdot\int_{0}^{r} E_D(r)\cdot dr = \left[2\cdot\alpha\cdot r + a\right]_0^r \quad \textit{(Eq. 2-36)}$$

$$\textit{With}\ \begin{cases} r = 0 \Rightarrow F_D(0) = a = 0 \\ r = R \Rightarrow F_D(R) = 2\alpha\cdot R = 1 \Rightarrow \alpha = 1/2\cdot R \end{cases} \quad \textit{(Eq. 2-37)}$$

From **Eq. 2-34-37**, the chord distribution, $E_D(lc)$ and cumulative distribution, $F_D(lc)$ functions in number are deduced for a sphere of diameter D:

$$\begin{cases} For\ l_C \le D \Rightarrow F_D(l_c) = \left(1 - \dfrac{(l_c/2)^2}{R^2}\right)^{1/2} = \left(1 - \dfrac{l_C^2}{D^2}\right)^{1/2} \\ For\ l_C > D \Rightarrow F_D(l_c) = 1 \end{cases} \quad \textit{(Eq. 2-38)}$$

$$\begin{cases} For\ l_C \le D \Rightarrow E_D(l_c) = \dfrac{l_c}{D}\cdot\left(D^2 - {l_c}^2\right)^{-1/2} \\ For\ l_C > D \Rightarrow E_D(l_c) = 0 \end{cases} \quad \textit{(Eq. 2-39)}$$

Then, the chord distribution function in number could be expressed as follows for a distributed population of sphere:

$$E_n(l_c) = \frac{\int_{D=0}^{D=\infty} E_D(l_c)\cdot D^3\cdot E_n(D)\cdot dD}{\int_{D=0}^{D=\infty} D^3\cdot E_n(D)\cdot dD} \quad \textit{(Eq. 2-40)}$$

With En(lc) as the chord length distribution function in number and En(D) as the diameter distribution function in number. **Eq. 2-40** could be generalised in the form of matrices:

$$E_n(l_c) = E_v(d)\cdot A \quad \textit{(Eq. 2-41)}$$

The matric A is the reference matric of chord length (l_c) distribution as a function of sphere diameter D. As defined by conditions above, if the matric A is invertible, it is possible to estimate a PSD in number and volume from a CLD in number (**Eq.2-42**):

$$E_v(d) = E_n(l_c) \times A^{-1}$$ *(Eq. 2-42)*

To convert automatically and systematically the experimental data, a program Matlab was written and used in version Matlab R2012.

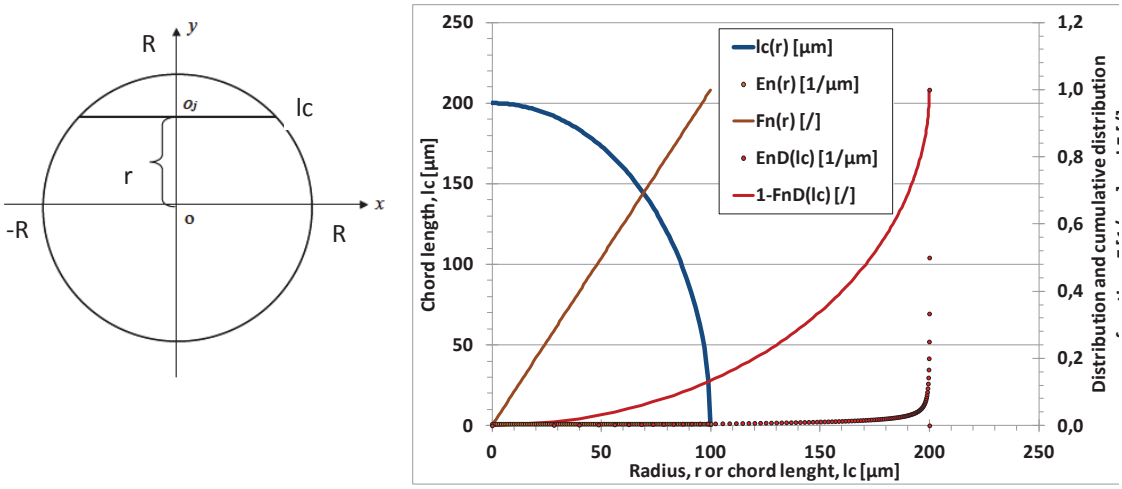

Figure 2-11: Chord cutting probability for a spherical particle – Evolution of chord length versus radius and evolution of chord length distribution and cumulative distribution functions in number versus chord length.

To summarise, the particle size analysis could be realised by four different optical methods: in-situ focus beam reflectance, diffraction laser scattering, microscopy and transmission & backscattering light (**Table 2-7**). Each technique presents several advantages and drawbacks associated to principle of technique, sample preparation, assumption used for signal treatment and data treatment and transformation. The FBRM allows monitoring in-situ and in real time the evolution of chord length during hydrolysis. Its sensor is easily implemented inside the bioreactor but raw data are based on numerous assumptions. A post-treatment to convert CLD into PSD should be realised in order to compare diameter distributions issued from different techniques. The DLS and Turbiscan Lab are limited by sample numbers and the conditions which are taken as references. The change of optic properties of fibres predominately affects to obtained results from these methods. The morpho-granulometry appears as the most reliable technique. It takes less theoretical hypotheses than other methods into account but their disadvantages come from the sample preparations (fibre dissociation) and the important quantity of data to process after measurements. The four techniques are associated to four different approaches to characterise the particle size and shape. In consequence, we developed a methodology to compare the results of these methods.

Table 2-7: Summary of particle size analysis techniques.

Method	FBRM	DLS	Morpho-granulometry	Turbiscan Lab
Measurement mode	In-situ	Ex-situ	Ex-situ	Ex-situ
Sample preparation	None	Dilution	Ultrasound + Dilution	None
Analyse	2D	3D	2D	3D
Measured quantity	l_c	D_{SE}	D_{CE}	d_s
Distribution	Number	Volume	Number	Volume

2.5 Methodology

2.5.1 Study strategy

This study aims to investigate the destructuration of fibre during enzymatic hydrolysis. Our strategy is built on a multi-scale approach using in-situ and ex-situ physico-chemical measurements. The lignocellulose matrices and their hydrolysis potentials were examined by considering various physical and biochemical analysis. **Figure 2-12** illustrates the three blocs corresponding to the three levels of observation: macro-scale with viscosimetry and rheometry, micro-scale with granulometry (DLS, PSD, CLD, d_s) and molecular scale with biochemistry (chemical analyses of soluble fraction and solid fraction).
The tripod frame leads to analyse and to compare the in-situ and ex-situ methods (excluded biochemical analysis). Then phenomenological models could be established and discussed in light of theory before to embrace all results and to provide a full overview of implied mechanisms. In this regard, the phenomenological models should respond to criteria, such as reliability, simplicity and homogeneity with the experimental information.

- for rheometry: integration of a phenomenological model of rheological behaviour considering volume fraction, size and shape of particles;
- for granulometry: morpho-granulometric analysis and associated distribution functions (mass and population balances);
- for biochemistry: integration of biochemical kinetic models.

A global result synthesized from these three blocks could provide a "knowledge block" to explain some scientific locks and lead to the implementation and intensification of new bioprocesses.
To respond to these scientific goals, this work is structured around three main actions:

- Matrices characterisation and rheology of suspensions,
- Hydrolysis under favourable conditions,
- Hydrolysis under high concentration with a strategy based on cumulative substrate adds.

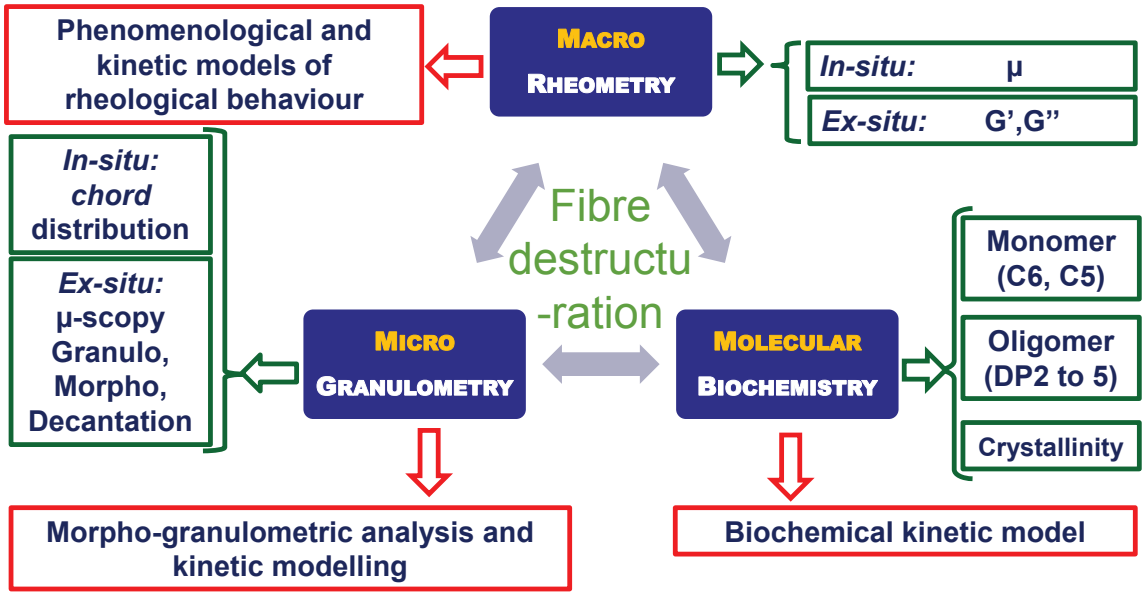

Figure 2-12: Experimental methodology and strategy.

2.5.2 Characterisation of substrates and rheology of suspension

Under the objective of knowledge development for fibre destructuration during hydrolysis, we choose five different matrices: MCC, BAG, WP, PP-27 and PP-31. To highlight the impact of matric on hydrolysis, it is necessary to characterise these substrates. Therefore, different physico-chemical-biological properties were determined (as presented above). This step will give us a general view for each matric mainly their level of complexity which could determine the bioconversion rate.

Firstly, we evaluate the interaction between the physical and chemical structure of the solid phase and performance of the bio-catalytic conversion by integrating the dynamic state change (transition from a solid state to a soluble state). The rheological characterisation of initial suspensions was investigated. This analysis consisted in suspending the substrates in 1300ml of water. Each cycle of suspension is composed of (i) a homogenization phase (100rpm for 300s) with substrate addition and (ii) torque measurement based on 100s phase with increasing and decreasing mixing rates (10, 50, 100, 155, 200, 300, 500, 650 and 800rpm) within viscometer torque capacity (N_{max}=800rpm, $C_{max}\approx$ 30 mN.m). The concentration chosen for a given experiment was reached by successive additions of substrate: 8x20g for MCC, 7x3g for WP, 11x12g for PP and 9x20g for BAG.

Secondly, the obtained results were used to build the phenomenological models which performed the relationship between suspension viscosities, shear rate and substrate concentrations. The goal is to give a unique model for each substrate, no matter the substrate concentration and the shear rates are. This model could be established using power-law model, Einstein model and Quemada's approach. All of this will be shown in chapter 3. When the model was established, we could try to determine the yield stress and critical concentration which indicated the transition between different regimes. Finally, the results of in and ex-situ measurement could be compared and discussed.

2.5.3 Enzymatic hydrolysis

Enzymatic hydrolysis were carried out at 40°C due to thermal enzymatic stability (activity reduction at high temperature); energy saving and considering the microbiological step during the fermentation process which will be added considering a simultaneous saccharification and fermentation (SSF) operation. The pH of the medium was adjusted to 4.8 using a solution of 85% ortho-phosphoric acid. To avoid contamination, 20µL of a solution of chloramphenicol ($5g.L^{-1}$) was added. Then enzymes were added when the suspension reached homogeneity and when the torque value was stabilised. Two strategies of hydrolysis were applied: in dilute condition (favourable condition) and with a cumulative feeding strategy of substrate.

In a first step, corresponding to favourable conditions, hydrolysis was investigated over 24h for the five substrates with a mixing rate of 100 rpm and using two substrate concentrations, 1% and 3%w/v, two enzyme/substrate ratio, 0.1 and 0.5mL enzyme/g cellulose (**Table 2-8**) (Experiments at 2% substrate for PP and WP were limited to viscosity investigation). These concentrations were chosen to obtain a significant initial torque (C>=2mN.m) and to ensure accurate monitoring of its derivation during hydrolysis. These concentrations ensure initial laminar regimes for WP and PP and transitional regime for MCC and BAG. They also correspond to a dilute regime that facilitates the enzyme attack.

These experiments for dilute concentration of matrices with two enzyme concentrations were carried out to explore the impact of substrate nature and enzyme ratio on fibre destructuration kinetics (bioconversion rate). After the consistency between physical properties (rheological behaviour, particle size) and hydrolysis kinetics (production of monomers) were analysed. This scientific information was used to define operating conditions for hydrolysis up to high concentration.

Table 2-8: Investigated operating conditions at low substrate conditions.

Substrate		MCC		WP		PP-27		PP-31		BAG	
Enzyme		0.1	0.5	0.1	0.5	0.1	0.5	0.1	0.5	0.1	0.5
	1%	X	X	X	X	X	X	X	X	X	X
Concentration	2%	-	-	X	X	X	X	X	X	-	-
	3%	X	-	X	X	X	X	X	X	X	X

Based on the results obtained in this first part of the study, a second part was developed to reach high concentration with a cumulative feeding strategy for substrate. Hydrolysis was investigated over 24h with PP-27 and WP. Enzyme and substrate adds were realised simultaneously each 30min (for WP) or 1h (for PP) which will be equivalent to three different flow rates (0.5mL enzyme/g cellulose) until total substrate concentration reached 10%. In addition, one experiment with total enzyme adds at initial time was done for PP-27. The aim was to increase the substrate concentration during hydrolysis in limiting the energy consumption. Beside it, we want to confirm the relationship between three blocks of parameters: rheology, morpho-granulometry and biochemistry for enzymatic hydrolysis.

In both strategies, suspensions were sampled with a 7mm diameter flexible connected to a 50mL syringe. In favourable condition, each sample was about 15mL for the moment of 0h, 15min, 1h, 2h, 3h, 5h, 7h, 10h and 24h of hydrolysis time. For feeding cumulative substrate strategy, one sample of 2mL (for biochemical analysis only) was taken before each substrate adds and one sample of 15mL was taken at 0h, 5h, 10h and 24h of hydrolysis time. The enzymatic reaction was stopped by add of 0.1mL NaOH 10N. The total volume of samples removed for both of two cases was approximately 130 mL (<10% of initial volume). This order of decrease of suspension volume causes negligible impact on the suspension viscosity (at the end, a difference of 1% to 7% may be observed). The samples were used for rheological, granulometric and biochemical analysis during enzyme degradation.

For characterisation of fibre in suspension and fibre destructuration during enzymatic hydrolysis, several of analysed methods were applied: two techniques in and ex-situ for three different parameter blocks. Then, the data treatment was investigated by crossing each of technique and blocks (**Figure 2-13**). A global view could be obtained as a summary of all of measured results.

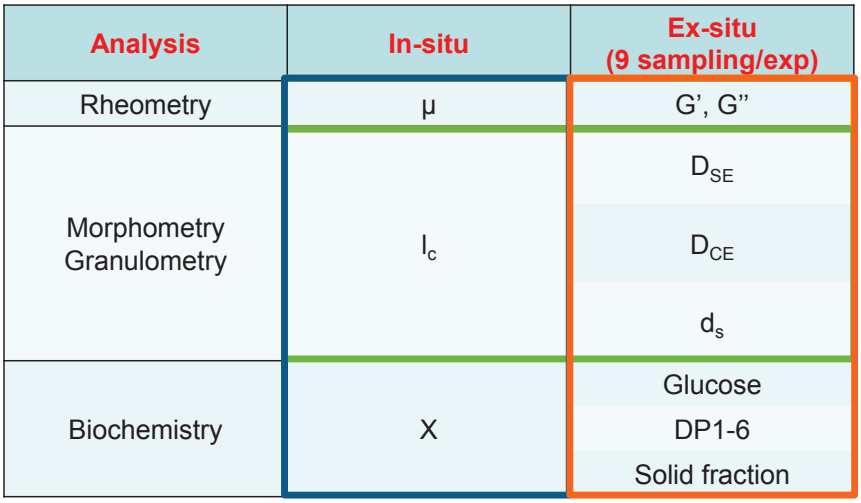

Figure 2-13: Data exploitation strategy.

3 RESULTS AND DISCUSSIONS

Table 3-1 summarises the aims, challenges and proposed strategy and methodology used in this work. The scientific complexity of the project corresponds to two degrees of freedom of the study related to (i) matrices (nature, structure, composition) and (ii) bio-catalysis operating conditions (high dry matter content, transfers and inhibition). The originality of our approach is based on:

1. The matrices considered which constitute a real economic and technological issue (paper pulp),
2. The study was carried out at substrate concentrations ranging from dilute up to high,
3. Multi-scale investigations using state-of-the-art analytical technologies involving a pluri-disciplinary approach (process engineering, bioengineering, fluid mechanics, chemical analysis and biochemistry),

Table 3-1 : Overview of scientific issues.

Overarching aim	- To improve bio-catalytic destructuration of lignocellulose biomass to produce concentrated fermentable substrates - To alleviate the scientific bottlenecks that lead to the development of new intensified bioprocesses.
Critical challenges	- Related to the development of phenomenological descriptions of the bio-catalytic processes that occur in industrial conditions.
Approach	- State of the art analytical technologies, coupled to significant methodological developments, and a multidisciplinary approach - To involve scientists possessing expertise in process engineering, bioengineering, fluid mechanics, chemical analysis and biochemistry.

The overarching aim of this thesis is to provide a "knowledge building-block" that will alleviate the current scientific bottlenecks and lead to the development of new intensified bioprocesses. The critical challenges in this work are related to the development of an integrated multi-scale (from molecular up to macroscopic scale) dynamic characterisation of the bio catalytic processes that occur under realistic industrial conditions.
In this chapter firstly the results obtained on initial and hydrolysed substrate suspensions are reported and secondly, the results are analysed more deeply and the scientific conclusions summarised. It is divided into two parts: sections 3.1 and 3.2 present “raw” data from these in-situ and ex-situ measurements; then analysis and discussion is developed in section 3.3.

3.1 Overview of substrates and experiments

In this first part, our aims are:

- To describe the raw material through biochemical, physical and thermal analyses.
- To provide the reader a full overview of the experiments and analyses conducted
- To illustrate each experimental results per analyses.

Each raw material was characterised by biochemical (composition, water content, and ash), physical (density, crystallinity, surface tension, decantation kinetics, granulometry) and thermal (calorimetry, thermogravimetry) analyses before experiments and/or during hydrolysis in various operating conditions. This chapter gives a general and multi-dimensional view of fibre restructuration before and during enzyme attack. When possible, a comparison between in-situ and ex-situ measurements is used to highlight changes in suspension viscosity, viscoelasticity, particle size, biological conversion and crystallinity.

3.1.1 Thermal, physical and chemical characterisations of the initial substrates

The first results presented are the thermo-physical-chemical characterisations (**Table 3-2**) of five substrates (**Figure 3-1**) ranked as a function of cellulose content.

- Chemical/Biochemical composition: water content, biochemical composition, ash content.
- Physical properties: morphological characterisation, equivalent diameter (DLS, morphology), hydrodynamic diameter, density, crystallinity and surface energy.
- Thermal properties: specific heat capacity, thermogravimetric destructuration.

The range and variability of the characteristic properties argue that the matrices selected should be suited to various operating conditions from hydrodynamic and bio-catalytic standpoints. They enable investigation of the impact of fibre morphologies, biochemical composition and structure and particle size distributions.

MCC

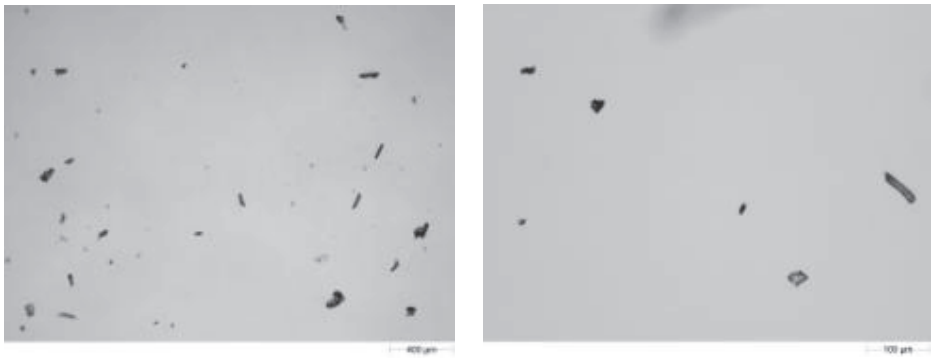

WP

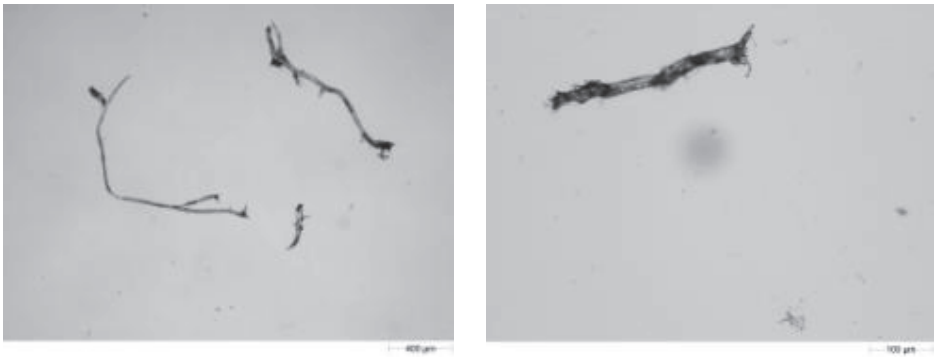

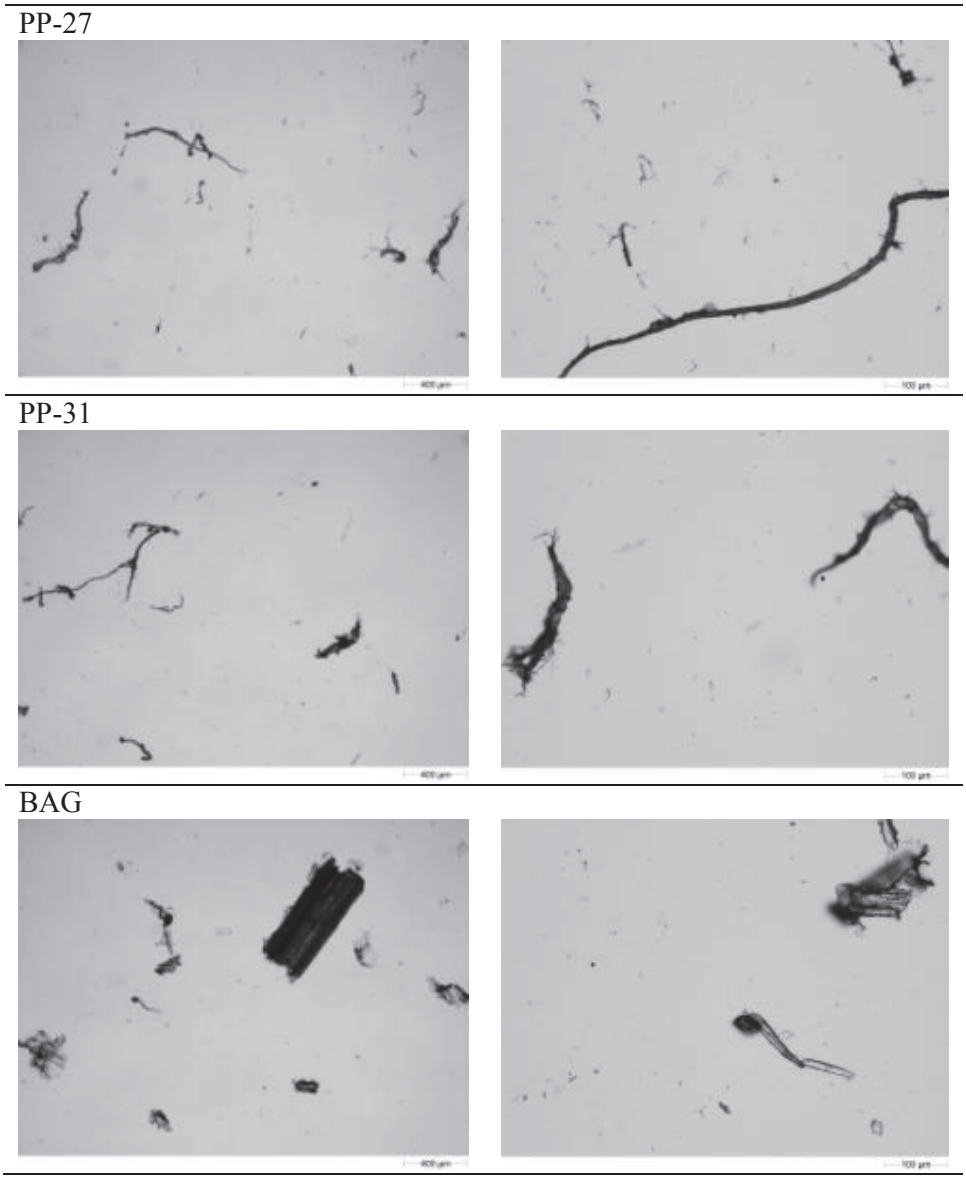

Figure 3-1: Microscopic observation of substrates (Morphology G3S, wet way, sample between slide and coverslip, diascopic illumination, optical magnification: left column x2.5 and right column x10). MCC: microcrystalline cellulose; WP: Whatman paper; PP-27: softwood paper pulp; PP-31: hardwood paper pulp; BAG: sugarcane bagasse

- Biochemical and chemical properties:

In **Table 3-2**, substrates are ranked in increasing order of cellulose content. They all exhibit a cellulose content ofover 75% of the dry matter except for bagasse (47%). **Table 3-3** compares our experimental data with existing literature.

Even though WP (Whatman paper) is not identified as a common substrate for second-generation biofuels (lack of data regarding hydrolysis), its initial composition is reported in literature (Kadolph & Langford, 1998; Samaniuk et al., 2011) and appears to be in agreement with our own data.

Paper pulps, PP-27 and PP-31, are coniferous (soft) and deciduous (hard) wood pulps after thermo-chemical and physical pre-treatment. The Kraft process consist in treating wood chips with a mixture of sodium hydroxide and sodium sulphide, known as white liquor, that breaks the bonds that link lignin to cellulose. Soft and hard wood paper pulps mainly differ in

hemicellulose content with respectively 8.0 and 19% and both have a negligible lignin content (<2.5%). and a high cellulose content (>75%) with a high degree of macroscopic restructuration. With paper pulps, overall results are very consistent with literature data (Lacerda et al., 2012; Le Moigne et al., 2010; Tu et al., 2009; Zhang et al., 2009).
Bagasse results from a single mechanical pre-treatment (milling). Consequently its composition and structure are close to that of a raw material with hemicellulose and lignin contents respectively around 30% and 20%. Our bagasse compositions (**Table 3-3**) are of the same order of magnitude as that reported by several authors (Carvalho et al., 2013; Mosier et al., 2005; Pereira et al., 2011). Considering the biochemical composition, the substrate complexity significantly increased from MCC and WP to PP27 and PP31 up to BAG.
Initial dry content is also an important parameter in industrial bioprocesses. In agro-food processes, water removal consumes energy and has an economic and environmental impact. The use of raw industrial or pre-treated material is consequently preferred. In our case, model matrices MCC and WP contain very little water (<1%) whereas our model industrial substrates (PP27 and PP31) contain around three-quarters water. Similar results were reported in the bibliography (Palmqvist et al., 2011; Szijarto et al., 2011; Tu et al., 2009; Wiman et al., 2010) for these industrial products. Bagasse exhibits a lower but significant water content (around 9%).

Table 3-2: Thermal, physical and biochemical properties of the substrates.

Matrices		MCC	WP	PP-27	PP-31	BAG
Biochemical-chemical composition						
Cellulose (%)		100	90	82	75	47
Hemicellulose (%)		-	-	8	19	29
Lignin (%)		-	-	2	2	21
Ash (%)		0.01	0.02	1.50	0.97	1.26
Dry matter (%)		99	99	28	26	91
Physical properties						
D[4,3] (µm) (DLS)		100±17	363±40	497±77	471±88	230±33
D[4,3] (µm) (Morphogranulometry)		105	312	187	222	352
Stockes's diameter (µm)		41	nd	nd	nd	63
Aspect ratio (width/length)		0.61 ± 0.03	0.45 ± 0.03	0.60 ±0.02	0.60 ± 0.02	0.61 ±0.02
Density, ρ_{HM} (kg.m^{-3}) at 20°C		1623±28	1200±2	1034±9	1025±8	1100±7
Density, ρ_{DM} (kg.m^{-3}) at 20°C		1633	1202	1133	1103	1110
Crystallinity (%)		82.4	90.7	76.8	78.3	57.1
Thermal properties						
Specific heat (J.kg^{-1}.K^{-1})		1356	1417	1361	1373	1653
Thermogravimetric analysis						
Pic 1	Tp (°C)	310	340	291.6	-	213.6
	dW (%)	~90	~75	~45	-	~45
Pic 2	Tp (°C)			330	-	260-300
	dW (%)			~10-15		~30-35
Pic 3	Tp (°C)					326.3
	dW (%)					~45
Surface energy						
Dispersive surface energy (mN.m^{-1})		43.6	45.5	43.2	44.6	37.2
Polar surface energy (mN.m^{-1})		21.4	22.2	21.7	21.0	12.2
Total surface energy (mN.m^{-1})		65.0	67.7	64.9	65.6	49.4
Surface free energy (solid-water, mN.m^{-1})		10.1	10.2	9.8	10.6	15.4

Gibbs energy ($mN.m^{-1}$)	-127.7	-130.3	-127.9	-127.8	-106.8

(MCC: microcrystalline cellulose; WP: Whatman paper; PP-27: softwood paper pulp; PP-31: hardwood paper pulp; BAG: sugarcane bagasse).

- Physical properties

Various physical properties of the initial matrices (morphology, granulometry, density, crystallinity and surface energy) were determined. Viscosimetry of the suspensions was dealt with separately and is presented in a §3.2.1. In future studies it could also be interesting to investigate porosity and specific surface area.

Crystallinity refers to the degree of structural order in a solid and is usually specified as a percentage of the volume of the material that is crystalline. The ratio between amorphous/crystalline cellulose is generally thought to provide information about the level of difficulty to enzymatically degrade a substrate but this simple vision is subject to controversial publications. Agarwal et al. (2012) reported an inverse linear relationship between the hydrolysis yield and CrI (crystallinity), i.e., the higher the CrI the lower the amount of cellulose that can be saccharified (for Whatman paper hydrolysis). In contrast, Bommarius et al. (2008) studied the hydrolysis of MCC and showed that the degree of crystallinity of cellulose in the samples does not appear to impact cellulase activity, suggesting that cellulose activity is not confined to non-crystalline regions. In our matrices, the CrI increased with level of biomass treatment: BAG<PP-27=PP-31<MCC<WP. With paper pulp, the same degree of crystallinity around 78% was found for both of PP-27 and PP-31. This value corresponds to that of Lacerda et al. (2012) reporting CrI=77% but is higher than (Le Moigne et al., 2010) with CrI= 46-49%. These differences could be explained by the origin of the material, the sample preparation method and the substrate pre-treatment (Stewart et al., 1997).

Densimetry brings useful additional information since it highlights the compactness or porosity of a material. The deviation of intrinsic density constitutes an indicator of hydrolysis susceptibility which could be discussed versus morphological and granulometric parameters. Densities of humid and dried material are reported in **Table 3-2**. As expected, the density of humid matter decreases as water content increases. The density of dried matter enlarges structural information. MCC and WP have higher densities, 1635 and 1202 $kg.m^{-3}$ compared to PP27, PP31 and BAG with a similar average density equal to 1100 $kg.m^{-3}$. This value for MCC was in full agreement with the literature. The intrinsic density of MCC ranges from 1512 to 1668 $kg.m^{-3}$, while the true density of a perfect cellulose crystal is 1582 and 1599 $kg.m^{-3}$ for alpha and beta polymorphs. Therefore, because native cellulose of higher plants is a mixture of alpha and beta cellulose, the true density of a 100% crystalline natural cellulose is between 1582 and 1599 $kg.m^{-3}$ (Sun, 2005) or Lu et al. (2014) reporting ρ=1560 $kg.m^{-3}$. However, the density of the humid BAG and PP are different from data found in the literature. Damani et al. (1993) gave a value of 356-538 ($kg.m^{-3}$) for PP and Pereira et al. (2011): 1420 ($kg.m^{-3}$) for BAG. MCC was the most compact substrate among the five studied. Its density is more than 45% higher than BAG, PP-27 and PP-31, and 33% higher than WP. This may account for the rapid decantation of MCC in suspension.

The surface energy (**Table 3-2**) showed that four substrates: MCC, WP, PP-27 and PP-31 exhibited similar values. Only BAG presented a surface energy that was notably different (about 25% that of the other matrices). This difference stresses the complexity of this natural substrate.

Beside biochemical differences, the substrates exhibit various morphologies and dimensions (**Figure 3-2**) as indicated by the distribution and the mean values of diameter, length, aspect ratio, circularity, etc. As described in §1.4.7, several techniques and particle equivalent diameters can be used. In our case, 3 ex-situ methods were investigated: (i) diffraction light

scattering (DLS), (ii) morpho-granulometry and (iii) falling velocity measurements, to estimate respectively sphere equivalent, circle equivalent and falling (hydrodynamic) diameters. For example, **Figure 3-2** reports the volume distribution function of sphere-equivalent diameters for the five initial substrates from DLS measurements. MCC and BAG indicate the same unimodal population whereas bimodal populations are observed with WP, PP-27 and 31. From **Figure 3-1**, MCC fibres appear as dense crystalline particles with an angular shape (rectangle, square) resembling crystals. BAG particles are larger than MCC, look like rectangular parallelepipeds or crystals resulting from a coarse milling. WP, PP-27 and PP-31 include long fibres with ramifications. Aspect ratios decreased from MCC to WP: 0.61 ± 0.03, 0.61±0.02, 0.60 ± 0.02, 0.60±0.02 and 0.45 ± 0.03 for MCC, BAG, PP-27, PP-31 and WP respectively.

Table 3-3: Biochemical compositions (%w/w) of Whatman paper, paper pulp and bagasse in recent literature.

Substrate	References	Cellulose (%)	Hemicellulose (%)	Lignin (%)	Ash (%)	Remarks
WP	(Kadolph & Langford, 1998)	95.0	-	-	-	
	(Samaniuk et al., 2011)	99.0	-	-	-	
PP	(Palmqvist & Liden, 2012)	50.2	6.4	36.8	-	Steam exploded pre-treatment
	(Pereira, 1988)	67.6	7.3	4.3	0.2	
	(Lacerda et al., 2012)	88.0	12.0	-	-	Sisal pulp - Kraft
	(Silva et al., 2011)	50.0	20.0	15.0	-	Eucalyptus wood
	(Prasad et al., 2007)	60.0	21.6	18.0	-	Organosolv pre-treatment
	(Wiman et al., 2010)	48.0	3.0	45.0	-	Steam exploded pre-treatment
	(Le Moigne et al., 2010)	90.0	3.5	1.8	-	
	(Zhang et al., 2009)	79.3	19.6	1.0	-	
	(Tu et al., 2009)	91.2	2.0	5.9	-	
BAG	(Carvalho et al., 2013)	88.2	-	5.4	0.7	Steam exploded pre-treatment
	(Mosier et al., 2005)	42.1	23.6	23.7	-	
	(Pereira et al., 2011)	43.6	8.8	33.8		

DLS granulometry showed that the mean volume diameters increased significantly from MCC to PP-27: 100±17, 230±33, 363±40, 471±88, and 497±77 µm for MCC, BAG, WP, PP-31 and PP-27 respectively. The mean diameter and the distribution of diameters are in agreement with the various preparation methods. The ranges covered by our five matrices are close to those of the majority of works reported in the literature (**Table 1-8** – Bibliography synthesis) which varied between 30 and 1000µm. The D[4,3] of PP-27 is similar to that of PP-31 but their standard deviation is high (~80µm) due to the configuration of the extruder, and hard of fibre dissociation during measurement. For MCC (often used as model material), this value is comparable to literature (Luukkonen et al., 2001; Rosell et al., 2009; Um & Hanley, 2008). However, for bagasse, the diameters found in the bibliography, are higher than our result. Pereira et al. (2011) worked with bagasse particles with a diameter of 2000µm; Geddes et al. (2010) used a 2500µm of bagasse particles. For PP, our results are in the same range as in the studies of (Samaniuk et al., 2011; Wiman et al., 2010). Other authors presented different results with the lowest value of 30µm (Bennington et al., 1990; Chen et al., 2003) up to the highest value of 1000-3000µm (Blanco et al., 2006; Chaussy et al., 2011; Damani et al., 1993; Derakhshandeh et al., 2010).

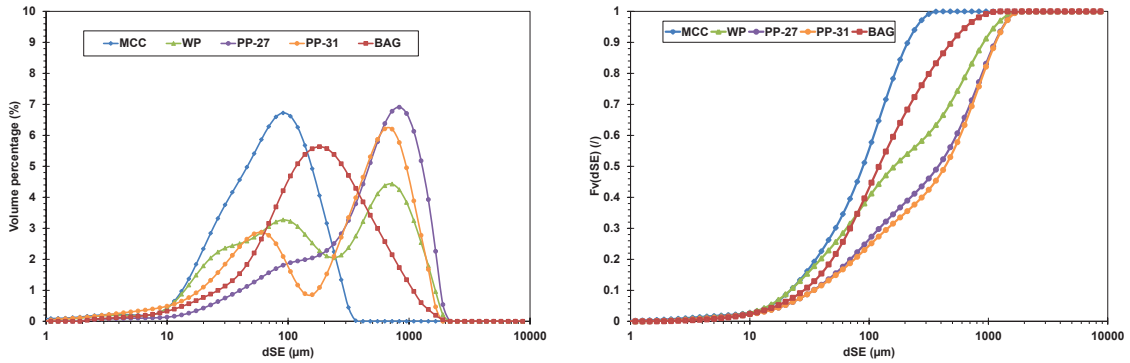

Figure 3-2: Volume distribution (left) and Cumulative volume distribution (right) of particle size for five substrates (DLS analysis).

- Thermal properties:

Lignocellulose matrices have been characterized with two additional thermal properties: (i) specific heat capacity and (ii) thermo-gravimetric restructuration. The literature reports a specific heat around 1546 $J.kg^{-1}.K^{-1}$ for cellulose. Our experimental measurements (mean values between 20 and 65°C) are coherent with the literature and consistent with the biochemical composition. MCC, WP, PP-27 and PP-31 have similar values whereas BAG exhibits higher values. For each matrix, high thermal dependency was noted.

Thermal analysis may be defined as a set of techniques used to describe the physical or chemical changes associated with substances as a function of temperature. It also informs about the structural and biochemical composition of the material as reported by Tsujiyama and Miyamori (2000) with cellulose/hemicellulose and lignin mixtures. Thermo-gravimetric analysis of MCC, WP, PP-27 and BAG was carried out and the pyrolysis characteristics, both TG (in weight %) and DTG (in $\%.°C^{-1}$) curves, of the four matrices are shown in **Figure 3-4** and analysed in **Table 3-2**. There are obvious differences between their behaviours.

With BAG, curves are defined by the pyrolysis of hemicellulose started at 220°C; its mass-loss rate (DTG curve) increases greatly with increasing temperature and reaches its maximum value at 260 °C. When the temperature is over 350°C, its weight-loss rate is low and the amount of solid residue left is high (>20%dm). The pyrolysis of cellulose is focused on a temperature range of 315-390 °C and lignin degradation requires temperatures higher than 400°C (Beall, 1971).

With PP, a first loss occurs around 290°C of 45% of weight and a second around 330°C of 10-15%. The solid residue remains greater than 30% above 350°C. This suggests a recalcitrant fraction.

With MCC and WP, which are almost pure cellulose, a single sharp mass loss is observed at 310 and 340°C respectively.

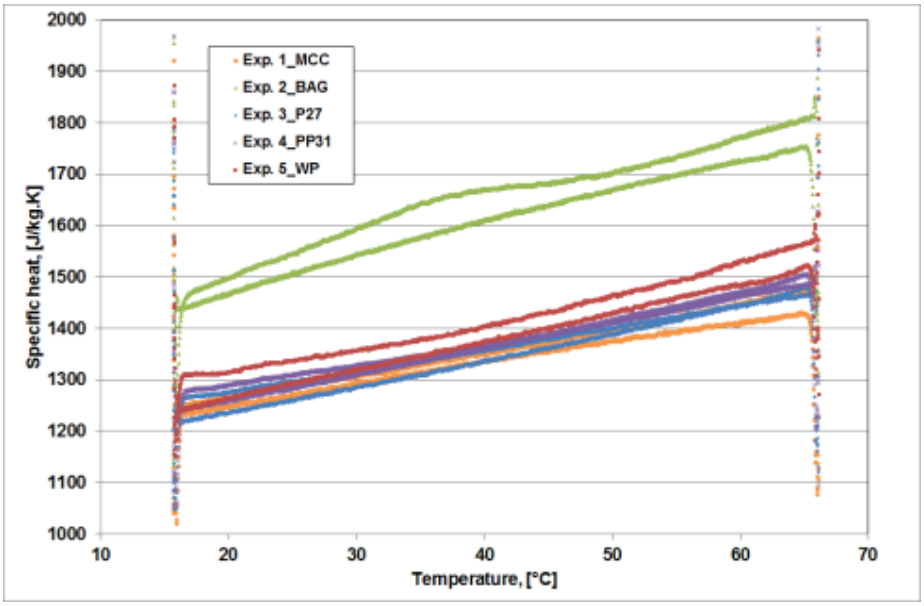

Figure 3-3: Specific heat capacities of MCC, WP, PP27, PP31 and BAG versus temperature (15 to 65°C).

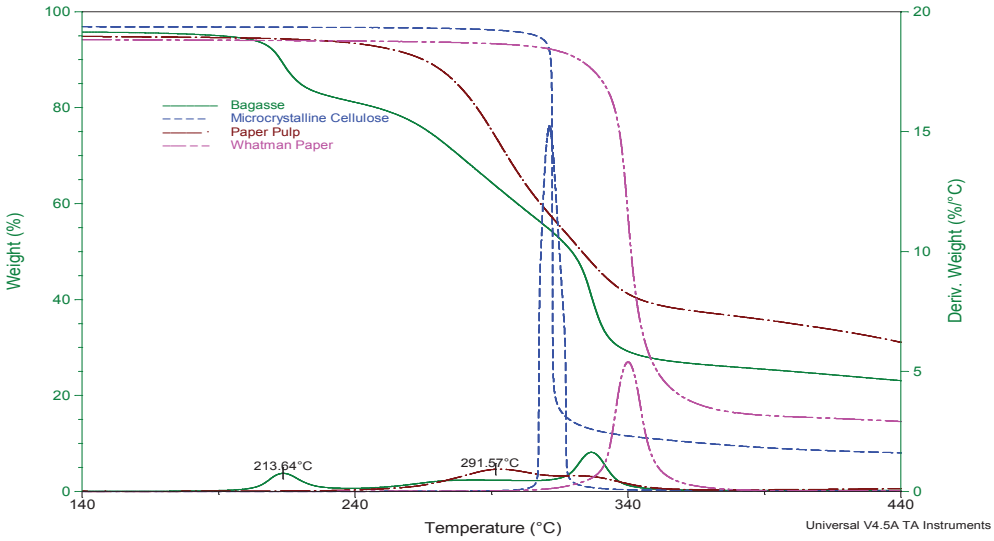

Figure 3-4: TG (in weight %) and dTG (in %°C^{-1}) curves as a function of temperature for MCC, WP, PP27 and BAG.

Considering the thermal, physical and biochemical criteria, these five matrices were ranked and are presented in **Table 3-4**. Globally, PP-27 and PP-31 present as the most promising substrate to convert into fermentable sugars in industrial bioprocesses. Among their biochemical properties, they have a high cellulose content with low lignin and inhibitors. Their physical properties include a low density and crystallinity. They are more easily degraded by heat than other substrates. However, because of their complex shape and size, mixing in suspensions requires more energy and know-how to obtain a homogeneous

suspension. These paper-pulps could be produced on a large scale and are favourable for bioethanol production in an industrial setting.

Table 3-4: Ranking of cellulose matrices versus physical, thermal and biochemical criteria in relation with hydrolysis bioprocesses (red: unfavourable; green: favourable).

Properties			MCC	WP	PP-27	PP-31	BAG
Industrial reliability							
Physical properties	Intrinsic density						
	Crystallinity						
	Diameter	Specific area					
		Suspension					
	Shape	Specific area					
		Suspension					
	Surface energy						
Thermal properties	Specific heat						
	Thermogravimetry						
Biochemical properties	Composition						
	Water content						

3.1.2 Hydrolysis experiments: from raw data up to scientific analysis.

This section provides an overview of all the hydrolysis experiments (operating conditions, physical and biochemical analysis). The experimental cartography defines the "raw data", and the results obtained from *in-situ* and *ex-situ* measurements (**Table 3-5**). Then, analysis and data treatment provide new and pertinent information supported through comparison with other analyses.

Table 3-5: Cartography of experimental strategy in relation with existing knowledge and industrial objectives.

Scale	In-situ	Ex-situ	
Macro	Viscosimetry	Oscillation (G', G'')	⇨ Rheological behaviour
Micro	Chord distribution	DLS Morpho-granulometry Falling diameter	⇨ Morphology and granulometry
Micro et molecular	∅	Dry matter, Concentration profile Monomer (C6, C5) Oligomer (DP<6)	⇨ Mass balance and biochemistry
↓			
Integration of "knowledge building blocks" dedicated to the dynamic description of consolidated and new intensified bioprocesses			

For example, in-situ rheometry basically uses torque and mixing rate measurements (raw experimental data) during experiments (suspension or hydrolysis). Knowing the power consumption curve leads to the construction of the flow curve (shear stress vs shear rate) and rheogram (viscosity vs shear rate) considering the restrictive assumption (laminar regime). A first level of analysis will consist in describing the rheological behaviour of suspensions under defined conditions (material, concentration, hydrolysis rate, temperature). A second level will establish a consolidated model ("knowledge building blocks") related to rheological behaviour by integrating additional parameters such as concentration, mean diameter,

morphological criteria, particle distribution, etc. A final step will compare in-situ and ex-situ measurements in order to assess the consistency of the two methodologies (average viscosity) and to highlight complementary criteria (flow threshold).
Table 3-6 gathers for all analyses, the links between raw data, experimental results and analyses and **Figure 3-5** (**Annexe 5**) illustrates this approach.

Table 3-6: Raw data, results and analyses carried out for all measurement techniques used

	Raw data	Results	Analyses
In-situ rheometry	Viscosimetry (torque, mixing rate)	Shear stress vs shear rate Viscosity vs shear rate	Rheological behaviour
Ex-situ rheometry	Oscillation (torque, deformation, amplitude, frequency	Elastic and viscous modules vs shear stress and frequency.	Viscosity, yield stress, rheological behaviour
Decantation kinetics	Transmitted and backscattered signals versus height and time.	Concentration profile vs time and height. Falling velocity	Falling diameter, size distribution, mass balance, critical settle concentration.
In-situ chord length measurement	Chord length distribution versus hydrolysis time	$En(l_c)$ vs time, chord number $N(l_c)$ vs time, specified values of l_c vs time, conversion CLD into PSD: $Ev(d_{SE})$	Evolution of $En(l_c)$, $N(l_c)$, $Ev(d_{SE})$; impact of hydrolysis, substrate, enzyme concentration
DLS	Raw signals of angular detectors	$Ev(d_{SE})$, obscuration vs sample concentrations	Evolution of $Ev(d_{SE})$; impact of hydrolysis, substrate, enzyme concentration; evolution of optical properties of substrate
Morpho-granulometry	Composed image	Particle identification and characterization based on image treatment, $Ev(d_{CE})$	Evolution of $Ev(d_{CE})$, morphological properties (intensity, elongation); impact of hydrolysis, substrate, enzyme concentration
YSI	Glucose concentration	Bioconversion rate	Hydrolysis efficiency discussion
HPLC	Monomers and oligosaccharides concentrations	Bioconversion rate	Hydrolysis efficiency discussion, dry matter content estimation
Wettability	Dry matter content vs hydrolysis time	-	Material balance

In the objective of further understanding the development of fibre restructuration under enzyme activities, hydrolysis was carried out in two conditions: under favourable conditions but also in suspensions with high dry matter content. We performed thirty nine hydrolysis experiments: twenty five for hydrolysis at dilute concentrations (1-3% DM) and fourteen for hydrolysis at high solid content using a cumulative feeding strategy (for PP-27 and WP) or not (for MCC and BAG) (**Table 3-7+3-8**). Three experiments were contaminated by yeast so

no results could be exploited (M23, 35 and 38); four experiments were carried out to examine viscosity variation so only in-situ viscosity was monitored (M25-28). The measurements of in-situ viscosity, DSL, dry matter YSI and HPLC analysis were applied to all the experiments. For ex-situ rheometry, the samples of MCC and BAG suspensions were impossible to measure because of their high decantation velocity. In-situ, a FBRM sensor and a Turbiscan Lab apparatus were used on selected experiments.
Our scientific strategy consisted in optimising our characterisation of the matrices and their suspension (rheological behaviour) before investigation using a multi-scale physical approach of their hydrolysis under favourable conditions (dilute suspension). After that, to choose a strategy which allows lignocellulose substrate load to be increased resulting in reduced energy consumption (revealed by suspension viscosity), we performed a cumulative feeding strategy for substrate and enzyme during hydrolysis. It was named semi-continuous mode.
Using the results of initial substrate suspension characterisation of rheological behaviour, we determined a critical substrate concentration, C* from which the suspension viscosity increased exponentially (indicating a high energy consumption) (detailed results in §3.3.4). Moreover, considering the results of viscosity variation during hydrolysis in dilute conditions, we defined a parameter t* as the time necessary for a reduction of 90% of the initial suspension viscosity: t(μ*=0.1) (detailed results in §3.3.2.3). From these two quantities, the critical substrate flow rate was calculated as follows considering broth volume:

$$Q_c = \frac{C^* \cdot V_{reactor}}{t\left(\mu^* = 0.1\right)} \quad \textit{(Eq. 3-1)}$$

Each substrate (PP-27 and WP) was hydrolysed at three different flow rates as presented in **Table 3-8** (for WP, Qc also signified maximal admissible flow rate so it was not possible to use a higher flow rate than this). To tend towards a continuous mode as much as possible, substrate (and enzyme) was added every hour (for PP-27) or every 30 minutes (for WP) until the total substrate concentration reached about ~ 10%dm. An experiment with the whole quantity of enzyme added at t=0h was carried out for comparison with PP-27 (M39). An experiment introducing the same substrate flow rate (4gdm/h) for WP and PP-27 was performed in order to increase the solid matter up to 20% and to compare the influence of substrate concentration on hydrolysis efficiency. Unfortunately, all three of these experiments were contaminated by yeast so no results could be exploited.
For a typical experiment with all the in-situ and ex-situ measurements, the results are presented in **Figure 3-5** below. Any given hydrolysis run can be characterised at three scales: macro, micro and molecular. We monitored the suspension viscosity in-situ in real time and also measured the viscoelasticity at specific times. The pattern of variation of mean particle chord length and total chord number were followed in-situ. The results of particle size analysis were completed by ex-situ measurements. We made different evaluations of the particle diameter: spherical equivalent diameter (D_{SE}) for DLS, circle equivalent diameter (D_{CE}) for morpho-granulometry versus hydrolysis time; morphological observations and data of different relevant shape parameters. The kinetics of decantation were measured and compared before and after enzyme attack. Finally, we zoomed onto the mono and olio-saccharides released during hydrolysis to calculate bioconversion.

Table 3-7: Overview of experiments in batch mode (M22-PP27-3%-0.5 signifies: experiment 22 with paper-pulp 27 matrix at a concentration of 3%dm w/v and a ratio of 0.5mL enzyme/g cellulose) (X= done; empty = not done).

Experiment	Rheometry Viscosimetry		Particle size analysis				Biochemical analysis			
	μ in-situ	G'& G"	FBRM	DSL	Morpho	Tur.Lab	YSI	HPLC	CrI	Dry matter
MCC										
M1-MCC-1%-0.1	X			X	X		X	X		X
M9-MCC-1%-0.5	X		X	X	X		X	X	X	X
M5-MCC-3%-0.1	X			X	X	X	X	X		X
M33-MCC-10%-0.5	X		X	X			X	X		X
M37-MCC-30%-0.5	X		X	X			X	X		X
WP										
M4-WP-1%-0.1	X			X	X		X	X		X
M13-WP-1%-0.5	X	X	X	X			X	X		X
M26-WP-2%-0.1	X		X	X			X	X	X	X
M27-WP-2%-0.5	X		X	X			X	X	X	X
M8-WP-3%-0.1	X	X		X	X		X	X		X
M14-WP-3%-0.5	X	X	X	X	X	X	X	X	X	X
PP-27										
M31-PP27-1%-0.1	X	X	X	X			X	X		X
M24-PP27-1%-0.5	X	X	X	X	X	X	X	X	X	X
M28-PP27-2%-0.1	X		X	X			X	X	X	X
M25-PP27-2%-0.5	X		X	X			X	X	X	X
M32-PP27-3%-0.1	X	X	X	X	X	X	X	X		X
M22-PP27-3%-0.5	X	X	X	X	X	X	X	X	X	X
PP-31										
M3-PP31-1%-0.1	X			X			X	X		X
M29-PP31-1%-0.5	X	X	X	X	X		X	X		X
M7-PP31-3%-0.1	X	X		X	X	X	X	X		X
M10-PP31-3%-0.5	X	X	X	X	X	X	X	X	X	X
BAG										
M2-BAG-1%-0.1	X			X	X		X	X		X
M11-BAG-1%-0.5	X		X	X			X	X		X
M6-BAG-3%-0.1	X			X			X	X		X
M12-BAG-3%-0.5	X		X	X	X	X	X	X	X	X
M36-BAG-10%-0.5	X		X	X			X	X		X

Table 3-8: Overview of experiments carried out in fed-batch mode with a cumulative-add strategy (M16-PP27-Qc*1.5-0.5 signifies: experiment n°16 with paper-pulp 27 matrix at a feed rate corresponding to critical flow rate x 1.5 and a ratio of 0.5mL enzyme/g cellulose) (X= done ; empty: not done).

Experiment	Rheometry Viscosimetry		Particle size analysis			Biochemical analysis			
	μ in-situ	G' & G"	FBRM	DSL	Morpho	Tur.Lab	YSI	HPLC	CrI	Dry matter
WP										
M17-WP-Qc/2-0.5	X		X	X			X	X		X
M18-WP-Qc/4-0.5	X		X	X			X	X		X
M19-WP-Qc/6.67-0.5	X		X	X			X	X		X
M35-WP-4g/h-0.5	X	Yeast contamination								
PP-27										
M16-PP27-Qc*1.5-0.5	X		X	X			X	X		X
M15-PP27-Qc-0.5	X		X	X			X	X		X
M39-PP-Qc-0.5-$E_{initial}$	X		X	X			X	X		X
M21-PP27-Qc/1.5-0.5	X		X	X			X	X		X
M23-PP27-4g/h-0.5	X	Yeast contamination								
M38-PP27-4g/h-0.5	X	Yeast contamination								

(0.1mL enzyme/g cellulose ≈ 5FPU/g cellulose; 0.5mL enzyme/g cellulose ≈ 25FPU/g cellulose)

MACRO-SCALE

Rheological behaviour	In-situ	Ex-situ
Raw data	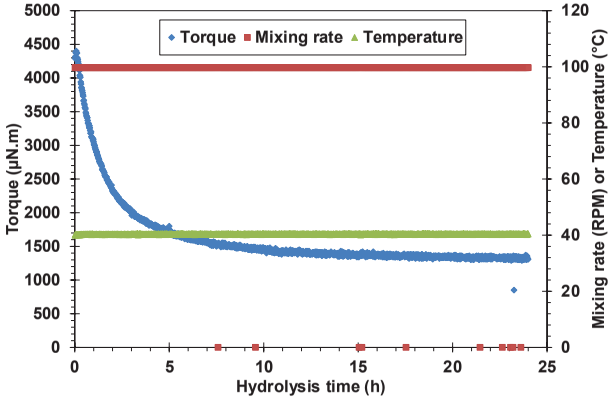	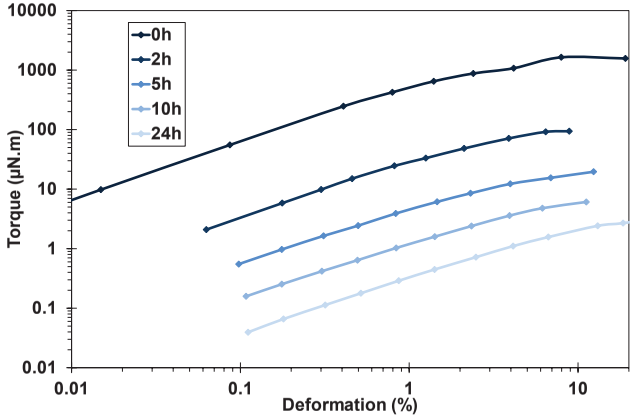
Experimental results	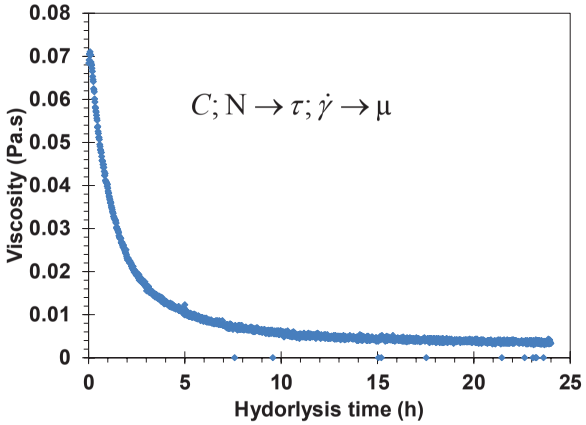	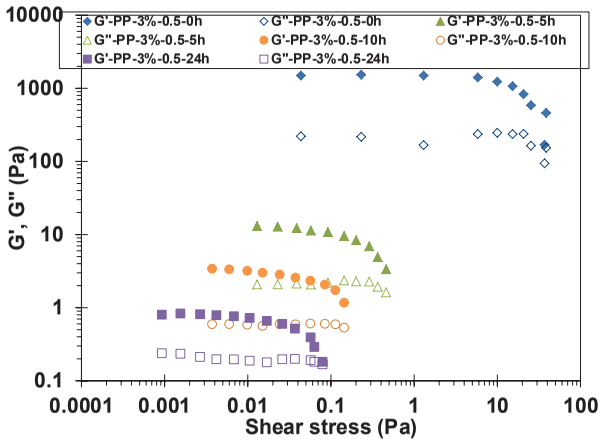

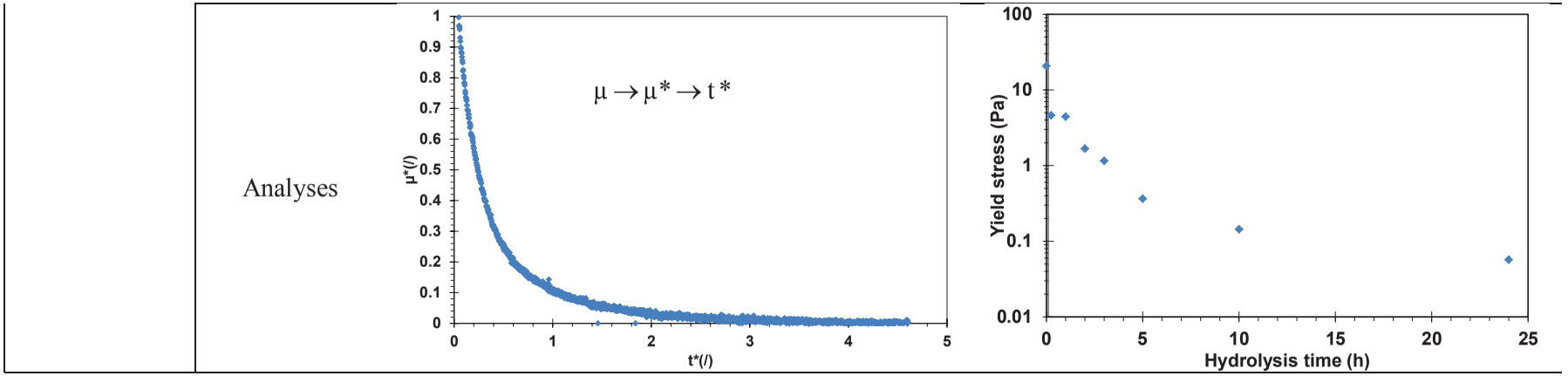

Figure 3-5: Cartography of a hydrolysis experiment (example for M22-PP27-3%-0.5) from raw data up to analyses.

3.2 Results

Raw data and results are described for the three levels of observation: macro-scale with rheometry and viscosimetry; micro-scale with morpho-granulometry (CLD, PSD) and molecular scale with biochemistry (chemical analysis of soluble and solid fraction).

3.2.1 Rheometry

Rheology describes the deformation and flow of matter. In the process of liquefaction and saccharification of lignocellulose biomass, the fundamental understanding of the rheology of these suspensions becomes a powerful tool in designing conversion equipment and processes (Ehrhardt et al., 2010; Knutsen & Liberatore, 2010; Stickel et al., 2009). The rheological behaviour of the suspension affects not only the hydrodynamic properties but also the dynamics of transfers (mass / heat) in suspension. However, it is not simple to characterise the rheological behaviour of a lignocellulose suspension, for two main reasons could explain this situation. Firstly, the rheological behaviour of suspensions is affected by multiple parameters: concentration, size, shape, density and surface properties, and biochemical properties of substrates. Secondly, there is no standard method to follow this quantity.

Our research used two different techniques to characterise the rheological behaviour of the suspension: in-situ viscosimetry and ex-situ oscillation measurements. This chapter will present (i) the rheological behaviour, viscosity, viscoelasticity of lignocellulose suspensions before hydrolysis; (ii) variation of flow properties during enzyme attack and (iii) the basis of a rheological model and identification of the relevant criteria.

Figure 3-6 shows the scientific approach used to characterise the rheological behaviour of lignocellulose suspensions during enzyme hydrolysis. Starting from different scientific issues linked to mass and heat transfers, the rheological behaviour of suspensions was characterised and modelled theoretically as a function of substrate concentrations and shear rate. This model was then developed by adding physical and morphological fibre properties. Finally, the enzyme hydrolysis kinetics was introduced into the model.

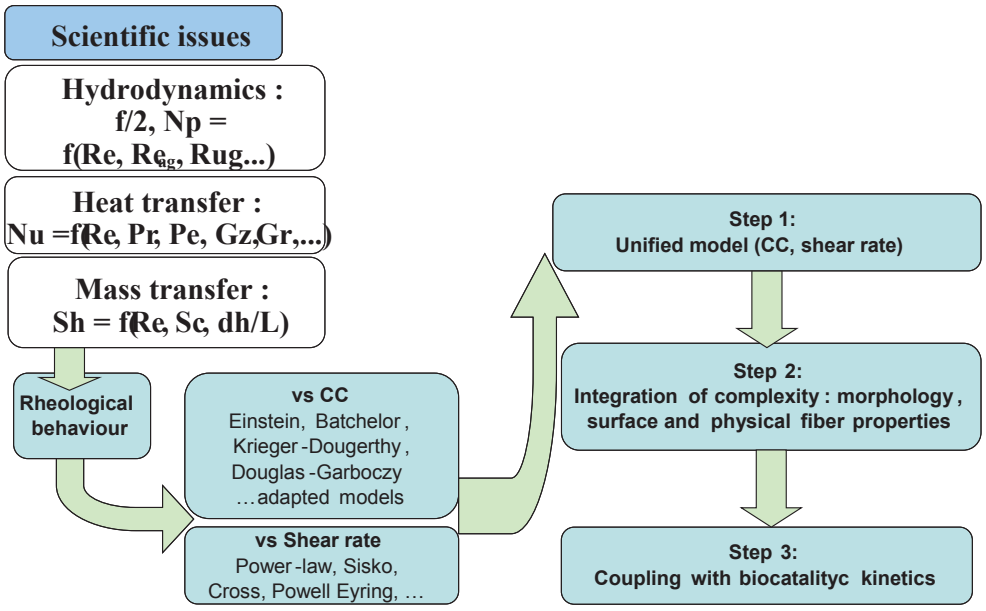

Figure 3-6: Approach for rheological characterisation of lignocellulose suspensions.

3.2.1.1 Initial suspensions

The in-situ viscometry of the initial suspension was followed by investigating the influence of concentration and mixing rate for the different substrates. All measurements were performed within the working zone of the torquemeter with a maximum torque of 30mN.m and a maximum mixing rate of 800rpm. The in-situ measurements were firstly used to establish rheograms (considering only results in the laminar regime) and to determine the rheological behaviour of the suspensions. In a second step, the impact of the particle volume fraction on the relative viscosity was investigated. This approach contributed to establishing a structured rheological model including several factors such as shear-rate, volume fraction and particle size. These rheograms, established in the first step, were subsequently used to develop the model. The ex-situ measurements provided further details for suspension rheological behaviour: the loss and storage modulus and the yield stress.

Figure 3-7 presents the rheograms for MCC, WP, PP-27, PP-31 and BAG. The paper pulps, PP-27 and PP-31, exhibited the same rheological behaviour. The in-situ rheograms presented superimposed laminar and transition regimes for the PP while WP was mainly in the laminar regime. In contrast, MCC and BAG were in the transition regime. For a given mixing rate and concentration, viscosity is ranked WP>PP (PP27 and PP31) >BAG >MCC. As an example, for a shear rate of $50s^{-1}$ (rotation speed 100rpm) and a substrate concentration close to 30gdm/L, the viscosities observed were μ_{WP}= 817mPa.s, $\mu_{PP\text{-}27}$=75mPa.s, $\mu_{PP\text{-}31}$=67mPa.s, μ_{BAG}=13mPa.s and μ_{MCC}=1mPa.s with volume fractions, ϕ_{WP}=0.024 (28.7gdm/L), $\phi_{PP\text{-}27}$=0.01 (29.2gdm/L), $\phi_{PP\text{-}31}$=0.01 (27gdm/L) ϕ_{BAG}=0.034 (34gdm/L) and ϕ_{MCC}=0.013 (20gdm/L) respectively. For MCC, the results are in agreement with reported data with an average fibre length and diameter of 1.7µm and 0.077µm, respectively exhibiting $0.01<\mu<10$Pa.s for 0.5<%dm<5% (Tatsumi et al., 1999). For PP, Blanco et al. (2006) reported results similar to ours: hardwood Kraft pulp suspension: $1<\mu<150$mPa.s for 0.8<%dm<2.8%. For all concentrations and suspensions, the viscosity decreased as the mixing rate increased indicating a Non-Newtonian behaviour. All the suspensions were found to be shear-thinning fluids.

Ex-situ measurements only made for WP, PP-27 and PP-31. Because of the rapid decantation of the other substrates (MCC and BAG) it was not possible to make measurements under oscillation which requires several minutes. When possible, this type of measurement allowed determination of the elastic (G') and viscous (G") moduli. They were first determined with increasing amplitude of deformation at 1Hz in order to determine the linear domain for the fluid (**Figure 3-8 A** and **C**). Then, choosing a deformation in the linear domain, measurements were performed for frequencies in the range 0.5 to 20 Hz. The results are presented in **Figure 3-8 B** and **D**. For all three substrates (WP, PP-27 and PP-31), the elastic modulus was always higher than the viscous modulus. A ratio of about 8-fold was found for these two moduli indicating that the suspensions presented a predominantly elastic behaviour under these conditions of solicitation. In addition, these two moduli remained stable on varying the oscillation frequency between 0.5 and 20Hz. The same conclusions were reported for microfibrillated cellulose by (Agoda-Tandjawa et al., 2010) in a concentration range between 0.5-3%w/w where G'>G" by about 10-fold and remained stable between 0.1-10Hz. This is characteristic of viscoplastic behaviour and a value for the yield stress is given by the maximum of the G"(t) curves (**Figure 3-8 A** and **C**).

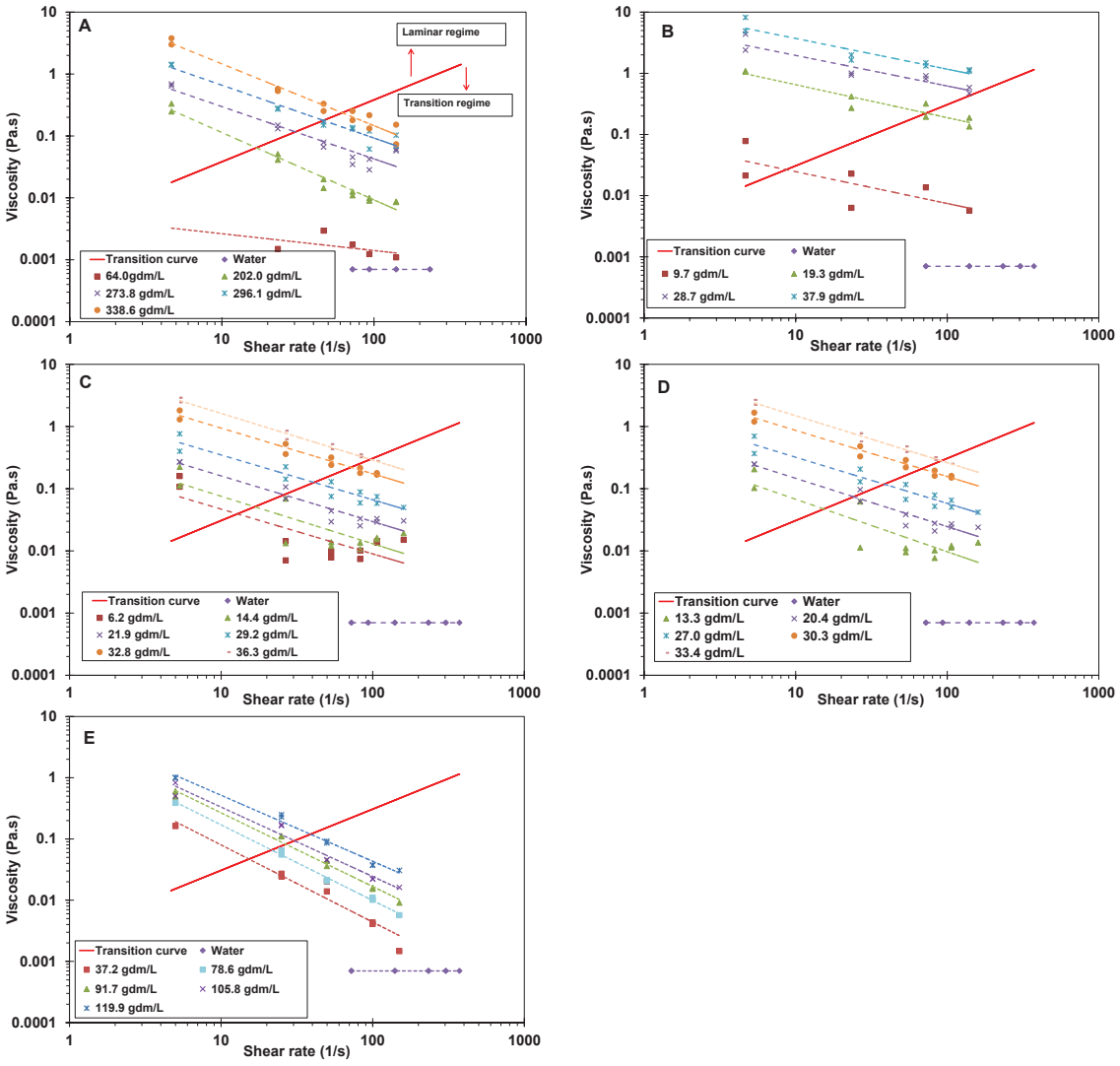

Figure 3-7: In-situ rheograms versus substrate concentrations for MCC(A), WP(B), PP-27(C), PP-31(D) and BAG(E)

There was no significant difference between the two types of paper pulp. They presented the same value range and trends for G' and G" (**Figure 3-8-A-B**). For both substrates, there was an increase of elasticity with an increase of substrate concentration (**Figure 3-8-C**). A dramatic increase from about 20 to 1000Pa for G' appeared on changing the dry matter concentration from 1 to 3%w/v. The yield stress was also greatly affected, rising from roughly 0.5Pa to 20Pa.

The PP (both of 27 and 31) had values of G' and G" higher than those of WP (about 3-fold), together with higher yield stresses. This signifies that the elastic behaviour of the PP suspension under the threshold is more pronounced that that of WP. This observation could be related with the morphological properties of fibres the very long and ramified fibres (Agoda-Tandjawa et al., 2010).

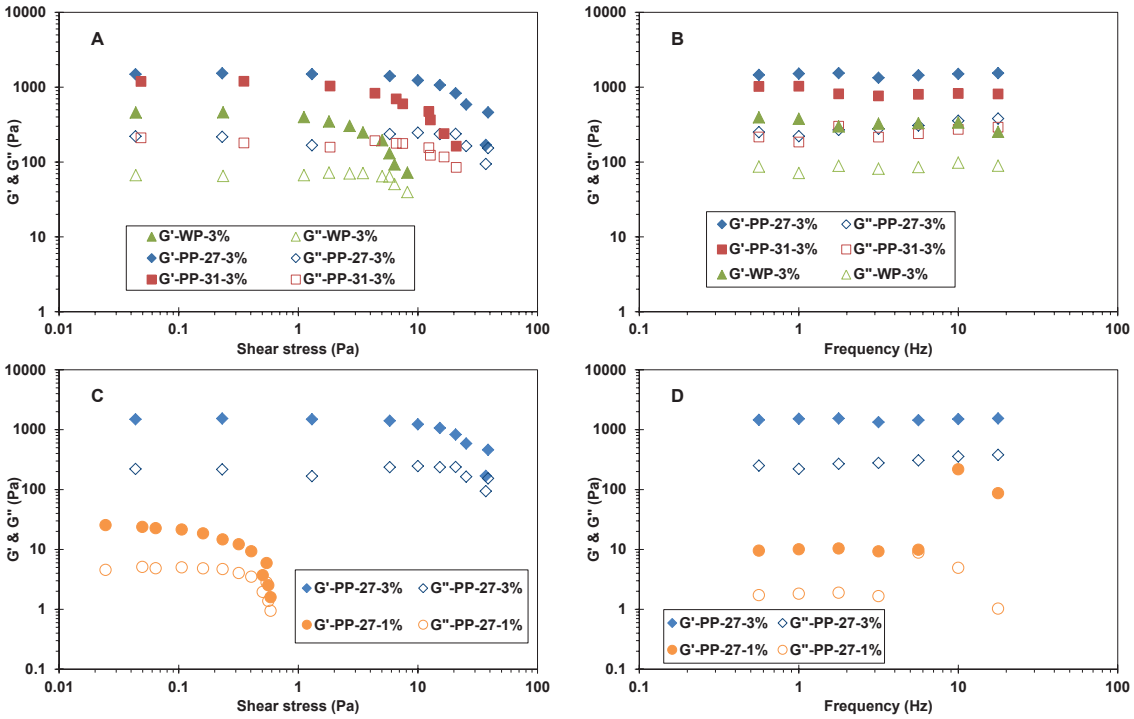

Figure 3-8: Viscous modulus (G") and elastic modulus (G') of lignocellulose suspensions as a function of shear stress (left) and frequency (right) (A-B: for Whatman paper, paper-pulp 27 and paper- pulp 31 at 3%w/v; C-D: for paper-pulp 27 1% and 3%w/v).

3.2.1.2 Hydrolysis of lignocellulose suspensions

Figure 3-9 illustrates the in-situ viscosimetry of suspensions as a function of hydrolysis progress. PP-27 and PP-31 exhibit the same trends, so the figures are restricted to PP-27 (PP-31 is in **Annexe 6**). As expected, slurry viscosity decreases during hydrolysis even though this phenomenon was less intense for MCC and BAG (**Figure 3-9-A**). Viscosity was greatly reduced at the beginning of hydrolysis, so a log-scale was used for time. For PP and WP, a sharp reduction in viscosity was observed whatever the concentration or enzyme/substrate ratio. In the same hydrolysis conditions: 3%dm, 0.1mL E/g cell, before hydrolysis (t=0h), the initial viscosities of the four suspensions were in accordance with established models (§ 3.3.2.1); $\mu_{WP}>\mu_{PP}>\mu_{MCC}$ and $_{BAG}$. During the bio-catalytic reaction, these values changed with two trends: viscosities of MCC and BAG remained almost constant and equal to water at 40°C (0.65mPa.s) whereas the viscosities of PP-27 and WP decreased from 68 and 624mPa.s to 12 and 6mPa.s respectively. This change in the physical appearance of the slurry is associated with the biochemical changes and particle morphology changes occurring in the fibres (Kaar & Holtzapple, 1998; Roche et al., 2009b). The drop in viscosity is a combination of the decrease of solids concentration and the fragmentation of the cellulose particles (Rosgaard et al., 2007; Vázquez et al., 2007). Under the action of enzymes, the cellulose chains are cut to give smaller particles and non-dissolved cellulose is converted into soluble compounds such as monomers and water-soluble oligomers. In addition, the decrease of viscosity is suggested to be strongly connected with the degradation and decrease of water binding capacity of the lignocellulose structures during the enzyme action (Chang et al., 1981).

For PP-27 and WP (**Figure 3-9-B and C**), the initial viscosities of 3% suspension were 12-15 fold higher than those of 1% suspension (~70-600mPa.s and ~5-50mPa.s respectively). This dependence of viscosity on concentration is expected and can be explained by an increase in

particle interactions, less free water, and hydrogen bonding between cellulose chains. As the solid concentration increases, the average distance between particles in the slurry decreases, leading to enhanced contact between particles, especially if there is an entanglement of amorphous fibres between particles (Dasari et al., 2009). During hydrolysis, a significant drop in slurry viscosity is observed within the first 10h of the hydrolysis reaction. These results are supported in the literature over a wide range of matrices, particle sizes and enzyme/cellulose ratios. For spruce pulp (initial diameter: 91µm), initial and final viscosities ($\mu_{initial}/\mu_{final}$) were 0.24/0.028, 0.4/0.058 and 0.84/0.087Pa.s for concentrations of 10, 15 and 20% (w/w), respectively (Um, 2007). For acid-pre-treated sugarcane bagasse, viscosity was reported to be reduced by 77% to 95% after 6h (Geddes et al., 2010) and by 75 to 82% within 10h (Pereira et al., 2011).

The effect of enzyme concentration (ratio E/g cell) was observed for both of PP and for WP (**Figure 3-9-B and C**). At the same substrate concentration, the higher the E/g cellulose ratio, the faster the viscosity decreased. For example, with PP-27, within 5h, the viscosity of a 3% suspension was reduced by 85% (from 68mPa.s to 10mPa.s) for 0.5mL E/g cellulose; whereas this value was limited to 40% (from 79mPa.s to 47mPa.s) for 0.1mL E/g cellulose. This conclusion is in agreement with other authors (Du et al., 2014; Geddes et al., 2010; Rosgaard et al., 2007; Tu et al., 2009). On the other hand, the decrease of viscosity depends on the type of substrate. For a 3% PP-27 suspension and 0.5 E/g cell, it took about 7h to reduce 90% of the initial viscosity whereas with WP only one hour was required. The various kinetics for viscosity reduction provide information about how to control enzyme hydrolysis processes, mainly for continuous mode concerning material flow rates, hydrolysis time, energy consumption, etc.

Figure 3-10 shows ex-situ rheological measurements reporting the variations in viscous and elastic moduli (G" and G' respectively) for PP-27 and WP. Both suspensions show a pseudo plastic (or shear-thinning) behaviour both initially and throughout hydrolysis. This result was also mentioned by other authors (Du et al., 2014; Pereira et al., 2011; Wiman et al., 2010).

Before the introduction of enzyme, the rheological behaviour for small deformations is mainly elastic with high value of G' (G'/G''> 4 to 10) for both substrates. For a 3%dm suspension at t=0h and in the linear domain, G' and G" reached about 1000 and 100 Pa for PP-27 and 350 and 90 Pa for WP. This is supported by the literature for different matrices. For corn stover, at 12%dm, G' and G" were reported as 2000 and 300 Pa (Stickel et al., 2009); for acid pre-treated soft wood, these values were 100 and 50 Pa respectively (Wiman et al., 2010). When increasing the shear stress, all the samples presented two zones: a first one where G' and G" did not depend on shear stress and a second one where both moduli decreased. In this second zone, G' deviated sharply from a stable curve and crossed (or tended to cross) G". The transition between these two regions will be used to give an estimation of the yield stress (§ 3.3.2.2).

During hydrolysis, a regular decrease of both moduli was observed and the high elastic character preserved. For example, with PP-27-3%-0.5, a reduction of 1000-fold for both of G' and G" was found after 24h of enzyme attack. Comparing the same substrate, *i.e.* PP-27, different enzyme concentrations caused differences in the behaviour of G' and G". The higher the enzyme activities, the faster the decrease of elasticity (in agreement with results of viscosity above). G' and G" for 3% PP-27 at E/S=0.1ml/g cell were 100 times lower than for E/S=0.5ml/g cell. This observation highlights yet again the strong impact of enzyme concentration on how the rheological behaviour varies during hydrolysis.

Comparing different substrates under the same conditions (3%, E/S=0.1ml/g cell), PP-27 exhibited a greater shear-thinning character than WP (Figure 3-10-C). The 3-fold difference between the elastic moduli of PP-27 and WP was maintained all along 24h of hydrolysis. This

difference may be correlated with the changes occurring in particle size and substrate concentration (§ 3.2.3).

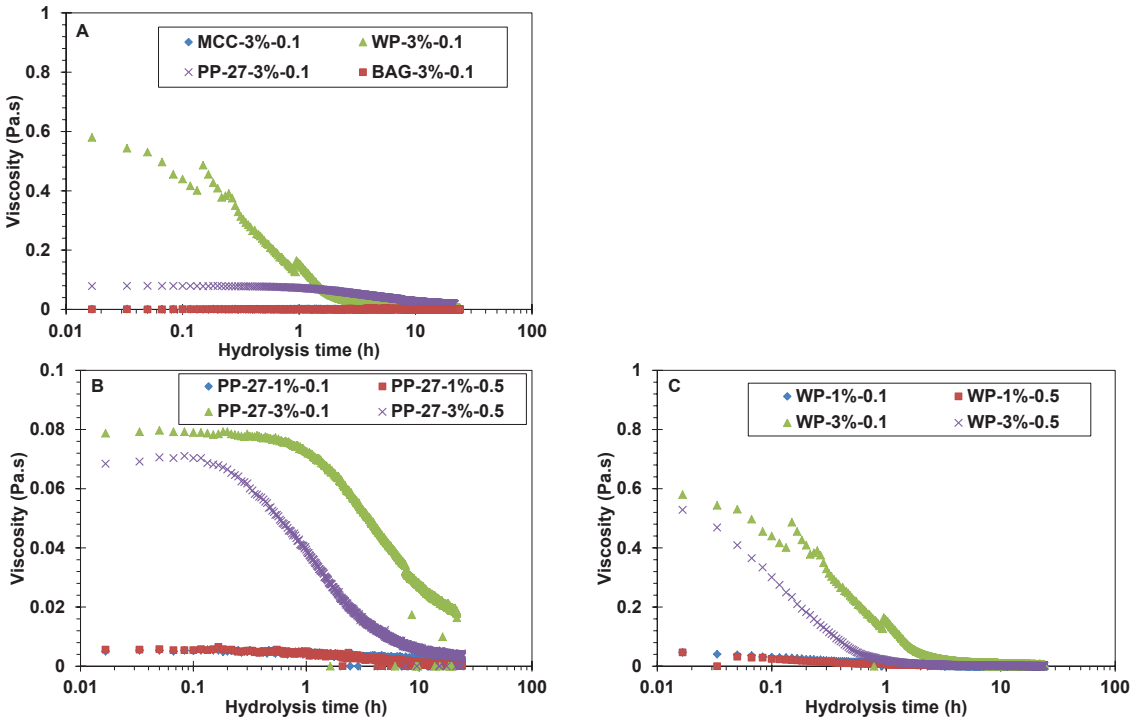

Figure 3-9: In-situ viscosimetry as a function of hydrolysis time. A: Comparison of the four substrates with 3%dm and E/S=0.1mL/g cellulose; B and C: Comparison of PP-27 and WP at 1 and 3% and E/S=0.1 and 0.5 mL/g cellulose.

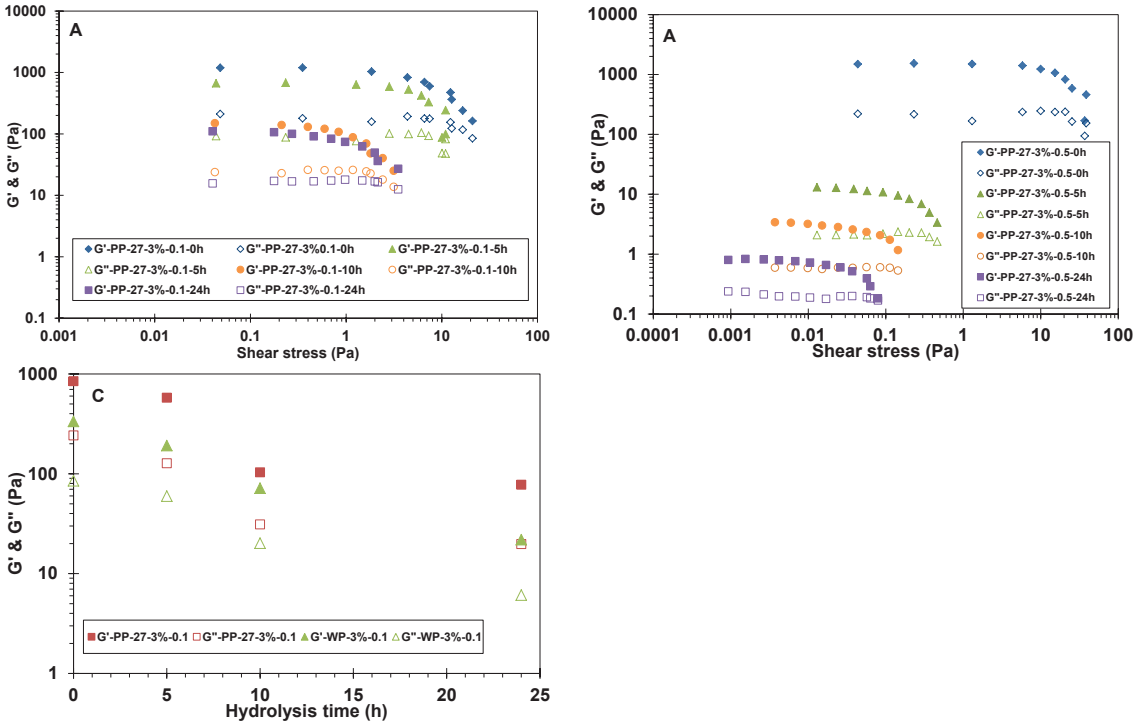

Figure 3-10: Viscous (G'') and elastic (G') modulus as a function of shear stress (A: PP-27-3%-0.1, B: PP-27-3%-0.5) and as a function of hydrolysis time (C: WP and PP-27 with 3%dm, 0.1mL E/g cellulose).

The following experiments under dilute conditions and considering E/S=0.5mL/g as the most efficient ratio to reduce viscosity, the semi-continuous hydrolysis mode was restricted to this ratio. Considering the critical parameters identified (C*, t* defining a critical feed flow rate, Qc, see § 3.3.2.3), our strategy and challenge consisted of analysing transfer limitation under varying viscosity as a function of glucose release kinetics but also of assessing the suitability of the established model under dilute conditions. Cumulative additions (enzyme, substrate) with defined quantities and hydrolysis time were then analysed.

If we now consider the cumulative addition strategy experiments (§3.1.2), **Figure 3-11** reports a comparison between three different substrate flow rates, all leading to the same total dry matter concentration of 10% for both substrates (WP, PP-27). Each hydrolysis run was performed for 24h and with the same final substrate quantity (around 10%) so that the higher the flow rate, the lower the number of additions required. The behaviour of viscosity can be divided into 2 steps. The first corresponds to the collection of the different "cycles" corresponding to substrate and enzyme addition (viscosity increase), and then a second step with hydrolysis alone (viscosity reduction). At the end of all the additions, the viscosity became drastically reduced following the hydrolysis kinetics. This trend is in total agreement with the results for hydrolysis under dilute conditions.

For PP-27, **Figure 3-11-A** illustrates the impact of substrate flow rate on the suspension viscosity up to 10%dm followed by the last phase corresponding to single hydrolysis phenomena. In this example, the viscosity reaches the maximum/minimum values of 277/28, 213/57 and 131/90mPa.s respectively for the flow rates Qc x1.5, Qc and Qc/1.5. The significant difference observed on the final viscosity could be easily explained by a longer hydrolysis time in the final phase for the highest flow rate. For an identical feed flow rate (Qc), two strategies for enzyme addition were tested: synchronous substrate and enzyme addition with E/S=0.5mL enzyme/g cellulose (M15), and an experiment where the total quantity enzyme was introduced at t_0 and only substrate was then added (M39). Consequently, the E/S ratio fell from about 8 down to 0.5mL enzyme/g cellulose. As expected, the viscosity kinetics was completely different with M39 viscosity remaining lower than that of M15. In this example, considering the highest and the final viscosities, μ_{max} for M39 was 79mPa.s (2.7-fold less than that of M15) and the μ_{final} was 30mPa.s (~half that of M15). These differences are due to hydrolysis conditions corresponding to enzyme excess. The greatest viscosity for M39 (79mPa.s) corresponded to the initial viscosity of 3% PP-27 (about 70mPa.s). This indicates that we could increase substrate concentration three-fold, from 3 to 10%w/v, keeping the viscosity maximum of the suspension at70-80mPa.s.

The influence of the enzyme feed strategy on suspension viscosity was also reported by Rosgaard et al. (2007) : working with barley straw, at the same final concentration of 15%w/w, the experiment with total enzyme quantity introduced at t = 0h presented a lower viscosity than the experiment with simultaneous addition of enzyme and substrate. After 24h of hydrolysis, these values were 90mPa.s and 240mPa.s respectively. However, when the hydrolysis time was prolonged, the difference became negligible. At 48h of hydrolysis, the viscosity of the two experiments reached the same level of about 30mPa.s.

For WP, the same experimental strategy was conducted and the same phenomenon observed. For example, the viscosities reached greatest/minimal values of 777/~20, 706/~20 and 555/~20mPa.s respectively for Qc/2, Qc/4 and Qc/6.67. The final viscosity, μ_{final}, reached the same values ~ 20mPa.s indicating that it is not flow rate dependent.

Figure 3-12 plots the viscosity minimum and the viscosity maximum versus time after each substrate addition for the different flow rates. With WP, interestingly, the minimum viscosity tended towards the same value irrespective of the flow rate. However, the viscosity maxima depended strongly on the flow rate, Qc/2 was half the viscosity of Qc/6.67. For PP-27, the same trend was observed for viscosity maxima and minima. The higher the flow rate, the higher the viscosity obtained. The enzyme ratio played an important role in viscosity decrease. With excess enzyme (orange line), the viscosity was always 2-fold less than those with synchronous enzyme-substrate feed (blue line) at the same flow rate.

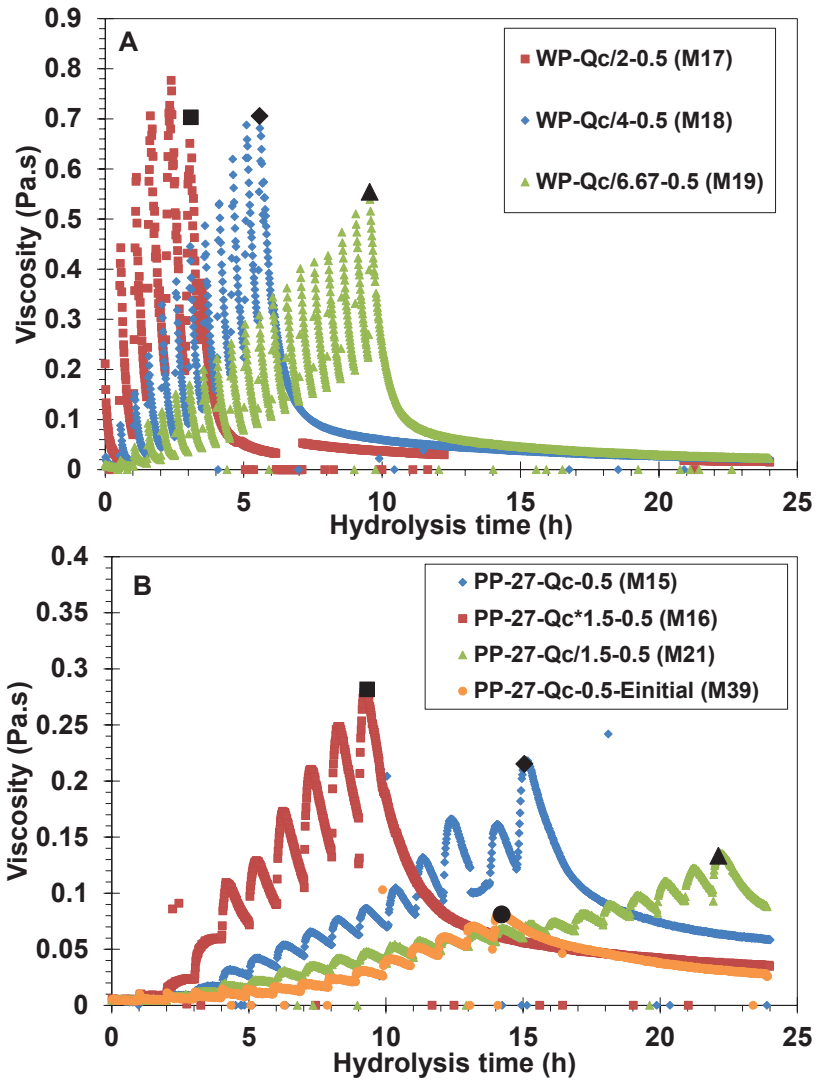

Figure 3-11: In-situ viscosimetry as a function of time during hydrolysis under semi-continuous mode (Maximum additions 10%, E/S=0.5mL/g cell, 40°C, pH4.8, substrate WP-A and PP-27-B, black point: the end of additions).

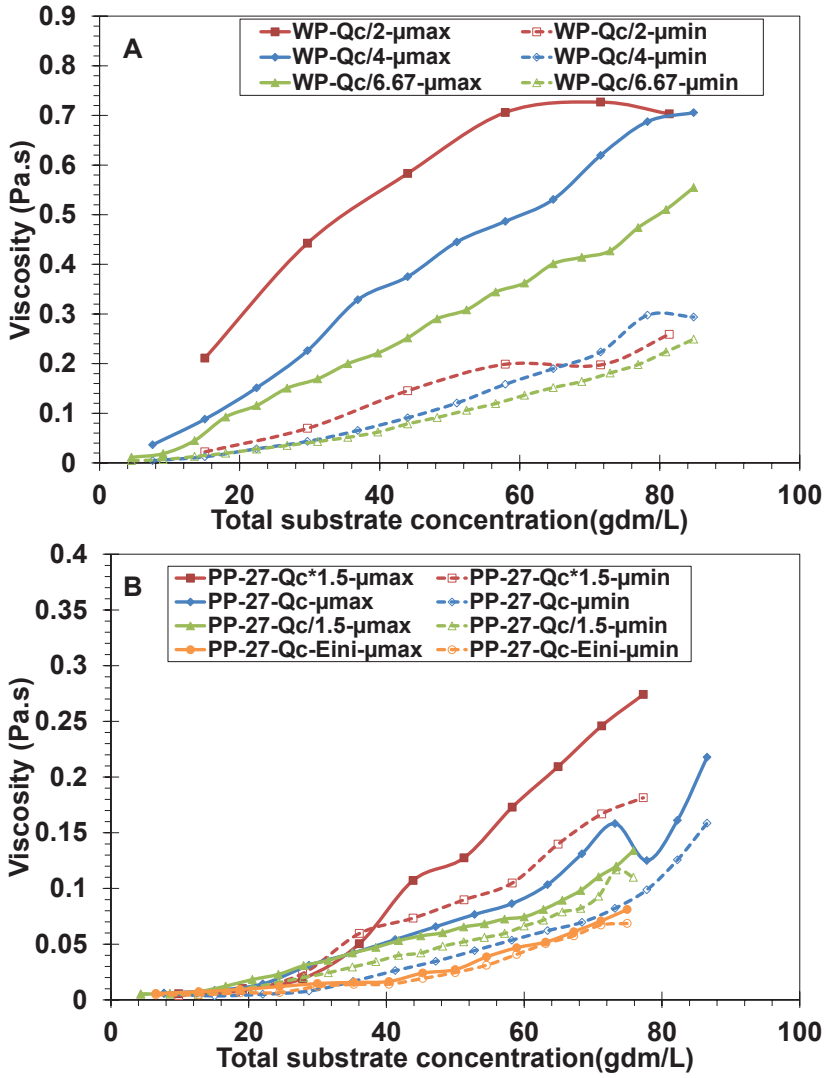

Figure 3-12: Maximal and minimal suspension viscosities under cumulative feeding strategy during hydrolysis. A-WP; B-PP-27.

3.2.2 Decantation kinetics

All substrate suspensions exhibited highly heterogeneous properties which caused difficulties in mixing during hydrolysis as well as in suspension characterisation. This disadvantage is partly due to the rapid decantation of fibres in suspension. So, a substrate decantation study is necessary to understand and characterise this property for each matrix and also to facilitate the bioprocess control. As presented in §2.4.4, this paragraph will focus on two steps: (i) comparison of decantation kinetics between the different substrates, (ii) determination of substrate concentration.

3.2.2.1 Comparison of decantation kinetics of a substrate suspension

As mentioned above, the lignocellulose suspensions contain fibres of diverse sizes, shapes and optical properties. To analyse and compare the decantation kinetics of different substrates is not simple. We wanted to find a way to characterise these kinetics that is easy, fast and qualitative. A new parameter named "sediment accumulation time index" was proposed to determine the time required for 90% of the total sediment to settle. Knowing that the square of backscattered light flux BS^2 is proportional to the substrate volume fraction, for a given

sample volume, at the end of the measurement when the suspension becomes stable, the total quantity of sediment is proportional to the square of the final back-scattering signal. We calculated the average value of BS in the zone defined as the sediment height H_s (**Figure 3-13**). Time t_i was defined as the time for $\overline{BS}_i^2 = 0.9 \cdot \overline{BS}_{fin}^2$. This t_i value provides information on the decantation rate. It is a quantity that is easy to use to compare different substrates. The results obtained for MCC, BAG, WP and PP suspensions at 1 and 3%w/v (0.1 and 0.5mL enzyme/g cellulose) before and after hydrolysis (samples were taken directly from the bioreactor) are presented in **Table 3-9**.

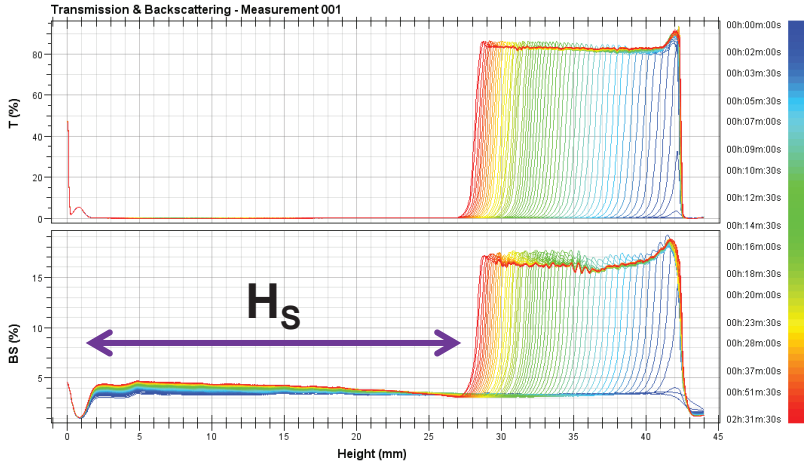

Figure 3-13: Sediment zone determination H_s (ex: PP-27-3%-0.5-24h).

Table 3-9: Sediment accumulation time index t_i for substrate suspensions before and after hydrolysis.

Experiment	Hydrolysis time (h)	t_i (s)
MCC-3%-0.1	0	240
	24	90
BAG-3%-0.5	0	1620
	24	90
WP-3%-0.5	0	nd
	24	150
PP-31-3%-0.1	0	150
	24	180
PP-31-3%-0.5	0	150
	24	330
PP-27-1%-0.5	0	240
	24	90
PP-27-3%-0.1	0	150
	24	180
PP27-3%-0.5	0	180
	24	540

Before hydrolysis (t=0h), the five substrates presented a strong difference in decantation kinetics. For PP (whether 27 or 31), the cellulose fibres formed a strong network and sediment accumulation take place faster by the decantation of coarse floc. It took about 150-180s to obtain 90% total sediment. MCC, which had the highest density, required 240s to deposit 90%

sediment. The BAG sample took more time to deposit because of its lower density (slightly higher than that of water) and its particle heterogeneity. Interestingly, WP did not deposit at any time during measurement (about 16h). This could be explained by the water retention of the paper fibre which occupied the whole volume of the experiment tube. So no decantation was observed for WP.
After 24h of hydrolysis, the decantation kinetics changed completely. For MCC, BAG and WP, the sediment accumulations were more rapid than before hydrolysis. The hydrolysed substrates took only 90s for 90%sediments accumulation. The main reason is fibre fragmentation under enzyme attack. The particle-particle interactions decreased so decantation was faster. With PP, the influence of enzyme concentration was highlighted. For the lowest quantity of enzyme used, t_i was unchanged during hydrolysis. The cellulose fibres were less attacked and their properties less modified. However, for higher enzyme concentrations (0.5mL E/cellulose), t_i increased from 150s to 330-540s. In this case, the particles were cut to give smaller, less compact particles. These fine populations exhibited slower decantation kinetics.

3.2.2.2 Estimation of instantaneous substrate concentration

The substrate concentration in suspensions (or substrate volume fraction) was determined though the calibration curves. For a given substrate, this curve was plotted by measuring different known substrate volume fractions ranging from 0.01 to 20% (v/v). Using these signals of transmission (T) and back-scattering (BS), we estimated a critical volume fraction ϕ_c which is the crossing point between the two curves of the signals T and BS (**Figure 3-14**). This method of ϕ_c determination is in agreement with methods reported in the literature (Buron et al., 2004; Mengual et al., 1999; Shih et al., 1999).
From **Eq. 2-17**, BS is proportional to the square root of the substrate volume fraction.
From **Eq. 2-19**, Ln(T) is proportional to the substrate volume fraction.
The equations relating these parameters are presented in **Table 3-10**. A critical value T_c for the transmission signal can be deduced from the critical substrate volume fraction. For $\phi_v < \phi_c$ (or $T>T_c$), the equation for transmission signal will be used to calculate the substrate volume fraction. For $\phi_v > \phi_c$ (or $T<T_c$), the equation for the back-scattering signal will be used.
Figure 3-15 presents the substrate volume fractions in analysis tubes for different suspensions before and after hydrolysis. PP-27 and PP-31 gave similar results. At t=0h, the decantation of MCC and BAG were almost finished after 15-30min. At the end of the measurement time, the sample is clearly divided into two zones: sediment and supernatant. The substrates formed a compact sediment whose volume fractions were 0.14 (MCC) and 0.1 (BAG) at about 4 and 7mm tube height respectively (**Table 3-11)**. In contrast, the suspension of WP revealed a relative homogeneity of the suspension in the tube and no decantation was observed right to the end of analysis time. The PP suspensions initial exhibited the same substrate concentration profile as WP. As result we obtained a smaller supernatant zone (>34mm) than for the initial suspension before hydrolysis.
With the slurry obtained after 24h hydrolysis, two inverse phenomena occurred in the matrices. The supernatant zone was enlarged for WP and PP; but reduced for MCC and BAG. For these latter matrices, the sediments were less compact and they reached twice the height after hydrolysis. The average substrate volume fraction decreased for both matrices (about 0.12 for MCC and 0.04 for BAG – **Table 3-11**). This could be explained by two main reasons: the decrease of solid content in samples under enzyme attack and the increase of the sediment zone. With PP and WP, these two zones of sediment and supernatant were clearly distinct compared with before hydrolysis. Due to hydrolysis, the solid matter decreased, in addition,

the supernatant zone increased; the substrate volume fraction of sediment was reduced for PP and kept a similar value for WP.

Let us highlight the discontinuation of substrate concentration profiles. We can observe the concentration jump in the zone around the critical volume fraction ϕ_c. This due to the transition of the concentration regime from diluted to semi- or concentrated regime and also to the inability of a single model being able to describe this intersection zone (the difference between model and experimented data: solid line and dotted line – **Figure 3-14**).

From the substrate volume fraction, we can calculate the total solid content (or the substrate concentration) present in the sample before and after hydrolysis. These results will be compared with results obtained by other methods and are detailed in §3.2.4.2.

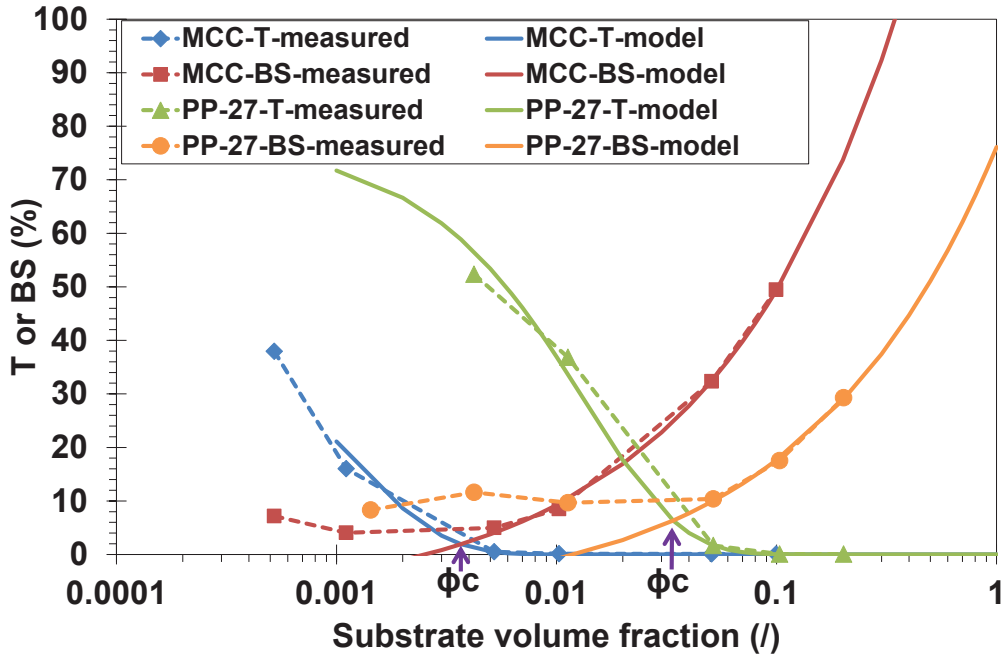

Figure 3-14: Critical substrate volume fraction determination from Transmitted, T and Back-scattered, B signals (example for MCC and PP-27 suspensions).

Table 3-10: Critical substrate volume fraction critical transmission value and equations for substrate concentration estimation (x= ϕ_v; y=ln(T); z= BS).

Substrate	ϕ_c (/)	T_c (/)	For transmission signal	For back-scattering signal
MCC	0.004	1.92	y = -894.46x + 3.9447	$z = 185.63x^{1/2} - 9.3403$
WP	0.003	2.53	y = -941.65x + 3.9526	$z = 168.69x^{1/2} - 7.0259$
PP-27	0.034	6.34	y = -73.779x + 4.3468	$z = 85.491x^{1/2} - 9.3894$
PP-31	0.032	3.13	y = -107.77x + 4.5619	$z = 94.654x^{1/2} - 13.728$
BAG	0.006	1.33	y = -587.27x + 3.9481	$z = 100.53x^{1/2} - 6.607$

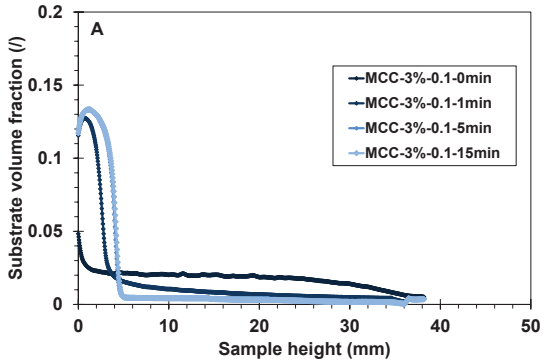
A
MCC-3%-0.1-0min
MCC-3%-0.1-1min
MCC-3%-0.1-5min
MCC-3%-0.1-15min
Substrate volume fraction (/)
Sample height (mm)

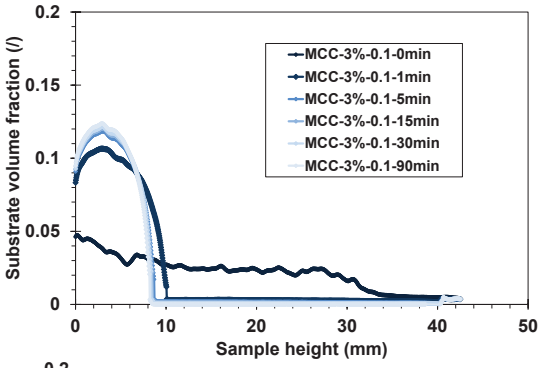
MCC-3%-0.1-0min
MCC-3%-0.1-1min
MCC-3%-0.1-5min
MCC-3%-0.1-15min
MCC-3%-0.1-30min
MCC-3%-0.1-90min
Substrate volume fraction (/)
Sample height (mm)

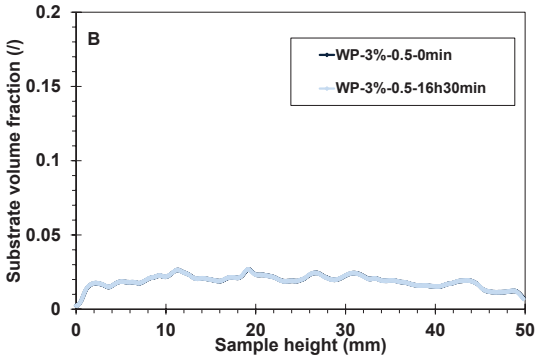
B
WP-3%-0.5-0min
WP-3%-0.5-16h30min
Substrate volume fraction (/)
Sample height (mm)

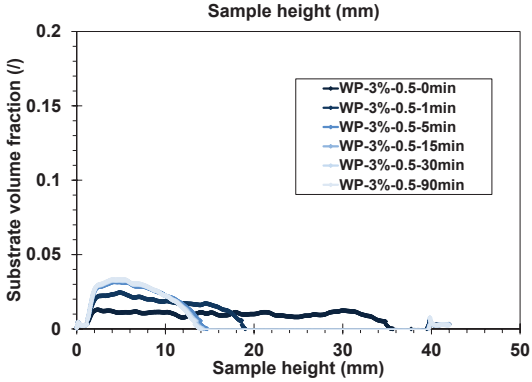
WP-3%-0.5-0min
WP-3%-0.5-1min
WP-3%-0.5-5min
WP-3%-0.5-15min
WP-3%-0.5-30min
WP-3%-0.5-90min
Substrate volume fraction (/)
Sample height (mm)

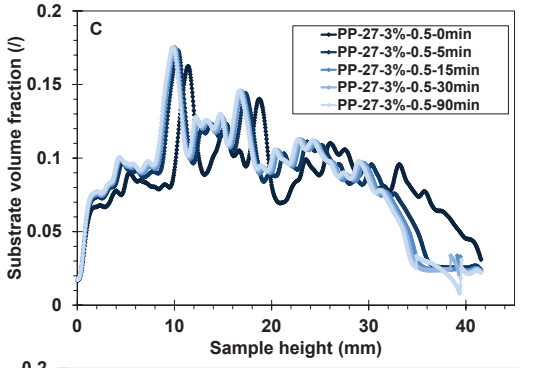
C
PP-27-3%-0.5-0min
PP-27-3%-0.5-5min
PP-27-3%-0.5-15min
PP-27-3%-0.5-30min
PP-27-3%-0.5-90min
Substrate volume fraction (/)
Sample height (mm)

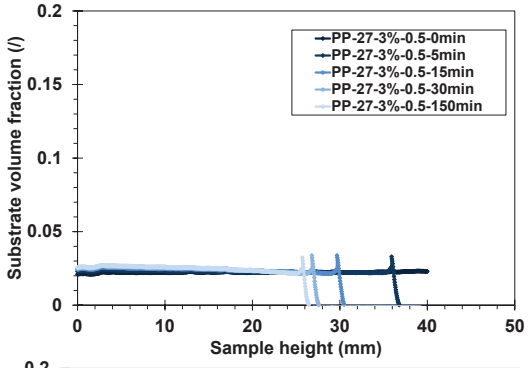
PP-27-3%-0.5-0min
PP-27-3%-0.5-5min
PP-27-3%-0.5-15min
PP-27-3%-0.5-30min
PP-27-3%-0.5-150min
Substrate volume fraction (/)
Sample height (mm)

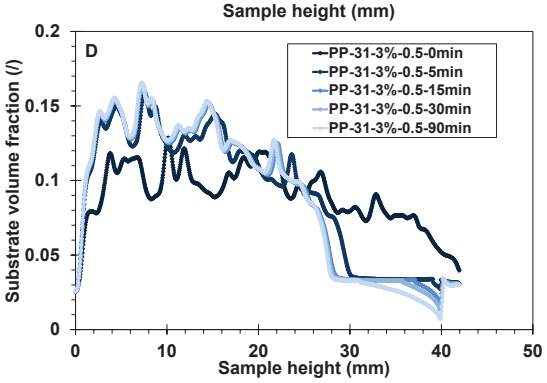
D
PP-31-3%-0.5-0min
PP-31-3%-0.5-5min
PP-31-3%-0.5-15min
PP-31-3%-0.5-30min
PP-31-3%-0.5-90min
Substrate volume fraction (/)
Sample height (mm)

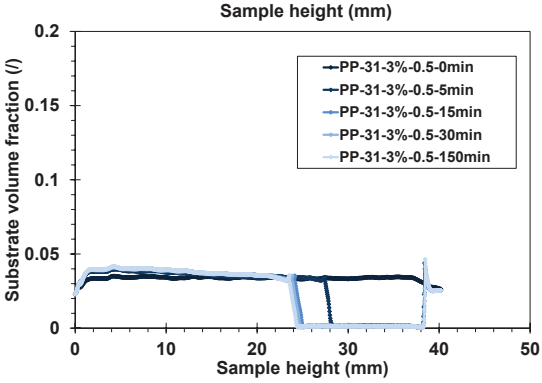
PP-31-3%-0.5-0min
PP-31-3%-0.5-5min
PP-31-3%-0.5-15min
PP-31-3%-0.5-30min
PP-31-3%-0.5-150min
Substrate volume fraction (/)
Sample height (mm)

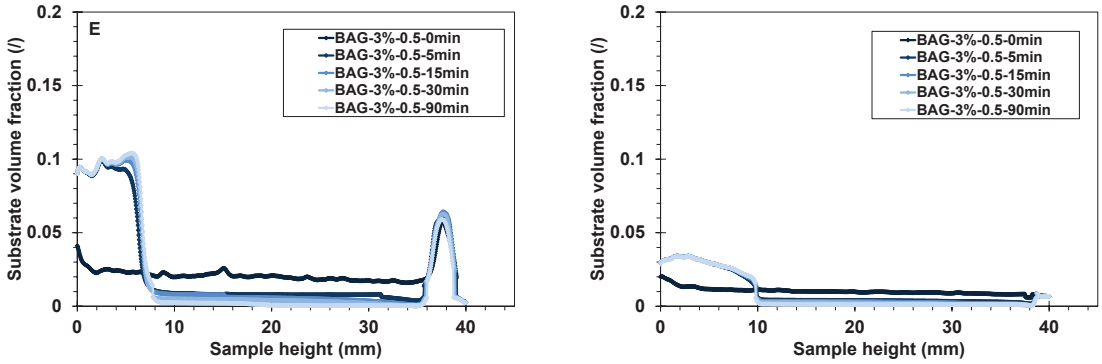

Figure 3-15: Decantation time-dependence of substrate volume fraction for material suspensions before (Left) and after (Right) hydrolysis. MCC (A), WP (B); PP-27 (C), PP-31 (D) and BAG (E) (for identical hydrolysis conditions: 3%w/v, 0.5 mL enzyme/g cellulose; excluded MCC 0.1mL enzyme/ g cellulose).

Table 3-11: Maximal volume fraction and occupied height of sediment for five substrates before (t=0h) and after (t=24h) hydrolysis (3%w/v, 0.5mL enzyme/g cellulose; excluded MCC 0.1mL enzyme/ g cellulose).

Experiment	Maximal volume fraction (/)		Height of sediment (mm)	
	0h	24h	0h	24h
MCC	0.14	0.13	4	8
WP	0.03	0.03	42	14
PP-27	0.15	0.04	34	26
PP-31	0.15	0.04	28	24
BAG	0.10	0.04	7	10

3.2.3 Morphology and granulometry

This part details the modifications of fibre size and morphology in slurry during enzyme hydrolysis. As mentioned above, four techniques were used for this characterisation. The results are presented successively for each technique: in-situ FBRM, ex-situ: DLS, morpho-granulometry and decantation kinetics. Considering different distributions (CLD and PSD), the particle population was divided into different classes and their behaviour followed during hydrolysis. The definition of four classes is presented in **Table 3-12** below. Taking the volume distribution of the initial population as a reference, the population balance of classes I to IV were monitored.

Table 3-12: Population class definition for different morpho-granulometry measurements.

Distribution	CLD $Fv(l_c)$	PSD $Fv(D_{SE}$ or $D_{CE})$
Class I	$l_c \leq l_c(Fv(l_c)=0.25)$	$D_{SE} \leq D_{SE}$ $(Fv(D_{SE})=0.25)$
Class II	$l_c(Fv(l_c)=0.25) < l_c \leq l_c(Fv(l_c)=0.5)$	$D_{SE}(Fv(D_{SE})=0.25) < D_{SE} \leq D_{SE}$ $(Fv(D_{SE})=0.5)$
Class III	$l_c(Fv(l_c)=0.5) < l_c \leq l_c(Fv(l_c)=0.75)$	$D_{SE}(Fv(D_{SE})=0.5) < D_{SE} \leq D_{SE}$ $(Fv(D_{SE})=0.75)$
Class IV	$l_c(Fv(l_c)=0.75) < l_c$	$D_{SE}(Fv(D_{SE})=0.75) < D_{SE}$

3.2.3.1 In-situ particle size analysis: from CLD to PSD

Focus beam reflectance measurement is a laser based technique giving information about the spectrum of chord length number and number (absolute or relative) distribution (cf. §2.4.7.4). Several results were extracted from raw data (**Table 3-13**) and from calculations considering

theoretical transformation based on selected assumptions (§2.4.7.4). For instance, variation of chord number, particular chord length (mean-lc in volume) and population balance (considering classes 0-25, 25-50, 50-75 and 75-100% in volume with initial population) as a function of hydrolysis time stand as points of interest. It is, however, necessary to introduce chord length distribution (CLD) transformation into particle size distribution (PSD) to enable comparison with other techniques (cf. §2.4.7.4). As indicated in **Table 3-13**, morphology and particle size can be investigated versus substrate nature, substrate concentration, enzyme ratio, hydrolysis mode (batch or semi-continuous).

Table 3-13: Overview of focus beam reflectance measurements with different operating conditions.

	Substrate concentration	1%		3%		10%	30%
	Enzyme ratio	0.1	0.5	0.1	0.5	0.5	0.5
Batch mode	MCC		X			X	X
	WP		X		X		
	PP27	X	X	X	X		
	PP31		X	X	X		
	BAG		X		X	X	
Semi-continuous mode	WP					X X X	
	PP27					X X X	

- Batch mode hydrolysis – CLD
  - Impact of substrate nature:

Figure 3-16 presents the time dependence of the number/volume distribution, En(l_c), Ev(l_c) and cumulative number distribution, Fn(l_c) of chord length for five substrates for the same conditions of hydrolysis (1%w/v; 0.5mL enzyme/g cellulose). This figure shows that there are four different trends. Firstly for MCC, the distributions of En and Ev shifted towards the fines population as hydrolysis progressed and absolute Fn increased sharply for the first 5 hours and then decreased. Secondly for PP-27 and PP-31, En and Ev indicated that the coarse population disappears in parallel with the reduction of the count number during enzyme hydrolysis. Thirdly for BAG, the disappearance of part of the fine population was observed in the first hours of hydrolysis. Beyond 5h changes in En, Ev or Fn were observed. Surprisingly, for WP, although count number increased, no transition of En and Ev was observed throughout hydrolysis.

Zooming in to population balance and specific chord values, **Figure 3-17** illustrates the evolution of mean chord, chord number and population balance versus hydrolysis progression. In agreement with the above observations, for MCC, an exponential increase of N_{lc} was observed in the first 6h of hydrolysis (about 5-fold from 8000 to 40 000) parallel with a drastic reduction of mean-l_c for the same period (about 2.5 times from 160µm to 60µm). During also 6h, the coarse and medium population (>150µm) disappeared and are replaced by the fine population (<100µm) which reached 90% of total population (in volume).

For WP, during hydrolysis, surprisingly the l_c decreased insignificantly from 88 to 78µm. For N_{lc} a dramatic increase (3-fold from about 5000 to 15 000) was observed within 1h, after that, it continued to increase at a lower rate and remained stable after 8h. This pattern is perfectly coherent with the decrease of WP suspension viscosity during the first hours of hydrolysis. The action of enzyme mainly dissociated the fibre structure or/and transformed the complex fibre network (macro-scale) into single fibres. After that, the speed of fibre defragmentation was equal to that of substrate solubilisation. This could explain the unchanged of N_{lc} from t=8h until the end of hydrolysis.

PP-27 and PP-31 exhibited the same pattern. A sharp decrease of mean chord length was observed for both within 6h (2-fold, from 120/140 to 60/70µm for PP-27 and PP-31

respectively). For population balance, the largest population decreased regularly parallel with the increase of the smallest population; the proportion of medium population was maintained throughout hydrolysis. For N_{lc}, a slight increase was found in the first 6h and then a steady reduction with hydrolysis time due to solubilisation of solid matter.
For BAG, the substrate the less attackable by enzyme, a slight change was observed for N_{lc} and population balance within about 4h. After that, no variations were found for l_c, for N_{lc} or for population balance.

- Impact of substrate concentration:

Figure 3-18 illustrates an example for MCC at three concentrations: 1, 10 and 30%w/v. All of these experiments showed the same phenomenon: an increase of N_{lc}, a decrease of mean chord length, disappearance of the coarse population and an increase of the fine population with hydrolysis time. However, the kinetics of these variations was strongly dependent on substrate concentration. For MCC-1%, it took only 6h to reach a steady state whereas for MCC-10%it was reached in about 12h. When the MCC concentration reached 30%, 24h was required for the coarse population to disappear.
In contrast, for dilute suspensions (1-3%w/v) no significant influence of substrate concentration was found. Example for PP-27 (**Figure 3-17-18**), at the same enzyme/cellulose ratio of 0.5; t=0h, the same l_c was found about 120µm; $N_{lc} \approx 13\,000$ and 4000 for 3% and 1% suspension respectively. This chord number was dependent on the initial substrate concentration (with a ratio 3/1 between the two concentrations). During enzyme hydrolysis, the l_c decreased sharply to reach the same value at the end of hydrolysis (about 60µm); the N_{lc} decreased until the end of hydrolysis. Fortunately, the final N_{lc} kept the ratio 3/1 for two initial substrate concentrations ($N_{lc} \approx 8200$ and 2600). From this "indicator", we can suggest that bioconversion had the same value whatever the substrate concentration.

- Impact of enzyme concentration:

Figure 3-18 illustrates an example for PP-27-3% at two enzyme ratios: 0.1 and 0.5mL enzyme/g cellulose. In the first hours of hydrolysis, the lc was reduced faster for the higher E/cellulose ratio. For example, at t=2.5h, the mean chord of PP-27-3%-0.5 is 25% less than that of PP-27-3%-0.1 (l_c=70 and 90µm respectively). The total chord number was found in the same range at t=0h (about 12 000) and during hydrolysis they increased during the first hours of hydrolysis for both of experiments, after that, for an E/ cellulose ratio of 0.5, the N_{lc} decreased until the end of hydrolysis; for ratio E/ cellulose of 0.1 in contrast, the N_{lc} continued the increase to reach a maximal value and remained stable thereafter. At t=24h, the N_{lc} of PP-27-3%-0.1 was 2.5 times higher than those of PP-27-3%-0.5 (about 21 000 compared to 9000). This augmentation of N_{lc} in these first hours could be explained by the defragmentation of cellulose fibres under enzyme activity. One coarse particle would be attacked and divided into several fine particles. After that, when the residual enzyme activities were still sufficiently high, these fine particles could be converted into dissolved compounds causing a reduction of chord number. This phenomenon also indicates the yield of bioconversion which depends strongly on enzyme concentration.

- Batch mode hydrolysis - PSD

Figure 3-19-20 presents the results for conversion from CLD into PSD. Surprisingly, the mean diameter in volume D[4,3] was significantly lower than the mean chord in volume l_c for all of five substrates. For example, the D[4,3]/l_c was 90/150; 61/90; 55/120; 54/140 and 60/230µm for MCC, WP, PP-27, PP-31 and BAG respectively. More interestingly, the D[4,3] of MCC (90µm) was higher than those of four other matrices which exhibited the same range of values (about 55-60µm). In spite of this difference of two quantities, all of observations for l_c, population balance were highlighted one more time.
A 2-fold reduction of particle diameter was observed for MCC as well as for PP-27 and PP-31 (from 90 to 40µm for MCC and from 60 to 30µm for PP) (**Figure 3-19-A, C-D**). The fine

population increased regularly during hydrolysis (from 25 to 70% for MCC and 25 to 40% for both of PP) parallel with the disappearance (for MCC) or decrease of the coarse population (for PP-27 and 31).
Neither WP or BAG presented any change in population balance or in D[4,3] (**Figure 3-19-B, E**).
The influence of substrate concentration and enzyme ratio are demonstrated in **Figure 3-20**. The slightest reduction of D[4,3] and percentage of coarse population was found for the higher substrate concentration (MCC-30%) and for the lower enzyme concentration (PP-27-0.1) compared to the lower substrate concentration (MCC-10%) and higher enzyme loading (PP-27-0.5). For example, the final D[4,3] for MCC-10% was 30% lower than those of MCC-30% (30µm compared to 45µm). The coarse population (>65µm) remained at 10% for PP-27-3%-0.5 at 24h but reached 20% for PP-27-3%-0.1 .
In conclusion, both chord length measurement and PSD conversion indicated for MCC, PP-27 and PP-31, during enzyme hydrolysis, the appearance of the fine population for the first 6-12h with an increase of N_{lc}, decrease of l_c and D[4,3]. The reduction of the solid fraction by its solubilisation led to the decrease of N_{lc} (from 6h) and the disappearance of the coarse population.

MCC

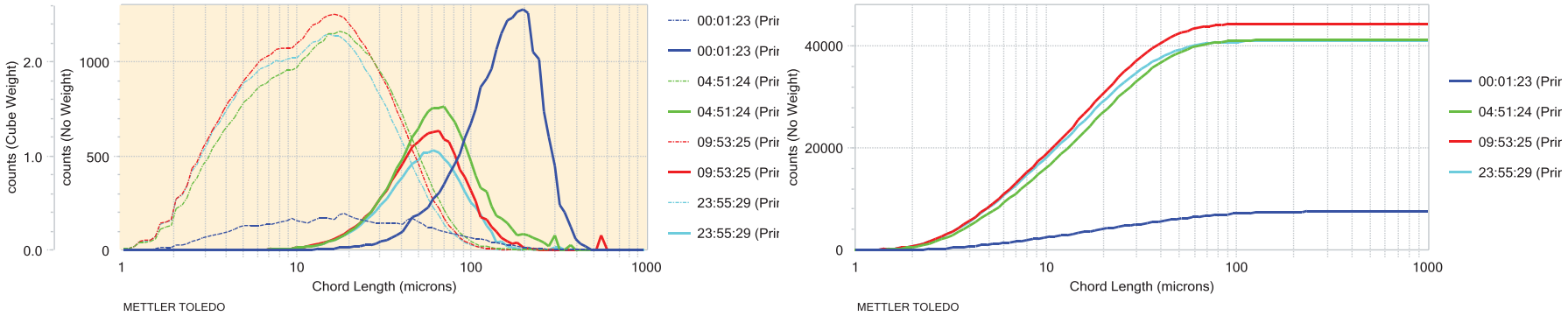
counts (Cube Weight)
counts (No Weight)
Chord Length (microns)
METTLER TOLEDO
00:01:23 (Prir
00:01:23 (Prir
04:51:24 (Prir
04:51:24 (Prir
09:53:25 (Prir
09:53:25 (Prir
23:55:29 (Prir
23:55:29 (Prir
counts (No Weight)
Chord Length (microns)
METTLER TOLEDO
00:01:23 (Prir
04:51:24 (Prir
09:53:25 (Prir
23:55:29 (Prir

WP

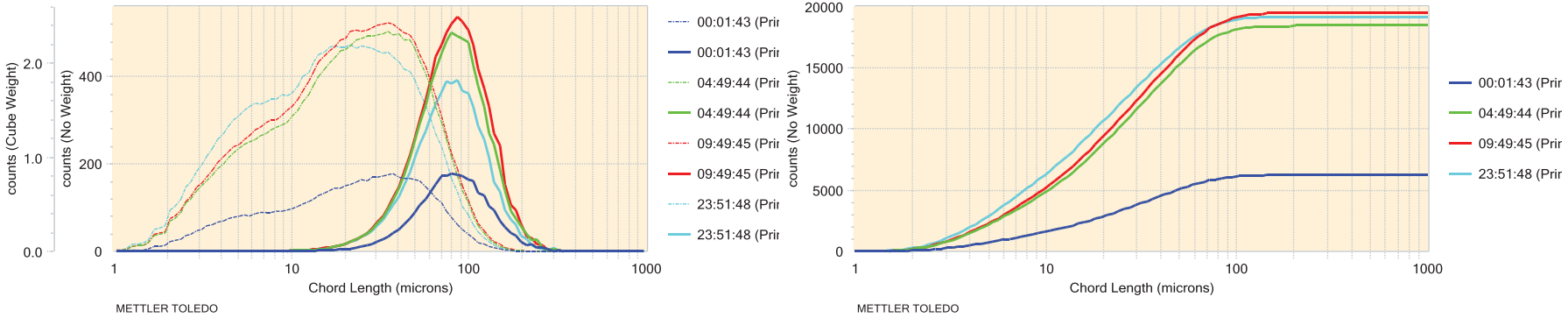
counts (Cube Weight)
counts (No Weight)
Chord Length (microns)
METTLER TOLEDO
00:01:43 (Prir
00:01:43 (Prir
04:49:44 (Prir
04:49:44 (Prir
09:49:45 (Prir
09:49:45 (Prir
23:51:48 (Prir
23:51:48 (Prir
counts (No Weight)
Chord Length (microns)
METTLER TOLEDO
00:01:43 (Prir
04:49:44 (Prir
09:49:45 (Prir
23:51:48 (Prir

PP-27

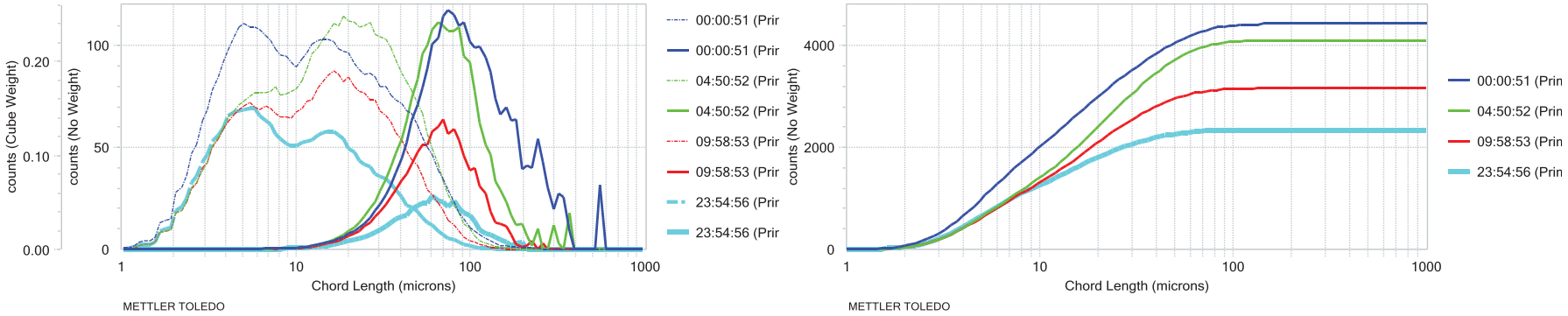
counts (Cube Weight)
0.00
0.10
0.20
counts (No Weight)
0
50
100
1
10
100
1000
Chord Length (microns)
METTLER TOLEDO
00:00:51 (Prir
00:00:51 (Prir
04:50:52 (Prir
04:50:52 (Prir
09:58:53 (Prir
09:58:53 (Prir
23:54:56 (Prir
23:54:56 (Prir
counts (No Weight)
0
2000
4000
1
10
100
1000
Chord Length (microns)
METTLER TOLEDO
00:00:51 (Prin
04:50:52 (Prin
09:58:53 (Prin
23:54:56 (Prin

PP-31

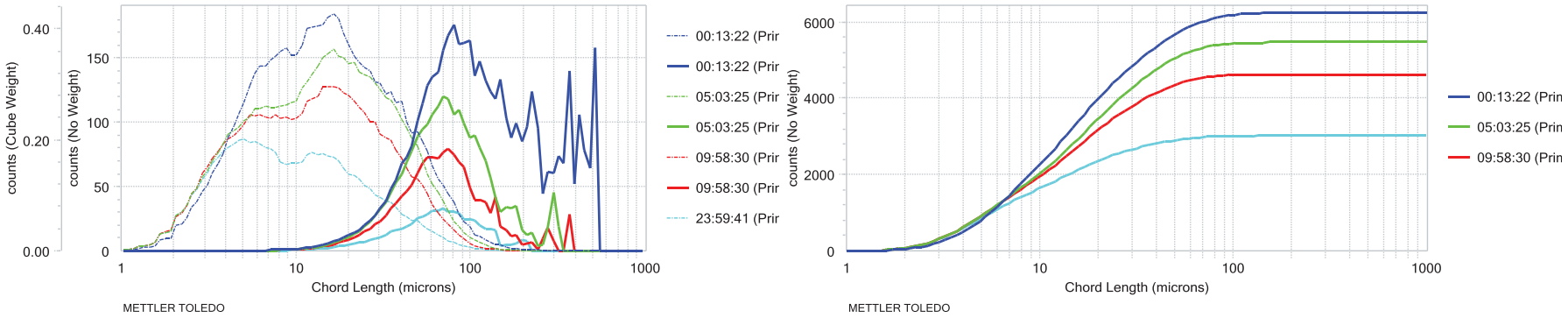
counts (Cube Weight)
0.00
0.20
0.40
counts (No Weight)
0
50
100
150
1
10
100
1000
Chord Length (microns)
METTLER TOLEDO
00:13:22 (Prir
00:13:22 (Prir
05:03:25 (Prir
05:03:25 (Prir
09:58:30 (Prir
09:58:30 (Prir
23:59:41 (Prir
counts (No Weight)
0
2000
4000
6000
1
10
100
1000
Chord Length (microns)
METTLER TOLEDO
00:13:22 (Prin
05:03:25 (Prin
09:58:30 (Prin

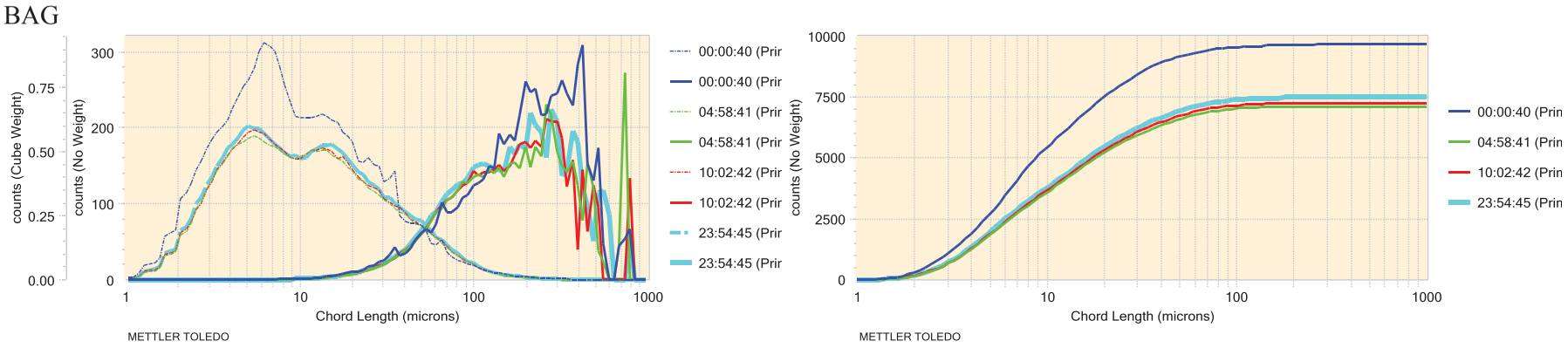

Figure 3-16: CLD analysis - Chord length distribution (Left) in volume, solid line: $Ev(l_c)$; in number, dotted line: $En(l_c)$ and cumulative distribution in number (Right) for five matrices (at 1%dm w/v, enzyme ratio 0.5mL/g cellulose) as a function of hydrolysis time (about 0h, 5h, 10h and 24h) (Cube Weight: in volume; No Weight: in number).

MCC

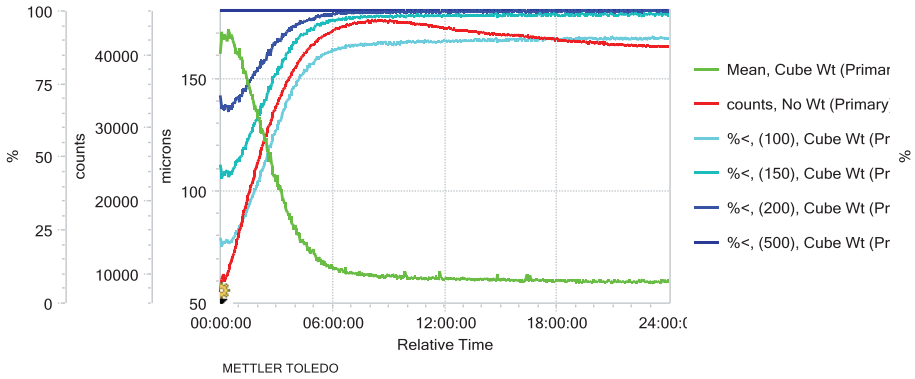

WP

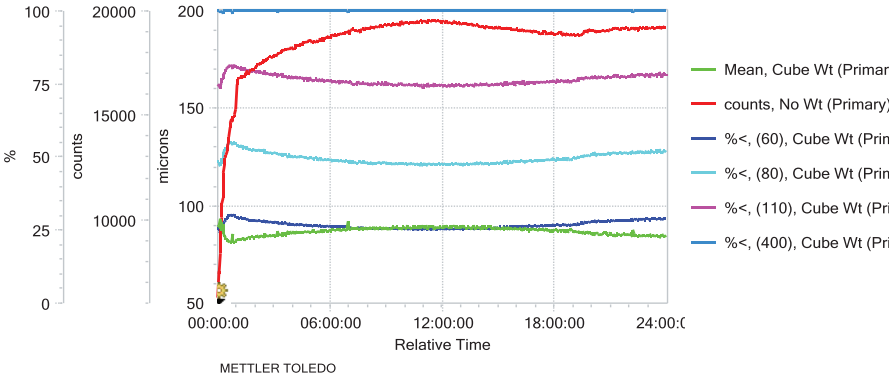

PP-27

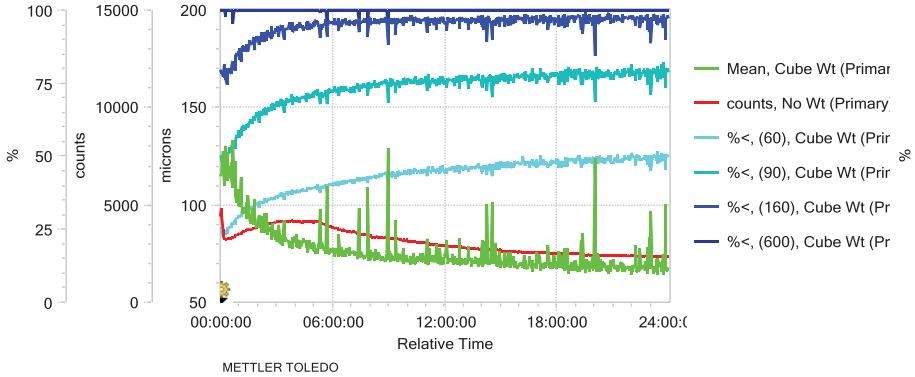

PP-31

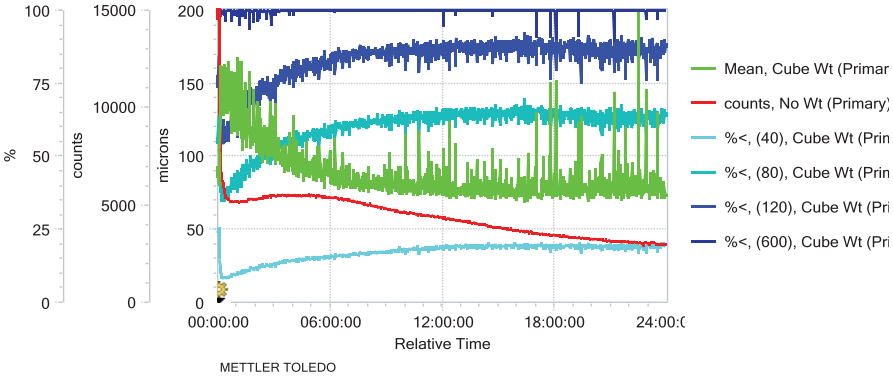

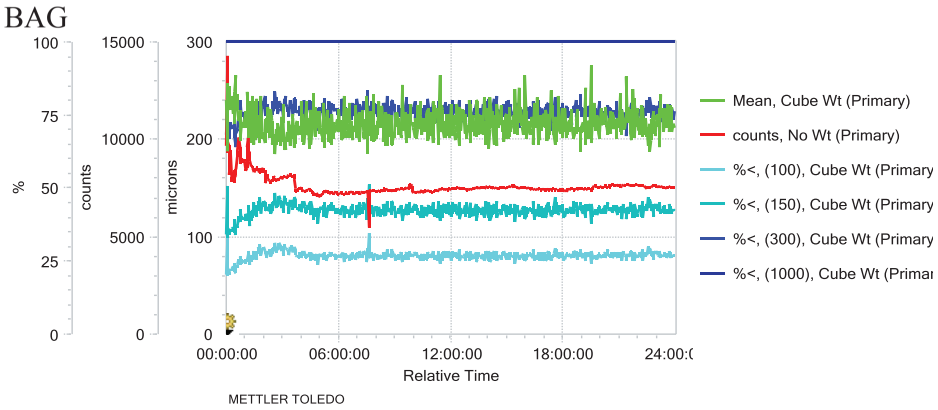

Figure 3-17: CLD analysis - Mean chord (in volume), chord number and population balance (class for 25, 50, 75 and 100% in volume of initial population) for five substrates (at 1%dm w/v, enzyme ratio: 0.5mL/g cellulose) during enzyme hydrolysis (%<(100) indicates the population percentage having the chord under 100µm) (Cube Wt: in volume; No Wt: in number).

MCC-1%-0.5

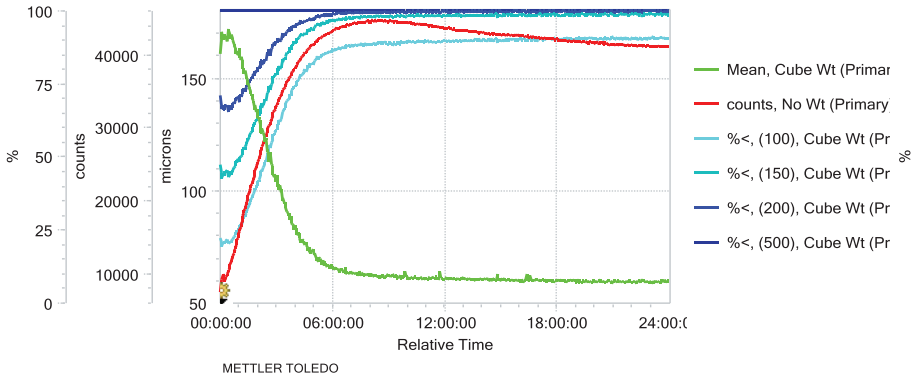

MCC-10%-0.5

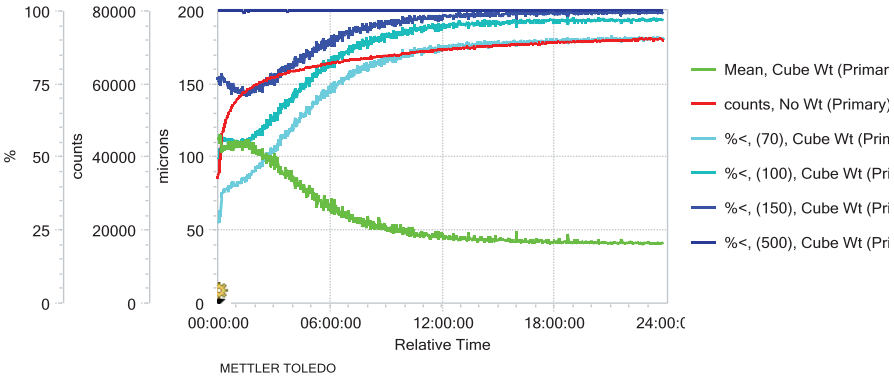

MCC-30%-0.5

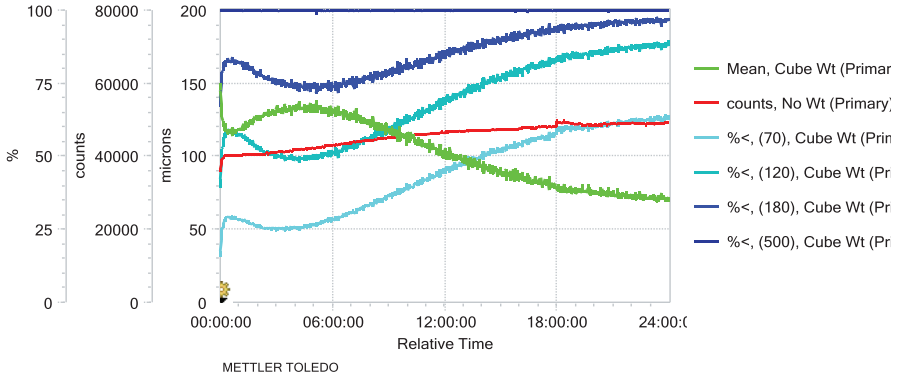

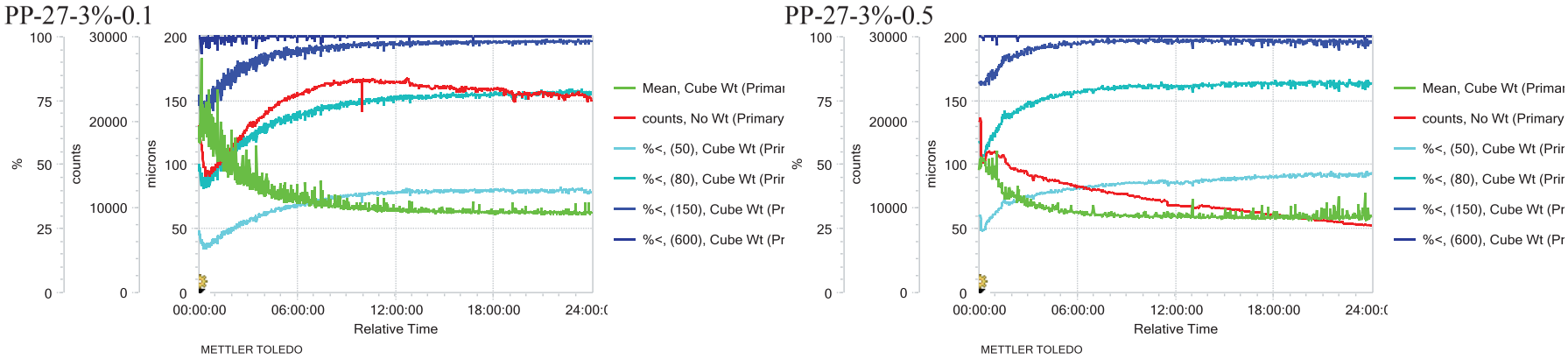

Figure 3-18: CLD analysis - Impact of substrate concentrations (MCC at three concentrations: 1%, 10% and 30%dm w/v) and impact of enzyme concentrations (PP-27-3% at two ratio E/S: 0.1 and 0.5mL/g cellulose) on mean chord (in volume), chord number and on population balance (class for 25, 50, 75 and 100% in volume of initial population) (%<(100) indicates the population percentage having the chord under 100µm) (Cube Wt: in volume; No Wt: in number).

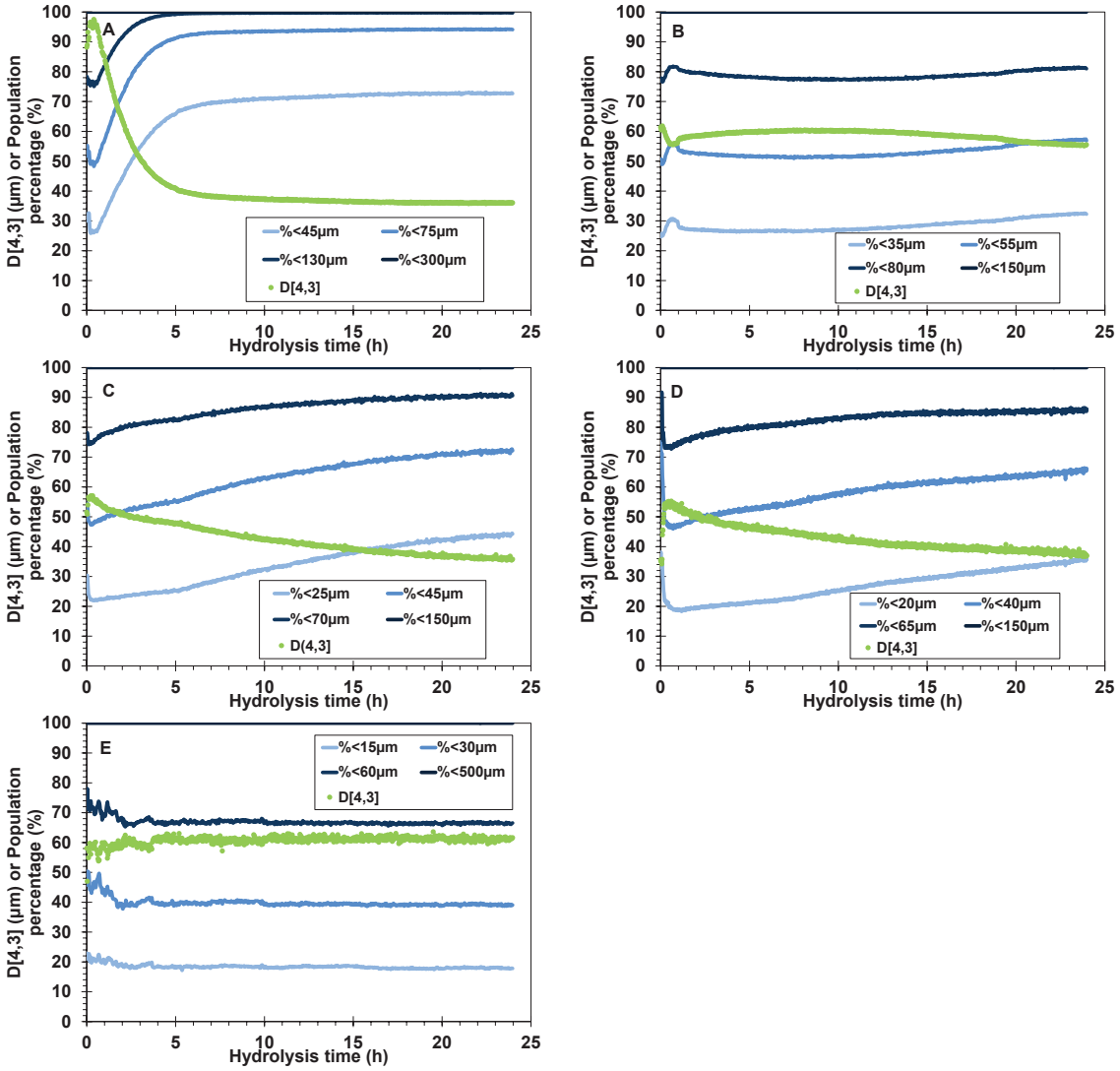

Figure 3-19: PSD analysis - D[4,3] and population balance (class for 25, 50, 75 and 100% in volume of initial population) versus hydrolysis time for the five substrates: MCC (A); WP (B); PP-27 (C); PP-31 (D) and BAG (E) in the same hydrolysis conditions (1%w/v, 0.5mL enzyme/g cellulose) (%<45µm indicates the percentage of the population with a diameter less than 45µm).

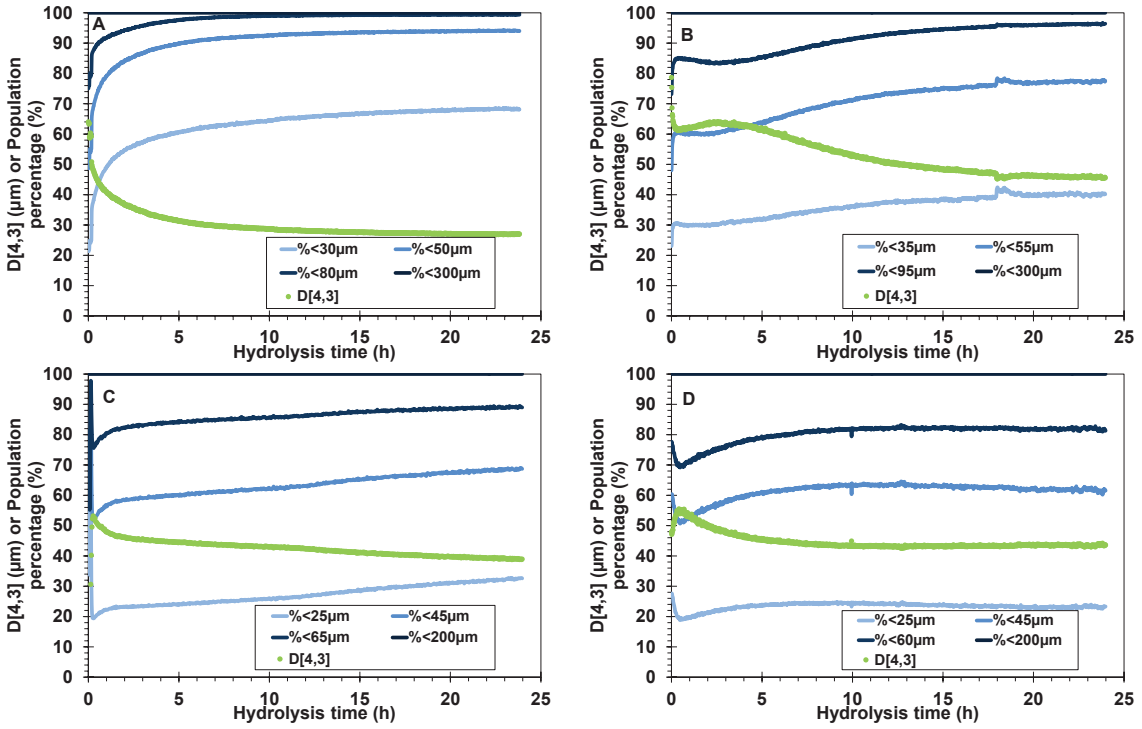

Figure 3-20: PSD analysis - Impact of substrate concentrations (MCC at two concentrations: 10% (A) and 30%dm w/v (B)) and impact of enzyme concentrations (PP-27-3% at two E/S ratios: 0.5 (C) and 0.1mL/g cellulose (D)) on D[4,3], population balance (class for 25, 50, 75 and 100% in volume of initial population) (%<30µm indicates the percentage of the population with a diameter under 30µm).

- Semi-continuous mode hydrolysis

Under semi-continuous mode, experiments were limited to WP and PP-27. Discussion concerns feed flow rate. As expected, the following main trends were noted: (i) the total number of chords increased during substrate additions; (ii) After the end of additions, chord number quickly increased before stabilising whereas mean chord length decreased before to stabilising. During each substrate feed, the same trends as in dilute conditions were observed.
In general, for 24h of hydrolysis, the mean chord decreased significantly for PP-27 but less so for WP (**Figure 3-21**). The initial/final mean chords were about 80/50µm and 150/50µm for WP and PP-27 respectively. Interestingly, irrespective of the flow rate, the same mean chord value was reached for both WP and PP-27 after 24h hydrolysis. This could be correlated to the same range of viscosity observed at the end of hydrolysis for these slurries.
At t=0h, the chord number corresponded to the initial substrate concentration. During hydrolysis, they increased at different speeds following the substrate feed flow rate. This development was faster with the higher flow rate. However, at the end of hydrolysis, the same value was reached whatever the substrate flow rate (~37000 for PP-27 and ~62000 for WP). According to the above results, the N_{lc} of WP was always higher than those of PP-27.

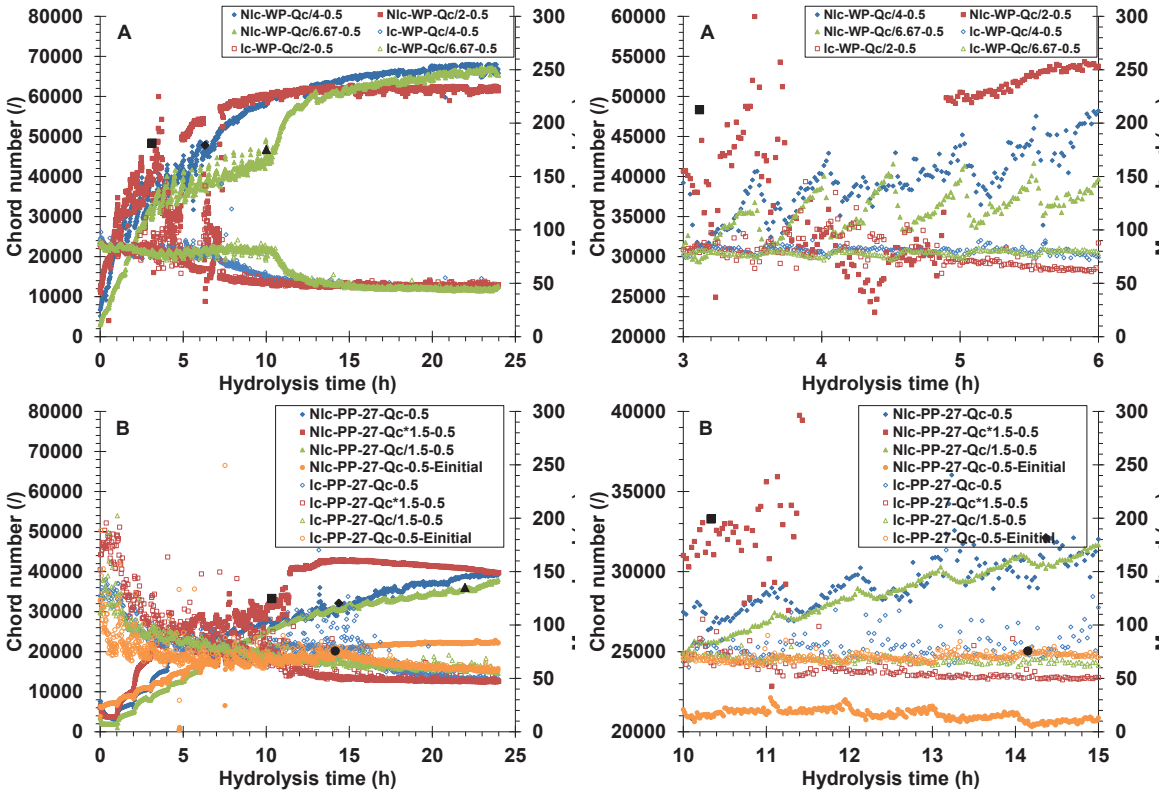

Figure 3-21: CLD analysis - Total chord number and mean chord length as a function of hydrolysis time under semi-continuous hydrolysis mode (A: WP and B: PP-27, Black dots indicate the end of substrate addition). Left: full experiment, Right: zoom of substrate addition.

Some experiments were conducted to compare two feed strategies: simultaneous enzyme/substrate addition (**Figure 3-21-B**- blue line) and introduction of the whole necessary enzyme quantity at the beginning of hydrolysis (**Figure 3-21-B**- orange line); we observed that both N_{lc} and l_c were lower all along hydrolysis when the enzyme was added at the beginning. At 24h, the final N_{lc} in this case was only about 20 000 which is about 50% of N_{lc} for simultaneous addition (~37 000). This is in agreement with the results of viscosity time

pattern (presented above) which demonstrated a ratio of 2 between final viscosities for these two experiments.
Zooming in on each of the substrate additions (**Figure 3-21-Right**), we observed exactly the same patterns as those observed in batch mode: a rising phase for both N_{lc} and l_c at the moment of substrate introduction and a descending phase which follows. Each substrate addition increases the solid concentration and thus increases Nlc and l_c also. The enzyme activity continues, the substrate is attacked and solid matter partially solubilised; this causes the decrease of N_{lc} and l_c.

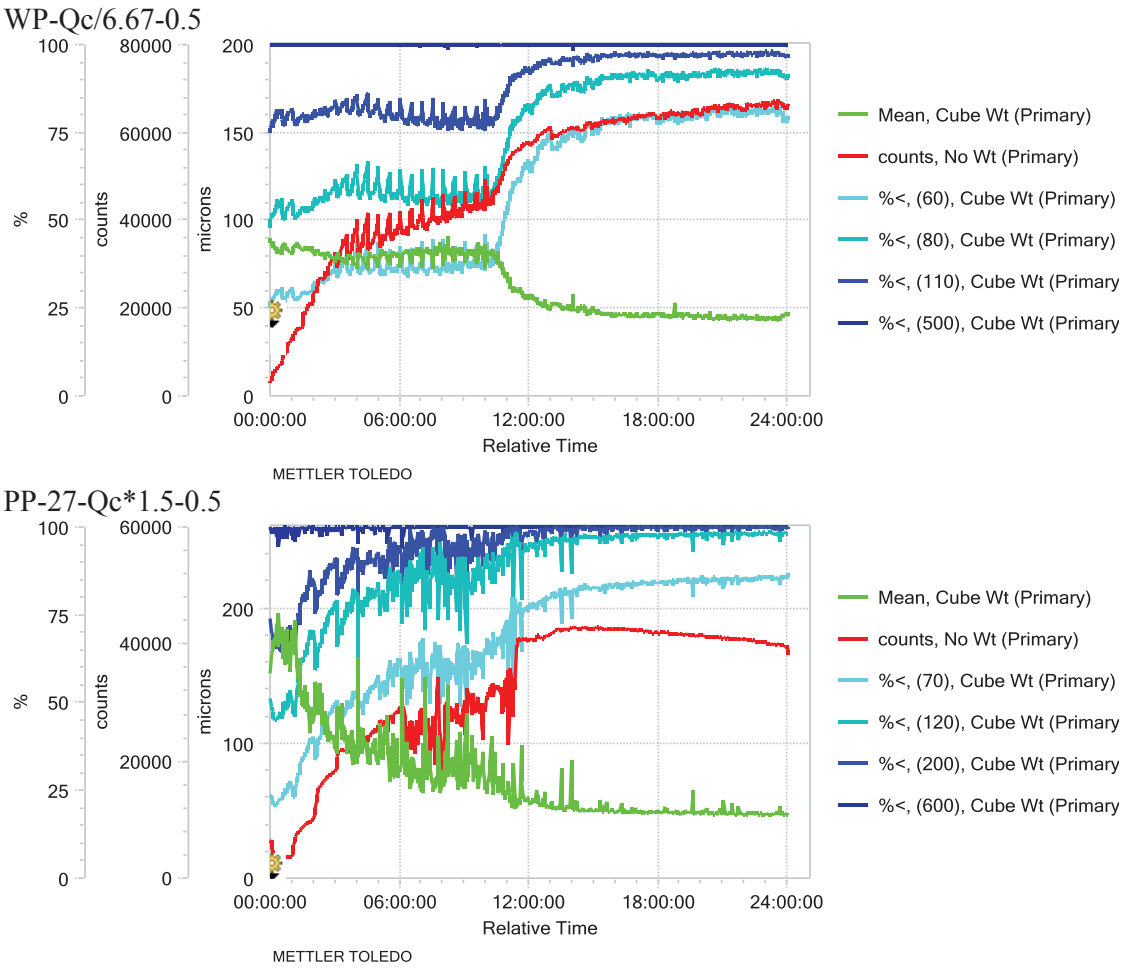

Figure 3-22: Mean chord (in volume), chord number and specific chord values (25, 50, 75, and 100% in volume of initial population) versus hydrolysis time under semi-continuous mode (top: WP at substrate feed rate of Qc/6.67 (Qc= 80gdm/h), ratio 0.5mL enzyme/g cellulose; bottom: PP-27 at substrate feed rate of Qc*1.5 (Qc= 8.67gdm/h), ratio 0.5mL enzyme/g cellulose).

Figure 3-22 illustrates population balance patterns for WP (Qc/6.67) and PP-27 (Qc*1.5) as hydrolysis progresses. It is clearly seen that, for both WP and PP-27, at the moment of substrate introduction, the percentage coarse population (lc>110µm for WP and lc>200µm for PP-27) increased rapidly in parallel with the decrease of the fine population. After that, the coarse population was degraded to form the smaller particles so their percentage decreased whereas the fine population increased.
Considering only the substrate feed period (about 0-12h-**Figure 3-22**), no significant change was observed in population balance for WP. However, for PP-27, the populations died vary.

After the period of substrate addition, results for both WP and PP-27 showed the disappearance of the biggest population and an exponential increase of the smallest population. As a result, at 24h, the fine population increased from 25% to 75% of the total population (in volume).

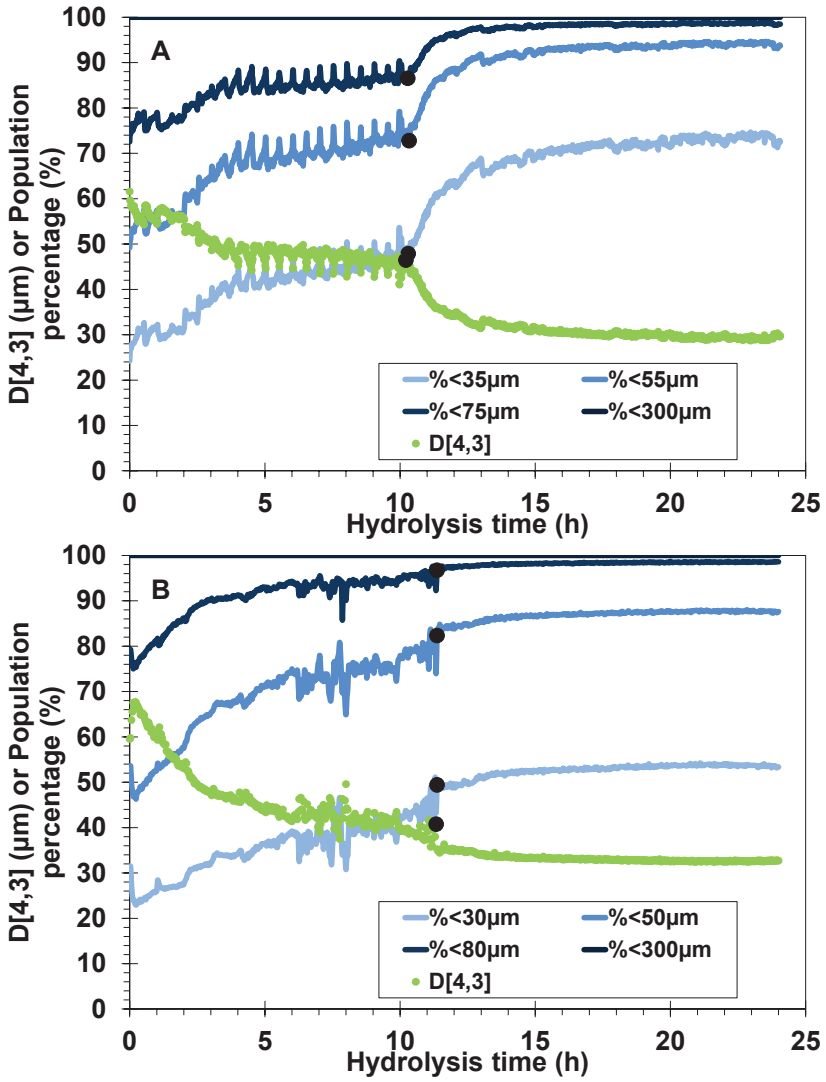

*Figure 3-23: PSD analysis - D[4,3] and population balance (25, 50, 75% in volume of initial population) versus hydrolysis time for WP-Qc/6.67 (A) (Qc= 80dm/h) and PP-27-Qc*1.5 (B) (Qc= 8.67gdm/h) (%<35µm indicates the percentage of the population with a diameter smaller than 35µm).*

All the above trends were confirmed when CLD was converted to PSD (**Figure 3-23**). Although the values of D[4,3] are significantly different from the mean chord values, the mean diameter (spherical equivalent) was halved from 60/70µm to 30/30µm for WP/PP-27. The coarse particles were completely degraded and the fine particles became the major population (70% for WP and 50% for PP-27 at 24h of hydrolysis).
We can conclude that for all CLD data and all PSD data, the kinetics of particle size (or chord) of fed-batch hydrolysis strategy can be considered as multiple batch mode experiments with the same kinetics.

3.2.3.2 Particle size distribution as determined by DLS (ex-situ)

The particle size distribution indicated firstly the proportion of laser obscuration and sample concentration and secondly the volume distribution of spherical equivalent diameter (D_{SE}). This measurement was performed for all experiments.

Figure 3-24-A illustrates the correlation between substrate concentration and laser obscuration for five substrates before hydrolysis at the same initial concentration of 3%w/v. For each substrate, three samples were prepared by dilution of an initial suspension with distilled water. The results showed that for all the suspensions, laser obscuration depended linearly on the substrate concentration. However, the actual proportion depended on the substrate nature, WP causing the most obscuration, giving MCC<BAG<PP-31≈PP-27<WP which highlights the difference in the optical properties of these five substrates.

As the particles were being degraded; a relationship was established between substrate concentration and laser obscuration (**Figure 3-24-B** for PP-31-3%**)** as a function of hydrolysis progress. For each hydrolysis time, the laser obscuration always depended linearly on sample concentration. Even so, the slope of these linear plots varied during hydrolysis time. We observed a significant increase of these slopes from 0h to 24h of hydrolysis. This signifies that the laser obscuration became increasingly dependent on the sample concentration or we can conclude that fibre optical parameters were modified during the enzyme attack. **Table 3-14** illustrates the time-dependence of the slope for these substrate concentration-obscuration curves: they increased during hydrolysis (excluding BAG). This pattern corresponds precisely to the enzyme progress which is more pronounced for the more attackable substrate while the slope remained stable for the less hydrolysable substrate (BAG). These observations demonstrate that under enzyme action, the lignocellulose fibres undergo not only particle size and shape modifications but also alterations of their optical properties.

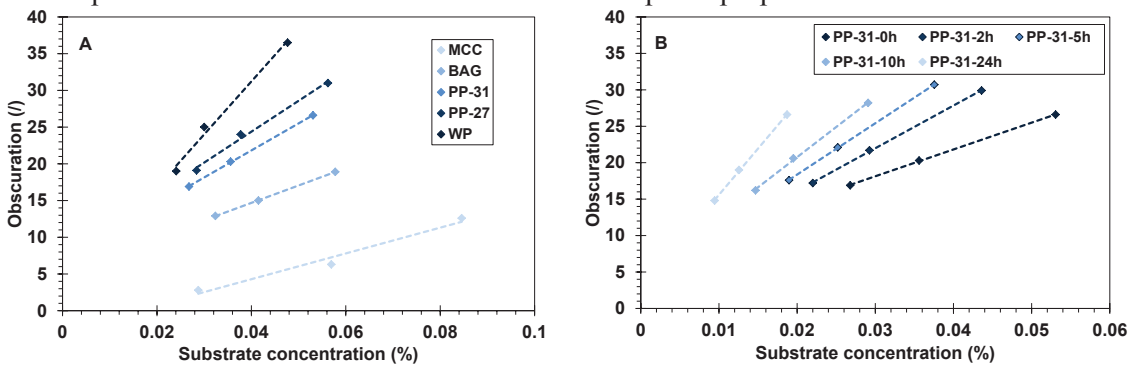

Figure 3-24: Relationship between substrate concentration and obscuration. (A)-For five substrates: MCC, WP, PP-27, PP-31 and BAG before hydrolysis at 3%w/v initial suspension; (B)-For PP-3%-0.5 during enzyme hydrolysis.

Table 3-14: Slope of substrate concentration-obscuration curve during hydrolysis for five substrates (initial suspension of 3%w/v; 0.5mL enzyme/g cellulose except MCC 0.1mL enzyme/g cellulose).

Time (h)	MCC	WP	PP-27	PP-31	BAG
0	175.4	410.0	420.6	368.1	236.6
2	368.2	-	428.8	506.1	-
5	402.3	504.8	577.3	703.4	-
10	420.0	557.3	808.0	828.0	231.8
24	480.6	651.3	1036.3	1268.3	227.4

- Batch mode hydrolysis

Figure 3-25 (Left) presents the volume distribution of D_{SE} for the five matrices under the same conditions: 1%w/v, 0.5mL enzyme/g cellulose. Before introducing enzyme, MCC and BAG presented a monomodal distribution, which was bimodal for WP, PP-27 and PP-31. During hydrolysis (except for BAG which did not undergo any change in particle diameter distribution) the population size shifted from coarse to fine particles. For MCC, the hydrolysis effect was mainly observed on coarse particles. The initial population tended towards a log-normal distribution. For WP coarse and fine populations were degraded giving four populations with average diameters of 3µm, 20µm, 75µm and 350µm after 24h indicating a macroscopic cutting effect on fibres. For PP-27 and 31, several mechanisms seem to occur. In the first step, the split between coarse and fine is strengthened. The fine population increases and shifts to a smaller diameter. The reduction process was observed later for the fine particles (from t=10h). The change in volume distribution of D_{SE} was clearly observed for 5h with MCC, 10h with WP and throughout the 24h for PP-27 and 31.

Figure 3-25 (Right) presents the trends of different populations corresponding to 25, 50 and 75% of the initial population. Excluding BAG, which presented no significant changes, the others showed similar patterns as hydrolysis progressed. The biggest population disappeared rapidly during hydrolysis (in the first five hours for MCC and in about the first ten hours for the three other matrices). In addition, the finest population increased. After 24 hours of hydrolysis, the percentage of fine population was multiplied by 3 for MCC (from about 25 to 75%) and by 2 for WP and PP-27 (from about 25 to 50%). Especially for PP-31, at the end of hydrolysis, we observed a degradation of the fine population; its percentage decreased between 10h and 24h (from about 45% to 30%) due to solid matter solubilisation.

Volume distribution functions of D_{SE}

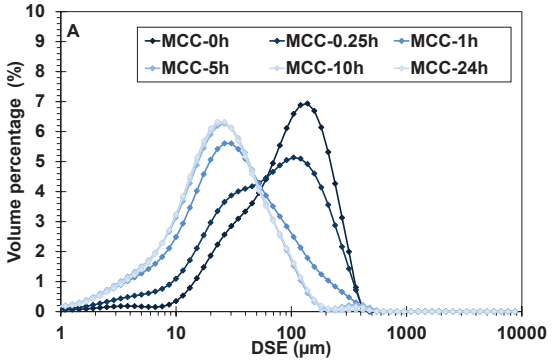

Population balance evolutions

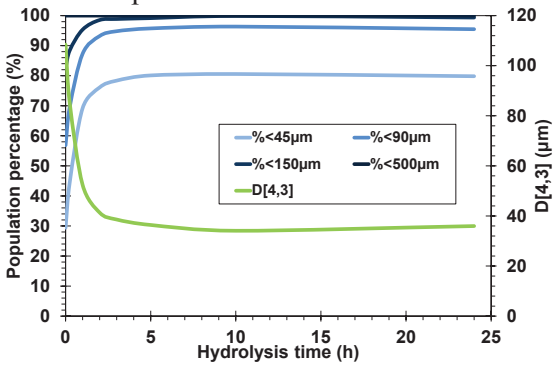

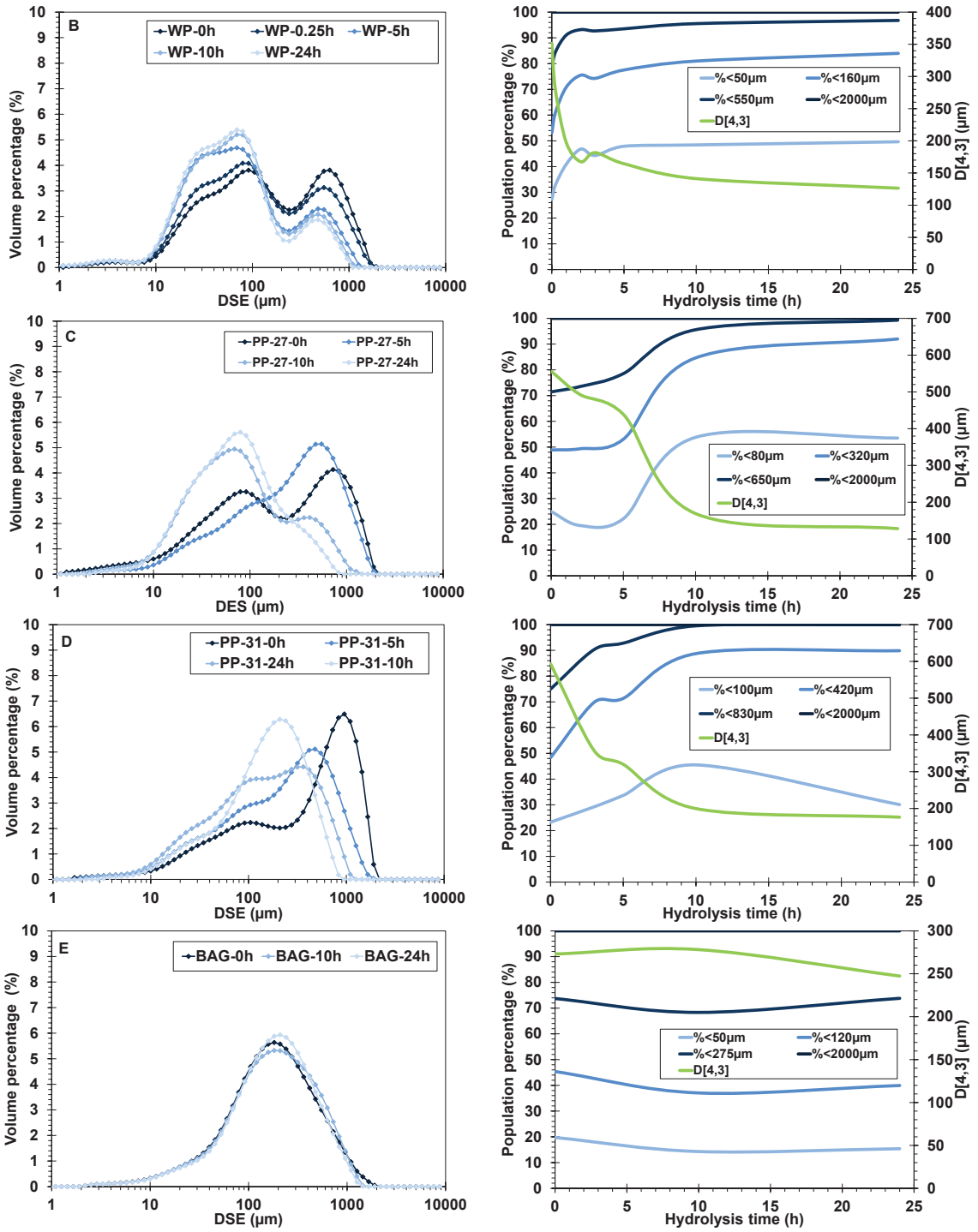

Figure 3-25: PSD analysis - Volume distribution versus spherical equivalent diameter (D_{SE}) (Left) and evolution of D[4,3] and population balance (25, 50, 75% in volume of initial population) during enzyme attack for the five substrates: (A) MCC, (B) BAG, (C) PP-27, (D) PP-31, (E) WP in the same hydrolysis conditions (1%w/v; 0.5mL enzyme/g cellulose) (%<45µm indicates the population percentage having diameter below 45µm).

Each population distribution can be characterised by different quantities linked to the distribution function or to the cumulative distribution. In the present case, we are interested in

a volume mean diameter D[4,3] and the special values based on volume cumulative distribution. We retained the following criteria: particle diameters for 10, 50 and 90% of the population are called $d_v(0.1)$, $d_v(0.5)$, $d_v(0.9)$. Results for these quantities are presented in **Table 3-15** for the five substrates. D[4,3] decreases regularly during enzyme hydrolysis (except BAG). Comparing initial and final values, a 3-fold reduction was found whatever the substrate (**Table 3-15**). This leads to the reduction of suspension viscosity. With MCC, halving the mean diameter of Solka floc within 25 hours has already been reported (Um & Hanley, 2008). A reduction of 40% of fibre length of Solka floc C100 was reported by Tozzi et al. (2014).

For hydrolysis of dilute acid pre-treated softwood (D[4,3]=109µm, concentration: 10%w/w): the coarse population (>100µm) decreased from 44.2% to 19.7% after 24h (Wiman et al., 2010). In the present work the mean diameter decrease occurred faster than for Wiman et al., 2011 reporting that the fibre diameter was stable for 10h and was then reduced by 20% at 24h. For cardboard waste, the mean length of fibre was decreased by 20% within 24h for 10%w/w suspension (Kinnarinen & Häkkinen, 2014).

The way $d_v(0.9)$ behaved indicated the reduction of coarse particles in suspension under enzyme attack. We also found a factor of 3 times for this decrease during 24h hydrolysis: from 221, 950, 1082 and 1332µm to 71, 380, 309 and 472µm for MCC, WP, PP-27 and PP-31 respectively.

In this study, the PSD measured showed almost no change during hydrolysis for BAG suspension, and even if cellulose degradation was observed, it seems that enzymes were not able to open the fibre networks and separate the fibres into smaller particles. This observation matches the results reported by Kadic et al. (2014) for a 13% spruce (w/w).

Comparing different hydrolysis conditions for a given matrix (ex. PP-27, **Table 3-16**), the decrease of the mean diameter was faster for higher concentrations of enzyme. For PP-27-3%-0.5, it takes only 5 hours to halve the initial D[4,3] while this value is 10 hours for PP-27-3%-0.1. At the end of hydrolysis the D[4,3] of PP-27-3%-0.1 was 50% higher than that of PP-27-3%-0.5. This observation could be one of the reasons that explain the difference of viscosity changes during hydrolysis.

This tendency was observed with all the substrates. For lower enzyme quantity, lower fibre degradation and higher particle diameters are observed.

- Semi-continuous mode hydrolysis

The variation of $d_v(0.1)$, $d_v(0.5)$, $d_v(0.9)$ and D[4,3] is presented in **Figure 3-26** for different hydrolysis times: 0h, 5h, 10h and 24h. Results for both PP-27 and WP show the decrease of $d_v(0.1)$, $d_v(0.5)$, $d_v(0.9)$ and D[4,3] with hydrolysis time. They exhibited similar kinetics whatever the substrate flow rate. Their values were totally comparable with those of experiments in dilute regime. For example, the D[4,3] of 0, 5, 10 and 24h for PP-27-Qc-0.5/PP-27-3%-0.5 were respectively 402/469, 202/170, 131/137 and 103/107µm. This signifies that there was no modification in the particle size domain when changing the substrate feed strategy. Then generally speaking, the variation of particle size depends only on the origin of the substrate and on the E/cellulose ratio. No effect of process strategy was found.

Table 3-15: Diameters $d_v(0.1)$, $d_v(0.5)$, $d_v(0.9)$ and D[4,3] during enzyme hydrolysis for five matrices for the same conditions: 1%dm, 0.5mL E/g cellulose.

		0h	0.25h	5h	10h	24h
MCC	$d_v(0.1)$	23.9±1.5	13.3±0.5	6.3±0.3	6.5±0.2	6.8±0.3
	$d_v(0.5)$	91.3±11.5	62.0±5.8	25.7±0.2	25.3±0.3	25.5±0.3
	$d_v(0.9)$	221.0±24.0	192.1±26.5	75.5±2.3	73.9±1.5	77.1±2.9
	D[4,3]	108.4±12.1	84.8±10.0	36.4±2.0	34.1±0.9	36.0±1.7
WP	$d_v(0.1)$	24.4±0.7	21.2±0.3	18.1±0.1	18.3±0.2	17.9±0.5
	$d_v(0.5)$	160.6±28.0	114.0±11.4	65.4±1.9	64.1±2.4	60.8±1.2
	$d_v(0.9)$	950.4±105.5	799.8±76.9	514.5±8.3	438.9±9.8	379.7±10.0
	D[4,3]	351.4±46.2	278.8±29.4	162.4±3.8	141.5±4.2	125.6±2.6
PP-27	$d_v(0.1)$	22.6±0.7	-	30.0±2.7	19.4±0.7	20.3±1.0
	$d_v(0.5)$	185.6±6.6	-	231.1±43.7	79.3±6.0	80.2±8.6
	$d_v(0.9)$	1082.3±24.6	-	817.9±74.4	481.9±43.4	308.7±30.0
	D[4,3]	402.1±9.1	-	338.9±38.8	169.1±15.1	128.3±13.2
PP-31	$d_v(0.1)$	38.8±2.0	-	31.2±0.8	21.5±0.6	35.6±5.5
	$d_v(0.5)$	510.3±41.7	-	250.1±11.7	106.7±7.0	186.8±40.3
	$d_v(0.9)$	1332.3±40.2	-	850.3±50.6	446.8±30.2	472.3±75.4
	D[4,3]	593.6±26.9	-	357.2±18.2	176.4±12.2	199.8±14.5
BAG	$d_v(0.1)$	37.8±6.2	-	-	44.4±2.8	42.0±5.4
	$d_v(0.5)$	169.7±17.9	-	-	195.0±10.4	177.4±18.5
	$d_v(0.9)$	657.3±35.9	-	-	638.4±26.1	546.2±45.0
	D[4,3]	278.2±10.7	-	-	278.2±10.8	247.3±19.9

Table 3-16: Comparison of $d_v(0.1)$, $d_v(0.5)$, $d_v(0.9)$ and D[4,3] between different hydrolysis conditions for PP-27.

	Quantities (µm)	0h	5h	10h	24h
PP-27-3%-0.1	$d_v(0.1)$	38.9±1.9	17.9±0.6	17.7±0.6	15.5±0.7
	$d_v(0.5)$	343.5±62.7	99.0±3.4	91.6±2.9	66.6±1.9
	$d_v(0.9)$	1190.3±71.8	800.1±100.6	655.5±66.2	452.6±26.5
	D[4,3]	456.0±43.9	264.6±25.7	223.8±18.2	154.9±9.0
PP-27-3%-0.5	$d_v(0.1)$	22.6±0.7	16.8±0.4	15.5±0.4	17.1±0.4
	$d_v(0.5)$	185.6±6.6	75.6±2.8	60.0±1.7	57.8±3.1
	$d_v(0.9)$	1082.3±24.6	612.0±92.8	384.0±17.4	257.7±6.7
	D[4,3]	402.1±6.1	201.4±25.8	131.0±3.8	103.4±2.9

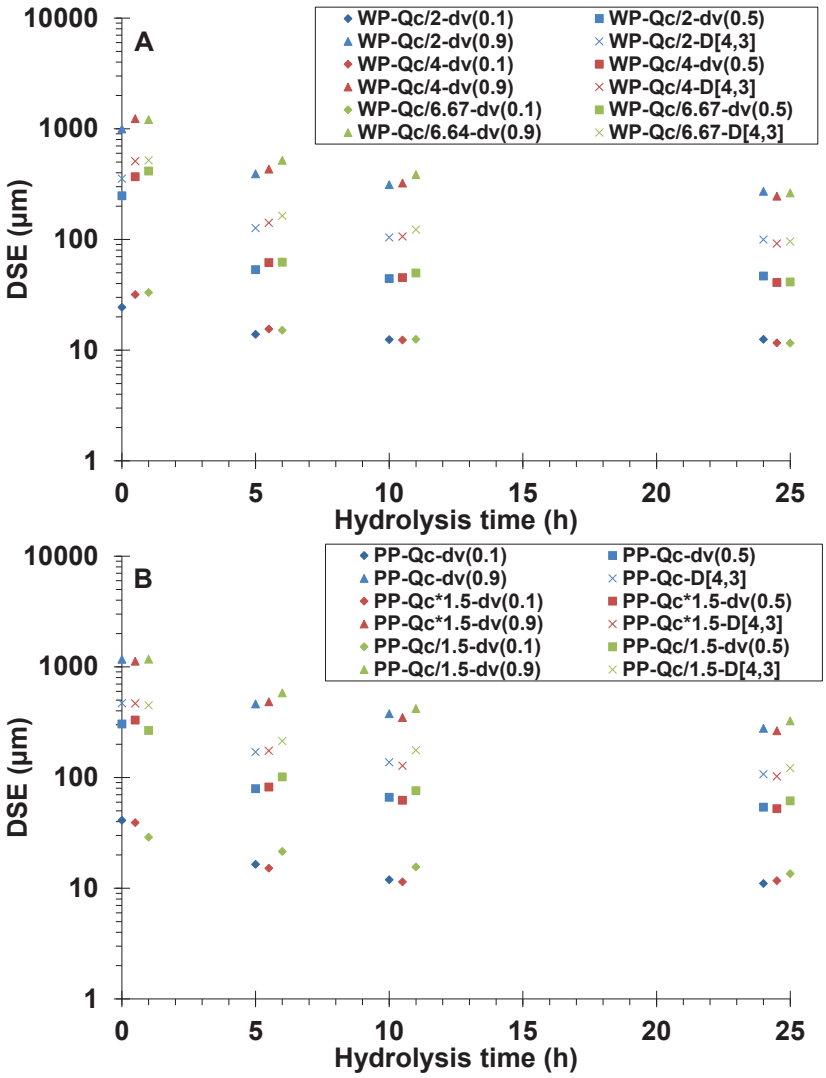

Figure 3-26: $d_v(0.1)$, $d_v(0.5)$, $d_v(0.9)$ and D[4,3] versus hydrolysis time for WP (A) and PP-27 (B) at semi-continuous mode.

3.2.3.3 Morpho-granulometry (ex-situ)

The morpho-granulometric studies provided detailed information on particle size and shape. Based on area measurement, this analysis gives us the circle equivalent diameter (D_{CE}) and its distribution together with particle geometrical properties. The results obtained here are limited to dilute concentration experiments.

Figure 3-27 presents optical observations of substrate suspensions at different hydrolysis times for MCC, BAG, WP, PP-27 and PP-31. The suspensions exhibited a heterogeneous character but during the hydrolysis, the shape and size of the particles changed drastically and the suspension heterogeneity became less pronounced as hydrolysis continued. For all matrices, the fibre structure became less compact. The coarse particles became divided into the smaller particles. We observed the appearance of fine particles while the larger particles disappeared. This phenomenon is widely mentioned in the literature (Alvira et al., 2010; Kinnarinen & Häkkinen, 2014; Tozzi et al., 2014; Wyman, 2007). Besides, the cellulose fibres became increasingly transparent, especially for MCC and PP.

Figure 3-28 (Left) assumes the hydrolysis time dependence of volume cumulative distribution of D_{CE} ($F_v(D_{CE})$) for five substrates: MCC, WP, PP-27 and PP-31 and BAG at different hydrolysis times: 0, 5, 10, 24h. Changes in $F_v(D_{CE})$ for BAG were not significant (**Figure 3-28-E**). The particle size distribution of each slurry illustrates, at t=0h, a population between 10 and 300µm for MCC and between 10 and 400µm for the three other matrices. During hydrolysis, these populations became steadily smaller. This change was observed clearly for 5h with MCC, for 10h with WP and all along hydrolysis time for PP. Taking, for instance, a value D_{CE}=100µm, the volume percentage of particles having D_{CE}<100µm is 54%, 3%, 19% and 10% for MCC, WP, PP-27 and PP-31. The enzyme decreased D_{CE} so these volume percentages increasedreaching 100, 30, 80 and 50% at the end of hydrolysis.

Considering the classes defined as 25, 50 and 75% of the initial population, their variations during the hydrolysis are presented in **Figure 3-28 (Right)** for five matrices in the same conditions (1%w/v, 0.5mL enzyme/g cellulose). Except for BAG which showed no significant variation of population balance, the substrates all exhibited the same trend. The coarse population disappeared within a few hours of hydrolysis and was replaced by the fine population. These observations are similar to the results obtained using DLS.

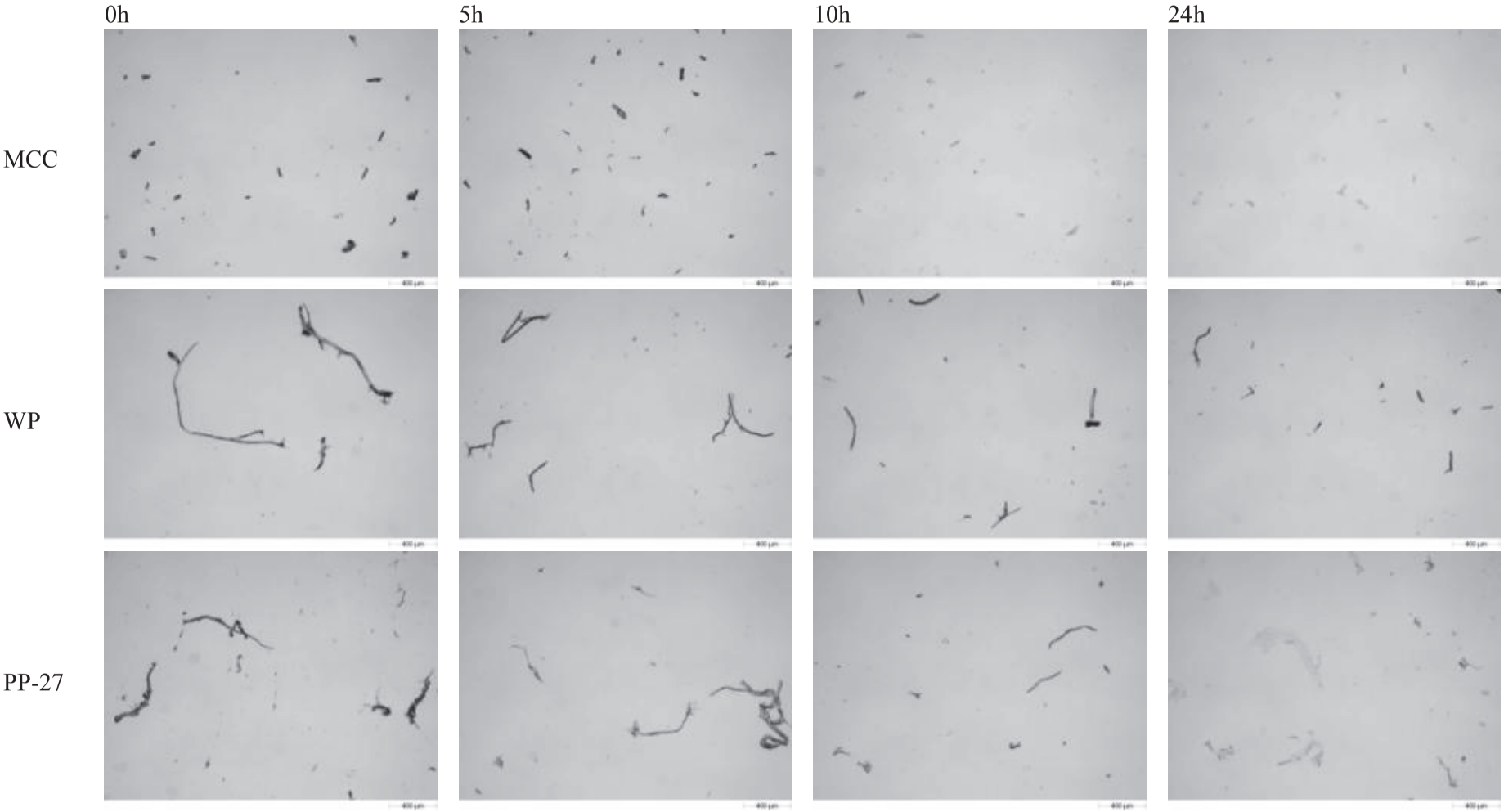
0h
5h
10h
24h
MCC
WP
PP-27

PP-31

BAG

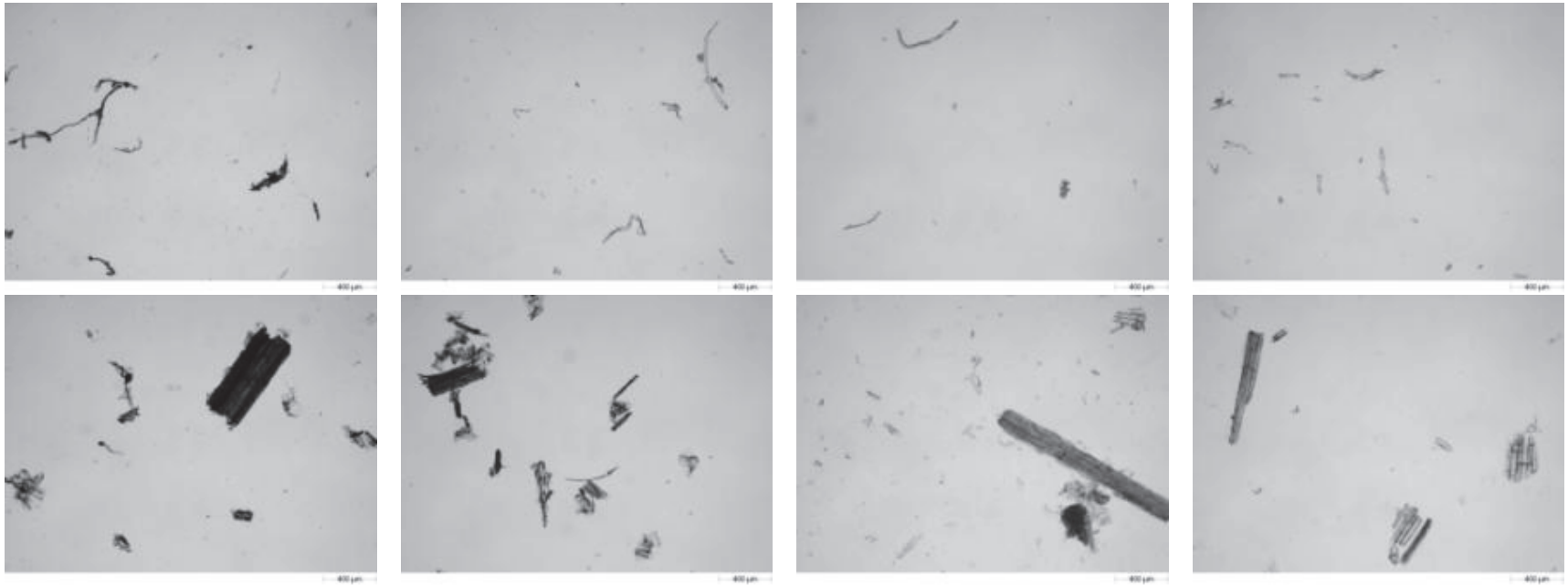

Figure 3-27: Fibre observations at different hydrolysis times: 0h, 5h, 10h, 24h for all substrates (optic x2.5; 3%w/v; 0.5mL enzyme/g cellulose excluded MCC 1%w/v).

Cumulative volume distribution of D_{CE}

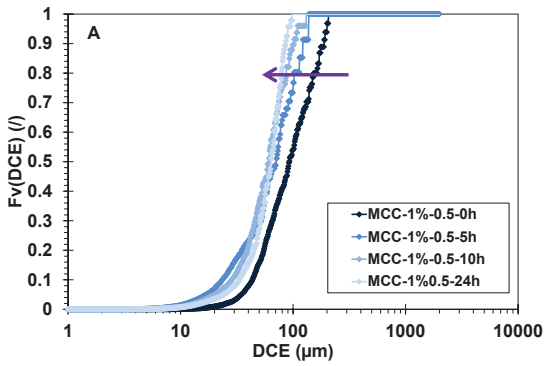

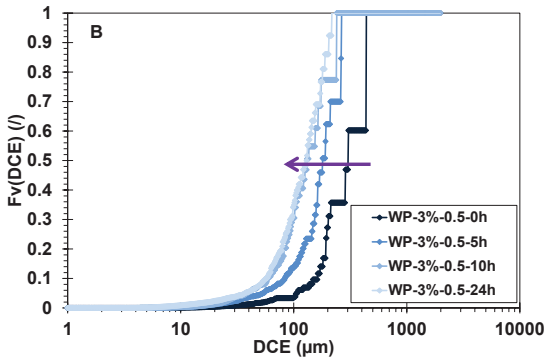

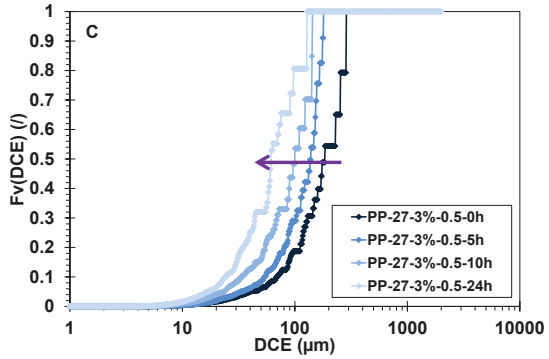

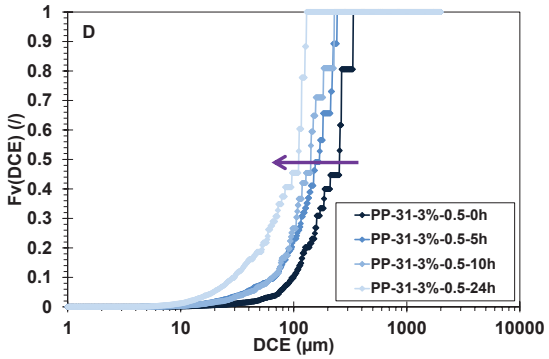

Population balance

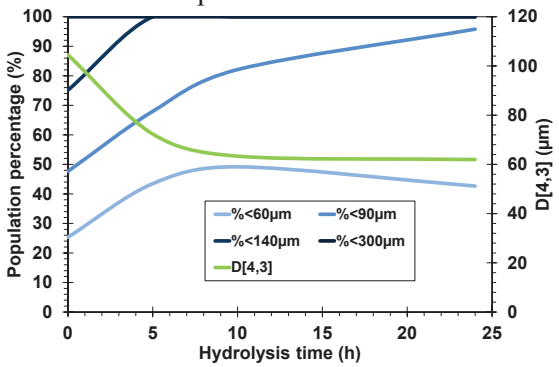

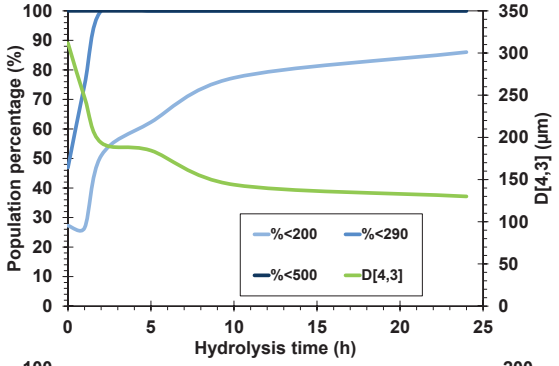

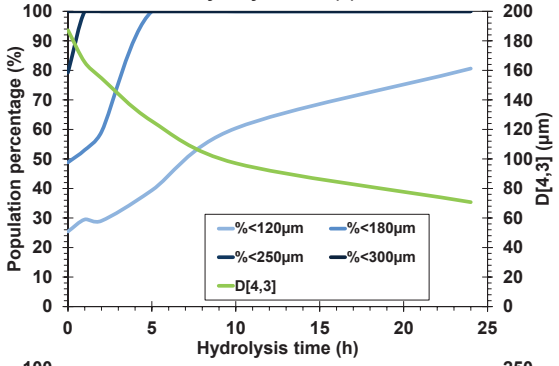

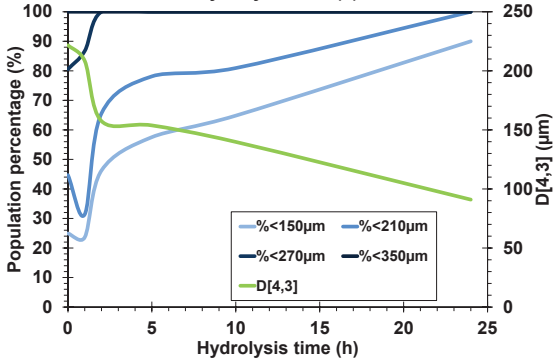

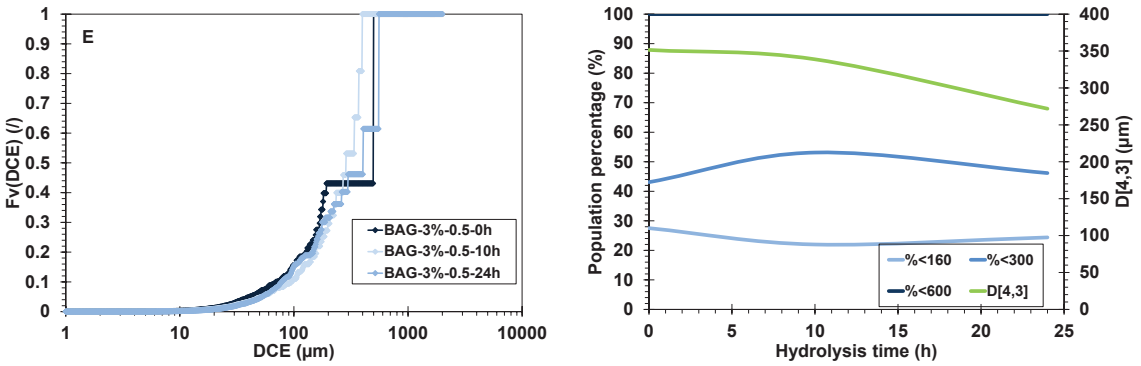

Figure 3-28: PSD analysis - Cumulative volume distribution as a function of circle equivalent diameter (D_{CE}) (Left) and D[4,3] and population balance (25, 50, 75% in volume of initial population) during enzyme attack for five substrates: (A) MCC, (B) WP, (C) PP-27, (D) PP-31, (E) BAG in the same hydrolysis condition (3%w/v; 0.5mL enzyme/g cellulose; except MCC: 1%w/v) (%<60µm indicates the percentage population with a diameter smaller than 60µm).

Together with the distribution function, the variation of particle size, represented by mean volume diameter, versus time is reported in **Table 3-17**. Surprisingly, the mean diameter of these substrates was lower than the values obtained by DLS. However, the trends noted for D_{CE} behaviour under enzyme activity was strengthened. This quantity decreased during enzyme attack for all the substrates (excluding BAG which remained fairly constant). After 10 hours of hydrolysis, initial particle diameter was halved, in complete agreement with the results obtained for DLS.

Table 3-17: Mean volume diameter as a function of hydrolysis time for five substrates in the same conditions: 3%dm, 0.5mL E/g cellulose (except MCC: 1%dm).

Time	MCC	WP	PP-27	PP-31	BAG
0h	104.5	311.8	187.2	221.7	171.0
1h	-	247.2	165.5	208.4	-
2h	-	193.7	154.7	157.4	-
5h	72.3	184.4	125.6	153.8	-
10h	63.3	143.9	97.1	139.8	168.4
24h	62.0	130.0	70.7	91.0	161.4

Considering the mean intensity – the average of the pixel greyscale levels for a particle – we observed a significant change for MCC and PP, but for two matrices: BAG and WP, the changes of mean intensity were weak. For greyscale images, the mean intensity varies between 0 (black) and 255 (white). When a fibre is more transparent, its mean intensity (Int_m) tends to 255.

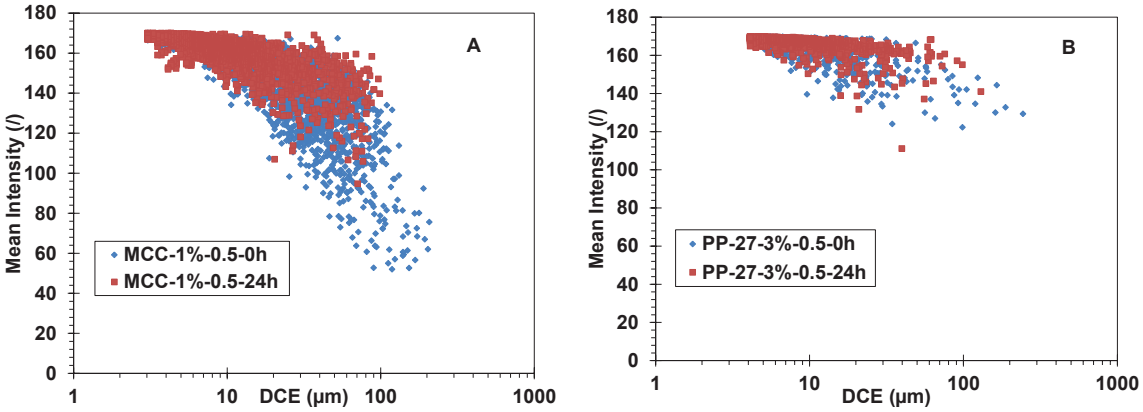

Figure 3-29: Mean intensity during hydrolysis for MCC (A) and PP-27 (B).

During hydrolysis, and simultaneously with the reduction of particle size; the white-level of the fibre increased. This phenomenon clearly observed for MCC substrate. Under enzyme, the fibre structure was deformed; the linkages between different fractions (hemicellulose – cellulose) were degraded to open the matrix to release the products such as glucose and xylose. The substrate became less compact, and increasingly transparent. **Figure 3-29** plots the mean initial intensity and after hydrolysis for two substrates: MCC and PP-27. It shows that at t=0h, the population of MCC particles was darker than those of PP-27 and after enzyme hydrolysis the Int_m decreased (e.g., with Int<150, particle volume percentage for MCC was 89%, whereas for PP-27 it was only 48%, after hydrolysis, these values fell to 26% and 6% for MCC and PP-27 respectively).
For the other substrates, no significant results were obtained, so the trend given by optical observations was not demonstrated perfectly. To our knowledge, no studies have focused on the relationship between fibre intensity and lignocellulose enzyme hydrolysis. However, we think that this will be a valuable approach to characterise the biodegradation of lignocellulose fibres. The difficulty with this approach is sample preparation (because of their heterogeneous properties) and intensity calibration (background, threshold determination).

3.2.3.4 Stockes's diameter from decantation kinetics (ex-situ)

This section firstly presents results concerning the settling velocity of particles, which was then used to determine the Stockes diameter. Of course, with substrates exhibiting no decantation during experiments, it was impossible to determine a falling diameter. In our experimental conditions, suspensions of WP 3%w/v and PP 3%w/v before hydrolysis presented no decantation so the Stockes diameter was obtained essentially for MCC and BAG. One experiment was performed for PP-27-1% to deduce its Stockes diameter.
The particle settling velocities of for MCC, PP-27 and BAG are presented in **Figure 3-30** as a function of their concentration. Comparing the suspension before and after hydrolysis, the settling velocity increased significantly for a given substrate concentration. This is coherent with the rapid sediment accumulation shown in §3.2.2. Matrices MCC and PP-27 exhibited similar settling velocities, higher than that of BAG. Interestingly, for PP-27, a 100-fold difference in settling velocity was found considering the initial and final suspension (at 0.3%w/w, $v_s \approx 10$ and $1000 mm.h^{-1}$ for t=0h and 24h respectively). This observation highlighted the important role of enzyme activity in modifying the fibre structure and properties.
Table 3-18 presents the mean diameters obtained for three substrates: MCC, PP-27 and BAG. The mean falling diameter (in volume) decreased in the order PP-27>BAG>MCC. These diameters became reduced as hydrolysis progressed (except for BAG). We found that MCC was halved (from 48 to 26µm) and that of PP-27 fell by about 30% after 24h hydrolysis. For

BAG, the mean diameter remained stable in spite of the enzyme attack. These observations are in full agreement with the results of the other measurement techniques.

Figure 3-31 gives an example of volume cumulative distribution of falling diameter for MCC before and after hydrolysis. Within 24h, degradation of the coarse population was observed to parallel solubilisation of the fine population. This figure is concordant with the conclusion from the morpho-granulometry measurements.

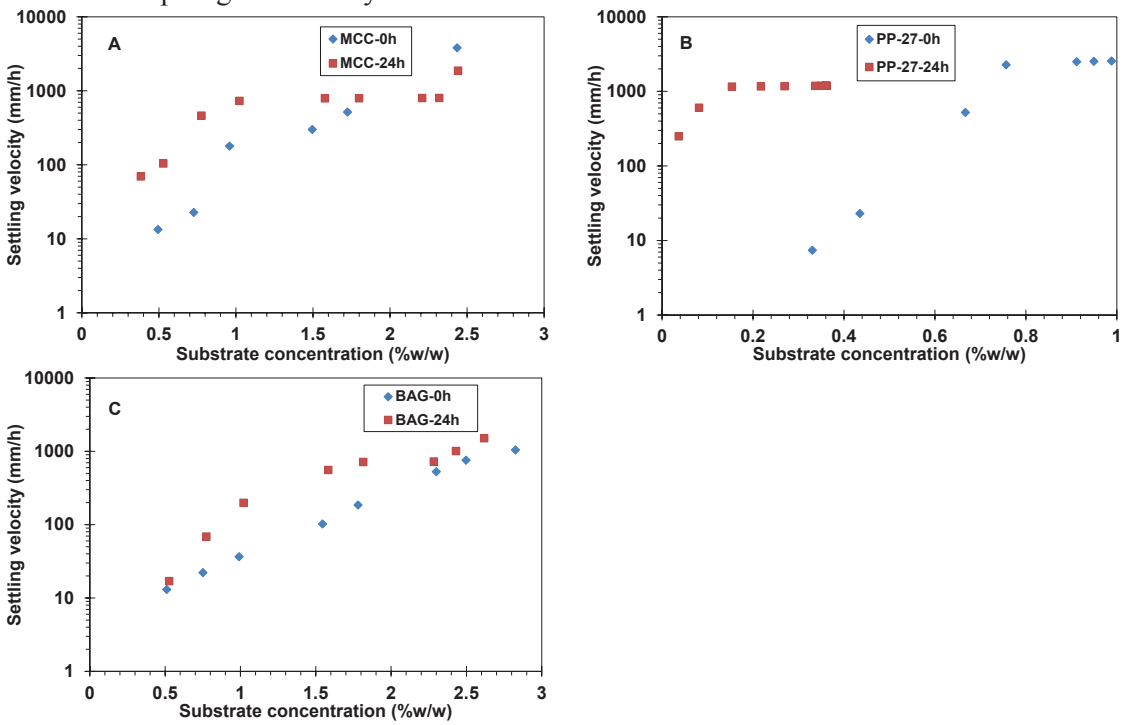

Figure 3-30: Settling velocity of particle for suspension before (t=0h) and after (t=24h) hydrolysis. A-MCC-3%-0.1; B-PP-27-1%-0.5; C-BAG-3%-0.5.

Table 3-18: Mean falling diameter for MCC, PP-27 and BAG substrates before and after hydrolysis.

Substrate	d_s (µm)	
	0h	24h
MCC-3%-0.1	48	26
PP-27-1%-0.5	194	133
BAG-3%-0.5	63	62

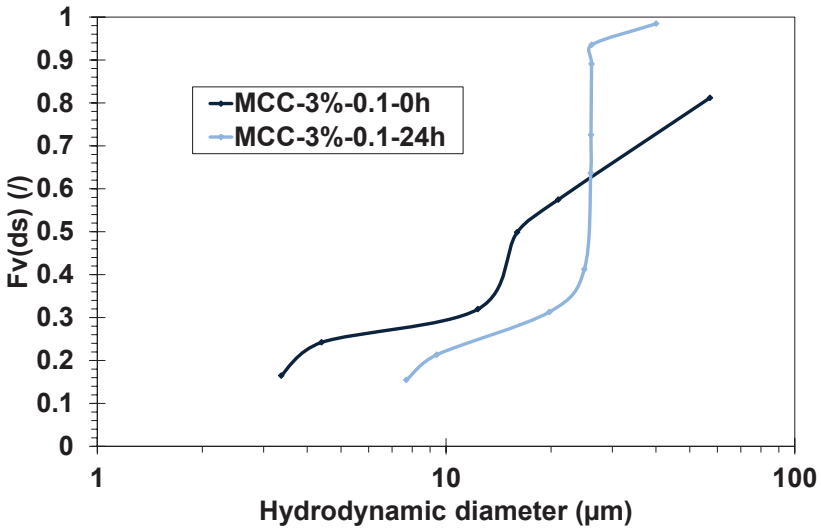

Figure 3-31: Volume cumulative distribution for MCC substrate before and after hydrolysis (3%w/v, 0.1mL enzyme/g cellulose).

3.2.4 Crystallinity index and biochemistry analysis

3.2.4.1 Crystallinity index

The crystallinity index (CrI) of biomass is thought to be correlated with enzyme saccharification into glucose (Kumar et al., 2009). However, there are always conflicting results regarding the role played in controlling the bioconversion rate and also its variation during hydrolysis. In our case, the CrI was measured by XRD before (t=0h) and after (t=24h) enzyme hydrolysis of the substrates. The results are reported in **Table 3-19** for the five substrates and for the same hydrolysis conditions (3%w/v, 0.5mL enzyme/g cellulose, except MCC-0.1mL enzyme/g cellulose). During enzyme attack, the substrate CrI tends to increase (except BAG) but not significantly (1.5% for WP to 5.5% for PP-31). BAG exhibited a reduction of 2% of CrI within 24h. In the literature, the CrI was reported to decrease significantly during hydrolysis (Agarwal et al., 2012; Bansal et al., 2010; Mansfield & Meder, 2003), or to remain constant (Bommarius et al., 2008; Lenz et al., 1990) and even to increase (Chen et al., 2007; Gan et al., 2003).

Table 3-19: Crystallinity index before and after enzyme hydrolysis (3%w/v, 0.5mL enzyme/g cellulose except MCC-0.1mL enzyme/g cellulose).

Substrate	Hydrolysis time (h)	CrI (%)
MCC	0	82.4
	24	-
WP	0	90.7
	24	92.2
PP-27	0	76.8
	24	79.9
PP-31	0	78.3
	24	83.7
BAG	0	57.1
	24	55.0

In our conditions, initial CrI had no influence on bioconversion rate (**Table 3-19**). For example, the CrI of WP was the highest (90.7%) but it presented a very high bioconversion

rate (77.8%) whereas BAG exhibited the lowest CrI (57.1%) but its bioconversion rate was also the lowest (13.7%). This suggests that CrI is not the main factor effecting enzyme hydrolysis of pre-treated biomass. We can also conclude that cellulose activity is not confined to non-crystalline regions (Bommarius et al., 2008).

3.2.4.2 Biochemical analysis

Biocatalysis kinetics were analysed by mass balance considering initial substrates, dry matter in suspension and intermediate and final soluble biodegradation products. Beside the knowledge bottleneck concerning fibre destructuration, the production of monomers (C6, C5) and water-soluble oligosaccharides is crucial for the development of new intensified bioprocesses.

First of all, the bioconversion rate was calculated only on the glucose produced. Based on **Eq. 1-9** and **1-10** (§1.1.5), our hydrolysis efficiency is defined by **Eq. 3-2**.

$$Bioconversion\ (\%) = \frac{[glu]_{measured}}{[glu]_{theory}}$$

$$[glu]_{theory} = \left(m_s \cdot \frac{DM}{100} \cdot \frac{Cellu}{100 \cdot 0.9} \right) \Big/ \left(V_w + \frac{m_s}{\rho_s} \right) \quad \textit{(Eq. 3-2)}$$

With [Glu]: glucose concentration ($g.L^{-1}$), Cellu: cellulose content (%), V_w: volume of introduced water (L), m_s: quantity of substrate (g) and ρ_s: substrate density ($g.L^{-1}$). The conversion coefficient from cellulose to glucose obtained was 0.9 (**Eq.1-1**).

On the other hand, the conversion of hemicellulose into xylose was taken into account only in the case of the material balance calculation. This quantity is defined by **Eq. 3-3,** based on **Eq. 1-12** (§1.1.5) as follow:

$$Bioconversion_{\,hemicellulose}\ (\%) = \frac{[xyl]_{measured}}{[xyl]_{theory}}$$

$$[xyl]_{theory} = \left(m_s \cdot \frac{DM}{100} \cdot \frac{Hemi}{100 \cdot 0.88} \right) \Big/ \left(V_w + \frac{m_s}{\rho_s} \right) \quad \textit{(Eq. 3-3)}$$

With [xyl]: xylose concentration ($g.L^{-1}$) and Hemi: hemicellulose content (%). 0.88 is the coefficient of conversion from xylan to xylose (**Eq. 1-3**).

In fact, hemicellulose is composed not only of xylan but also of mannan and other polysaccharides (the case of softwood), so the conversion rate above is considered as a partial conversion rate of hemicellulose.

In order to investigate hydrolysis kinetics, the soluble monomers and oligomers (DP≤5) of cello-oligosaccharides were quantified (§2.3.3). All analyses are reported in **Annexe 7**.

For dilute concentrations, **Figure 3-32** (A, B, C, D and E) reports oligomer and monomer concentrations ($g.L^{-1}$) for the five substrates (3%w/v, 0.5mL enzyme/g cellulose, excluded MCC: 0.1mL enzyme/g cellulose). Oligomers with DP≥2 were not detected for any of the dilute experiments. Xylose was quantifiable only for PP-27 and 31 at 3%w/v.

Under enzyme activity, the polymeric cellulose chain is broken down to produce monomers. As expected, the concentration of monomers (glucose, xylose) increases with hydrolysis time (**Figure 3-32**). For example, for PP-31 (3%w/v), the monomer concentration increased regularly during hydrolysis with an impact of enzyme loading (0.1 to 0.5) on the quantity of glucose released (4.42 to 18.23g/L) corresponding to 18.8 to 78.5% bioconversion (**Table 3-20**). Similar yields were found for all the substrates when dilute (**Table 3-20**). In agreement

with substrate characterization (§3.1.1), bagasse was found to be the most recalcitrant substrate. Its bioconversion remained in the range 10.6 to 17.6%. This result again highlights the complexity of this substrate not only regarding its physical properties but also its biochemical characteristics. So, pre-treatment of such a complex substrate is indispensable (Karunanithy et al., 2013; Taherzadeh & Karimi, 2008). The MCC was the second least attackable. The two other substrates, with high enzyme loading, were the most hydrolysable and had the highest bioconversion yields (~75-80%). The PP then appears to be an interesting raw material for the production of fermentable sugars because of its low price and high bioconversion yield.

A limited number of articles have examined the evolution of water-soluble cello-oligosaccharides. Sun and Cheng (2002) analysed the hydrolysis of microcrystalline cellulose ($10 g.L^{-1}$) by cellulase produced by *Cellulomonas fimi.* They did not detect soluble oligomers with DP≥4 but the cellotriose concentration varied between 0.2 and $0.6 g.L^{-1}$ depending on the enzyme used: endo-glucanase and cellobiohydrolase. Solubilisation reached 61% and 50% respectively for each enzyme separately. In contrast to our study, the intermediates of cellulose hydrolysis were not found because the Accelarase 1500 cocktail has all the required activities to rapidly degrade these intermediates during hydrolysis.

Our bioconversion yields are comparable to data reported in the literature. Carvalheiro et al. (2008) presented glucose conversion for a 2% (w/w) suspension of oven-dried corncob after 24h hydrolysis. It varied between 30 and 82% for 6 and 30 (FPU/g). Pierre et al. (2011) worked on the hydrolysis of a pre-treated wheat straw suspension at 1% (w/v) and doubled bioconversion (from 45.9 to 87%) after 18h with enzyme loading between 9.6 and 57.6 (FPU/g). With more concentrated suspensions, the reported bioconversion was 45% for bagasse suspension (10%w/w, 36h, 10 FPU/g, Pereira et al. (2011)), 25-40% for MCC suspension (10-20%w/w, 24h, 30 FPU/g, Um (2007)), 17.6% for bagasse suspension (10%w/w, 24h, 5 FPU/g, Geddes et al. (2010)).

Under a fed-batch process, the results are limited for WP and PP-27. No oligosaccharides (DP>2) were detected during enzyme attack. Cellobiose and glucose were found for both WP and PP-27. Xylose was detected only for PP-27.

Generally, the monomers increased regularly with hydrolysis time for all substrates (**Figure 3-33-A-B**). The cellobiose concentrations increased during the five first hours and appeared to be stable beyond. Bioconversion rates reached similar levels about 35-45% for all the experiments after 24h. **Table 3-21** indicates that our results are consistent with those of the literature. Interestingly, the substrate and enzyme feeding flow-rate did not affect the bioconversion kinetics (**Figure 3-33-B**). Nevertheless, bioconversion yields after 24h were lower than those of dilute experiments.

Identical final bioconversion rates can be explained by hydrolysis inhibition by the substrate. For a given flow rate, when we compared two enzyme feed strategies, a difference clearly appears (**Figure 3-33-C**). The bioconversion of experiment PP-27-$E_{initial}$ was always higher than that of PP-27-0.5. Finally, it was more efficient and reached 45% i.e. 8% more than the bioconversion percentage of PP-27-Qc-0.5. This observation be explained an extend enzyme working condition in the first 15 hours of hydrolysis. It could also be correlated with variations in the viscosity. In the literature, with barley straw at a final concentration of 15%w/w, Rosgaard et al. (2007) concluded that there was a slight difference at 24h between glucose concentrations with total enzyme introduced initially and the levels obtained when enzyme was loaded together with the substrate during the reactions (about 6.5%). At 72h, the difference became insignificant.

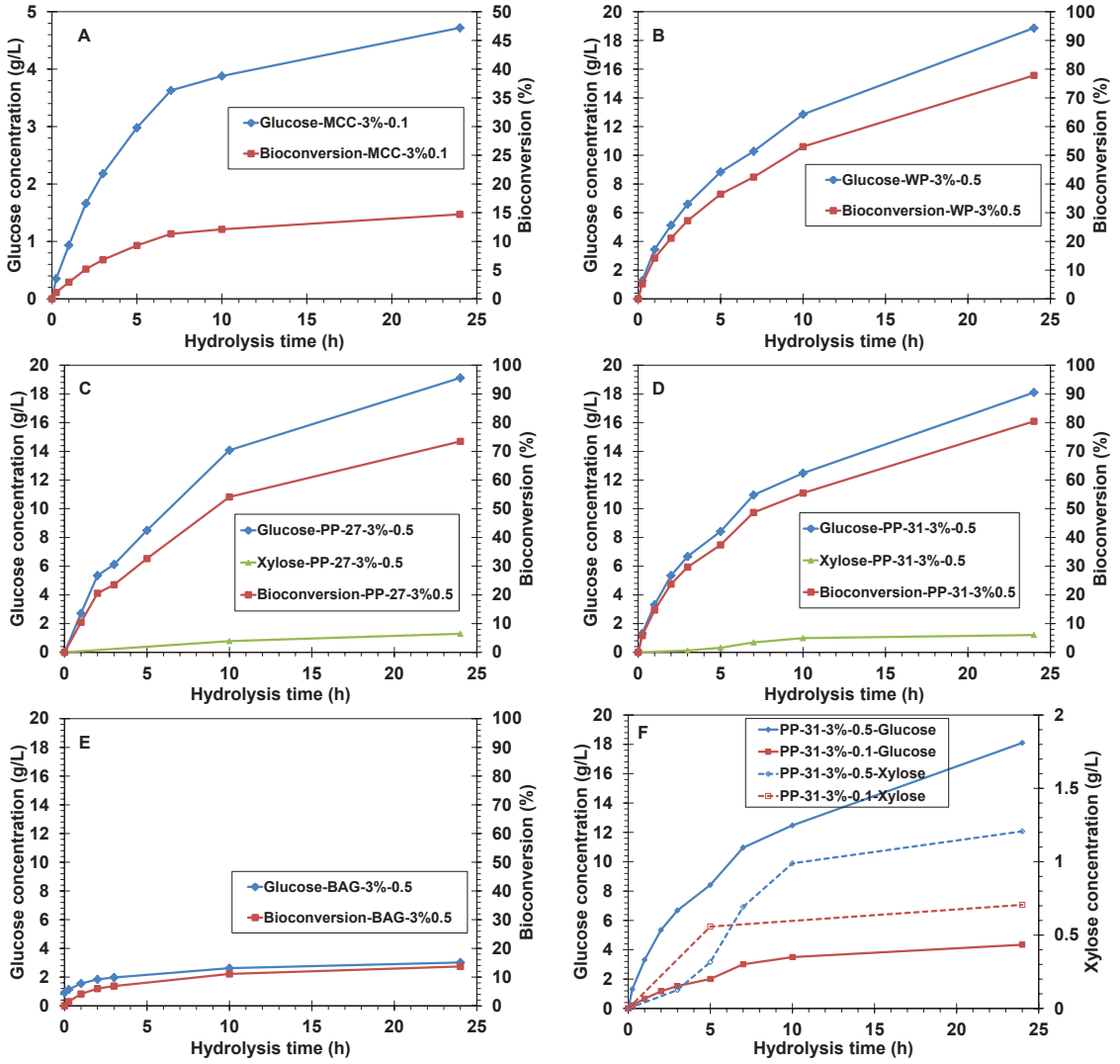

Figure 3-32: Monomer (glucose, xylose) concentrations and bioconversion rate as a function of hydrolysis time for five substrates: MCC (A); WP (B); PP-27 (C); PP-31 (D); BAG (E) at 3%w/v, 0.5mL enzyme/g cellulose excluded MCC (0.1mL enzyme/g cellulose); comparison between PP-31-3%-0.5 and PP-31-3%-0.1 (F).

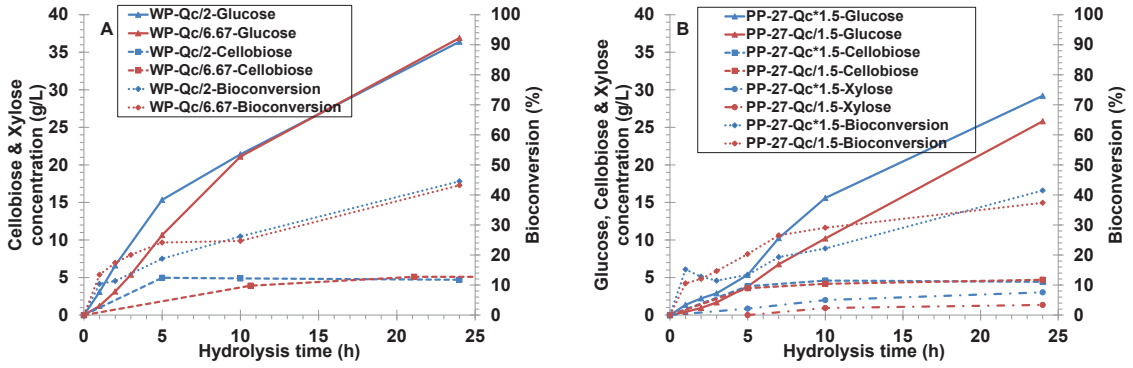

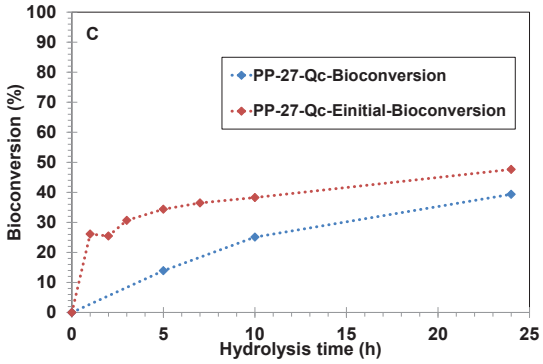

*Figure 3-33: Bioconversion, concentration of cellobiose, glucose and xylose for (A)-WP (Qc/2 and Qc/6.67; Qc=80gms/h); (B)-PP-27 (Qc*1.5 and Qc/1.5; Qc=8.67gms/h); (C)-PP-Qc with cumulative enzyme addition and total enzyme introduced initially.*

Table 3-20: Bioconversion after 24h of hydrolysis.

Substrate	Experiment	Bioconversion (%)
MCC	1%-0.1	35.4
	1%-0.5	62.2
	3%-0.1	14.7
	10%-0.5	34.1
	30%-0.5	30.0
BAG	1%-0.1	15.4
	1%-0.5	17.6
	3%-0.1	10.6
	3%-0.5	13.7
	10%-0.5	16.6
WP	1%-0.1	11.9
	1%-0.5	78.2
	3%-0.1	12.8
	3%-0.5	77.8
PP-27	1%-0.1	18.7
	1%-0.5	76.0
	3%-0.1	13.0
	3%-0.5	71.7
PP-31	1%-0.1	13.6
	1%-0.5	81.2
	3%-0.1	18.8
	3%-0.5	78.5
WP	Qc/2	44.5
	Qc/4	43.0
	Qc/6.67	43.2
PP	Qc/1.5	35.4
	Qc	37.2
	Qc*1.5	39.5
	$Qc\text{-}E_{initial}$	45.2

Table 3-21: Literature results summary for fed-batch hydrolysis strategy.

References	Substrate	Strategy (%w/w)	Bioconversion (%)
(Rosgaard et al., 2007)	Barley straw	5 + E (0h); 5 (6h); 5 (24h);	43
		5 + E (0h); 10 (24h);	44
		5 + E (0h); 5 + E (6h); 5 + E (24h);	49
		5 + E (0h); 10 + E (24h);	44
(Hodge et al., 2009)	Corn stover	12 + E (0h); 5 +E (12h); 2 + E (24h)	45
(Yang et al., 2010)	Corn stover	10 + E (0h, 8h and 16h)	67

3.2.4.3 Mass balance

The goal of this chapter is (i) to monitor the material balance in suspension during hydrolysis, (ii) to compare the dry matter measured by different methods, (iii) to correlate the material balance with the progress of enzyme hydrolysis.

Changes in dry matter content were monitored by determining the water content (§2.3.1) in the sample at different hydrolysis times. This technique involves the error inherent to sampling heterogeneous suspensions. Beside this technique, the dry matter content was also determined from dissolved and undissolved substrate measurements. Under hypothesis the of conservation of substrate mass before and after hydrolysis, the dry matter in suspension can be deduced from the initial quantity and the hydrolysed quantity (which released soluble components: monomers and cello-oligosaccharides). As reported in the previous section, the water soluble cello-oligosaccharides with DP>2 were not quantifiable, so only glucose, xylose and cellobiose were used to calculate the quantity of substrate hydrolysed. The equation is written as follow:

$$DM_{fin}(\%) = \frac{m_s \cdot DM_{ini} - (BC_{glu} \cdot m_{cellu} + BC_{biose} \cdot m_{cellu} + BC_{xyl} \cdot m_{hemi}) \cdot 10^{-2}}{m_{tot}} \cdot 100 \quad \textit{(Eq. 3-4)}$$

With DM_{fin}, DM_{ini}: final and initial dry matter percentage (%).
m_s, m_{tot}: mass of substrate and total mass (suspending fluid + substrate) (g).
m_{cellu}, m_{hemi}: cellulose and hemicellulose content in initial substrate (g).
BC_{glu}, BC_{biose}, BC_{hemi}: bioconversion of glucose, cellobiose and xylose (%).

For dilute concentration, during hydrolysis, part of the substrate was broken down to give a soluble fraction. Therefore, the dry matter content decreased regularly as a function of hydrolysis time (**Figure 3-34**). However, the rate of the decreases depended on the rate of bioconversion. **Figure 3-34** illustrates the time dependence of dry matter content and hydrolysed substrate mass converted into glucose for the five substrates, for the same substrate concentration 1%w/v and for two enzyme ratios: 0.1 and 0.5mL/g cellulose (the mass balance was performed with 5% variance). For the higher enzyme concentration, the reduction of dry matter content was closely correlated to the increase of released glucose. For the same concentration of substrate, at t=24h, the final DM was 2-3 times smaller for 0.5mL/g enzyme than for 0.1 enzyme (except for BAG, **Figure 3-34-A-D**). For example, the final dry

matter contents for experiments with 0.1 and 0.5mL/g cellulose were 0.7/0.4; 0.9/0.3; 0.9/0.3 and 0.9/0.3% for MCC, WP, PP-27 and PP-31 respectively (1%dm initial). For BAG suspensions, the dry matter content again indicated their low bioconversion. For example, at 1%dm, for 24h, only about 10% dry matter content reduction was observed irrespective of the enzyme concentrations (**Figure 3-34-E**). This confirms the difficulty and inefficiency of enzyme attack on non-pre-treated matrices.

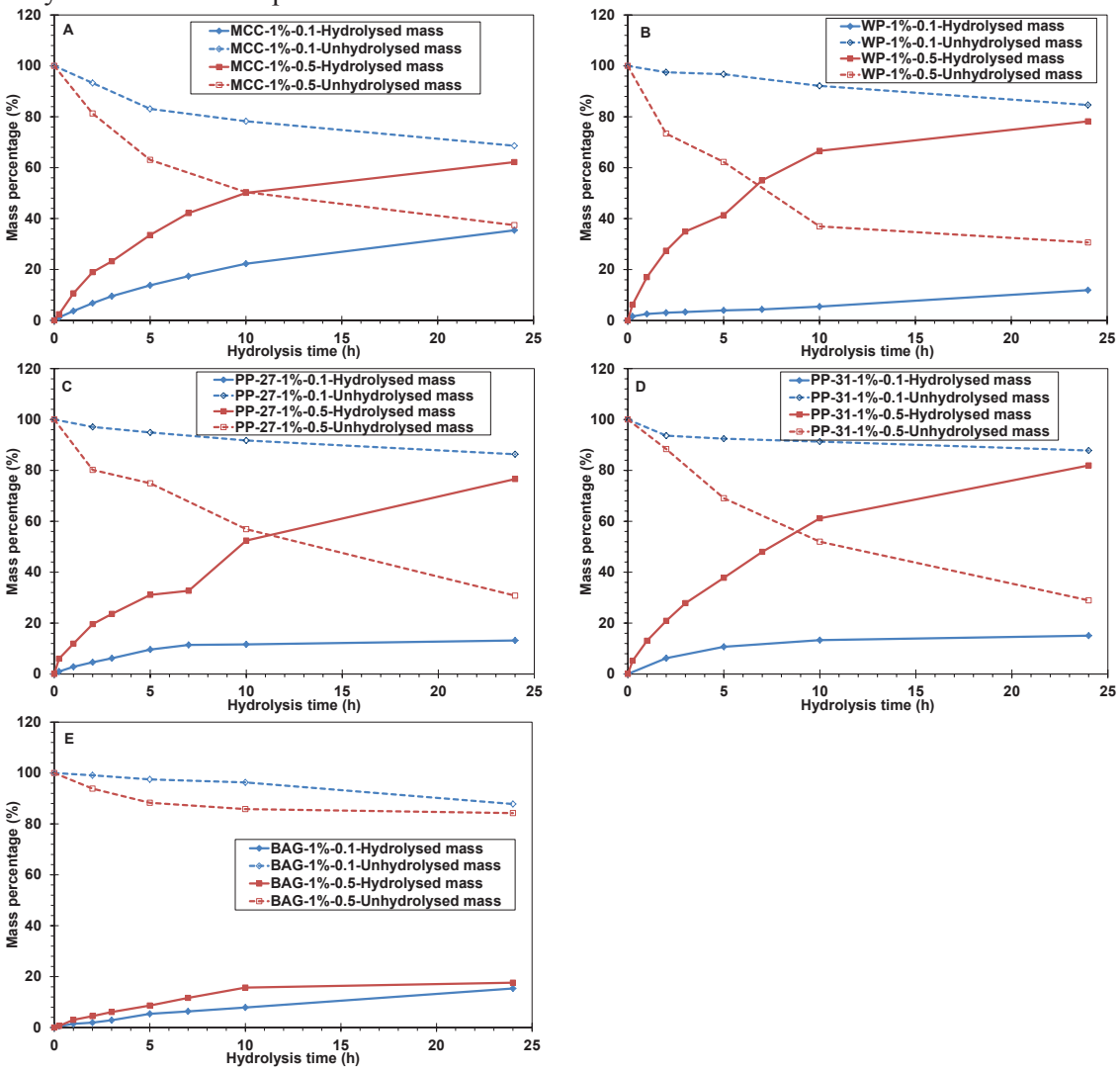

Figure 3-34: Hydrolysed and unhydrolysed percentage of substrate as a function of hydrolysis time. (A)-MCC-1%; (B)-BAG-1%; (C)-WP-3%; (D)-PP-31-3%; (E)-BAG-1% (for 0.1 and 0.5mL enzyme/g cellulose).

Under high substrate concentrations (cumulative substrate additions), the same tendency was observed. During substrate additions, the solubilisation rate was slower than that of feeding substrate; we found a sharp increase of dry matter content. After this period, the DM decreased regularly because of enzyme activity. **Figure 3-35** shows an example for WP and PP-27 suspensions at one substrate flow rate (Qc/4 for WP (Qc=80gdm/h); 1.5*Qc for PP-27(Qc=8.67gdm/h)).

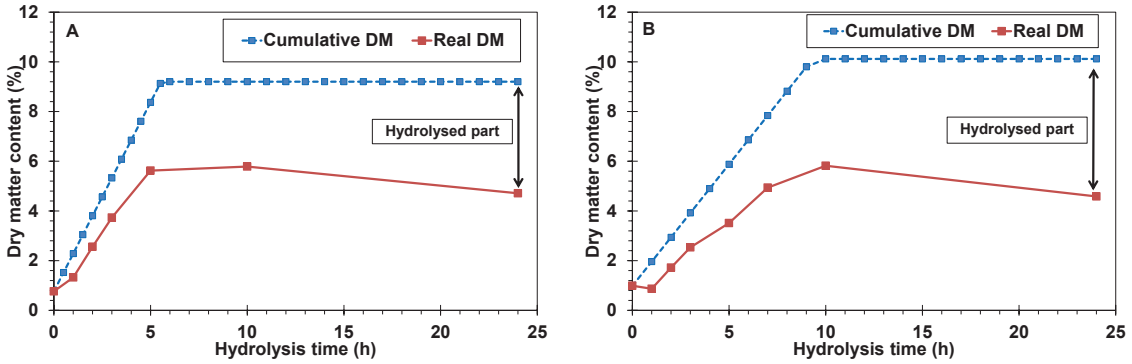

*Figure 3-35: Hydrolysis time dependence of dry matter content for (A)-WP-Qc/4-0.5 (Qc=80gdm/h) and (B)-PP-Qc*1.5-0.5 (Qc=8.67gdm/g).*

The crucial point of the cumulative feeding strategy is to keep a low solid concentration in the bioreactor during hydrolysis time. As presented in **Figure 3-35**, the maximum substrate concentration was always less than or equal to 60% of the cumulative DM. This promoted the action of enzyme and decreased the high solid content effect together with saving energy consumption.

Beside the two techniques presented, the substrate concentrations can be estimated from decantation kinetics measurements (Turbiscan Lab). Taking the profile of the substrate volume fraction in the measuring tube, we were able to deduce the quantity of substrate in the sample. **Table 3-22** illustrates the comparison between substrate concentration estimated from Tusbiscan measurements and those of the water content technique.

Table 3-22: Dry matter content from Turbiscan measurements and water content measurements for initial and hydrolysed suspensions (initial suspension of 3%w/v; 0.5mL enzyme/g cellulose excluded MCC 0.1mL enzyme/g cellulose).

Experiment	Time (h)	Dry matter content (%)	
		Turbiscan Lab	Dry matter measurement
MCC	0	2.96	3.00
	24	2.80	2.46
BAG	0	2.93	2.94
	24	2.58	2.68
WP	0	2.60	2.43
	24	1.06	0.72
PP-27	0	3.17	2.86
	24	1.16	1.15
PP-31	0	3.10	2.82
	24	1.22	1.02

This table shows that the DM of initial suspensions (t=0h) determined by the two techniques were comparable, especially for MCC, BAG, WP (<±5%). However, at the end of hydrolysis, a large difference was found (>±10%). The first explanation could be the change of substrate densities. During hydrolysis the fibre structure is modified and this can lead to a modification of substrate densities. The second could be due to substrate water retention. For PP which has a high water content, the restructuration of fibre possibly changes its water retention capacity thus modifying the decantation kinetics.

3.2.4.4 Energy consumption

The objective of this paragraph is to compare the energy consumption in experiments using a high solid content between the different substrate flow rates. The average mechanical power consumption was determined as follows:

$$\overline{P} = \frac{1}{T} \cdot \int_0^T P(t) \cdot d(t) = \frac{1}{\sum_{i=1}^{\infty} \Delta t_i} \cdot \sum_{t=1}^{\infty} P_i \cdot \Delta t_i \qquad \textit{(Eq. 3-5)}$$

$$P = C \cdot 2\pi \cdot N$$

with $\overline{P}$, P_i: average mechanical power and mechanical power at time i (W).
T: total time of hydrolysis (h).
Δt_i: time period between measurements i and i+1 (h).
C: torque (N.m).
N: rotation speed (revolutions per second).

$\overline{P}$ was determined for all the substrate flow rates at two moments: at the end of substrate addition and when hydrolysis was stopped. The results obtained are presented in **Table 3-23.**

Table 3-23: Average mechanical power for cumulative feeding substrate experiments.

Substrate	Flow	$\overline{P}_{24h}$ (mW/L)	$\overline{P}_{endofadd}$ (mW/L)	Bioconversion (%)
PP-27	Qc*1.5	28	32	22.2
	Qc	26	24	25.2
	Qc/1.5	22	21	34.6
	Qc-$E_{initial}$	16	14	32.4
WP	Qc/2	37	107	11.6
	Qc/4	39	70	18.2
	Qc/6.67	39	56	24.7

In this table, the average mechanical power was expressed in mW per litre of suspension. Generally, the mechanical power of PP-27 suspensions was lower than those of WP because of their lower viscosities.

For WP, the same value of $\overline{P}_{24h}$ is coherent with the identical viscosity patterns, hydrolysis kinetics and bioconversion rates observed for these three different flow rates. However, the substrate addition flow rate clearly affects the mechanical power consumption during the substrate feeding period. This quantity was halved for a three-fold decrease of substrate addition flow rate (from 107 to 56mW/L for from Qc/2 to Qc/6.67). Power consumption considerations stress the importance of the cumulative feeding strategy.

For PP-27, the average mechanical power (mean of two values) tended to decrease as the substrate flow rate decreased. This variance between the highest and lowest flow rates was successively 10% and 35% for $\overline{P}_{24h}$ and $\overline{P}_{endofadd}$. On the other hand, correlated to the lowest viscosity and to the highest bioconversion rate, the average mechanical power consumption of experiment PP-27-Qc-$E_{initial}$ proved to be the most economical for enzyme hydrolysis. We found a difference of about 40% in P values at the same substrate flow (Qc).

(Fan et al., 2003) investigated the power required to mix paper sludge (at 100 rpm) as a function of solids concentration (0-10%w/w). Their results indicate that the power requirement increases sharply with increasing solids concentration for unhydrolysed or partially hydrolysed sludge. However, a two-fold reduction of the mixing power was observed with 15% hydrolysis of substrate at the same solid concentration (4%w/w). In addition, there

was no discernible increase in the power required for mixing the residue resulting from sludge that had been completely hydrolysed.
In the light of these results, a continuous or semi-continuous operating strategy appears to be advantageous as compared to batch operation considering the goal of mixing power required (Fan et al., 2003). In particular, it is desirable in order to have a reasonable substrate feeding flow rates that correlated with particular times have a high bioconversion.

3.3 Discussion and modelling

Based on our results, this chapter aims to analyse and model the phenomena observed. The different in and ex-situ measurement techniques investigated the relationship between physical and biochemical kinetics. Different phenomenological and kinetic models are proposed to represent the changes occurring in the physical-biochemical quantities during hydrolysis. Structured into three parts corresponding to the three study scales: macro, micro and molecular, this chapter offers a global view of enzyme hydrolysis of lignocellulose suspensions.

3.3.1 Rheometry and viscosimetry

In this step the rheological modelling of suspensions before hydrolysis and also substrate dependence on yield stress during hydrolysis are introduced.

3.3.1.1 Rheological model for suspensions before hydrolysis

The on-line measurements were firstly used to establish rheograms (considering only results in the laminar regime §3.2.1.1) and to determine the rheological behaviour of the suspensions. In a second step the impact of particle volume fraction on relative viscosity was investigated. This approach contributed to establishing a structured rheological model including several factors such as shear rate, volume fraction and particle dimension.

Based on the concept of Metzner & Otto, rheograms are identified under the laminar flow regime (Re≤30). Data obtained with the microcrystalline cellulose and sugarcane bagasse suspensions were outside the laminar regime, so rheograms were only established for WP and PP.

The different suspensions are yield stress fluids. Focusing now on the shear-thinning behaviour of these fluids (for 'large' shear rates), different models can be used: power-law, Sisko, Cross, Powell-Eyring, Carreau and "local" power-law models. In the conditions investigated, the power-law model adopted was:

$$\mu = k \cdot \dot{\gamma}^{n-1} \quad \textit{(Eq. 3-6)}$$

This model was fitted to the viscometric data in **Figure 3-7**. For substrates WP and PP, the rheological behaviour was described as a function of concentration and modelled by linear and exponential relationships for the power law index and for consistency (**Table 3-24**). The patterns observed are similar to those reported by Bayod et al. (2005) and Luukkonen et al. (2001). In the concentration range studied power-law indices range between 0.28 and 0.50 for WP and between 0.57 and 0.68 for PP. Consistencies range between 88.8 and 6.2 $Pa.s^n$ for WP and between 18.0 and 3.5 $Pa.s^n$ for PP.

Similar results are reported in the literature: for a 10%dm concentration and shear rates ranging from 1 to $100s^{-1}$, the viscosity of corn stover (maize thresh and residue) and pre-treated softwood suspensions, decreased from 1.87 to 0.03 and 9 to 0.20 Pa.s respectively (Pimenova & Hanley, 2004; Wiman et al., 2010) (**Table 3-25**). Considering dimension criteria, these values are higher than those for MCC found in the present work.

Surprisingly, the viscosity appears to be of the same order of magnitude for dilute and concentrated MCC suspensions (Bayod et al., 2005; Luukkonen et al., 2001) (**Table 3-25**). For an MCC concentration of 40%dm and for shear rates ranging from 1 to $100s^{-1}$, the viscosity of the suspension decreased from 8.0 to 0.3 Pa.s (Luukkonen et al., 2001). This is similar to the values we measured.

In dilute suspensions, there are few interactions between particles and a linear relationship between viscosity and volume fraction is observed. The relative viscosity can be modelled by the Einstein equation:

$$\frac{\mu}{\mu_s} = 1 + k_1 \cdot \phi = 1 + [\mu] \cdot Cm \quad \textit{(Eq. 3-7)}$$

For semi-dilute suspensions, the particles begin to interfere and can at first be taken into account by introducing a quadratic term:

$$\frac{\mu}{\mu_s} = 1 + \alpha \cdot \phi + \beta \cdot \phi^2 \quad \textit{(Eq. 3-8)}$$

The third regime corresponds to concentrated suspensions with a lot of contact between the particles. The viscosity of the suspension increases rapidly with volume fraction. When ϕ reaches a critical value, each particle is confined in a cage formed by its nearest neighbours. For volume fractions above this value, only vibration of the particles inside the cage remains possible, and this disappears completely when ϕ reaches the value of dense packing.
Covering all concentration ranges, the most commonly used relationship between relative viscosity and volume fraction is that of Krieger-Dougherty.

$$\frac{\mu}{\mu_s} = \left(1 - \frac{\phi}{\phi_{\max}}\right)^{-q} \quad 1 \le q \le 2 \quad \textit{(Eq. 3-9)}$$

The relative viscosity μ / μ_{water} is plotted versus the volume fraction at the same rotation speed for four suspensions (**Figure 3-36**). In the plot of PP-27 (the same results for PP-31) and WP, three regions are observed corresponding to two concentrations: (i) a dilute/semi-dilute concentration range exhibiting a low relative apparent viscosity (μ/μ_0<100 under 100rpm) and a quasi-Newtonian behaviour (low viscosity variations with the rotation frequency) and (ii) a semi-dilute/concentrated regime with higher relative viscosity (μ/μ_0>100) and a striking shear-thinning behaviour (displayed by the decreasing values of the relative viscosity as the mixing rate increases) and a strong increase with volume fraction. For WP and PP-27, the transition between these two regimes takes place around ϕ=0.01-0.1. The changes in relative viscosity at dilute/semi-dilute regime and concentrated regime respected a linear equation and quadratic function respectively. However, the model in **Eq. 3-9** presented not enough for viscosity modelling. Firstly, our fibres are deformable and often observed under fibre network forms; secondly, it is not simple to estimate the substrate volume fraction, especially for humid substrates such as PP. The substrate volume fraction could be calculated based on apparent density or intrinsic density and also based on real occupied volume (measured by morpho-granulometry). This property was seen to change drastically during hydrolysis (see on results of decantation kinetics §3.2.2). Consequently, for our lignocellulose matrices, the Krieger-Dougherty model is of limited applicability.
From **Figure 3-36**, a critical volume fraction ϕ_c may be assumed at the transition between two concentration regimes for all suspensions. With an identical substrate volume fraction and rotation speed, the relative viscosity decreased from WP, PP, BAG to MCC. This could be linked to the differences in particle size and morphology. For all suspensions, a transition from semi-dilute to concentrated regime is observed. A linear variation was shown for MCC and BAG in dilute regime. For an identical rotation speed (100rpm≈50s^{-1}), one critical volume fraction was identified for each suspension $\phi_c \approx 0.03$; 0.1, >0.12 and >0.24 for WP, PP and MCC respectively (**Table 3-26**). Luukkonen et al. (2001) proposed a critical volume fraction (equivalent to 47%dm) for MCC.
These results show that the viscosity of suspensions is strongly dependent on physical fibre properties among which size and shape as appear to make the major contributions (Horvath & Lindstrom, 2007; Lapierre et al., 2006; Wiman et al., 2010).

Table 3-24: Power-law (n) and consistency (k) indices versus substrate concentration (Cm gdm.L^{-1}) - (WP: Whatman paper and PP: extruded paper pulp).

Substrate	n	k
WP: 20-40gdm.L^{-1} (ϕ=0.016-0.032)	n= -6.10^{-3}Cm + 0.701	k=0.724e$^{0.075Cm}$
PP: 20-40gdm.L^{-1} (ϕ=0.067-0.134)	n= -9.10^{-3}Cm + 0.555	k= 0.017e$^{0.175Cm}$

Table 3-25: Overview of published results.

Author	Substrate	D[4,3] (µm)	Cm (%)	n	k (Pa.s^n)
(Pimenova & Hanley, 2004)	corn stover	120	5-30	0.9-0.05	0.05-1684
(Wiman et al., 2010)	dilute acid pre-treated softwood	109	4-12	0.4-0.15	1-16
(Bayod et al., 2005)	MCC	33	0-7	0.9-0.8	0.8-2.5
(Luukkonen et al., 2001)	MCC	60	40-55	0.29-0.14	8-177

Table 3-26: Critical volume fractions and substrate concentrations.

	MCC	BAG	WP	PP
ϕ_c	>0.24	>0.12	0.03	0.1
C_{HM} (g/L)	390	220	36.0	103.5
C_m (gdm/L)	386	200	35.3	29.0

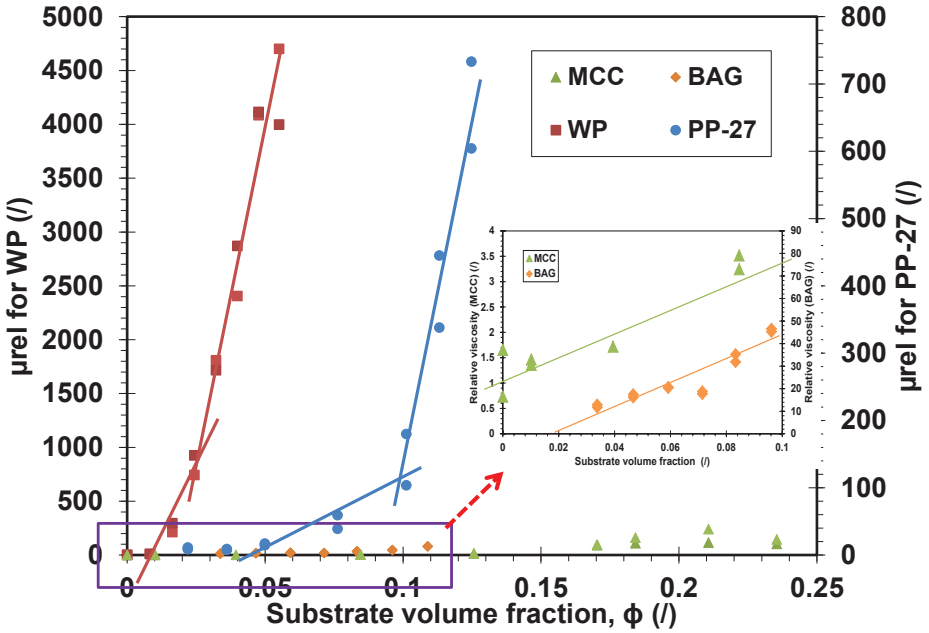

Figure 3-36: Relative viscosity versus substrate volume fraction at rotation speed of 100rpm ($\dot{\gamma} \approx 51 s^{-1}$).

3.3.1.2 Changes in yield stress during enzyme hydrolysis

The five suspensions exhibited a shear-thinning behaviour. Ex-situ rheometry measurements showed them to be viscoplastic. As viscometric yield stress measurements are not possible for these suspensions, this yield stress τ_0 was deduced from the elastic modulus (G') obtained with oscillatory measurements. Several methods can be used for the determination of the yield stress. It could be interpreted as the stress amplitude at which the elastic modulus G' becomes smaller than the shear modulus G", or at which the loss modulus G'' presents a maximum. It

can also be identified as the maximum elastic stress given by $\tau_0 = G'\gamma$ (Damani et al., 1993; Shih et al., 1999; Walls et al., 2003; Yang et al., 1986) where γ is the strain amplitude. Especially for lignocellulose substrates, it could be defined as the first departure from the linear viscoelasticity region (Stickel et al., 2009; Wiman et al., 2010). In the present study, we chose as a criterion for this departure a reduction of 20% of the value of G' in the linear region (see **Figure 3-37-A)**. Yield stress could be regarded as the stress required to initiate a flow. Because of the complexity of suspensions (decantation, heterogeneous character), this measurement was not applied to all slurries. Only the results of dilute PP-27 slurries (1% and 3%dm) are reported.

Yield stress values between 1 and 20Pa were determined for PP-27 at 1% and 3%dm (w/v) before hydrolysis (**Figure 3-37-B**). With an increase of the substrate concentration from 1% to 3%, the yield stress increased 20 times. It confirmed the critical substrate concentration (≈3% determined by in-situ measurement) where the viscosity increased exponentially. Our results were slightly higher than with pre-treated softwood: 0-28Pa for 4-12% substrate concentration (Wiman et al., 2010) or pre-treated corn stover: 0.26-22.9Pa for 5-17%dm (Pimenova & Hanley, 2004). This difference could be due to the nature of the matrices and mainly to the method used to determine the yield stress.

During hydrolysis, the values of yield stress decreased sharply as the enzyme attack progressed. This decrease can be explained by the drop in the solid content in suspension which involves a reduction of fibre-fibre interactions. **Figure 3-37-B** shows that the decrease of yield stress is was greater for experiments with higher enzyme concentrations. The final yield stress (at 24h hydrolysis) of PP-27-3%-0.1 was 10 times higher than that of PP-27-3%-0.5. This observation is directly correlated to the impact of enzyme activities on fibre degradations. In addition, the yield stress of the hydrolysed samples (PP-27-3%-0.5 at 24h) showed lower values for similar DM content compared to the original material (yield stress at 0h of PP-27-1%-0.5) (**Figure 3-37-B**). This can be explained by modification of fibre structure, diameter and shape. Decreasing yield stress during enzyme hydrolysis was previously reported for corn stover (Roche et al., 2009a) and pre-treated softwood (Wiman et al., 2010). These two studies also reported a lower yield stress value for hydrolysed slurries when compared to un-hydrolysed slurries at the same solid content.

Figure 3-38 shows the dependence of yield stress on dry matter content (A) and on bioconversion rate (B) for PP-27. Yield stress collapses onto a single curve when plotted against DM and/or bioconversion (considering the yield stress for PP-27-1% is negligible – red series in the figure). It decreased exponentially with the decrease of DM or with the increase of the bioconversion rate. If we take the criterion that the fluid behaves as a pourable liquid at yield stress below 1Pa, **Figure 3-38-B** shows that this criterion is reached for a bioconversion rate >25%. This has a real significance for the choice of the substrate flow rate for the cumulative feed strategy or if the slurry has to be pumped into another bioreactor. For a bioconversion rate over 50%, the yield stress became negligible. Therefore the yield stress of biomass slurries is reduced to a negligible value once enough insoluble biomass is converted into soluble components.

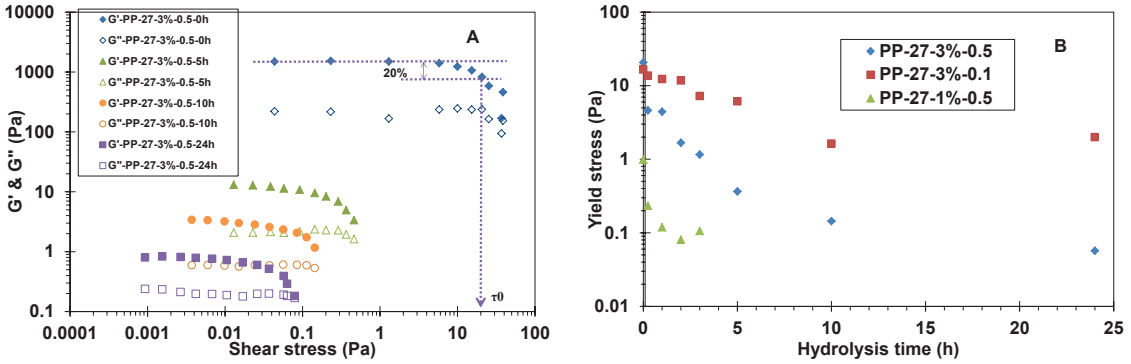

Figure 3-37: (A)-Example for yield stress determination; (B)-Yield stress versus hydrolysis time for PP-27.

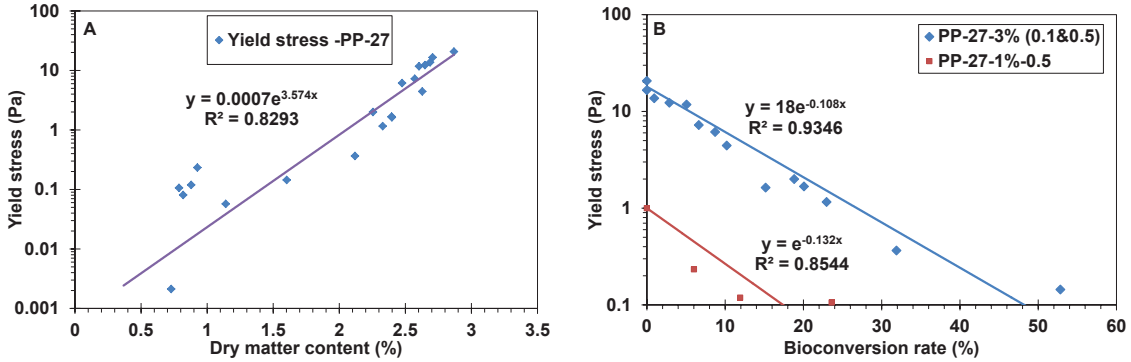

Figure 3-38: Dry matter content dependence (A) and Bioconversion dependence (B) of yield stress (PP-27-3%-0.1 and 0.5mL enzyme/g cellulose; PP-27-1%-0.5).

3.3.1.3 Uniqueness of dimensionless viscosity-time curves

In order to explore the change of viscosity during enzyme hydrolysis and to compare its kinetics between different experimental conditions and substrates, a critical time which signifies the decrease of suspension viscosity was determined.
In dilute conditions, the suspension viscosity decreased as a function of hydrolysis time only for WP, PP-27 and PP-31. The slurry viscosity was normalised as follows:

$$\mu^* = \frac{\mu_t - \mu_{fin}}{\mu_0 - \mu_{fin}} \quad \textit{(Eq. 3-10)}$$

Where μ*: dimensionless viscosity; μ_0, μ_t, μ_{fin}: viscosity at t=0h, t_i and 24h of hydrolysis.
μ* then describes the reduction of viscosity during enzyme hydrolysis. It varies between 1 (t=0h) and 0 (t=24h). From this quantity, a critical time which corresponds to a 90% reduction of the initial suspension viscosity is defined. It is noted t(μ*=0.1). Then, the hydrolysis time (t) was normalised with this critical time as **Eq. 3-11:**

$$t^* = \frac{t}{t(\mu^* = 0.1)} \quad \textit{(Eq. 3-11)}$$

Table 3-27 presents the critical time as a function of substrate (WP, PP-27 and PP-31) and hydrolysis conditions (1-3%w/v, 0.1-0.5mL enzyme/g cellulose). In general, this t(μ*=0.1) varies slowly with substrate concentration (for the range studied). However, it clearly depends upon the enzyme concentration used. We observed more or less the same value of t(μ*=0.1) for the same enzyme ratio, i.e. for WP-0.5, the critical time was about 0.5h; whereas a

difference of 2 to 3-fold was found on varying the enzyme ratio. For instance, with a concentration of 3%w/v, it took less than 3 times to reduce 90% initial viscosity for WP (from 1.6 to 0.5h) and about 2 times for both of PP-27 and 31 (from 11.7 to 5.2 for PP-27; from 8.4 to 4.4 for PP-31).

Considering the impact of the type of substrate, the results showed that with WP suspensions, viscosity decreased more rapidly during hydrolysis than with PP-27 or PP-31. For example, at 3%-0.5, the critical time for PP (27 and 31) was 10-fold higher than that of WP (5.2/4.4 compared to 0.5). The effect of fibre dissociation during the first hours for WP is assumed to make the main contribution. PP-31 presented a lower value of t(μ*=0.1) than PP-27. This difference was negligible at high enzyme concentration but more pronounced at low enzyme ratio (i.e. 11.7 and 8.4h for PP-27 and PP-31 respectively at 3%-0.1). The type of matrix (softwood and hardwood) could be the main reason underlying this difference.

The dimensionless time-viscosity curves are plotted in **Figure 3-39**. Interestingly, WP (**Figure 3-39-A**) and PP (**Figure 3-39-B**) exhibit a single curve. This uniqueness of dimensionless time-viscosity curves was observed no matter what the hydrolysis conditions (substrate concentrations, enzyme ratio). These results suggest that during the period of reduction of 90% initial viscosity, a similar degradation mechanism could be assumed.

Data were collected from the literature to estimate whether a unique tendency between viscosity decrease and hydrolysis time can also be observed (**Figure 3-40**). However, as mentioned in the bibliography, a "cloud" of data representing t(μ*=0.1) as a function of cellulase activity is observed. The various types of substrate, differing enzyme activities together with the great variation in hydrolysis conditions (temperature, concentration) all contribute to explaining this dispersion. Within a single data series, the critical time value is seen to decrease with the increase of enzyme activity. Our results for WP are in agreement with those of Samaniuk et al. (2011).

Nevertheless, it is interesting to demonstrate the existence (or not) of the uniqueness of the dimensionless viscosity-time curve for concentrated regimes.

Table 3-27: Critical time t(μ*=0.1) for experiments in dilute WP, PP-27 and PP-31.

Substrate	Conditions	t(μ*=0.1) (h)
WP	1%-0.1	1.7
	1%-0.5	0.6
	2%-0.1	2.1
	2%-0.5	0.5
	3%-0.1	1.6
	3%-0.5	0.5
PP-27	1%-0.5	7.6
	2%-0.5	4.0
	3%-0.1	11.7
	3%-0.5	5.2
PP-31	1%-0.5	5.2
	3%-0.1	8.4
	3%-0.5	4.4

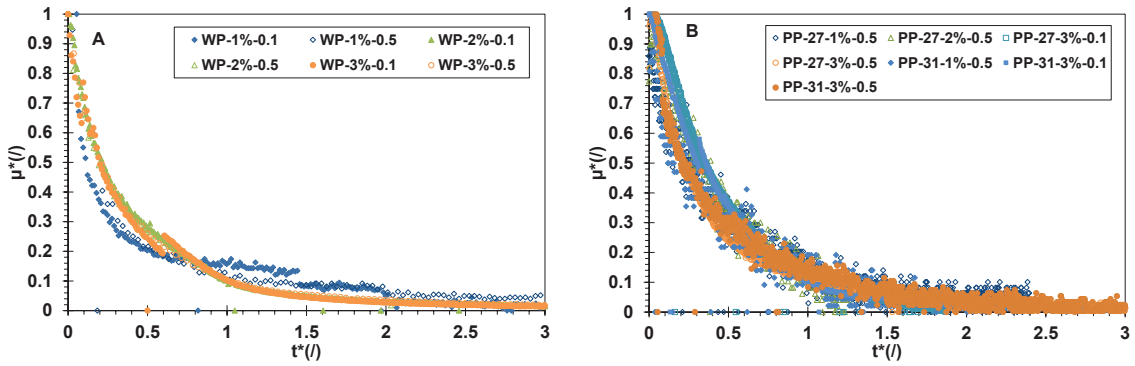

Figure 3-39: Dimensionless viscosity-time hydrolysis curves (μ=f(t*)) with dilute substrate for WP (A) and PP (B).*

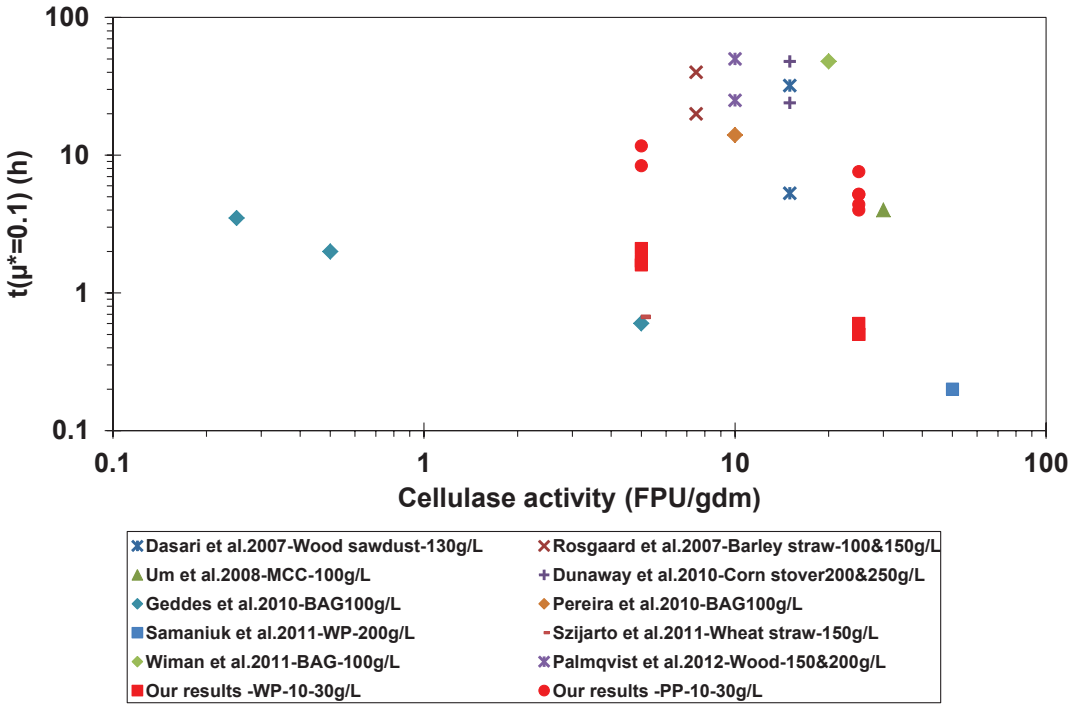

Figure 3-40: Critical time t(μ=0.1) versus cellulase activity reported in different studies.*

3.3.2 Particle size analysis: comparison between techniques

Particle size was characterised by four methods: focus beam reflectance, diffraction laser scattering, optical microscopy and falling velocity measurement.

The techniques canbe classed into 2 groups: diffraction or reflectance techniques and image analysis techniques. Each measurement technique is affected by various technical specifications and assumptions. For image analysis methods, particle shape and orientation are the major parameters; for diffraction/reflectance method: refractive index (particle, supernatant), isotropy, shape + orientation, particle surface area, wavelength and polarity of incident light can be mentioned.

After measurement, each technique makes a hypothesis to determine the "particle size", for DLS: spherical model, for morpho-granulometry: circle model. With FBRM, it gave us the chord length of the particle and it is not easy to compare this technique with the others; we used a spherical model to convert chord length distribution CLD into particle size distribution

PSD (§2.4.7.4). PSD was taken as reference considering the homogeneity of model of other methods.

As presented in §3.2, the PSD calculated from CLD showed exactly the same trends therefore, only the data PSD will be used for comparison with other methods. As expected and considering theory, the mean diameters of the equivalent sphere are always lower than the mean chord length. For FBRM, the reliability of CLD to PSD conversion depends on the initial CLD material size (number of chord length bands).

Figure 3-41 illustrates the volume cumulative distribution of particle diameter before and after hydrolysis for five substrates (the results obtained for Stoke diameter was limited so only three other measurements were taken in account for comparison). All three methods described the same tendency for variation of particle diameter during hydrolysis (excluding FBRM with WP– **Figure 3-41-B**). The shift from coarse to fine particles was observed for MCC, PP-27 and PP-31. All techniques indicate no change in Fv(d) for BAG during enzyme attack (**Figure 3-41-E**). Surprisingly, while DLS and morpho-granulometry showed a clear evolution of Fv(d) during hydrolysis, the results of FBRM did not present any changes.

At t=0h, for MCC, the cumulative distribution of volume was totally comparable between three methods (**Figure 3-41-A**). This observation is supported by the value of D[4,3] presented in **Table 3-28** which indicates the same range of mean particle diameter (from 95 to 108µm). Nearer to the spherical shape, the MCC particle appears to be the most favourable substrate to use all the hypotheses mentioned in determining the particle size. After hydrolysis, the results of FBRM and DLS came to the same value (34-36µm) whereas morpho-granulometry presented a value 2-fold higher (62µm).

For the four other matrices, the absolute value was different. It decreased from the DLS measurement to morpho-granulometry and to FBRM. For example, with PP-27, the D[4,3] decreased from 497 to 187 to 52µm for DLS, morpho-granulometry and FBRM respectively (**Table 3-28**). The various variables cited above affected the long fibres more. DLS measurement also detected coarse particles which was in fact the flocculation of fibres. That explains why this technique always gave the highest diameters. For morpho-granulometry, after measurement, the sample was filtered to remove the agglomerations. For FBRM, lignocellulose the fibres always present an elongated shape so the probability of cutting the fibre width is greater than fibre length. Therefore FBRM presented the lower results than other methods.

In the literature, numerous researches compared different methods using a model suspension as reference. Andrès et al. (1996) used 52 and 260µm polystyrene spheres. They investigated 2 methods of diffraction and image analysis. A qualitative comparison showed the same results for both techniques while a statistical approach demonstrated differences.

Yu and Erickson (2008) used FBRM and DLS to characterise PVC spheres with diameters ranging between 90 and 300µm. The results showed that the median diameter of DLS was 2 times higher than the median chord length.

Hamilton et al. (2012) worked with MCC (Avicel) which was characterised by FBRM and DLS. Their results highlighted the lower value for FBRM measurement compared with DLS measurement.

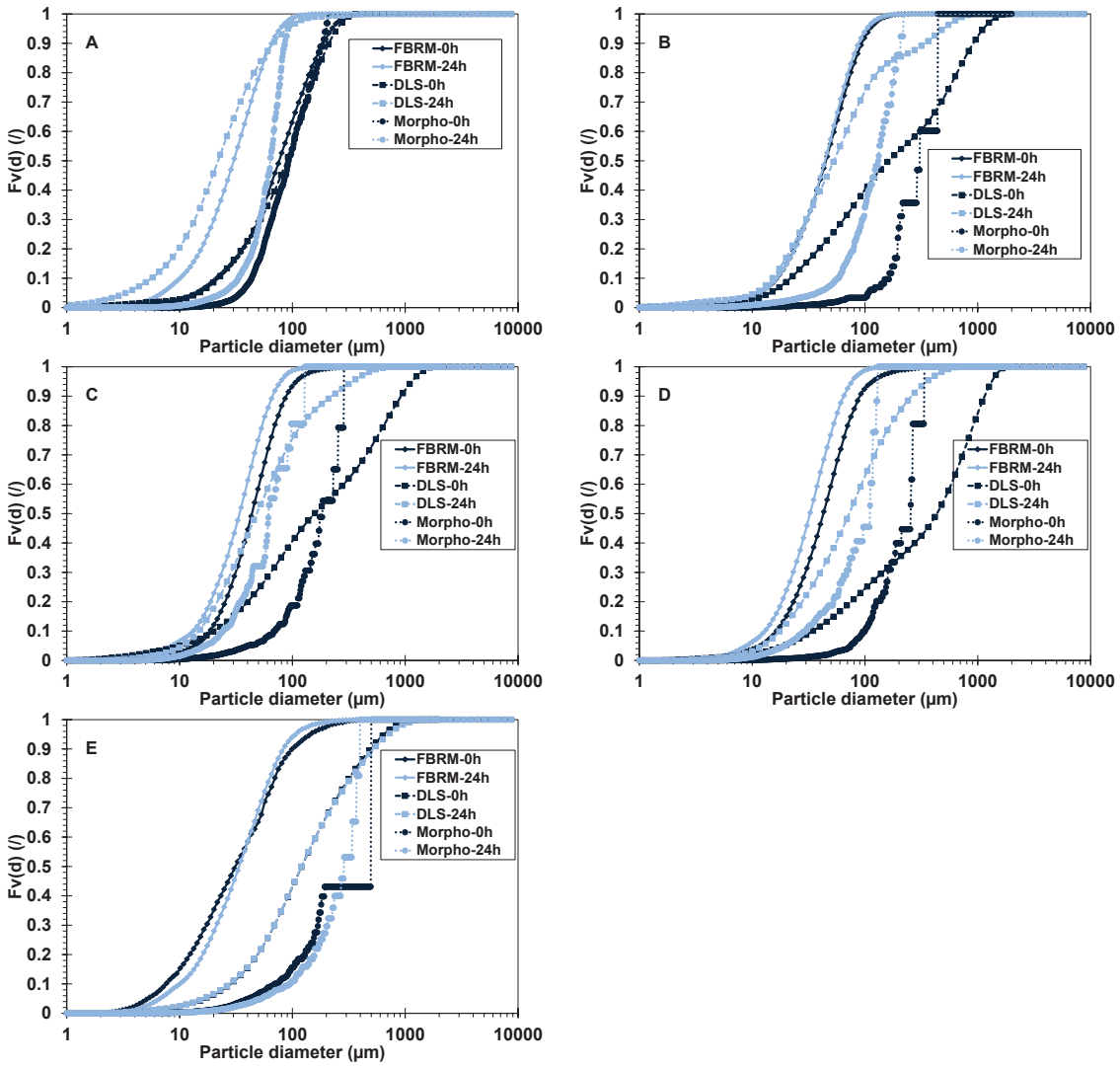

Figure 3-41: Volume cumulative distribution of particle diameter before and after hydrolysis for five substrates MCC (A); WP (B); PP-27 (C); PP-31 (D); BAG (E) under the same conditions: 3%w/v, 0.5mL enzyme/g cellulose (excluded MCC-1%w/v).

Figure 3-42 illustrates the population balance and its variation as hydrolysis progresses for MCC. We present the behaviour of four population taking 25, 50, 75 and 100% of the initial population (in volume). All three measurements showed the same trends for these populations. We observed that the largest population disappeared within the first 5 hours parallel to the increase of fine population.

In conclusion, all particle size measurement techniques presented comparable qualitative trends. Absolute particle size of granular particles appears to be the most accurate criterion.

Table 3-28: Comparison of volume mean diameter D[4,3] of different measurement techniques for five substrates (3%w/v, 0.5mL enzyme/g cellulose; excluded MCC-1%w/v).

Substrate	Technique	0h	2h	5h	10h	24h
MCC	FBRM	95	64	41	37	36
	DLS	108	41	39	36	34
	Morpho	105	-	72	63	62
WP	FBRM	53	53	52	51	51
	DLS	351	162	136	124	114
	Morpho	312	194	184	144	130
PP-27	FBRM	52	46	44	43	39
	DLS	497	-	201	130	103
	Morpho	187	155	126	97	70
PP-31	FBRM	53	46	42	40	38
	DLS	471	295	216	136	126
	Morpho	222	157	154	140	91
BAG	FBRM	51	51	45	45	44
	DLS	227	-	-	229	221
	Morpho	171	-	-	168	161

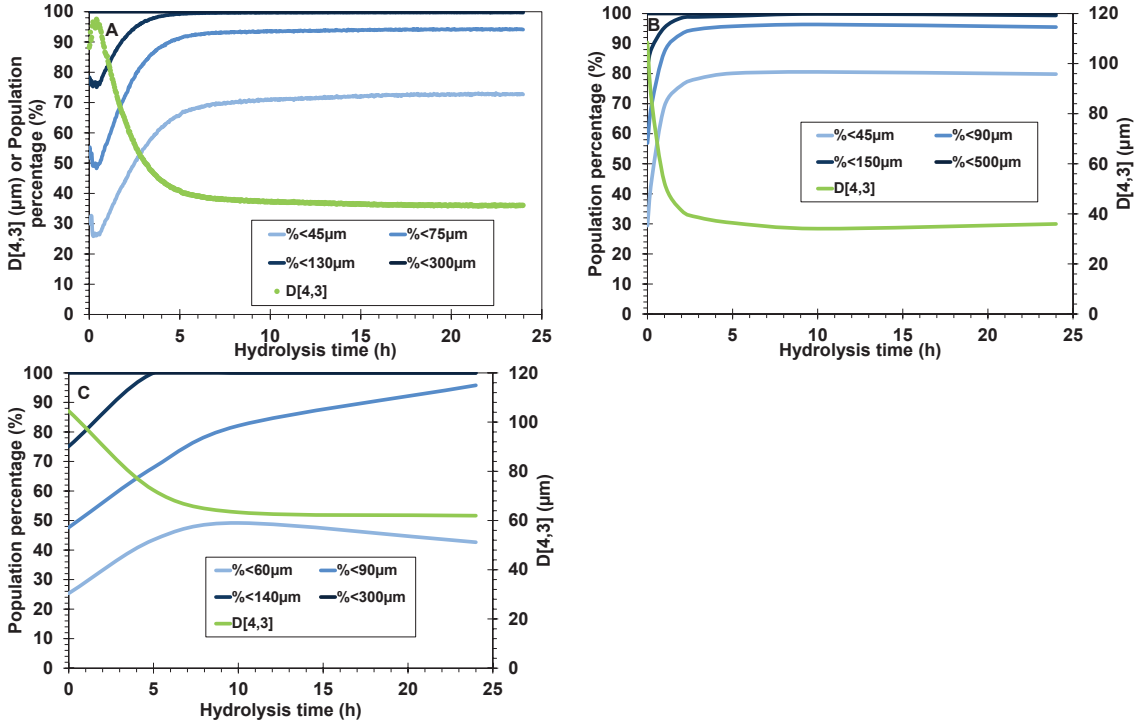

Figure 3-42: Population balance during hydrolysis – Comparison of three measurement methods: FBRM (A); DLS (B) and morpho-granulometry (C) – Example for MCC (1%w/v, 0.5mL enzyme/g cellulose); (population class considering 25, 50, 75% of initial population); (%<45µm indicates the percentage of the population having a diameter of less than 45µm).

3.3.3 Modelling of kinetics

During hydrolysis of lignocellulose matrices, kinetics of macro (viscosity), micro (particle size and shape) and biochemical properties stand as key indicators for process control and performance. Assuming a single kinetic behaviour, bioreaction was investigated from a physical and biochemical stand point.

3.3.3.1 Biochemical kinetics

The kinetics of the bio-chemical reaction has been regularly investigated in the literature. Many enzyme reactions (e.g. hydrolysis, oxidation, and reduction or cofactor mechanisms) are second or higher order reversible reactions. Many are diffusion limited and the time curves depend strongly on the heterogeneous rate-limiting structures of the enzyme system. Adsorption (reaction) in high molecular weight structures (for example, proteins, polynucleotides, polysaccharides or heterogeneous protein-phospholipid, protein-nucleotide and protein-polysaccharide structures) is more complex.
Among the numerous models reported, one of the best-known is the Michealis-Menten equation (Michaelis & Menten, 1913). The model describes the rate of enzyme reactions, by relating reaction rate, the concentration of a substrate. We can find a model describing the concentration of a substance versus hydrolysis time (first order model) reported by Chrastil (1988). The concentration-time curve of substrate, S, is defined by the general equation below:

$$-\frac{dS}{dt} = k_{bio} \cdot S^{\alpha} \quad \textit{(Eq. 3-12)}$$

where S is the hydrolysable substrate concentration ($g.g^{-1}$); k_{bio} the bio-kinetic constant ($(g/g)^{1-\alpha}.s^{-1}$) and α the model order (/).
For different model orders, the equations presented in **Table 3-29** can be used:

Table 3-29: Kinetic models for different orders.

Model order	Differential equation	Model equation
0	$-\frac{dS}{dt} = k_{bio} \cdot S^{0}$	$S = (S_0 - S_\infty) - k_{bio} \cdot t + S_\infty$
1	$-\frac{dS}{dt} = k_{bio} \cdot S^{1}$	$S = (S_0 - S_\infty) \cdot e^{-k_{bio} \cdot t} + S_\infty$
2	$-\frac{dS}{dt} = k_{bio} \cdot S^{2}$	$S = \frac{S_0 - S_\infty}{(S_0 - S_\infty) \cdot k_{bio} \cdot t + 1} + S_\infty$
3	$-\frac{dS}{dt} = k_{bio} \cdot S^{3}$	$S = \frac{S_0 - S_\infty}{\sqrt{2 \cdot k_{bio} \cdot t \cdot (S_0 - S_\infty)^2 + 1}} + S_\infty$

Note that the initial substrate S (%) is the hydrolysable fraction rather than the total introduced substrate.

$$S = S_0 - S_\infty \quad \textit{(Eq. 3-13)}$$

where S_0 and S_∞ are the total substrate and non-hydrolysable substrate.
In our case, the enzyme cocktail (Accellerase 1500) contained only cellulase and hemicellulase so the lignin fraction can be considered as part of the non-hydrolysable fraction. For MCC and WP, $S_\infty = 0$; for PP-27 and PP-31, $S_\infty < 2\%$ which can be ignored; for BAG, $S_\infty = 21\%$. The model was adjusted by the least squares method of S.

Figure 3-43 (**Annexe 8**) illustrates the coherence between experimental data and models of different orders for the behaviour of dry matter content of WP and PP-27-3%. A second order model accurately describes the time dependence of dry matter consumption and monomer production.

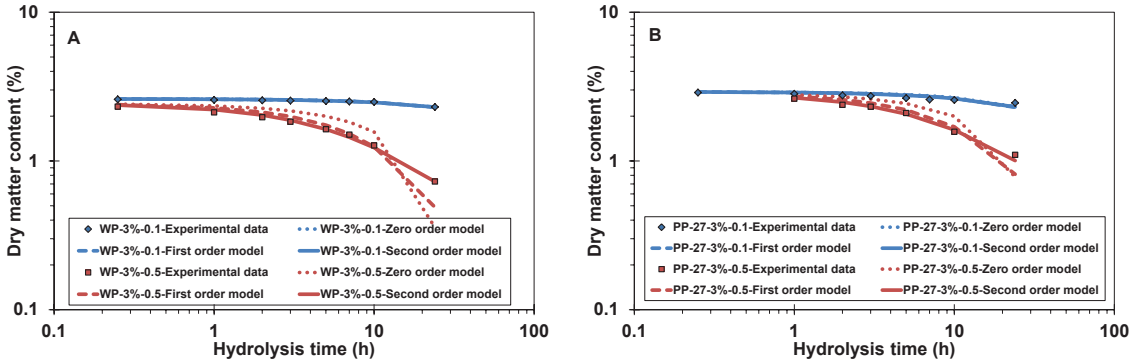

Figure 3-43: Model of dry matter content –time dependence for WP (A) and PP-27 (B) at 3%w/v; 0.1 and 0.5mL enzyme /g cellulose.

Constant k_{bio} characterises bio-kinetics for each substrate in different hydrolysis conditions presented in **Table 3-30**. In general, the results for PP-27 and PP-31 were similar. Effects of enzyme and substrate concentrations were observed clearly for all matrices. The increase of the E/S ratio from 0.1 to 0.5mL/g cellulose created an increase of about 4, 20 and 8-10 times for MCC, WP and PP respectively. With BAG, the influence of enzyme concentration was not significant. When the initial substrate concentration increased from 1 to 3%w/v, a reduction of 2-3 times was found for all substrates.

Table 3-30: Bio-kinetic coefficients for different substrates.

Substrate	1%		3%	
	5 FPU/g	25 FPU/g	5 FPU/g	25 FPU/g
MCC	0.027	0.100	0.001	-
WP	0.006	0.140	0.002	0.040
PP-27	0.008	0.072	0.004	0.027
PP-31	0.007	0.080	0.004	0.032
BAG	0.004	0.005	0.001	0.002

3.3.3.2 Rheological kinetics

Assuming a similarity to biochemical kinetics, suspension viscosity is modelled by an identical structure as below:

$$-\frac{d\mu}{dt} = k_{visco} \cdot \mu^{\alpha} \quad \textit{(Eq. 3-14)}$$

where μ, suspension viscosity (Pa.s); k_{visco}, visco-kinetic constant ($Pa^{1-\alpha}.s^{-\alpha}$); α: model order (/)

Viscosity, μ is defined as the subtraction of measured from final viscosity, μ_∞ which corresponds to the viscosity of a suspension containing all soluble fractions (total conversion). In our case, this value was approximately equal to supernatant fluid (1mPa.s) consequently μ_∞ became negligible compared with μ. The model was adjusted by the least squares method of ln(μ).

Figure 3-44 illustrates the different models for PP-27-3%-0.5.

In agreement with the observation for biochemical kinetics, the second order model gives the best description of the viscosity kinetics during enzyme attack in our conditions.
Table 3-31 shows the visco-kinetic coefficients obtained for WP and PP. The similarity of k_{bio} with k_{visco} demonstrated the pronounced impact of enzyme and substrate concentrations on the variation of suspension viscosity during hydrolysis. The same order of multiplication was concluded: 12- and 8-fold for the impact of enzyme concentration with WP and PP res., and 4-fold for the impact of substrate concentration).

Table 3-31: Rheological kinetic coefficients for different substrates.

Substrate	1%		3%	
	5 FPU/g	25 FPU/g	5 FPU/g	25 FPU/g
WP	14.023	155.400	6.609	76.296
PP-27	-	61.476	2.104	15.253
PP-31	-	64.371	1.784	14.563

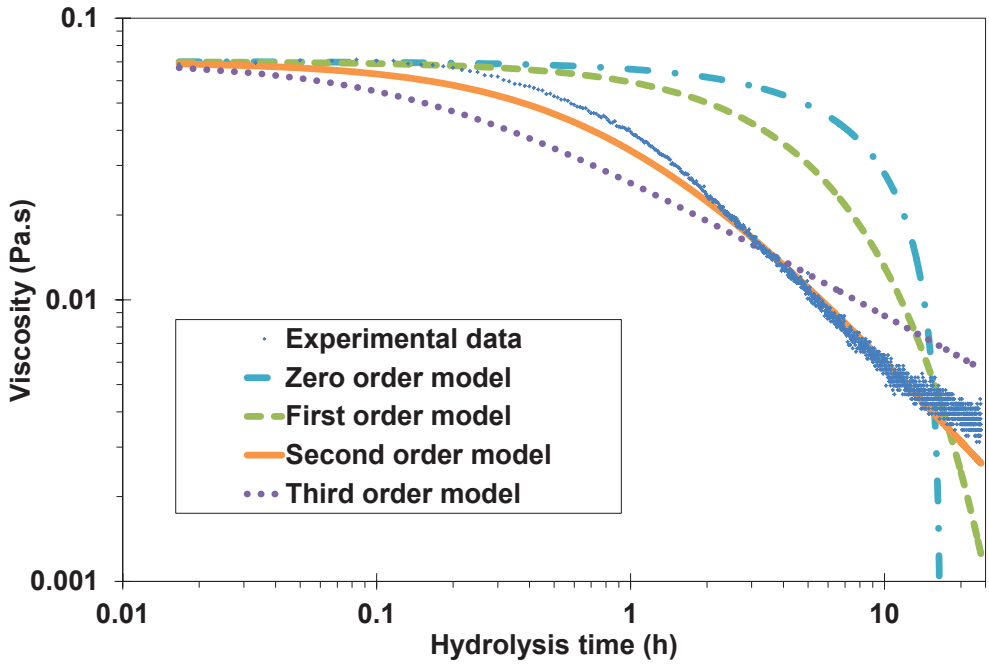

Figure 3-44: Modelling of viscosity time dependence for PP-27-3%-0.5.

3.3.3.3 Granulometric kinetics

Considering the model of biochemical and rheological kinetics, a second-order model was found to describe the time dependence of particle mean diameter. The results of PSD (from FBRM) were used as reference. The relationship between D[4,3] and hydrolysis time was defined as below:

$$D[4,3] = \frac{D[4,3]_0 - D[4,3]_\infty}{\left(D[4,3]_0 - D[4,3]_\infty\right) \cdot k_{granulo} \cdot t + 1} + D[4,3]_\infty \quad \textit{(Eq. 3-15)}$$

where $D[4,3]_0$ and $D[4,3]_\infty$, volume mean diameter for initial and final suspension (µm); $k_{granulo}$, granulo-kinetics constant ($\mu m^{-1}.s^{-1}$).
In ideal conditions, all solid fractions should be converted into soluble fractions, the $D[4,3]_\infty$ would then tend to zero. However, there is always a part of non-hydrolysable substrate then

$D[4,3]_\infty$ is not negligible compared to $D[4,3]_0$. The model was adjusted by least squares method of ln(D[4,3]).

Figure 3-45 presents the model of mean diameter-time dependence for PP-27-3% at two enzyme ratios 0.1 and 0.5. The model proposed fits the experimental data. For lower enzyme ratios, an increase of mean diameter during first hour is noticeable. So the model in **Eq. 3-15** was applied only from the maximal value of μ until end of hydrolysis for experiments with 0.1mL enzyme/g cellulose. This increase of D[4,3] could first be explained by fibre swelling and unwinding under limited enzyme activity.

Table 3-32 shows the kinetic coefficients obtained for PP-27 and PP-31. In general, the results of PP-27 were identical with those of PP-31. Absolute values of $k_{granulo}$ seemed identical in magnitude, however, we can only distinguish the impact of enzyme ratio by the final value of the mean diameter, $D[4,3]_\infty$. The higher the enzyme concentration, the lower the value of $D[4,3]_\infty$, which reached about 35-39μm, and likewise, the lower the E/S ratio, the higher the $D[4,3]_\infty$ obtained (20% addition).

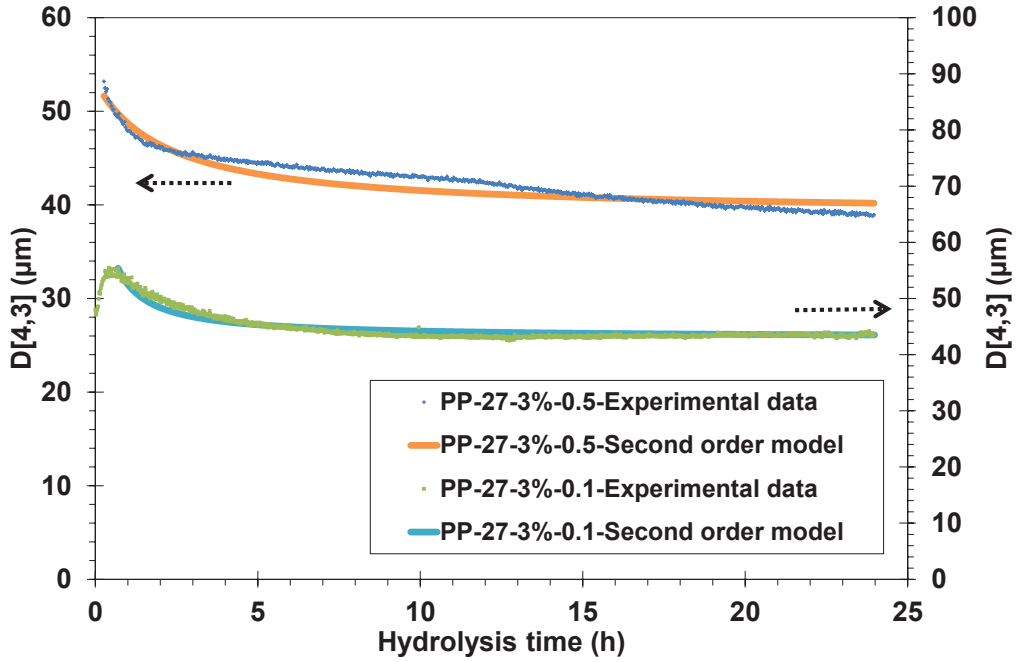

Figure 3-45: Modelling of mean diameter-time dependence curve for PP-27: 3%w/v; 0.1 and 0.5mL enzyme/g cellulose.

Table 3-32: Morpho-granulometric kinetic coefficients and $D[4,3]_\infty$ (in brackets) for different substrates.

Matrice	1%		3%	
	5 FPU/g	25 FPU/g	5 FPU/g	25 FPU/g
PP-27	0.047 (42)	0.012 (35)	0.090 (43)	0.032 (39)
PP-31	-	0.020 (37)	-	0.035 (37)

As presented in the previous paragraphs, all the physical and biochemical kinetics respected the second order model. Using these models, the relationship between suspension viscosity, substrate content and particle mean volume diameter are presented in **Figure 3-46**. The similarity in the dependence of PP-27 and PP-31 at the same hydrolysis conditions is clear. The visco-bio-kinetics for WP were faster than those of PP. The impact of enzyme

concentration was more pronounced for WP than PP with visco-bio-kinetics. In contrast, it is clearly observed with PP for visco-granulo kinetics (**Figure 3-46**).
To sum up, the values of the physical-biochemical coefficients reinforced the identical kinetics of viscosity, particle diameter reduction, substrate consumption and glucose production.

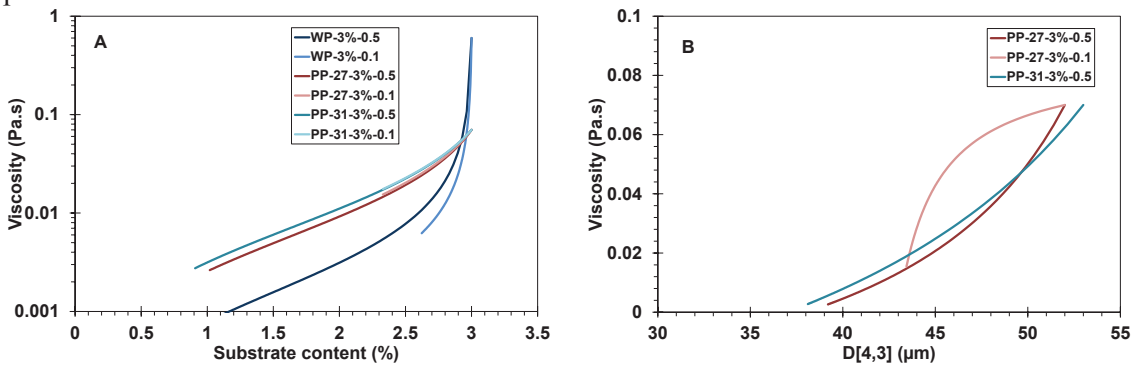

Figure 3-46: Relationship between viscosity and substrate content (A); between viscosity and volume mean diameter of particle (B) as a function of substrate and hydrolysis conditions.

3.3.4 Hydrolysis of lignocellulose matrices: overview and final observations

Destructuration of lignocellulose matrices during biocatalytic hydrolysis was considered by a multi-scale approach based on physical and biochemical investigations. Rheometry, morpho-granulometry and biochemistry stand as our tripod frame to enable us to scrutinise transfer limitations.
Obviously, hydrolysis kinetics depend on the type of substrate, its concentrations and enzyme ratios. These kinetics were similar for the pre-treated substrates: MCC, WP, PP-27 and PP-31 (bioconversion, variation of particle size). For non-pretreated BAG, the hydrolysis efficiency was not useful. PP-27 was taken as an example.
Under dilute conditions, (**Figure 3-47)** the enzyme hydrolysis of PP-27 (3%-0.5) with mass balance (bioconversion rate based on glucose released, dry matter); viscosity (initial suspension, estimated viscosity and measured viscosity) and particle size (mean diameter, population balance) variations were followed. During hydrolysis, the solid matter was degraded into water-soluble fractions, therefore the decrease of dry matter and the increase of glucose or bioconversion rate are concomitant (**Figure 3-47-A**). Mass balance (reported in §3.2.4.3) is verified instantaneously (kinetics) and in the overall experiment (up to final bioconversion rate). Flow properties (suspension viscosity) are the result of dry matter concentration, fibre structure and particle size. **Figure 3-47-B** reports the dry matter concentration and in-situ viscosity. The viscosity at initial total substrate concentration (not hydrolysed) and of the solid fraction (not hydrolysed) are calculated with established rheological models and compared to the in-situ viscosity. The contribution of two major effectors on viscosity is then highlighted: (i) the reduction of dry matter concentration and (ii) fibre destructuration due to hydrolysis reactions. The balance between the effectors cannot be considered as constant during the bioreaction. For example, at t=5h, the ratios $\mu_{initial\ total\ substrate}/\mu_{solid\text{-}fraction}$ and $\mu_{solid\text{-}fraction}/\mu_{in\text{-}situ}$ were similar (factor of about 3-fold); however, at the end of hydrolysis t=24h, these values are about 20 and 2 times respectively.
Assuming that fibre destructuration can be described by particle diameter, **Figure 3-47-C** shows the behaviour of different populations and the reduction of D[4,3] during hydrolysis. Interestingly, the impact of diameter reduction is maintained stable throughout hydrolysis. We observed the same reduction factor for both of t=5h and t=24h (about 15% reduction of D[4,3]).

For each batch mode hydrolysis run, the kinetics of physical and biochemical parameters under enzyme attack can be described by a second-order reaction. For example, with PP-27 (3%-0.5), **Table 3-33** reports kinetics constants. The variation of suspension viscosity, particle diameter and also glucose production can be estimated easily at any given hydrolysis time.

Our next scientific objective was to integrate these kinetics into a cumulative feed strategy and to compare simulated and experimental data related to suspension viscosity, particle diameter and glucose production.

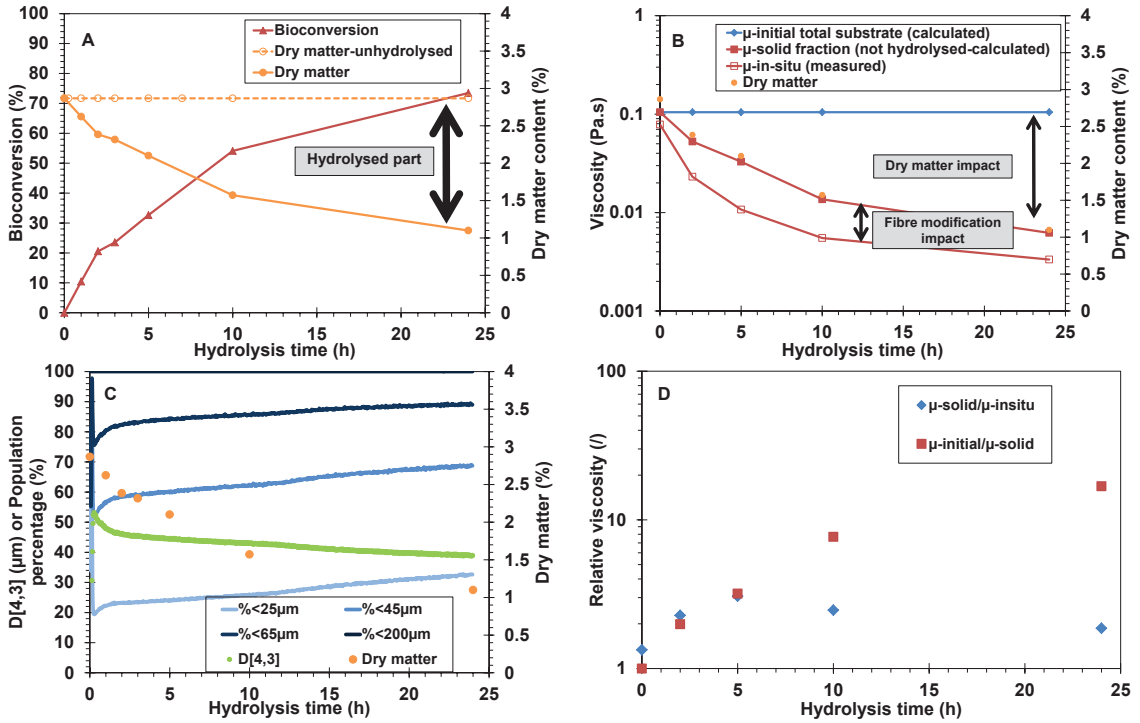

Figure 3-47: Enzyme hydrolysis under dilute conditions of PP-27 (3%w/v, 0.5mL enzyme/g cellulose). A-Dry matter and bioconversion rates; B-Impact of hydrolysis on suspension viscosity (µ-initial total and µ-solid fraction, are estimated with the rheological model for the initial suspension); C-Population balance during hydrolysis (data PSD from FBRM measurement); D-Relative viscosity versus hydrolysis time.

Table 3-33: Kinetic models for PP-27-3%w/v; 0.5mL enzyme/g cellulose.

Kinetic	Model
Bio-kinetic	$S = \frac{S_0}{S_0 \cdot 0.027 \cdot t + 1}$
Visco-kinetic	$\mu = \frac{\mu_0}{\mu_0 \cdot 15.253 \cdot t + 1}$
Granulo-kinetic	$D[4,3] = \frac{D[4,3]_0 - 39}{(D[4,3]_0 - D[4,3]_\infty) \cdot 0.032 \cdot t + 1} + 39$

Figure 3-48 illustrates an example for PP-27 (Qc*1.5-0.5). As in previous experiments under dilute conditions, the results highlight the impact of substrate solubilisation and morphological modifications on viscosity. In these conditions, the impacts were more

pronounced. As observed, the value of $\mu_{initial\ total\ substrate}/\mu_{solid\text{-}fraction}$ and $\mu_{solid\text{-}fraction}/\mu_{in\text{-}situ}$ are unbalanced at the end of substrate additions (about 27 and 71 times respectively); however, for t=24h, we found the inverse phenomenon of these impacts on viscosity ($\mu_{initial\ total\ substrate}/\mu_{solid\text{-}fraction}$ and $\mu_{solid\text{-}fraction}/\mu_{in\text{-}situ}$ were 45 and 230) corresponding also a 2-fold reduction of particle size (D[4,3]) and the disappearance of the coarse population steadily replaced by the fine population. These results demonstrate that no transfer limitations occurred to control glucose released kinetics under the cumulative feeding strategy reaching 10%w/v. This strategy offers a new approach to regulate suspension viscosity and fermentable carbon production by a defined feed strategy.

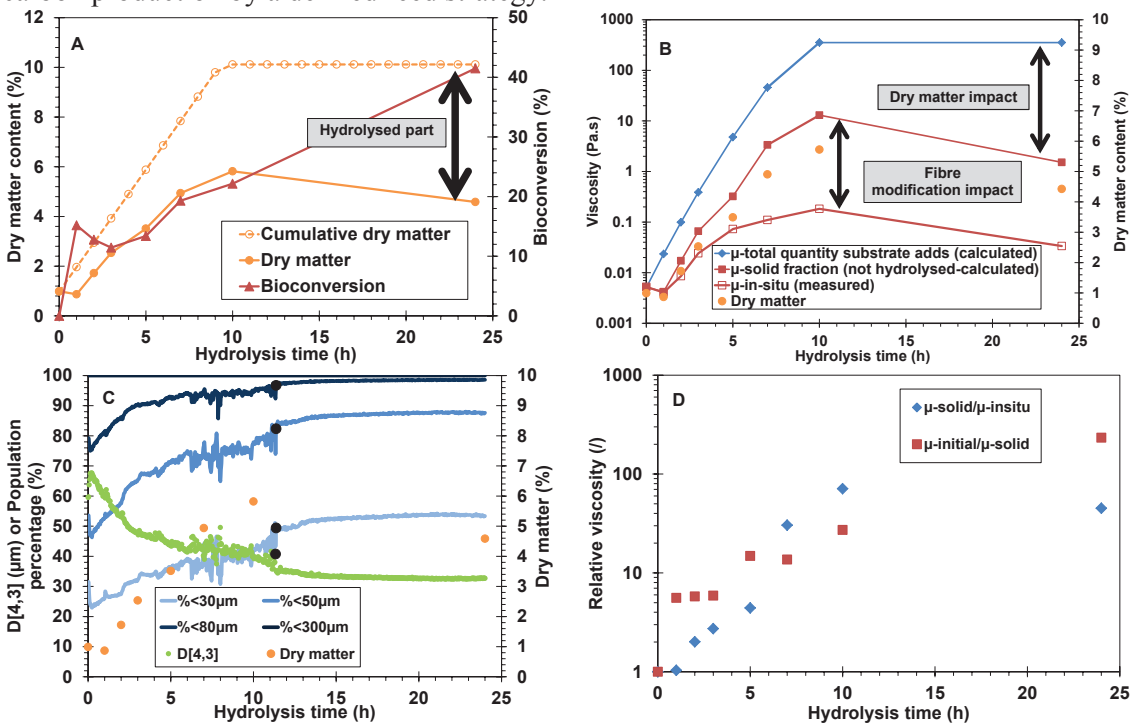

Figure 3-48: Enzyme hydrolysis under semi-continuous strategy of PP-27 (Qc*1.5-0.5), (Qc=8.67gdm/h, 0.5mL enzyme/g cellulose). A-Dry matter and bioconversion yield; B-Impact of hydrolysis on suspension viscosity (µ-total and µ-solid are estimated with rheological model for initial suspension); C-Population balance evolution during hydrolysis (data PSD from FBRM measurements); D-Relative viscosity versus hydrolysis time.

CONCLUSION

In this conclusion, firstly the social, economic, environmental and scientific contexts of the present work are briefly summed up. A second part draws attention to the limits and the aims of the work done during this PhD, highlighting the scientific issues raised as well as the domain investigated. Then, the main points concerning (i) Materials & Methods, (ii) Substrate characterisation and rheology of suspensions, (iii) hydrolysis under dilute conditions and (iv) hydrolysis up to high dry matter content are reported. The final part deals with the scientific perspectives of future work by considering the lack of knowledge concerning the substrates, weaknesses to interpret/understand physical and biochemical mechanisms and the potential of new instrumentations and/or process control/command abilities.

Firstly, terrestrial biodiversity (the extraordinary variety of ecosystems, species and genes) is a natural capital, providing humanity with food, water and a variety of materials and therapeutic products that underpin global economy, societies and individual well-being. Genetic resources support a wide range of market sectors (e.g., cosmetics, pharmaceuticals, biotechnology, agriculture and food industry), while maintaining and expanding the options for the transition to a resource-efficient economy and sustainable development. However, environmental impacts associated with land-use change, over-exploitation of biodiversity, spread of invasive alien species, pollution and climate change, and have triggered species redistribution and/or translocation in many parts of the world, accelerating the deterioration and loss of biodiversity, making the transition towards a more climate-resilient and low carbon economy mandatory. Recently, new environmental policies and societal concerns have triggered intensive research efforts into the production of specialised high value compounds, chemicals and biomaterials from cost-effective and readily accessible biochemical technologies benign to the environment.

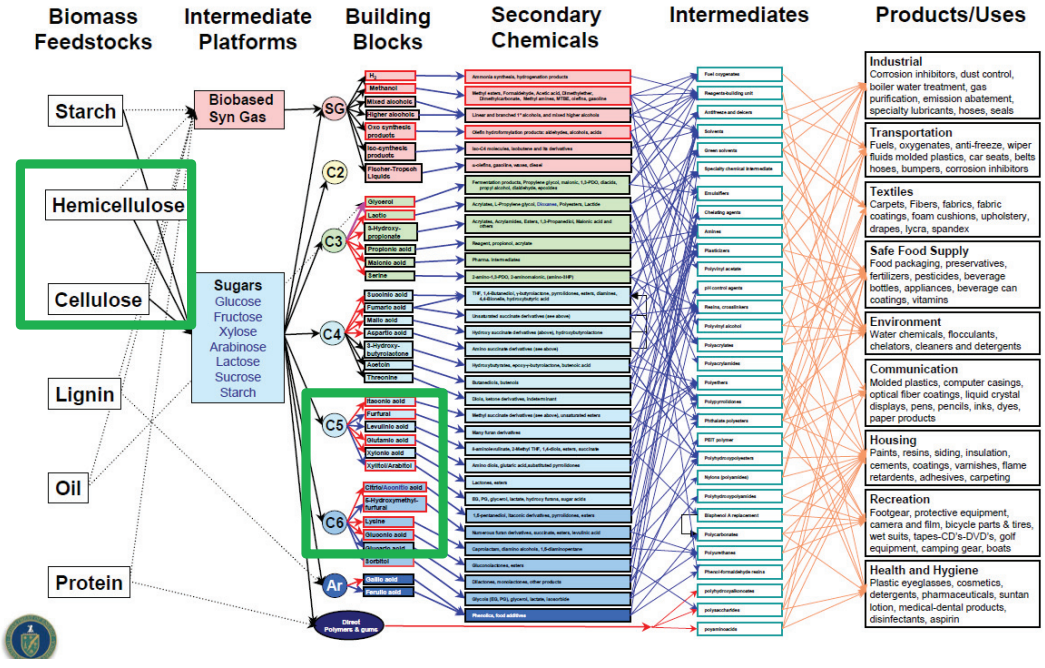

Figure 4-1: Analogous model of biobased product flow-chart for biomass feedstocks (Werpy et al., 2004).

Plant biomass, a completely renewable resource, has the potential to satisfy European needs in chemicals, materials and specialty products, while minimising environmental impact and increasing sustainability. Contrary to conventional hydrocarbons, biomass-derived components are highly functionalised compounds that minimise the need for oxidative and in general conventional chemistry, during their treatment, and thus, the use of toxic heavy metal catalysts and other noxious chemicals. Plant biomass is typically derived from wood, agricultural and agro industry residues, forestry waste and municipal solid wastes which are excellent examples of sustainable, low-cost carbon biomass feedstock with a large potential for flexible synthesis of novel high-value bio-based products. Plant lignocellulose, the most abundant and most underutilised polysaccharide-containing biomass available in the world (i.e., 1011 tonnes/yr production), is an extremely complex and widely varying nano-scale composite, comprising cellulose, hemicellulose and lignin, along with a variable level of extractive molecules (e.g., alkaloids, phenolics). In general, lignocellulose biomass consists of 40-50% cellulose, 25-30% hemicellulose and 15-20% lignin, with woody species having more lignin than the herbaceous plants. Cellulose is a linear polymer of glucose, linked by glycosidic bonds whereas hemicellulose is a branched hetero-polymer containing both five- (D-xylose, L-arabinose) and six-carbon sugars (D-mannose, D-glucose, D-galactose). Lignin is a complex hydrophobic, cross-linked aromatic polymer mainly composed of three major phenolic components, namely p-coumaryl, coniferyl and sinapyl alcohols. The degradation of the main polymeric fractions of lignocellulose into simpler molecules is a prerequisite for the integrated utilization of this resource in a biorefinery concept.
Currently, the bioconversion technologies available for the production of bio-based products are limited since the cell wall matrix is naturally resistant to decomposition and present technologies are not fully viable at a commercial scale. In particular, the currently employed processes for the fractionation of the lignocellulose matrices into its components and the hydrolysis of cellulose and hemicellulose into the corresponding monomeric sugars are not economically feasible. Sustainable production and utilization of high value plant products from integrated bioprocessing of lignocellulose biomass has an enormous potential for Europe's bioproducts market. Currently, most R&D studies focus on the design and operation of individual biochemical process units (e.g., enzyme hydrolysis, fermentation, saccharification, etc.) as well as on the synthesis of specific bioproducts. To gain full benefits, however, it is important to investigate the production and utilization cycles in an integrated way and to consider all important aspects involved in the consolidated biomass processing operation (i.e., conversion technologies, flexibility of end-product synthesis, integrated process optimization, efficient separation and purification, product life cycle analysis, environmental and climate change aspects, etc.).

Secondly, my PhD work stands as a contribution to the understanding and establishment of a novel integrated biomass processing technology for the efficient synthesis of high value energy sources, from selected lignocellulose biomass exhibiting industrial relevance. In the light of this, the pulp and paper industry can provide pre-treated cellulose materials, free of or with a low lignin content and reduced levels of microbial inhibitors, for enzyme and microbial treatment. The feedstock materials must undergo physical-biochemical treatments to release the fermentable cellulose carbon at concentrations and operating conditions compatible with realistic transfer to industry (at high dry matter content) and bioprocess scale-up. The understanding of the mechanisms of liquefaction of complex cellulose substrates at high total solids concentrations is still limited and requires detailed and exhaustive characterisation. Several scientific and technical questions for bioprocess intensification and biochemical engineering also need to be investigated. The central scientific question is: What are the physical and biochemical phenomena that limit performance? The scientific issues are centred

on the study of coupled transfers in bioreactors along two main lines: (i) the physical properties of complex biological suspensions and transfer limitations and (ii) the bio-performances under specific hydrodynamic constraints.

My PhD experimentation aimed to investigate the breakdown of fibre during enzyme hydrolysis and more precisely focused on "In-situ and ex-situ multi-scale physical metrologies to understand the mechanisms of fibre degradation in lignocellulose matrices and release kinetics of fermentable cellulose carbon". It is related to the identification of the rate limiting steps of biomass liquefaction using physical and biochemical characterization of model (Microcrystalline cellulose, Whatman paper) and industrial (Paper pulp, Sugarcane bagasse) matrices at the macroscopic scale (power consumption, viscosimetry and rheometry), microscopic scale (particle size, morphology) and molecular scale (chemical analysis). Operating conditions covered various concentrations from dilute (1% to 3%w/v, batch mode) to concentrated (around 10% up to 30%w/v, semi-continuous mode) and two enzyme/substrate ratios (0.1 and 0.5 mL/g cellulose i.e. 5 and 25 FPU/g cellulose) with an industrial cellulolytic enzyme cocktail, Accellerase 1500 from Genencor). All experiments were conducted at 40°C, pH=4.8 (compatible with microorganism culture conditions) and during 24h (relevant period to assess transfer limitations and representative of substrate additions in agro-industrial process). To respond to these scientific questions, this work is structured around three main actions:

- Raw material characterisation and rheology of suspensions,
- Hydrolysis under dilute conditions,
- Hydrolysis up to high dry matter content with a strategy based on cumulative substrate feed.

Figure 4-2 reports the three blocs corresponding to the three levels of observation: macro-scale with viscosimetry and rheometry, micro-scale with morpho- and granulo-metry (DLS, PSD, CLD, d_{St}) and molecular scale with biochemistry (chemical analyses of soluble fraction and solid fraction). The three-angled framework led us to analyse and to compare the in-situ and ex-situ methods (excluding biochemical analysis). Then phenomenological models could be established and discussed in the light of theory before including all results and providing a full overview of the mechanisms involved. In this regard, the phenomenological models should respond to criteria such as reliability, simplicity and homogeneity with the experimental information.

- for rheometry: integration of a phenomenological model of rheological behaviour considering volume fraction, size and shape of particles;
- for granulometry: morpho-granulometric analysis and associated distribution functions (mass and population balances);
- for biochemistry: integration of biochemical kinetics models.

A global result from these three blocks could provide a "knowledge block" to explain some scientific questions and lead to the implementation and intensification of new bioprocesses. The main challenge was related to the integration of dynamic description (kinetics) and multi-scale (molecular, microscopic and macroscopic) characterisations of physical and biological phenomena.

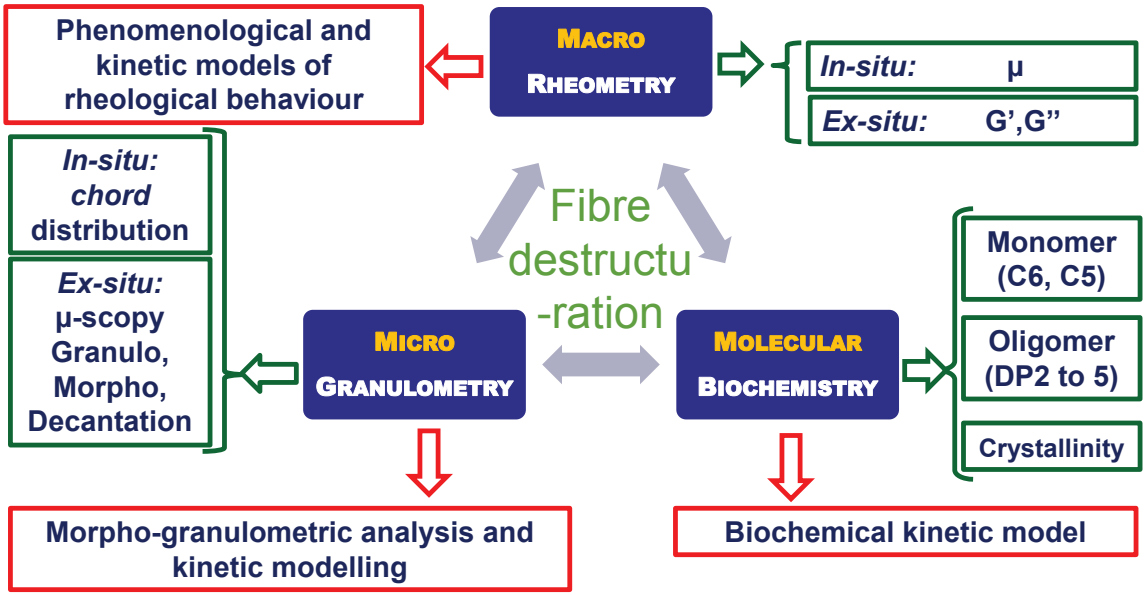

Figure 4-2: Objectives and strategy of study.

Thirdly, our main contributions can be presented considering methodological advances and progress in the three main actions. This work is primarily based on the development of a specific experimental set-up allowing the measurements and the control of different physical-biochemical parameters. The design of the experimental set-up (bioreactor and peripheral accessories) and the selection of in- & ex-situ physical and biochemical sensors/analyses (torque, rotation speed, rheometry, FBRM, DLS, morpho-granulometry, decantation, etc.) single out our scientific approach. Based on theoretical foundations of measurements, all raw data was interpreted, modified and compared. Then, the experimental set-up was fully characterized (power consumption curve associated with Metzner & Otto concept and Rieger & Novak's approach) in order to monitor the viscosity in-situ with Newtonian and non-Newtonian homogeneous suspensions. Regarding granulo- and morpho-metry, all raw data (FBRM, DLS, Decantation and Morphology) may be transformed and compared on the basis of restrictive assumptions, for example, the successful conversion of CLD into PSD, using the spherical particle model as reference.

Regarding (i) raw material characterisation and rheology of suspensions, (ii) hydrolysis under dilute conditions and (iii) hydrolysis up to high dry matter contents with a strategy based on cumulative substrate additions, the different questions, to which responses have been provided, may be inventoried and major results recapped. Our strategy to exploit experimental data (**Table 2-13**) is based on a comparison of in and ex-situ measurements (macro (rheometry) and micro-scale (morpho-granulometry)). At a molecular scale, mass balance and biochemical kinetics are characterised.

- Rheometry/Viscosimetry of lignocellulose suspension:

(i) What is the importance of the scientific literature and its indications on the physical properties of lignocellulosic suspensions before and during enzyme hydrolysis?

→ Considering the study of rheometry and viscosimetry, the literature overview focussing on "lignocellulosic fiber suspension / particle size or rheometry/biocatalytic hydrolysis" is still limited. Approximately 40 publications and two reviews are reported.

(ii) What is (are) the rheological behaviour(s) of these suspensions before hydrolysis and their behaviour as hydrolysis progresses?

→ Our results showed that a shear-thinning rheological behaviour was demonstrated for all substrates. This behaviour is conserved during enzyme attack but its magnitude is progressively reduced. In addition, the oscillatory measurements indicate a non-negligible yield stress for the initial suspension of WP and PP. This yield stress rapidly disappears within the first five hours of enzyme attack. During hydrolysis, viscosity depends on the type of substrate and the enzyme concentration (ratio E/S).

(iii) Can suspension viscosity be described by a single mechanism during hydrolysis?

→ A dimensionless viscosity-time curve was established and the uniqueness of this curve indicated the same visco-kinetics. The critical time, $t(\mu^*=0.1)$ was identified irrespective of the substrate and enzyme concentrations. This critical time corresponding to 90% reduction of the initial viscosity was taken into account to define (i) dimensionless time and (ii) critical (reference) feeding flow rate.

(iv) Could we identify the technological criteria (concentration, viscosity, hydrolysis time) defining the favourable conditions to control hydrolysis without transfer limitation?

→ A phenomenological model, describing the viscosity versus shear rate and substrate concentration, was established. The critical (technical) concentrations, C* indicates the passage from dilute/semi-dilute to concentrated regimes for all matrices. These values were >396; 35; 29; >200gdm/L for MCC, WP, PP (27 and 31) and BAG respectively. The critical time $t(\mu^*=0.1)$ was also used to determine a critical (reference) substrate feed rate in semi-continuous mode. This operating parameter, Qs is defined by the ratio $C^*/t(\mu^*=0.1)$. The results of viscosity change for the cumulative feeding strategy experiments demonstrated the same phenomenon as observed for batch mode experiments. The reference flow rates enable us to control the rheological behaviour of the suspension, to maintain low viscosity and to control glucose release without transfer limitation.

- Morpho-granulometry

(i) How do the particle size and shape vary?

(ii) Are the different measurement techniques (FBRM, DLS, MG, Turbiscan) comparable?

(iii) Can coherence between raw data (from the various techniques) and transformed data (En(d_{EC}, lc, etc) up to Fv(d_{EC}, lc,…)) be demonstrated?

→ All analyses for all substrates (except BAG) indicated reduction of particle size under the action of the enzymes; the disappearance of the coarse population and the increase of fine particles. The conversion from CLD into PSD and also from En/Fn(d_{EC}, lc, etc) into Ev/Fv(d_{EC}, lc, etc) was successful. Morpho-granulometry analysis demonstrated the strong coherence between different in-situ and ex-situ techniques. The evolution of particle size could be correlated with viscosity changes during hydrolysis.

- Bio-chemical analysis and mass balance

(i) How do monomer (glucose, xylose) and oligomer (DP≤5) concentrations vary during enzyme hydrolysis?

(ii) Does the high dry matter content may significantly affect the hydrolysis efficiency under cumulative feed strategy?

→ The impact of enzyme concentration was clearly observed on hydrolysis efficiency. A five-fold difference in bioconversion rate (in glucose equivalent) was found when the enzyme activities were multiplied by five (except BAG). A bioconversion of around 80% was obtained for dilute substrate concentration (1-3%w/v, 25FPU/g cellulose). No significant accumulation of intermediate compounds (DP≥2) was observed during the 24h test run. Interestingly for the semi-continuous mode, no transfer limitations controlling glucose release kinetics were found. The final bioconversion rates were identical no matter what the flow rates were. As expected, the initial additions of enzyme were much more effective in reducing suspension viscosity and increasing biomass conversion into glucose.

- Modelling of kinetics

(i) Can we propose a single kinetic model for physical-biochemical parameters?

→ As reported in the literature our multi-scale investigation confirmed that the evolution of suspension viscosity was affected by (i) the dissolution of solid matter and (ii) the morphological modifications of fibres. In a more original way, the results obtained enabled ud to quantify the relative contributions (on viscosity) of substrate solubilisation and fibre degradation during the bio-reaction. The kinetics of physical (viscosity, particle size) and biochemical parameters were analysed. Interestingly, a single model (assuming a second order reaction) accurately described all quantities. Consequently, the ability to interpret physical and biochemical variables and associated rates is now feasible.

Finally, this PhD work contributed to investigating the dynamics of transfer phenomena and the limitation of bio-catalytic reactions with lignocellulose resources under high concentrations. This research was centred on the development of in-situ and ex-situ physical and biochemical analyses to complete the comprehension of fibre breakdown mechanisms and to characterise the release kinetics of glucose in order to ultimately control microbial cultures.

The above assessments enable the identification of perspectives for the future. Three main axes (technology, experimentation and modelling) may contribute to deepening and enlarging this research.

- From a technological standpoint, the implementation of the experimental set-up can be considered on the basis of:

(i) Upgrading of in-situ instrumentation (e.g.: in-situ optical measurements with multi-wavelength sensors to discriminate particles)

(ii) Enlarged performance including operating conditions (e.g.: max and min torque measurement, improved accuracy)

(iii) Development of accurate and flexible control/command of inlets (substrate, enzyme, microorganism) (e.g.: substrate feeding strategy),

(iv) Integration of cell culture specifications (e.g.: to ensure sterility and sterilisation of experimental set-up),

- From experimental standpoint:

(i) Extensive characterisation of complex lignocellulose substrates (e.g.: porosity and specific surface area measurement with tomography, variation of interfacial surface tension (hydrophilicity) along hydrolysis reactions),

(ii) Identification and quantification of soluble fractions (up to DP<16) to build the profile of lignocellulose degradation compounds and to investigate its impact on suspension viscosity

(iii) Quantification of enzyme efficiency by assaying the residual activity,

(iv) Investigation the impact of single biocatalytic activities (e.g.: endo-glucanase, β-glucosidase, xylanase, etc.) on physical parameters,

(v) Achievement of high dry matter content (up to 30%w/v) under controlled substrate feed strategy,

(vi) Supernatant fermentability testing (e.g.: inhibitor identification),

Consolidation with extrusion-enzyme reaction and fermentation processes,

- For modelling kinetics:

(i) Interpretation of physical and biochemical variables and associated rates,

(ii) Establishment of "knowledge building-blocks" by integrating rheometry, morpho-granulometry and biochemistry models,

(iii) Simulation and validation of phenomenological models for the semi-continuous mode.

"Lời quê chắp nhặt dông dài
Mua vui cũng được một vài trống canh"
- Nguyễn Du -

REFERENCES

Agarwal, U.P., Zhu, J.Y., Ralph, S.A. 2012. Enzymatic hydrolysis of loblolly pine: effects of cellulose crystallinity and delignification. *Holzforschung 2013*, **67**(4), 371-377.

Agbor, V.B., Cicek, N., Sparling, R., Berlin, A., Levin, D.B. 2011. Biomass pretreatment: Fundamentals toward application. *Biotechnology Advances*, **29**(6), 675-685.

Agoda-Tandjawa, G., Durand, S., Berot, S., Blassel, C., Gaillard, C., Garnier , C., Doublier, J.-L. 2010. Rheological characterization of microfibrillated cellulose suspensions after freezing. *Carbohydrate Polymers*, **80**, 677-686.

Allen, T. 1968. *Particle size measurement*. Chapman & Hall, London.

Alves, E.F., Bose, S.K., Francis, R.C., Colodette, J.L., Iakovlev, M., Van Heiningen, A. 2010. Carbohydrate composition of eucalyptus, bagasse and bamboo by a combination of methods. *Carbohydrate Polymers*, **82**(4), 1097-1101.

Alvira, P., Negro, M.J., Ballesteros, M. 2011. Effect of endoxylanase and alpha-L-arabinofuranosidase supplementation on the enzymatic hydrolysis of steam exploded wheat straw. *Bioresource Technology*, **102**(6), 4552-4558.

Alvira, P., Tomás-Pejó, E., Ballesteros, M., Negro, M.J. 2010. Pretreatment technologies for an efficient bioethanol production process based on enzymatic hydrolysis: A review. *Bioresource Technology*, **101**(13), 4851-4861.

Andrès, C., Réginault, P., Rochat, M.H., Chaillot, B., Pourcelot, Y. 1996. Particle-size distribution of a powder: Comparison of three analytical techniques. *International Journal of Pharmaceutics*, **144**(2), 141-146.

Araki, J., Wada, M., Kuga, S., Okano, T. 1998. Flow properties of microcrystalline cellulose suspension prepared by acid treatment of native cellulose. *Colloids and Surfaces a-Physicochemical and Engineering Aspects*, **142**(1), 75-82.

Ballesteros, M., Oliva, J.M., Manzanares, P., Negro, M.J., Ballesteros, I. 2002. Ethanol production from paper material using a simultaneous saccharification and fermentation system in a fed-batch basis. *World Journal of Microbiology & Biotechnology*, **18**(6), 559-561.

Bansal, P., Hall, M., Realff, M.J., Lee, J.H., Bommarius, A.S. 2010. Multivariate statistical analysis of X-ray data from cellulose: A new method to determine degree of crystallinity and predict hydrolysis rates. *Bioresource Technology*, **101**(12), 4461-4471.

Barnes, H.A. 1997. Thixotropy - A review. *Journal of Non-Newtonian Fluid Mechanics*, **70**(1-2), 1-33.

Barnes, H.A., Hutton, J.F., Walters, K. 1989. *An Introduction to rheology*. Elsevier.

Barrett, P., Glennon, B. 1999. In-line FBRM monitoring of particle size in dilute agitated suspensions. *Particle & Particle Systems Characterization*, **16**(5), 207-211.

Bayod, E., Bolmstedt, U., Innings, F., Tornberg, E. 2005. Rheological Characterization of Fiber Suspensions Prepared from Vegetable Pulp and Dried Fibers. A Comparatible Study. *Annual Transactions of The Nordic Rheology Society*, **13**, 249-253.

Beall, F.C. 1971. Differential calometric analysis of wood and wood components. *Wood Science and Technology*, **5**(3), 159-175.

Bennington, C.P.J., Kerekes, R.J., Grace, J.R. 1990. THE YIELD STRESS OF FIBER SUSPENSIONS. *Canadian Journal of Chemical Engineering*, **68**(5), 748-757.

Blanco, A., Negro, C., Fuente, E., Tijero, J. 2006. Rotor selection for a Searle-type device to study the rheology of paper pulp suspensions. *Chemical Engineering and Processing*, **46**, 37-44.

Boluk, Y., Lahiji, R., Zhao, L., McDermott, M.T. 2011. Suspension viscosities and shape parameter of cellulose nanocrystals (CNC). *Colloids and Surfaces a-Physicochemical and Engineering Aspects*, **377**(1-3), 297-303.

Bommarius, A.S., Katona, A., Cheben, S.E., Patel, A.S., Ragauskas, A.J., Knudson, K., Pu, Y. 2008. Cellulase kinetics as a function of cellulose pretreatment. *Metabolic Engineering*, **10**(6), 370-381.

Brittain, H.G. 2001. Particle size distribution, Part I: Representation of particle shape, size and distribution. *Pharmaceutical Technology*, **25**, 38-45.

Bru, P., Brunel, L., Buron, H., Cayré, I., Ducarre, X., Fraux, A., Mengual, O., Meunier, G., de Sainte Marie, A., Snabre, P. 2004. Particle Size and Rapid Stability Analyses of Concentrated Dispersions: Use of Multiple Light Scattering Technique. in: *Particle Sizing and Characterization*, Vol. 881, American Chemical Society, pp. 45-60.

Buron, H., Mengual, O., Meunier, G., Cayré, I., Snabre, P. 2004. Optical characterization of concentrated dispersions: applications to laboratory analyses and on-line process monitoring and control. *Polymer International*, **53**(9), 1205-1209.

Cara, C., Ruiz, E., Oliva, J.M., Sáez, F., Castro, E. 2008. Conversion of olive tree biomass into fermentable sugars by dilute acid pretreatment and enzymatic saccharification. *Bioresource Technology*, **99**(6), 1869-1876.

Carvalheiro, F., Duarte, L.C., Gírio, F.M. 2008. Hemicellulose biorefineries: a review on biomass pretreatments. *Journal of Scientific & Industrial Research*, **67**, 849–864.

Carvalho, M.L., Sousa, R., Rodriguez-Zuniga, U.F., Suarez, C.A.G., Rodrigues, D.S., Giordano, R.C., Giordano, R.L.C. 2013. KINETIC STUDY OF THE ENZYMATIC HYDROLYSIS OF SUGARCANE BAGASSE. *Brazilian Journal of Chemical Engineering*, **30**(3), 437-447.

Chandra, R.P., Au-Yeung, K., Chanis, C., Roos, A.A., Mabee, W., Chung, P.A., Ghatora, S., Saddler, J.N. 2011. The influence of pretreatment and enzyme loading on the effectiveness of batch and fed-batch hydrolysis of corn stover. *Biotechnology Progress*, **27**(1), 77-85.

Chang, M., Chou, T.C., Tsao, G. 1981. Structure, pretreatment and hydrolysis of cellulose. in: *Bioenergy*, Vol. 20, Springer Berlin Heidelberg, pp. 15-42.

Chaussy, D., Martin, C., Roux, J.C. 2011. Rheological Behavior of Cellulose Fiber Suspensions: Application to Paper-Making Processing. *Industrial & Engineering Chemistry Research*, **50**(6), 3524-3533.

Chen, B., Tatsumi, D., Matsumoto, T. 2003. Fiber orientation and flow properties of pulp fiber suspensions under shear flow conditions. *Sen-I Gakkaishi*, **59**(12), 471-478.

Chen, Y., Stipanovic, A., Winter, W., Wilson, D., Kim, Y.-J. 2007. Effect of digestion by pure cellulases on crystallinity and average chain length for bacterial and microcrystalline celluloses. *Cellulose*, **14**(4), 283-293.

Chrastil, J. 1988. ENZYMIC PRODUCT FORMATION CURVES WITH THE NORMAL OR DIFFUSION LIMITED REACTION-MECHANISM AND IN THE PRESENCE OF SUBSTRATE RECEPTORS. *International Journal of Biochemistry*, **20**(7), 683-693.

Cullen, P.J., O'Donnell, C.P., Houska, M. 2003. Rotational rheometry using complex geometries - A review. *Journal of Texture Studies*, **34**(1), 1-20.

Damani, R., Powell, R.L., Hagen, N. 1993. VISCOELASTIC CHARACTERIZATION OF MEDIUM CONSISTENCY PULP SUSPENSIONS. *Canadian Journal of Chemical Engineering*, **71**(5), 676-684.

Dasari, R., Dunaway, K., Berson, R. 2009. A scraped surface bioreactor for enzymatic saccharification of pretreated corn stover slurries. *Energy Fuel*, **23**, 492 - 497.

Dasari, R.K., Berson, R.E. 2007. The effect of particle size on hydrolysis reaction rates and rheological properties in cellulosic slurries. *Applied Biochemistry and Biotechnology*, **137**, 289-299.

Demirbas, A. 2005. Bioethanol from Cellulosic Materials: A Renewable Motor Fuel from Biomass. *Energy Sources*, **27**(4), 327-337.

Derakhshandeh, B., Hatzikiriakos, S.G., Bennington, C.P.J. 2010. Rheology of pulp suspensions using ultrasonic Doppler velocimetry. *Rheologica Acta*, **49**(11-12), 1127-1140.

Dhawan, S., Kaur, J. 2007. Microbial Mannanases: An Overview of Production and Applications. *Critical Reviews in Biotechnology*, **27**(4), 197-216.

Di Risio, S., Hu, C.S., Saville, B.A., Liao, D., Lortie, J. 2011. Large-scale, high-solids enzymatic hydrolysis of steam-exploded poplar. *Biofuels, Bioproducts and Biorefining*, **5**(6), 609-620.

Dibble, C.J., Shatova, T.A., Jorgenson, J.L., Stickel, J.J. 2011. Particle morphology characterization and manipulation in biomass slurries and the effect on rheological properties and enzymatic conversion. *Biotechnology Progress*, **27**(6), 1751-1759.

Du, J., Zhang, F.Z., Li, Y.Y., Zhang, H.M., Liang, J.R., Zheng, H.B., Huang, H. 2014. Enzymatic liquefaction and saccharification of pretreated corn stover at high-solids concentrations in a horizontal rotating bioreactor. *Bioprocess and Biosystems Engineering*, **37**(2), 173-181.

Dunaway, K.W., Dasari, R.K., Bennett, N.G., Berson, R.E. 2010. Characterization of changes in viscosity and insoluble solids content during enzymatic saccharification of pretreated corn stover slurries. *Bioresource Technology*, **101**(10), 3575-3582.

Ebringerova, A., Hromadkova, Z., Heinze, T. 2005. Hemicellulose. *Adv Polym Sci*, **186**, 1-67.

Ehrhardt, M.R., Monz, T.O., Root, T.W., Connelly, R.K., Scott, C.T., Klingenberg, D.J. 2010. Rheology of Dilute Acid Hydrolyzed Corn Stover at High Solids Concentration. *Applied Biochemistry and Biotechnology*, **160**(4), 1102-1115.

Elliston, A., Collins, S.R.A., Wilson, D.R., Roberts, I.N., Waldron, K.W. 2013. High concentrations of cellulosic ethanol achieved by fed batch semi simultaneous saccharification and fermentation of waste-paper. *Bioresource Technology*, **134**, 117-126.

Esterbauer, H., Steiner, W., Labudova, I., Hermann, A., Hayn, M. 1991. Production of Trichoderma cellulase in laboratory and pilot scale. *Bioresource Technology*, **36**(1), 51-65.

Fan, L.T., Gharpuray, M.M., Lee, Y.H. 1987. *Cellulose Hydrolysis*. Springer Verlag, Berlin.

Fan, Z.L., South, C., Lyford, K., Munsie, J., van Walsum, P., Lynd, L.R. 2003. Conversion of paper sludge to ethanol in a semicontinuous solids-fed reactor. *Bioprocess and Biosystems Engineering*, **26**(2), 93-101.

Fillaudeau, L., Babau, M., Cameleyre, X., Lombard, E., Anne-Archard, D. 2011. Libération de substrats fermentescibles à partir de matrices lignocellulosiques issues de l'industrie papetière. *Récents Progrès en Génie des Procédés*, **101**.

FitzPatrick, M., Champagne, P., Cunningham, M.F., Whitney, R.A. 2010. A biorefinery processing perspective: Treatment of lignocellulosic materials for the production of value-added products. *Bioresource Technology*, **101**(23), 8915-8922.

Fowkes, F.M. 1964. Attractive Forces at Interfaces. *Industrial & Engineering Chemistry* **56**(12), 40-52.

Gan, Q., Allen, S.J., Taylor, G. 2003. Kinetic dynamics in heterogeneous enzymatic hydrolysis of cellulose: an overview, an experimental study and mathematical modelling. *Process Biochemistry*, **38**(7), 1003-1018.

Gandjbakhche, A.H., Mills, P., Snabre, P. 1994. Light-scattering technique for the study of orientation and deformation of red blood cells in a concentrated suspension. *Applied Optics*, **33**(6), 1070-1078.

García-Aparicio, M., Ballesteros, I., González, A., Oliva, J., Ballesteros, M., Negro, M. 2006. Effect of inhibitors released during steam-explosion pretreatment of barley straw on enzymatic hydrolysis. *Applied Biochemistry and Biotechnology*, **129**(1-3), 278-288.

García-Aparicio, M., Ballesteros, M., Manzanares, P., Ballesteros, I., González, A., José Negro, M. 2007. Xylanase contribution to the efficiency of cellulose enzymatic hydrolysis of barley straw. *Applied Biochemistry and Biotechnology*, **137-140**(1-12), 353-365.

García-Cubero, M.T., González-Benito, G., Indacoechea, I., Coca, M., Bolado, S. 2009. Effect of ozonolysis pretreatment on enzymatic digestibility of wheat and rye straw. *Bioresource Technology*, **100**(4), 1608-1613.

Geddes, C.C., Peterson, J.J., Mullinnix, M.T., Svoronos, S.A., Shanmugam, K.T., Ingram, L.O. 2010. Optimizing cellulase usage for improved mixing and rheological properties of acid-pretreated sugarcane bagasse. *Bioresource Technology*, **101**(23), 9128-9136.

Ghose, T.K. 1987. Measurement of cellulase activities. *Pure Appl. Chem.*, **57**, 257-268.

Gibbons, W.R., Hughes, S.R. 2009. Integrated biorefineries with engineered microbes and high-value co-products for profitable biofuels production. *In Vitro Cellular & Developmental Biology - Plant*, **45**(3), 218-228.

Gírio, F.M., Fonseca, C., Carvalheiro, F., Duarte, L.C., Marques, S., Bogel-Łukasik, R. 2010. Hemicelluloses for fuel ethanol: A review. *Bioresource Technology*, **101**(13), 4775-4800.

Gonzalez-Labrada, E., Gray, D.G. 2012. Viscosity measurements of dilute aqueous suspensions of cellulose nanocrystals using a rolling ball viscometer. *Cellulose*, **19**(5), 1557-1565.

Govumoni, S.P., Koti, S., Kothagouni, S.Y., S, V., Linga, V.R. 2013. Evaluation of pretreatment methods for enzymatic saccharification of wheat straw for bioethanol production. *Carbohydrate Polymers*, **91**(2), 646-650.

Goyal, A., Ghosh, B., Eveleigh, D. 1991. Characteristics of fungal cellulases. *Bioresource Technology*, **36**(1), 37-50.

Grammont, V. 2006. Les carburants à partir de ressources lignocellulosics: Présentation des filières et identification des risques. *Rapport INERIS direction de la certification*.

Gupta, R., Kim, T., Lee, Y. 2008. Substrate Dependency and Effect of Xylanase Supplementation on Enzymatic Hydrolysis of Ammonia-Treated Biomass. *Applied Biochemistry and Biotechnology*, **148**(1-3), 59-70.

Ham, J.H., Platzer, B. 2004. Semi-empirical equations for residence time distributions in disperse systems - Part 1: Continuous phase. *Chemical Engineering & Technology*, **27**(11), 1172-1178.

Hamilton, P., Littlejohn, D., Nordon, A., Sefcik, J., Slavin, P. 2012. Validity of particle size analysis techniques for measurement of the attrition that occurs during vacuum agitated powder drying of needle-shaped particles. *Analyst*, **137**(1), 118-125.

Herrera, A., Téllez-Luis, S.J., Ramírez, J.A., Vázquez, M. 2003. Production of Xylose from Sorghum Straw Using Hydrochloric Acid. *Journal of Cereal Science*, **37**(3), 267-274.

Hodge, D.B., Karim, M.N., Schell, D.J., McMillan, J.D. 2009. Model-Based Fed-Batch for High-Solids Enzymatic Cellulose Hydrolysis. *Applied Biochemistry and Biotechnology*, **152**(1), 88-107.

Horvath, A.E., Lindstrom, T. 2007. The influence of colloidal interactions on fiber network strength. *Journal of Colloid and Interface Science*, **309**(2), 511-517.

Hukkanen, E.J., Braatz, R.D. 2003. Measurement of particle size distribution in suspension polymerization using in situ laser backscattering. *Sensors and Actuators B: Chemical*, **96**(1–2), 451-459.

Ingram, L.O., Doran, J.B. 1995. Conversion of cellulosic materials to ethanol (English)

Beyond 2000Â : chemicals from biotechnology (English). *FEMS microbiol. rev.*, conf start date: 10-18-1994

cover date: 1995. Blackwell, Oxford. pp. 235.

Ingram, T., Wörmeyer, K., Lima, J.C.I., Bockemühl, V., Antranikian, G., Brunner, G., Smirnova, I. 2011. Comparison of different pretreatment methods for lignocellulosic materials. Part I: Conversion of rye straw to valuable products. *Bioresource Technology*, **102**(8), 5221-5228.

Ishimaru, A., Kuga, Y. 1982. Attenuation constant of a coherent field in a dense distribution of particles. *Journal of the Optical Society of America*, **72**(10), 1317-1320.

Jäger, G., Büchs, J. 2012. Biocatalytic conversion of lignocellulose to platform chemicals. *Biotechnology Journal*, **7**(9), 1122-1136.

Jahangiri, M., Golkar-Narenji, M.R., Montazerin, N., Savarmand, S. 2001. Investigation of the viscoelastic effect on the Metzner and Otto coefficient through LDA velocity measurements. *Chinese Journal of Chemical Engineering*, **9**(1), 77-83.

Jorgensen, H., Vibe-Pedersen, J., Larsen, J., Felby, C. 2007. Liquefaction of lignocellulose at high-solids concentrations. *Biotechnology and Bioengineering*, **96**(5), 862-870.

Kaar, W.E., Holtzapple, M.T. 1998. Benefits from Tween during enzymic hydrolysis of corn stover. *Biotechnology and Bioengineering*, **59**(4), 419-427.

Kadic, A., Palmqvist, B., Liden, G. 2014. Effects of agitation on particle-size distribution and enzymatic hydrolysis of pretreated spruce and giant reed. *Biotechnology for Biofuels*, **7**(1), 77.

Kadolph, S.J., Langford, A.L. 1998. *Textiles*. Prentice Hall, New Jork.

Kail, N., Briesen, H., Marquardt, W. 2007. Advanced Geometrical Modeling of Focused Beam Reflectance Measurements (FBRM). *Particle & Particle Systems Characterization*, **24**(3), 184-192.

Kamm, B., Kamm, M., Gruber, P. 2006. Biorefinerie Systems: An overview. *WILEY-VCH*, **1**, 3-40.

Kamm, B., Kamm, M., Soyez, K. 1997. Die Grüne Bioraffinerie/The Green Biorefinery. in: *1st International Symposium Green Biorefinery/Grüne Bioraffinerie*. Neuruppin, Germany.

Karunanithy, C., Muthukumarappan, K., Gibbons, W.R. 2013. Effect of Extruder Screw Speed, Temperature, and Enzyme Levels on Sugar Recovery from Different Biomasses. *ISRN Biotechnology*, **2013**, 13.

Kerker, M. 1969. *The scattering of light*. Academic Press, New York.

Keshwani, D.R., Cheng, J.J. 2010. Microwave-based alkali pretreatment of switchgrass and coastal bermudagrass for bioethanol production. *Biotechnology Progress*, **26**(3), 644-652.

Kinnarinen, T., Häkkinen, A. 2014. Influence of enzyme loading on enzymatic hydrolysis of cardboard waste and size distribution of the resulting fiber residue. *Bioresource Technology*, **159**(0), 136-142.

Knauf, M., Moniruzzaman, M. 2004. *Lignocellulosic biomass processing: A perspective*. Informa Healthcare, London, ROYAUME-UNI.

Knutsen, J.S., Liberatore, M.W. 2010a. Rheology Modification and Enzyme Kinetics of High-Solids Cellulosic Slurries: An Economic Analysis. *Energy & Fuels*, **24**, 6506-6512.

Knutsen, J.S., Liberatore, M.W. 2010b. Rheology Modification and Enzyme Kinetics of High Solids Cellulosic Slurries. *Energy & Fuels*, **24**, 3267-3274.

Koo, B.-W., Kim, H.-Y., Park, N., Lee, S.-M., Yeo, H., Choi, I.-G. 2011. Organosolv pretreatment of Liriodendron tulipifera and simultaneous saccharification and fermentation for bioethanol production. *Biomass and Bioenergy*, **35**(5), 1833-1840.

Kristensen, J., Felby, C., Jørgensen, H. 2009. Determining Yields in High Solids Enzymatic Hydrolysis of Biomass. *Applied Biochemistry and Biotechnology*, **156**(1-3), 127-132.

Kuhad, R., Singh, A., Eriksson, K.-E. 1997. Microorganisms and enzymes involved in the degradation of plant fiber cell walls. in: *Biotechnology in the Pulp and Paper Industry*, (Eds.) K.E.L. Eriksson, W. Babel, H.W. Blanch, C.L. Cooney, S.O. Enfors, K.E.L. Eriksson, A. Fiechter, A.M. Klibanov, B. Mattiasson, S.B. Primrose, H.J. Rehm, P.L. Rogers, H. Sahm, K. Schügerl, G.T. Tsao, K. Venkat, J. Villadsen, U. von Stockar, C. Wandrey, Vol. 57, Springer Berlin Heidelberg, pp. 45-125.

Kumar, P., Barrett, D.M., Delwiche, M.J., Stroeve, P. 2009. Methods for Pretreatment of Lignocellulosic Biomass for Efficient Hydrolysis and Biofuel Production. *Industrial & Engineering Chemistry Research*, **48**(8), 3713-3729.

Lacerda, T.M., de Paula, M.P., Zambon, M.D., Frollini, E. 2012. Saccharification of Brazilian sisal pulp: evaluating the impact of mercerization on non-hydrolyzed pulp and hydrolysis products. *Cellulose*, **19**(2), 351-362.

Ladisch, M.R., Flickinger, M.C., Tsao, G.T. 1979. Fuels and chemicals from biomass. *Energy*, **4**(2), 263-275.

Lapierre, L., Bouchard, J., Berry, R. 2006. On the relationship between fibre length, cellulose chain length and pulp viscosity of a softwood sulfite pulp. *Holzforschung*, **60**(4), 372-377.

Laureano-Perez, L., Teymouri, F., Alizadeh, H., Dale, B. 2005. Understanding factors that limit enzymatic hydrolysis of biomass. *Applied Biochemistry and Biotechnology*, **124**(1-3), 1081-1099.

Le Moigne, N., Jardeby, K., Navard, P. 2010. Structural changes and alkaline solubility of wood cellulose fibers after enzymatic peeling treatment. *Carbohydrate Polymers*, **79**, 325-332.

Lee, J. 1997. Biological conversion of lignocellulosic biomass to ethanol. *Journal of Biotechnology*, **56**(1), 1-24.

Lenz, J., Esterbauer, H., Sattler, W., Schurz, J., Wrentschur, E. 1990. Changes of structure and morphology of regenerated cellulose caused by acid and enzymatic hydrolysis. *Journal of Applied Polymer Science*, **41**(5-6), 1315-1326.

Leonowicz, A., Matuszewska, A., Luterek, J., Ziegenhagen, D., Wojtaś-Wasilewska, M., Cho, N.-S., Hofrichter, M., Rogalski, J. 1999. Biodegradation of Lignin by White Rot Fungi. *Fungal Genetics and Biology*, **27**(2–3), 175-185.

Li, M., Wilkinson, D. 2005. Determination of non-spherical particle size distribution from chord length measurements. Part 1: Theoretical analysis. *Chemical Engineering Science*, **60**(12), 3251-3265.

Lowys, M.-P., DesbrieÁres, J., Rinaudo, M. 2000. Rheological characterization of cellulosic microfibril suspensions. Role of polymeric additives. *Food Hydrocolloids*, **15**, 25-32.

Lu, A., Hemraz, U., Khalili, Z., Boluk, Y. 2014. Unique viscoelastic behaviors of colloidal nanocrystalline cellulose aqueous suspensions. *Cellulose*, **21**(3), 1239-1250.

Lu, Y.F., Wang, Y.H., Xu, G.Q., Chu, J., Zhuang, Y.P., Zhang, S.L. 2010. Influence of High Solid Concentration on Enzymatic Hydrolysis and Fermentation of Steam-Exploded Corn Stover Biomass. *Applied Biochemistry and Biotechnology*, **160**(2), 360-369.

Luukkonen, P., Newton, J.M., Podczeck, F., Yliruusi, J. 2001. Use of a capillary rheometer to evaluate the rheological properties of microcrystalline cellulose and silicified microcrystalline cellulose wet masses. *International Journal of Pharmaceutics*, **216**(1-2), 147-157.

Lynd, L.R., CUSHMAN, J.H., NICHOLS, R.J., WYMAN, C.E. 1991. Fuel Ethanol from Cellulosic Biomass. *Science*, **251**(4999), 1318-1323.

Lynd, L.R., Weimer, P.J., van Zyl, W.H., Pretorius, I.S. 2002. Microbial Cellulose Utilization: Fundamentals and Biotechnology. *Microbiology and Molecular Biology Reviews*, **66**(3), 506-577.

Malherbe, S., Cloete, T.E. 2002. Lignocellulose biodegradation: Fundamentals and applications. *Re/Views in Environmental Science & Bio/Technology*(1), 105-114.

Mansfield, S., Meder, R. 2003. Cellulose hydrolysis – the role of monocomponent cellulases in crystalline cellulose degradation. *Cellulose*, **10**(2), 159-169.

Marti, I., Hofler, O., Fischer, P., Windhab, E.J. 2005. Rheology of concentrated suspensions containing mixtures of spheres and fibres. *Rheologica Acta*, **44**(5), 502-512.

Martín, C., Thomsen, M.H., Hauggaard-Nielsen, H., BelindaThomsen, A. 2008. Wet oxidation pretreatment, enzymatic hydrolysis and simultaneous saccharification and fermentation of clover–ryegrass mixtures. *Bioresource Technology*, **99**(18), 8777-8782.

McMillan James, D. 1994. Pretreatment of Lignocellulosic Biomass. in: *Enzymatic Conversion of Biomass for Fuels Production*, Vol. 566, American Chemical Society, pp. 292-324.

Mengual, O., Meunier, G., Cayré, I., Puech, K., Snabre, P. 1999. TURBISCAN MA 2000: multiple light scattering measurement for concentrated emulsion and suspension instability analysis. *Talanta*, **50**(2), 445-456.

Menon, V., Rao, M. 2012. Trends in bioconversion of lignocellulose: Biofuels, platform chemicals & biorefinery concept. *Progress in Energy and Combustion Science*, **38**(4), 522-550.

Michaelis, L., Menten, M.L. 1913. Die Kinetik der Invertinwirkung. *Biochem*, **49**, 333-369.

Mills, P., Snabre, P. 1994. Settling of a Suspension of Hard Spheres. *EPL (Europhysics Letters)*, **25**(9), 651.

Monsalve, G., John, F., Medina, P., Ruiz, C., Adriana, A. 2006. Ethanol production of banana shell and cassava starch. *Dyna Rev fac nac minas*, **73**, 21-27.

Morice, E. 1972. Tests de normalité d'une distribution observée. *Revue de statistique appliquée*, **20**, 5-35.

Mosier, N., Wyman, C., Dale, B., Elander, R., Lee, Y.Y., Holtzapple, M., Ladisch, M. 2005. Features of promising technologies for pretreatment of lignocellulosic biomass. *Bioresource Technology*, **96**(6), 673-686.

Nguyen, Q.D., Boger, D.V. 1992. MEASURING THE FLOW PROPERTIES OF YIELD STRESS FLUIDS. *Annual Review of Fluid Mechanics*, **24**, 47-88.

Ogier, J.C., Ballerini, D., Leygue, J.P., Rigal, L., Pourquie, J. 1999. Ethanol production from lignocellulosic biomass. *Oil & Gas Science and Technology-Revue D Ifp Energies Nouvelles*, **54**(1), 67-94.

Palmqvist, B., Liden, G. 2012. Torque measurements reveal large process differences between materials during high solid enzymatic hydrolysis of pretreated lignocellulose. *Biotechnology for Biofuels*, **5**.

Palmqvist, B., Wiman, M., Liden, G. 2011. Effect of mixing on enzymatic hydrolysis of steam-pretreated spruce: a quantitative analysis of conversion and power consumption. *Biotechnol Biofuels*, **4**, 10.

Peng, L., Chen, Y. 2011. Conversion of paper sludge to ethanol by separate hydrolysis and fermentation (SHF) using Saccharomyces cerevisiae. *Biomass and Bioenergy*, **35**(4), 1600.

Pereira, H. 1988. Variability in the chemical composition of plantation eucalypts (Eucalyptus globulus Labill.). *Wood and Fiber Science*, **20**(1), 82-90.

Pereira, L.T.C., Pereira, L.T.C., Teixeira, R.S.S., Bon, E.P.D., Freitas, S.P. 2011. Sugarcane bagasse enzymatic hydrolysis: rheological data as criteria for impeller selection. *Journal Of Industrial Microbiology & Biotechnology*, **38**(8), 901-907.

Pessani, N.K. 2011. Simultaneous saccharification and fermentation of switchgrass by thermotolerant Kluyveromyces marxianus IMB3: Effect of enzyme loading, temperature and operating mode. in: *Biosystems & Agricultural Engineering*, Oklahoma State Universit. Oklahoma.

Pierre, G., Maache-Rezzoug, Z., Sannier, F., Rezzoug, S.A., Maugard, T. 2011. High-performance hydrolysis of wheat straw using cellulase and thermomechanical pretreatment. *Process Biochemistry*, **46**(11), 2194-2200.

Pimenova, N.V., Hanley, A.R. 2004. Effect of corn stover concentration on rheological characteristics. *Applied Biochemistry and Biotechnology*, **113**, 347-360.

Poulard, C. 2005. Dynamiques de gouttelettes mouillantes, Université Paris VI. Paris, France, pp. 163.

Prasad, S., Singh, A., Joshi, H.C. 2007. Ethanol as an alternative fuel from agricultural, industrial and urban residues. *Resources, Conservation and Recycling*, **50**(1), 1-39.

Quemada, D. 2006. *Modélisation Rhéologique Structurelle. Dispersions Concentrées et Fluides Complexes*. Lavoisier.

Rabinovich, M.L., Melnik, M.S., Bolobova, A.V. 2002. Dedicated to the memory of I.V. Berezin and R.V. Feniksova Microbial Cellulases (Review). *Applied Biochemistry and Microbiology*, **38**(4), 305-322.

Rao, M.A. 1975. MEASUREMENT OF FLOW PROPERTIES OF FOOD SUSPENSIONS WITH A MIXER. *Journal of Texture Studies*, **6**(4), 533-539.

Rieger, F., Novak, V. 1973. Power Consumption of Agitators in Highly Viscous non-Newtonian Liquids. *Trans. Instn. Chem. Engrs*, **51**, 105-111.

Roche, C.M., Dibble, C.J., Knutsen, J.S., Stickel, J.J., Liberatore, M.W. 2009a. Particle Concentration and Yield Stress of Biomass Slurries During Enzymatic Hydrolysis at High-Solids Loadings. *Biotechnology and Bioengineering*, **104**(2), 290-300.

Roche, C.M., Dibble, C.J., Stickel, J.J. 2009b. Laboratory-scale method for enzymatic saccharification of lignocellulosic biomass at high-solids loadings. *Biotechnology for Biofuels*, **2**.

Rosell, C.M., Santos, E., Collar, C. 2009. Physico-chemical properties of commercial fibres from different sources: A comparative approach. *Food Research International*, **42**(1), 176.

Rosgaard, L., Andric, P., Dam-Johansen, K., Pedersen, S., Meyer, A.S. 2007. Effects of substrate loading on enzymatic hydrolysis and viscosity of pretreated barley straw. *Applied Biochemistry and Biotechnology*, **143**(1), 27-40.

Rude, M.A., Schirmer, A. 2009. New microbial fuels: a biotech perspective. *Current Opinion in Microbiology*, **12**(3), 274-281.

Ruf, A., Worlitschek, J., Mazzotti, M. 2000. Modeling and experimental analysis of PSD measurements through FBRM. *Particle & Particle Systems Characterization*, **17**(4), 167-179.

Rushton, J., Costich, W., Everett, J. 1950. Power Charateristics of Mixing Impeller I and II. *Chemical Engineering Progress*, **46**(9), 467-476.

Saarikoski, E., Saarinen, T., Salmela, J., Seppala, J. 2012. Flocculated flow of microfibrillated cellulose water suspensions: an imaging approach for characterisation of rheological behaviour. *Cellulose*, **19**(3), 647-659.

Saha, B.C. 2003. Hemicellulose bioconversion. *Journal of Industrial Microbiology and Biotechnology*, **30**(5), 279-291.

Samaniuk, J.R., Scott, C.T., Root, T.W., Klingenberg, D.J. 2011. The effect of high intensity mixing on the enzymatic hydrolysis of concentrated cellulose fiber suspensions. *Bioresource Technology*, **102**(6), 4489-4494.

Sánchez, C. 2009. Lignocellulosic residues: Biodegradation and bioconversion by fungi. *Biotechnology Advances*, **27**(2), 185.

Santamaria-Holek, I., Mendoza, C.I. 2010. The rheology of concentrated suspensions of arbitrarily-shaped particles. *Journal of Colloid and Interface Science*, **346**(1), 118-126.

Schacht, C., Zetzl, C., Brunner, G. 2008. From plant materials to ethanol by means of supercritical fluid technology. *The Journal of Supercritical Fluids*, **46**(3), 299-321.

Segal, L., Creely, J.J., Martin, A.E., Conrad, C.M. 1959. An Empirical Method for Estimating the Degree of Crystallinity of Native Cellulose Using the X-Ray Diffractometer. *Textile Research Journal*, **29**(10), 786-794.

Shih, W.Y., Shih, W.-H., Aksay, I.A. 1999. Elastic and Yield Behavior of Strongly Flocculated Colloids. *Journal of the American Ceramic Society*, **82**(3), 616-624.

Silva, N., Betancur, G., Vasquez, M., de Barros Gomes, E., Pereira, N. 2011. Ethanol Production from Residual Wood Chips of Cellulose Industry: Acid Pretreatment Investigation, Hemicellulosic Hydrolysate Fermentation, and Remaining Solid Fraction Fermentation by SSF Process. *Applied Biochemistry and Biotechnology*, **163**(7), 928.

Sim, R., Taylor, M., Saddler, J.N., Mabee, W. 2008. From 1st to 2nd generation biofuel technologies - An overview of current industry and R&D activities. *OECD/IEA Bioenergy*.

Singh, R., Varma, A.J., Seeta Laxman, R., Rao, M. 2009. Hydrolysis of cellulose derived from steam exploded bagasse by Penicillium cellulases: Comparison with commercial cellulase. *Bioresource Technology*, **100**(24), 6679-6681.

Snabre, P., Arhaliass, A. 1998. Anisotropic scattering of light in random media: incoherent backscattered spotlight. *Applied Optics*, **37**(18), 4017-4026.

Snabre, P., Brunel, L., Meunier, G. 2004. Multiple Light Scattering Methods for Dispersion Characterization and Control of Particulate Processes. in: *Particle Sizing and Characterization*, Vol. 881, American Chemical Society, pp. 33-44.

Stewart, D., Azzini, A., Hall, A.T., Morrison, I.M. 1997. Sisal fibres and their constituent non-cellulosic polymers. *Industrial Crops and Products*, **6**(1), 17-26.

Stickel, J.J., Knutsen, J.S., Liberatore, M.W., Luu, W., Bousfield, D.W., Klingenberg, D.J., Scott, C.T., Root, T.W., Ehrhardt, M.R., Monz, T.O. 2009. Rheology measurements of a biomass slurry: an inter-laboratory study. *Rheologica Acta*, **48**(9), 1005-1015.

Sun, C. 2005. True density of microcrystalline cellulose. *Journal of Pharmaceutical Sciences*, **94**(10), 2132-2134.

Sun, R.C., Tomkinson, J. 2002. Characterization of hemicelluloses obtained by classical and ultrasonically assisted extractions from wheat straw. *Carbohydrate Polymers*, **50**(3), 263-271.

Sun, Y., Cheng, J. 2002. Hydrolysis of lignocellulosic materials for ethanol production: a review. *Bioresource Technology*, **83**(1), 1-11.

Szijarto, N., Siika-aho, M., Sontag-Strohm, T., Viikari, L. 2011. Liquefaction of hydrothermally pretreated wheat straw at high-solids content by purified Trichoderma enzymes. *Bioresource Technology*, **102**(2), 1968-1974.

Taherzadeh, M., Karimi, K. 2008. Pretreatment of Lignocellulosic Wastes to Improve Ethanol and Biogas Production: A Review. *International Journal of Molecular Sciences*, **9**(9), 1621-1651.

Tatsumi, D., Hitoshi, K., Chen, B., Matsumoto, T. 2008. Effect of natural additives on the rheological

properties of cellulose fiber disperse systems. *Colloids and Surfaces A: Physicochem. Eng. Aspects*, **316**, 151-158.

Tatsumi, D., Ishioka, S., Matsumoto, T. 2001. Effect of Fiber Concentration and Axial Ratio on the Rheological Properties of Cellulose Fiber Suspensions. *Journal of Society of Rheology*, **30**(1), 27-32.

Tatsumi, D., Ishioka, S., Matsumoto, T. 1999. Effect of particle and salt concentrations on the rheological properties of cellulose fibrous suspensions. *Nihon Reoroji Gakkaishi*, **27**(4), 243-248.

technologies, A.d. 2009. *Les Biocarburants*.

Tozzi, E.J., McCarthy, M.J., Lavenson, D.M., Cardona, M., Powell, R.L., Karuna, N., Jeoh, T. 2014. Effect of fiber structure on yield stress during enzymatic conversion of cellulose. *Aiche Journal*, **60**(5), 1582-1590.

Tsujiyama, S.-i., Miyamori, A. 2000. Assignment of DSC thermograms of wood and its components. *Thermochimica Acta*, **351**(1–2), 177-181.

Tu, M., Zhang, X., Paice, M., MacFarlane, P., Saddler, J.N. 2009. The potential of enzyme recycling during the hydrolysis of a mixed softwood feedstock. *Bioresource Technology*, **100**(24), 6407.

Um, B.-H. 2007. Optimization of Ethanol Production from Concentrated Substrate, Auburn University, pp. 268.

Um, B.H., Hanley, T.R. 2008. A comparison of simple rheological parameters and simulation data for Zymomonas mobilis fermentation broths with high substrate loading in a 3-L bioreactor. *Applied Biochemistry and Biotechnology*, **145**(1/3), 29-38.

Vallette, P., De Choudens, C. 1987. *Le bois, la pêtes, le papier*. Cartons et Celluloses, Centre Technique de l'Industrie des papiers.

Vázquez, M., Oliva, M., Téllez-Luis, S.J., Ramírez, J.A. 2007. Hydrolysis of sorghum straw using phosphoric acid: Evaluation of furfural production. *Bioresource Technology*, **98**(16), 3053-3060.

Viamajala, S., McMillan, J.D., Schell, D.J., Elander, R.T. 2009. Rheology of corn stover slurries at high solids concentrations - Effects of saccharification and particle size. *Bioresource Technology*, **100**(2), 925-934.

Villermaux, J. 1993. *Genie de la reaction chimique*. *2 ed*. Lavoisier, New York.

Walls, H.J., Caines, S.B., Sanchez, A.M., Khan, S.A. 2003. Yield stress and wall slip phenomena in colloidal silica gels. *Journal of Rheology (1978-present)*, **47**(4), 847-868.

Werpy, T.A., Holladay, J.E., White, J.F. 2004. Top Value Added Chemicals From Biomass: I. Results of Screening for Potential Candidates from Sugars and Synthesis Gas. PNNL-14808; Other: BM0102070; TRN: US200807%%599 United States10.2172/926125Other: BM0102070; TRN: US200807%%599Thu Apr 17 07:23:15 EDT 2008PNNLEnglish.

Wilson, C.A. 2013. Effect of endoxylanase and alpha-L-arabinofuranosidase supplementation on the enzymatic hydrolysis of steam exploded wheat straw. in: *Chemical & Biomedical Engineering*, Florida State University. Florida, pp. 170.

Wiman, M., Palmqvist, B., Tornberg, E., Liden, G. 2010. Rheological Characterization of Dilute Acid Pretreated Softwood. *Biotechnology And Bioengineering*, **108**(5), 1031-1041.

Worlitschek, J., Mazzotti, M. 2004. Model-Based Optimization of Particle Size Distribution in Batch-Cooling Crystallization of Paracetamol. *Crystal Growth & Design*, **4**(5), 891-903.

Wu, Q., Meng, Y.J., Wang, S.Q., Li, Y.J., Fu, S.Y., Ma, L.F., Harper, D. 2014. Rheological Behavior of Cellulose Nanocrystal Suspension: Influence of Concentration and Aspect Ratio. *Journal of Applied Polymer Science*, **131**(15).

Wyman, C.E. 2007. What is (and is not) vital to advancing cellulosic ethanol. *Trends in Biotechnology*, **25**(4), 153-157.

Wynn, E.J.W. 2003. Relationship between particle-size and chord-length distributions in focused beam reflectance measurement: stability of direct inversion and weighting. *Powder Technology*, **133**(1–3), 125-133.

Xue, Y., Jameel, H., Phillips, R., Chang, H.-m. 2012. Split addition of enzymes in enzymatic hydrolysis at high solids concentration to increase sugar concentration for bioethanol production. *Journal of Industrial and Engineering Chemistry*, **18**(2), 707-714.

Yang, J., Zhang, X.P., Yong, Q., Yu, S.Y. 2010. Three-stage hydrolysis to enhance enzymatic saccharification of steam-exploded corn stover. *Bioresource Technology*, **101**(13), 4930-4935.

Yang, M.C., Scriven, L.E., Macosko, C.W. 1986. Some Rheological Measurements on Magnetic Iron Oxide Suspensions in Silicone Oil. *Journal of Rheology (1978-present)*, **30**(5), 1015-1029.

Yu, W., Erickson, K. 2008. Chord length characterization using focused beam reflectance measurement probe - methodologies and pitfalls. *Powder Technology*, **185**(1), 24-30.

Zeng, M., Mosier, N.S., Huang, C.-P., Sherman, D.M., Ladisch, M.R. 2007. Microscopic examination of changes of plant cell structure in corn stover due to hot water pretreatment and enzymatic hydrolysis. *Biotechnology and Bioengineering*, **97**(2), 265-278.

Zhang, X., Qin, W., Paice, M.G., Saddler, J.N. 2009. High consistency enzymatic hydrolysis of hardwood substrates. *Bioresource Technology*, **100**(23), 5890-5897.

Zhao, X., Cheng, K., Liu, D. 2009. Organosolv pretreatment of lignocellulosic biomass for enzymatic hydrolysis. *Applied Microbiology and Biotechnology*, **82**(5), 815-827.

APPENDIX

Appendix 1: Composition of wood and paper-pulp before bleaching

Procédé	Pâte	Matrice	Rende-ment [%]	Composition								
				Cellulose	Hemi cellulose	pentosanes	mannanes	galactanes	Lignines	Substance protéique	Résines	Cendres
	Pâte de bois râpé	R	>90	40-50								
Pâtes mécaniques	Pâte mécanique de meule	R	>90		25-30				25-30		1-5	
	Pâte mécanique de copeaux	R	>90									
Pâtes thermo-mécanique	Pâte thermo-mécanique	R+F	>90									
ou chimico-thermo-mécanique	Pâte chimico-thermo-mécanique	R+F	80-90									
	Pâte à la soude à froid		70-80									
Pâtes mi-chimiques	Pâte aux sulfites neutres de sodium et d'ammonium		70-80									
Pâtes chimiques	Pâtes au sulfate écrue (Kraft) ou soude-anthraquinone		45-55									
	Pâtes aux bisulfites		45-55									
Bois résineux	(référence / tendre) (Vallette & De Choudens, 1987)			40-51 *40-55* *45-50*	*25-40* *25-35*	10-12	10-15		24-27 *15-35* *25-35*			
	Sapin			48.2	20.5	10.2	9.3	1.0	26.9	0.6	/	0.66
	Pin sylvestre			46.8	25.3	11.5	10.5	3.3	24.2	1	2.5-4.8	1.7
	Pin maritime			47.1	25.2	12.3	9.9	3.0	25.6	0.9	2-4	0.30
Bois feuillus	(référence / dur) (Vallette & De Choudens, 1987)			40-51 *38-49* *40-55*	*19-26* *24-40*	20-30	0-3		18-23 *23-30* *18-25*			
	Peuplier			51.1	21.4	21.4	0	0	22.7	0.8	1-2.7	0.4
	Hêtre			44.8	38.2	37.2	1.0	0	22.5	1.1	0.3-0.9	0.83
	Chêne			44.0	19.0	19.0	/	/	20.0	/	0.7	0.40

Appendix 2: Bioreactor characterisations

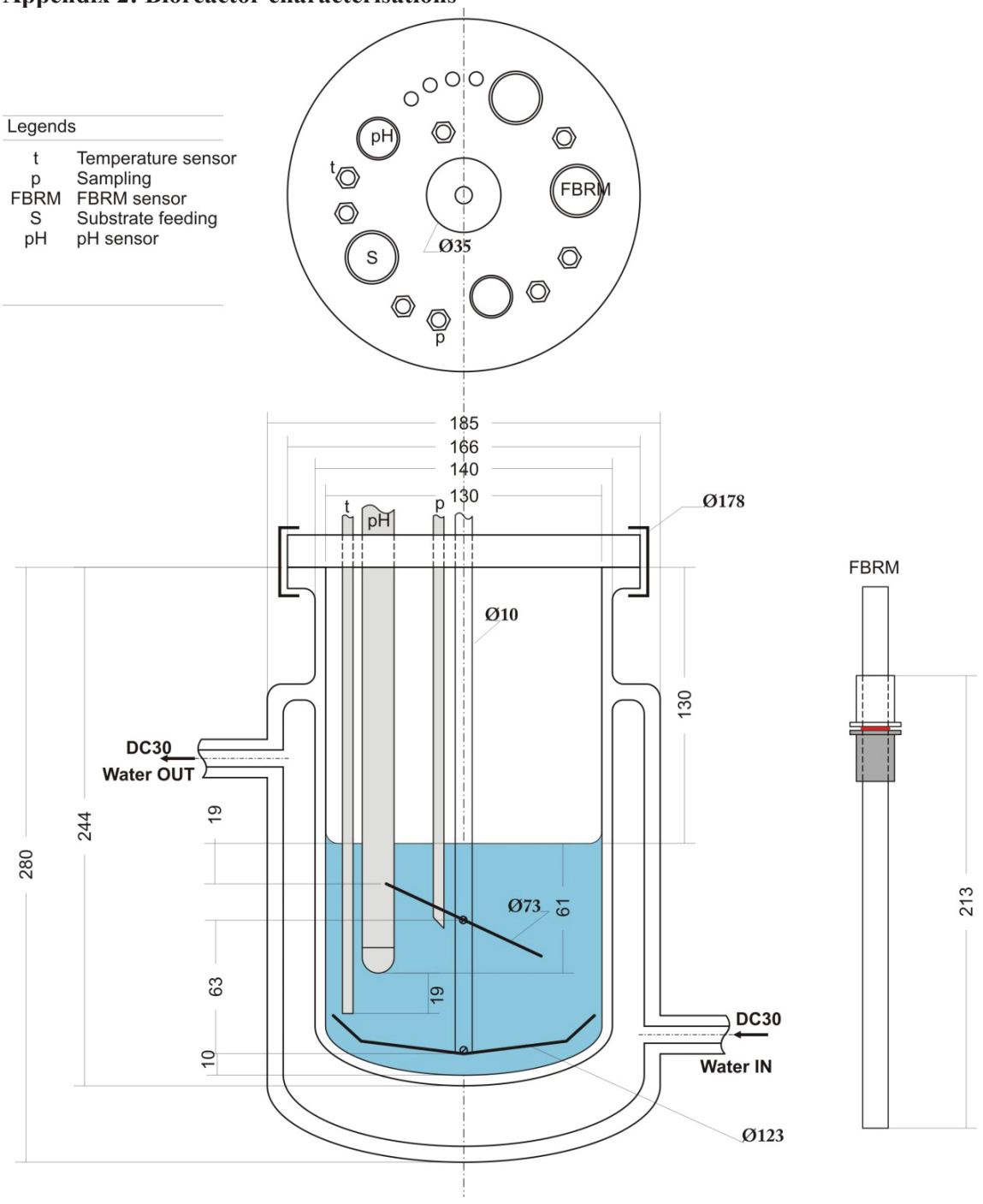

Appendix 3: Agitator characteristics

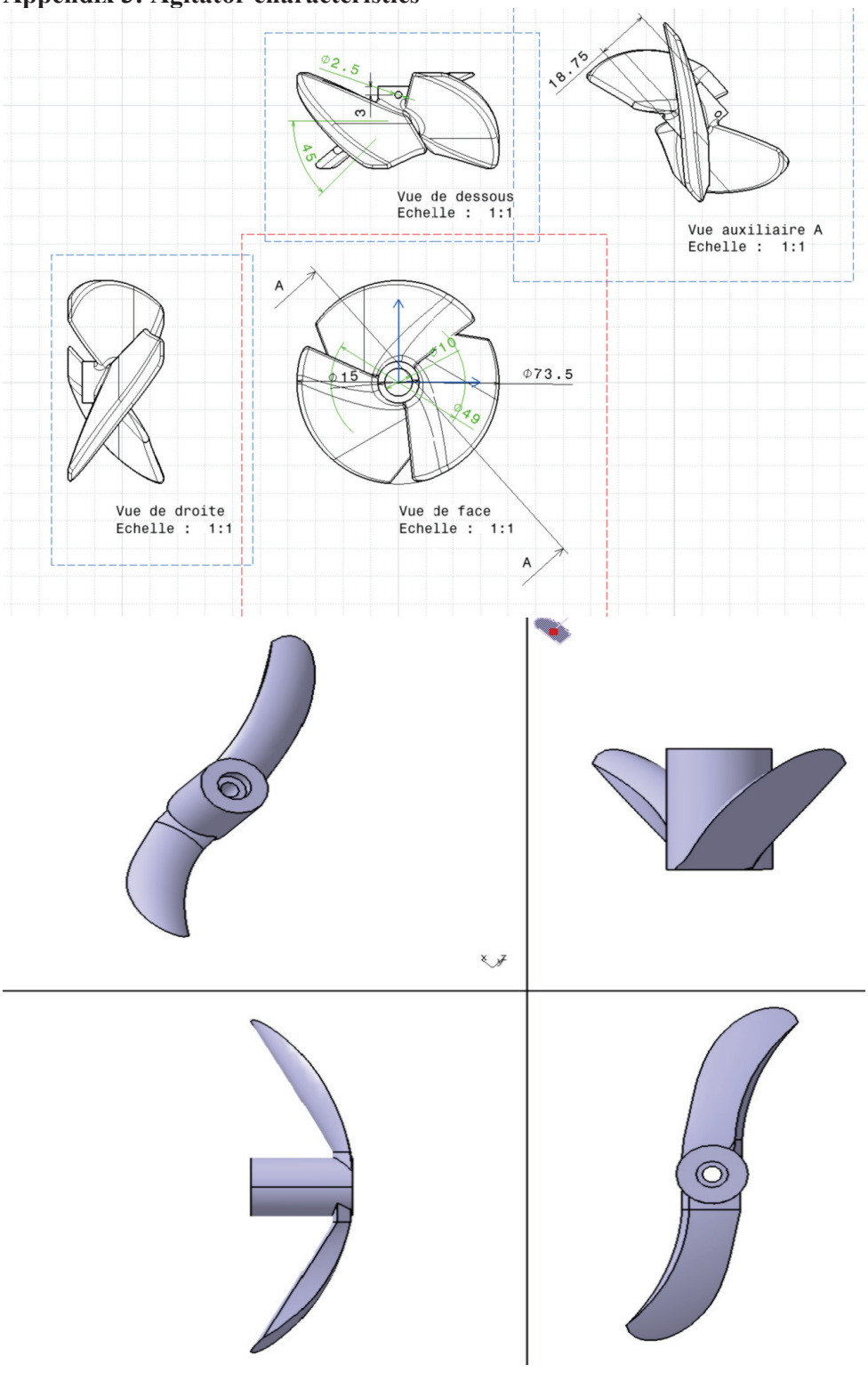

Appendix 4: Accellerase 1500 characteristics

GENENCOR®
A Danisco Division

ACCELLERASE® 1500

Cellulase Enzyme Complex for Lignocellulosic Biomass Hydrolysis

Product Information

DESCRIPTION

ACCELLERASE® 1500 cellulase is an enzyme complex intended specifically for the lignocellulosic biomass processing industries, including renewable fuels and chemicals. Designed as a replacement for ACCELLERASE® 1000, **ACCELLERASE® 1500** is a significant step toward more cost-effective commercial scale production of cellulosic ethanol and will facilitate process development and scale up in this emerging industry. Key features that are expected to be important at commercial scale biorefineries are already built in to this product. Benefits observed with the proprietary enzyme complex and the unique product formulation of **ACCELLERASE® 1500** compared to conventional cellulases include:

- More cost-effective than ACCELLERASE® 1000.
- Enhanced saccharification performance on a variety of feedstocks.
- Ability to operate in simultaneous saccharification and fermentation (SSF) processes, two step sequential hydrolysis and fermentation (SHF) processes, or hybrid saccharification and fermentation (HSF) processes.
- Even higher beta-glucosidase activity than ACCELLERASE® 1000 to minimize residual cellobiose, which may lead to higher rates of saccharification and ultimately to a faster ethanol fermentation. Yields may also be improved.
- Unclarified product. The remaining nutrients from enzyme production are available to the yeast in addition to the fermentable sugars produced by saccharification. This may lead to faster ethanol fermentations, reduce the cost of ethanol fermentation raw materials, and possibly even improve ethanol yields.
- Improved formulation to reduce the risk of inhibition of fermentative organisms, especially at high solids processing. The formulation does not interfere with saccharification carbohydrate profile analysis.

ACCELLERASE® 1500 enzyme complex contains a potent combination of enzymes which effectively modify and digest non-starch carbohydrates, the structural material of lignocellulosic biomass. Lignocellulosic material is composed mainly of cellulose, hemicellulose, and beta-glucans which are associated with each other and also with lignin, pectins, proteins, starch, and lipids. **ACCELLERASE® 1500** is capable of efficiently and synergistically hydrolyzing lignocellulosic biomass into fermentable monosaccharides. **ACCELLERASE® 1500** contains higher levels of beta-glucosidase activity than all other commercial cellulases available today, to ensure almost complete conversion of cellobiose to glucose.

ACCELLERASE® 1500 is produced with a genetically modified strain of *Trichoderma reesei*. The production host is inactivated at the end of the controlled fermentation.

TYPICAL CHARACTERISTICS

ACCELLERASE® 1500 enzyme complex contains multiple enzyme activities; mainly exoglucanase, endoglucanase, hemi-cellulase and beta-glucosidase. The endoglucanase activity is standardized on the basis of its activity on carboxymethylcellulose (CMC). Beta-glucosidase activity is standardized on the basis of activity on pNP-glucoside. The biomass hydrolysis performance of this enzyme complex is a result of the synergistic effect of all the main and accessory activities and cannot be completely evaluated on the basis of the declared activities alone.

Endoglucanase Activity:	2200 - 2800 CMC U/g
Beta-Glucosidase Activity:	525 - 775 pNPG U/g
Appearance:	Brown liquid
pH:	4.6 - 5.0

The activity of **ACCELLERASE® 1500** enzyme complex is expressed in carboxymethycellulose (CMC U) activity units. One CMC U unit of activity liberates 1 µmol of reducing sugars (expressed as glucose equivalents) in one minute under specific assay conditions of 50° C (122° F) and pH 4.8. Beta-glucosidase is reported in pNPG units. One pNPG unit denotes 1 µmol of Nitrophenol liberated from para-nitrophenyl-B-D-glucopyranoside per minute at 50° C (122° F) and pH 4.8. Detailed assay methods are available upon request.

APPLICATION RECOMMENDATIONS

ACCELLERASE® 1500 enzyme complex will hydrolyze the lignocellulosic carbohydrates into fermentable monosaccharides as well as aid materials handling by liquefaction and viscosity reduction. Feedstocks including paper pulp, corn stover and cob, sugarcane bagasse, wheat straw, wood chips, waste paper and many others can all be hydrolyzed using **ACCELLERASE® 1500**. **ACCELLERASE® 1500** can work with a variety of pretreatments including dilute acid, ammonia fiber-expansion (AFEX) and steam expansion. This can be done using simultaneous saccharification and fermentation (SSF), in a two step sequential hydrolysis and fermentation (SHF), or hybrid saccharification and fermentation (HSF) configuration. **Please be aware that the pH and temperature stability optima and limits of the enzyme in use will depend upon the other operating parameters and your process configuration.** Saccharification performance may be enhanced by the addition of other Genencor® enzymes depending on the composition of the pretreated feedstock.

DOSAGE GUIDELINES

The optimum dosage levels of **ACCELLERASE® 1500** enzyme complex will vary considerably with different substrates and their associated pretreatment technologies and conditions. Operating conditions such as pH, temperature and reaction time may also affect enzyme performance. An **ACCELLERASE® 1500** dosage rate of 0.1 - 0.5 mL per gram cellulose or roughly 0.05 to 0.25 mL per gram of biomass (depending on biomass composition) is recommended as a starting point for optimization of enzyme dosage. **ACCELLERASE® 1500** rapidly liquefies and hydrolyzes a variety of substrates within 24 hours, with some additional benefit by extending the time. Small-scale experiments are recommended to determine optimum enzyme

accellerase®
FUELING THE BIOBASED ECONOMY

Together we can fuel the future with biomass.

Appendix 5: Experiment cartography (Example for PP-27-3%-0.5)

		In-situ	Ex-situ	
		FBRM	DLS	MG
MICRO-SCALE	Raw data	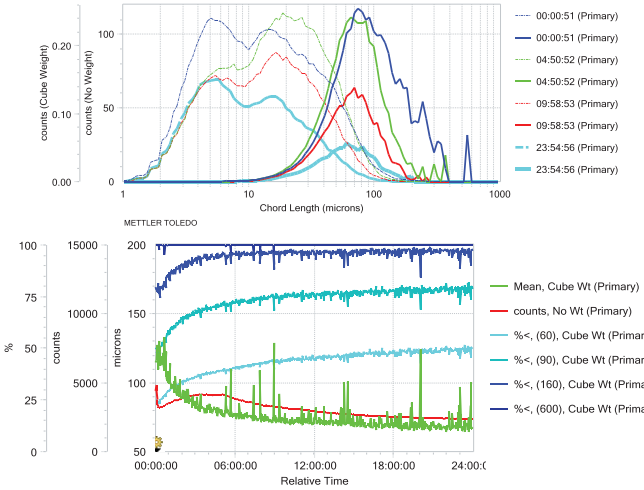	Raw signals of angular detectors	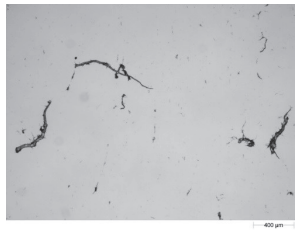
	Results	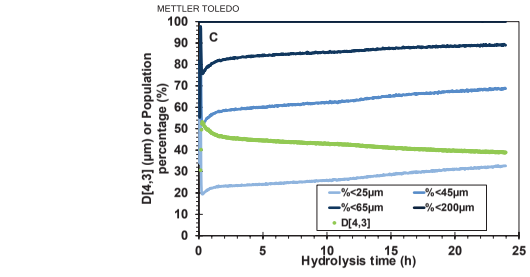	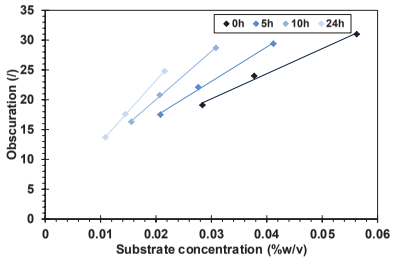 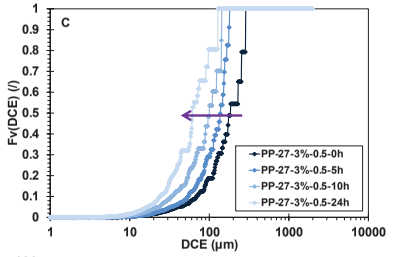 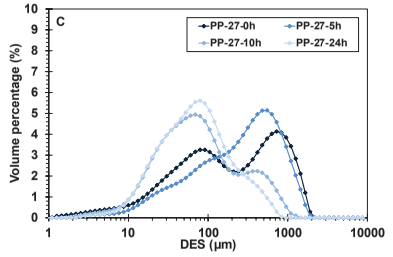 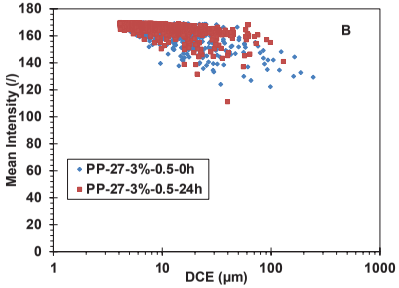	
	Analysis	Impact of hydrolysis, substrate and concentrations		
			YSI	HPLC
MOLECULAR SCALE	Raw data & Results	-	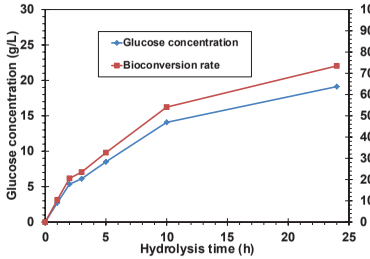	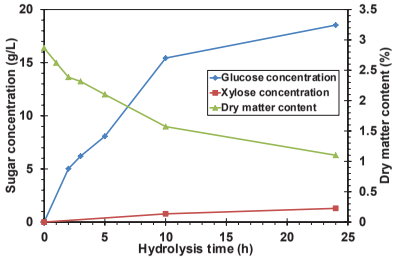
	Analysis		Hydrolysis efficiency discussion; mass balance calculation	

Appendix 6: Viscosity evolution of PP-31 suspensions during hydrolysis

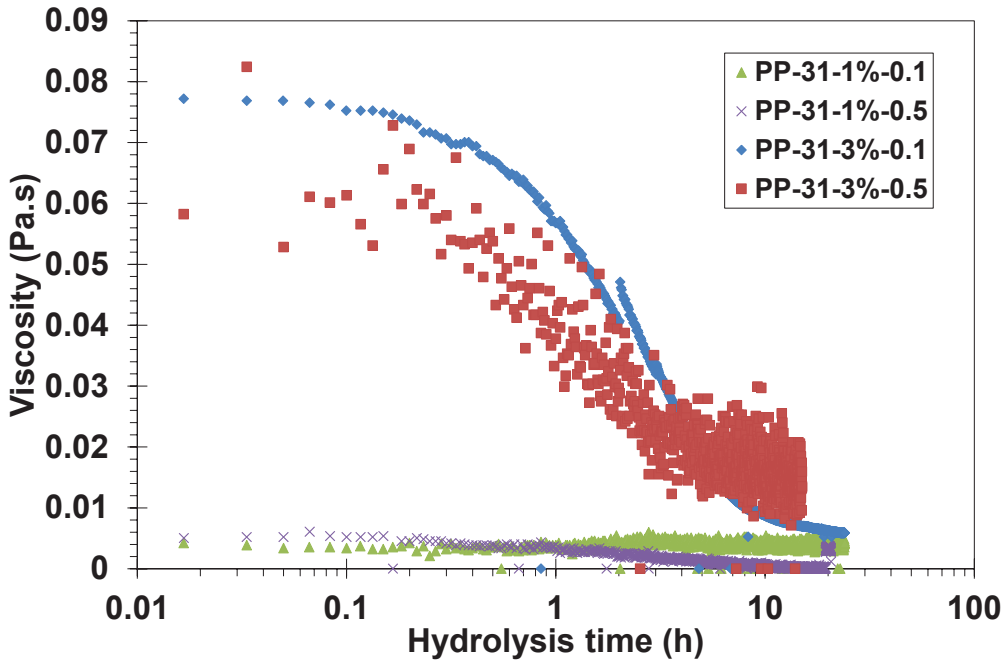

Appendix 7: Water soluble sugar (glucose, xylose and cellobiose) during hydrolysis for MCC (A), WP (B), PP-27 (C), PP-31 (D), BAG (E) at 1%w/v, 0.1 and 0.5mL enzyme/g cellulose; WP-Qc (F) and PP-27-Qc (G)

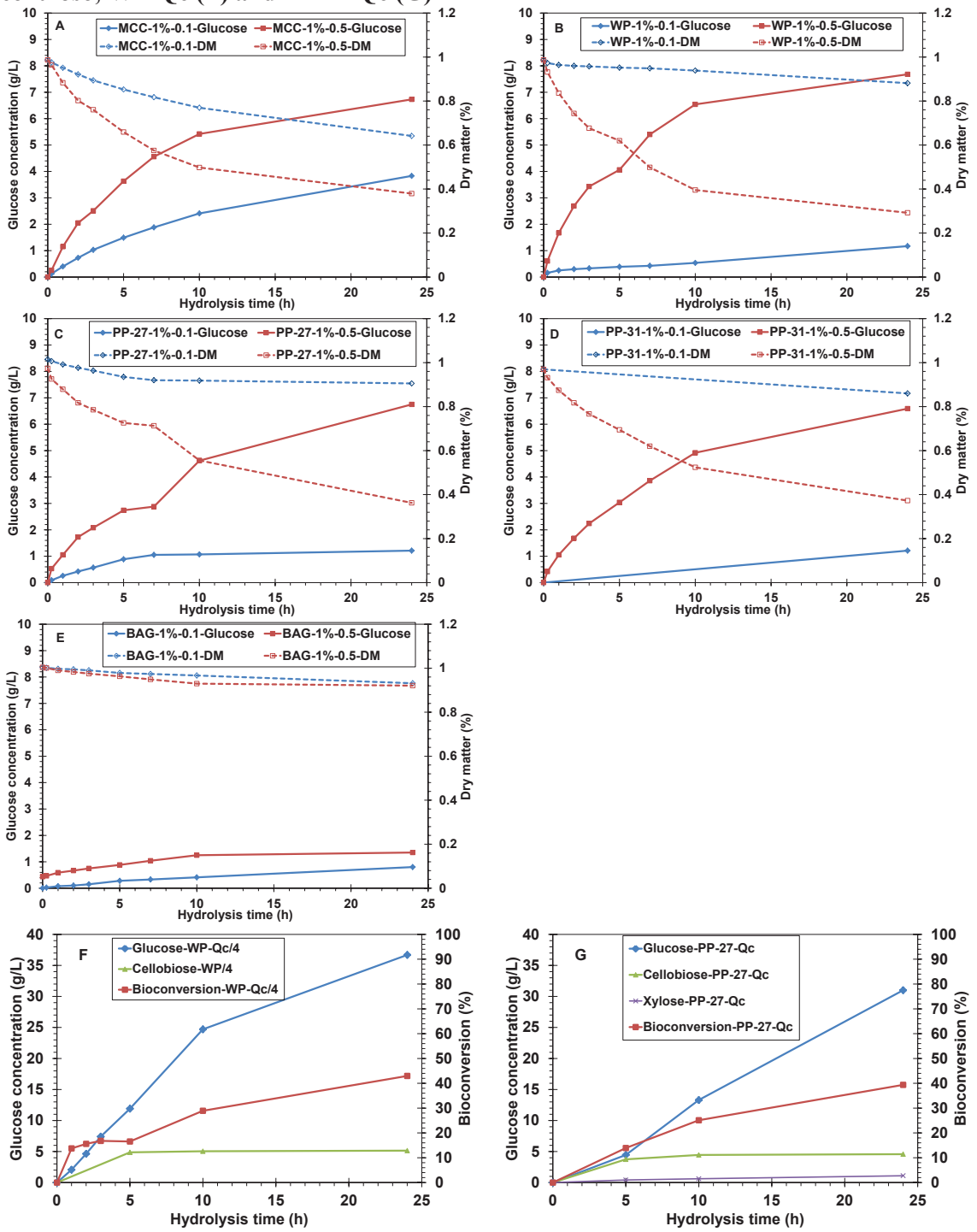

Appendix 8: Modelling of bio-kinetics MCC (A), WP (B), PP-27 (C), PP-31 (D)

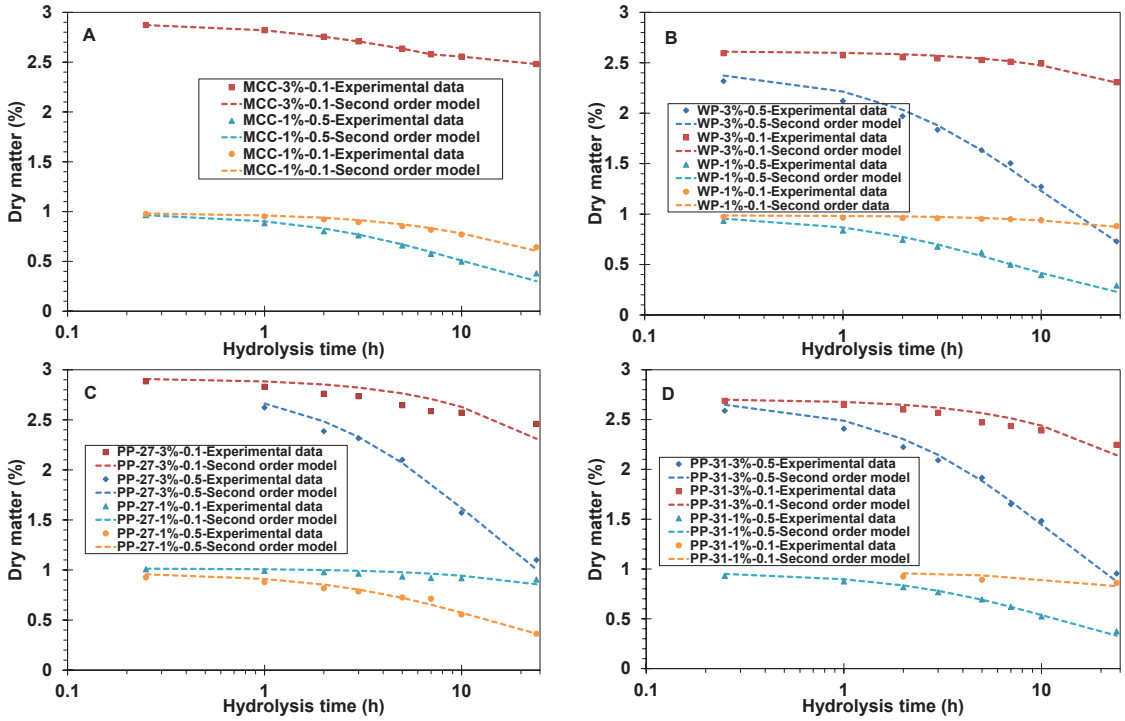

RESUME ETENDU

Titre : Métrologies physiques multi-échelles in-situ et ex-situ pour étudier les mécanismes de déstructuration des matrices lignocellulosiques et les cinétiques de libération de carbone cellulosique fermentescible.

Auteur : Tien Cuong NGUYEN
Directeurs de thèse : Luc FILLAUDEAU (CR INRA, LISBP, Toulouse), Kim Anh TO (PR, HUST/SBFT, Hanoï, Viet-Nam)
Ecole doctorale : ED SEVAB : Ingénieries microbienne et enzymatique
Laboratoire de recherche : Laboratoire d'Ingénierie des Systèmes Biologiques et des Procédés (LISBP, CNRS UMR5504, INRA UMR792, INSA)

Résumé
La bioconversion des biomasses lignocellulosiques est actuellement un grand défi pour le développement de technologies de bio-raffinage. Le manque de connaissances des mécanismes de liquéfaction et de saccharification est l'un des principaux facteurs qui pénalisent le développement des procédés de bio-raffinage. Ce travail est centré sur le développement d'analyses physiques et biochimiques in-situ (viscosimétrie, focus beam reflectance measurement) et ex-situ (rhéométrie, granulométrie laser, morpho-granulométrie, sédimentation…) pour améliorer la compréhension des mécanismes de déstructuration des fibres lignocellulosiques et caractériser les cinétiques de libération de carbone fermentescible. Des substrats modèles (cellulose microcristalline, papier Whatman) et industriels (pâte à papier, bagasse de canne à sucre) ont été utilisés avec différentes conditions d'hydrolyse (1% à 30%w/v, 0.1 à 0.5mL enzyme/ g cellulose). Les résultats obtenus ont permis:

- de proposer et de valider les mesures in-situ de la viscosité de la suspension et de la distribution des longueurs de corde des particules, ainsi que sa conversion en distribution de diamètre.
- de montrer l'impact de la nature et de la concentration du substrat et des ratios enzyme/substrat sur les évolutions des paramètres physico-biochimiques lors de l'hydrolyse. Ces effets ont été quantifiés sur les limitations de transfert.
- d'établir un modèle phénoménologique de comportement rhéologique des suspensions initiales.
- de montrer que les cinétiques physico et biochimiques sont du second ordre.
- de montrer que, pour des hydrolyses à haute teneur en matière sèche, on peut réduire considérablement la limitation des transferts liée aux hautes concentrations et contrôler la cinétique de production de glucose par une stratégie d'ajouts cumulés de substrat.

Mots-clés : bio-raffinage, lignocellulose, pâte à papier, déstructuration des fibres, limitation de transfert, rhéométrie, viscosimétrie, morphométrie, granulométrie, taille de particule, ajouts cumulés, glucose, bioconversion.

Ce résumé étendu décrira successivement les informations suivantes :

- Cadre administratif
- Contexte, enjeux scientifiques et présentation des travaux
- Matériels, méthodes et stratégie d'étude
- Résultats et Discussion
- Conclusion & Perspectives

Cadre administratif

Ces recherches reposent sur un partenariat scientifique (Laboratoire d'Ingénierie des Systèmes Biologiques et des Procédés, Institut de Mécanique des Fluides de Toulouse, Laboratoire de Chimie des Polymères Organiques) et technologique (Unité de service Toulouse White Biotechnologies, Fédération de Recherche FERMAT) inter-régional (Midi-Pyrénées et Aquitaine) associant 2 instituts nationaux de recherche (INRA, CNRS) et, en collaboration avec deux structures internationales (Université de Warterloo - CAN et Institut polytechnique de Hanoï -VN). Ce doctorat bénéficie d'un financement par l'ambassade de France au Vietnam dans le cadre du programme « bourses d'excellence ». Au sein du LISBP, ce doctorat s'intègre dans le projet ProBio3 (ANR Investissement d'Avenir) portant sur la « Production biocatalytique de bioproduits lipidiques à partir de matières premières renouvelables et coproduits industriels : application bio-kérosène ». Il constitue l'action principale de la sous-tache 1.2: « Etude des interactions biocatalyseurs-matrices et identification des phénomènes limitant avec le matériel lignocellulosique sous condition de haute teneur en matière sèche (HTMS) ». Il s'affiche dans la continuité des programmes de recherche précédents étudiant (i) la valorisation et la diversification des produits de l'industrie papetière, y compris les contraintes énergétiques et environnementales ainsi que les critères économiques et sociaux et (ii) la diversification des substrats et l'obtention de carbone cellulosique fermentescible pour le contrôle des cultures microbiennes appliquées aux biotechnologies blanches (programmes ANR-05-BIOE-007 et BIP ADEME - Prepilpat impliquant LCPO (ex-USBB), LISBP et Tembec SAS, Futurol OSEO).

Contexte, enjeux scientifiques et présentation des travaux

Dans un contexte de changement climatique, d'aide à l'indépendance énergétique et de réduction des ressources fossiles, les biocarburants de 2ème génération basés sur la bioconversion de la biomasse cellulosique offrent le plus grand potentiel de réduction de coût et permettent d'envisager une production à grande échelle et à long terme. Les ressources lignocellulosiques doivent subir des traitements physico-chimiques et enzymatiques pour libérer les substrats fermentescibles en concentrations compatibles avec une transposition industrielle réaliste. L'étude de cette liquéfaction du substrat nécessite la caractérisation physique, chimique et biochimique des matrices complexes et la caractérisation de leur potentiel fermentaire avec des questions scientifiques et technologiques relevant du génie des bioprocédés.

La biomasse lignocellulosique représente une des ressources renouvelables les plus abondantes et certainement une des moins coûteuses. Sa conversation en éthanol carburant pourrait subvenir à une partie significative des besoins énergétiques. Les premières méthodes d'hydrolyses utilisées étaient initialement chimiques mais à l'heure actuelle, elles sont moins compétitives à cause du coût élevé des réactifs et de la formation de sous-produits ainsi que de composés inhibiteurs. Ces méthodes sont maintenant concurrencées par les méthodes enzymatiques qui permettent grâce à des activités plus spécifiques d'atteindre de meilleurs rendements d'hydrolyse dans des conditions moins sévères (Ogier et al., 1999). Un procédé enzymatique peut être divisé en quatre étapes principales : (1) le prétraitement: à cause de la nature rigide des lignocelluloses natives, des traitements physiques/chimiques sont nécessaires pour obtenir un matériel convertible; (2) l'hydrolyse enzymatique: dégradation de la cellulose et l'hémicellulose en sucres monomères par action d'enzymes; (3) la fermentation: conversion des sucres monomères en éthanol notamment par les levures et enfin (4) la distillation: étape de récupération de l'éthanol (Bommarius et al., 2008; Zhang et al., 2009). Les substrats utilisés sont variés et concernent à la fois le bois (bois durs et bois tendres), les sous-produits de l'agriculture (paille) ou les déchets lignocellulosiques des industries agro-alimentaires et/ou des papèteries.

Afin d'atteindre une viabilité économique, le bio-raffinage des ressources lignocellulosiques doit être opéré à une haute teneur en matière première. Néanmoins, la liquéfaction et la saccharification enzymatique de toutes les matrices lignocellulosiques complexes sont soumises aux mêmes contraintes et nécessitent notamment un prétraitement pour lequel des méthodes alternatives peuvent être envisagées : explosion à la vapeur ou hydrolyse par acide dilué par exemple. Par conséquent, une meilleure connaissance scientifique ainsi qu'une maîtrise des techniques de ces réactions biocatalytiques, qui impliquent des matrices complexes à haute teneur en solide, constitue actuellement un défi majeur qui doit être relevé afin de faciliter l'intensification des opérations de bio-raffinage.

Parmi les principaux verrous, les phénomènes et les propriétés physiques régissant les transferts, comme le comportement rhéologique des suspensions, la morpho-granulométrie des particules et les mécanismes de déstructuration des fibres, apparaissent comme des facteurs déterminant de l'efficacité du processus. Les propriétés rhéologiques du matériel prétraité aura ainsi un impact important sur l'équipement et sur les stratégies à utiliser (Wiman et al., 2010). En outre, les transferts de chaleur et/ou de matière, ainsi que la réduction de taille des particules/agglomérats, sont des phénomènes favorisés par l'agitation et le mélange qui initient et favorisent la réaction biochimique. La nature du système d'agitation influence la bioconversion de la cellulose en sucres simples (Um, 2007). Cela exige une connaissance détaillée du comportement rhéologique des suspensions de substrat. Toutefois, ces suspensions présentent des propriétés complexes et variées et il n'existe pas de méthodes standards pour décrire la déformation du réseau de fibres et le comportement à l'écoulement des pâtes à papiers (Blanco et al., 2006).

L'écoulement de suspensions de fibres est un facteur clé et des études approfondies sont reportées dans la littérature scientifique liée à l'industrie des pâtes et papier. Des fibres cellulosiques en suspension forment un réseau tridimensionnel qui présente des propriétés viscoélastiques et viscoplastiques. La mesure des propriétés rhéologiques des suspensions de fibres est complexe, et dépend de multiples facteurs: (i) les propriétés physiques et mécaniques de fibres et les gammes de concentration, (ii) les contacts entre fibres et les forces de surface, et (iii) les forces sur les fibres et la floculation. Le comportement rhéologique des suspensions de fibres est généralement décrit par une contrainte seuil et un comportement rhéofluidifiant (modèles de Bingham et de Hershel-Buckley)et son élasticité. Il existe de nombreuses études rhéologiques à différentes températures et concentrations, de solutions diluées de 0,2 à 3,0% (Ferreira et al., 2003) à des solutions concentrées 10 - 20% (Um, 2007; Zhang et al., 2009). Chacune de ces études conclue à un comportement rhéo-fluidifiant pour les suspensions de substrats lignocellulosiques: cellulose microcristalline (Um et al., 2008) pâte à papier de bois dur (Blanco et al., 2006); pâte à papier de bois résineux (Wiman et al., 2010); bagasse de canne à sucre (Pereira et al., 2011). La viscosité de la suspension dépend non seulement de la température et de la concentration (Ferreira et al., 2003) mais aussi de la longueur moyenne des fibres (Lapierre et al., 2006).Une fibre longue a un plus haut degré de polymérisation et génère une plus grande viscosité. Au cours de l'hydrolyse biologique, les fibres lignocellulosiques sont déstructurées ce qui conduit à une diminution du degré de polymérisation. La viscosité apparente des suspensions diminue (Pereira et al., 2011; Um, 2007) parallèlement à une diminution de la taille des particules (Wiman et al., 2010).

Traditionnellement, ce sont les viscosimètres rotatifs qui sont utilisés (Bennington et al., 1990). Toutefois, comme mentionné, les viscosimètres commerciaux standards ne génèrent pas un mélange suffisant pour maintenir une distribution homogène des fibres, ce qui peut fausser de façon drastique les valeurs de viscosité mesurées .Par conséquent, il n'existe pas de méthode standard pour étudier les propriétés rhéologiques des suspensions de fibres. Plusieurs appareils de mesure sont décrits dans la littérature (Derakhshandeh et al., 2011; Pereira et al., 2011); les systèmes basés sur le couple présentent la meilleure résolution et

permettent de conserver une homogénéité macroscopique de la suspension. Ils sont, à ce titre, utilisés pour déterminer le comportement rhéologique de suspensions fibreuses. Une difficulté réside dans la définition de critère pour définir la viscosité apparente de suspensions hétérogènes, qui est initialement définies pour des fluides homogènes dans un régime d'écoulement laminaire. Pour atteindre la fluidisation, la contrainte seuil apparente doit être dépassée dans toute la suspension. Bien que la fluidisation généralement se produise en régime turbulent, un comportement de type « fluide » pour un floc peut être atteint sous des conditions d'écoulement non turbulentes. Un exemple est l'écoulement induit dans un système rotatif à faible vitesse d'agitation juste au-dessus de la contrainte seuil apparente ; un autre exemple est trouvé dans les lits fluidisés (Derakhshandeh et al., 2011).

Plus précisément, les ressources lignocellulosiques à haute teneur initiale en matière sèche doivent subir des traitements physico-chimiques et enzymatiques pour libérer les substrats fermentescibles en concentration compatible avec une transposition industrielle réaliste. Au cours de ces traitements, la matrice solide complexe évolue d'une structure solide fibreuse mise en suspension, vers une dégradation (fragmentation sous l'action de biocatalyseur enzymatique et microbien) jusqu'à une solubilisation (liquide). La dynamique de ces mécanismes, où interviennent des transferts couplés de matière, chaleur et quantité de mouvement, est liée à la diffusion (dans les phases solide ou liquide), à la convection (dispersion mécanique, agitation mélange et pompage) et à la libération d'inhibiteur (gradient de concentration). L'étude de cette liquéfaction du substrat nécessite la caractérisation physique, chimique et biochimique d'une matrice complexe et la caractérisation de son potentiel fermentaire avec des questions scientifiques et technologiques relevant du génie des bioprocédés. Cette thèse est ainsi centrée sur **le développement d'analyses physiques et biochimiques *in-situ* (viscosimétrie, réflectométrie) et *ex-situ* (rhéometrie, diffraction multiple de la lumière, morpho-granulométrie, cinétique de sédimentation, analyses biochimiques) pour améliorer la compréhension des mécanismes de déstructuration des fibres lignocellulosiques et caractériser les cinétiques de libération de carbone cellulosique fermentescible.**

L'originalité de cette approche se trouve dans:

- les matrices utilisées, qui répondent à un besoin économique et technologique de la filière des pâtes et papiers,
- les concentrations investiguées, qui recouvrent du régime dilué au concentré,
- la métrologie multi-échelle *in* et *ex-situ* mise en place, qui reposent sur des techniques d'analyse innovantes et de pointe et implique une approche pluridisciplinaire (sciences pour l'ingénieur, sciences du vivant et biochimique…).

Tableau 1: Les enjeux scientifiques.

Objectifs généraux	- Améliorer la déstructuration des matrices lignocellulosiques en produisant la haute teneur en sucres fermentescibles. - Alléger des difficultés scientifiques pour le développement des nouveaux bioprocédés intensifiés.
Défit critique	- Relier le développement des descriptions phénoménologiques de bioprocédé dans les conditions industrielles.
Approches	- Etat de lieu de technologies analytiques couplées aux développements méthodologiques importants et à l'approche multidisciplinaire. - Impliquer les expertises en génie des procédés, en génie biologique, en mécanique des fluides, en analyse chimique et biochimique

Matériels, méthodes et stratégie d'étude

Des travaux exploratoires (MSc Maud BABAU, Cédric BINET, Arthur NOUHEN) et une analyse bibliographique de l'état de l'art ont permis de concevoir, dimensionner et instrumenter un dispositif expérimental spécifique et dédié à nos questionnements scientifiques. Il comprend un bioréacteur (V=2L) double enveloppe multi-instrumenté (température, pH, vitesse d'agitation, couple, distribution de cordes) équipé d'un mobile d'agitation singulier assurant un mélange axial et radial, empêchant la décantation (Figure 5-1) et permettant un échantillonnage du moût.

Cinq matrices lignocellulosiques (académiques et industrielles) ont été sélectionnées et étudiées car elles présentent des morphologies de fibres, des compositions/structures biochimiques et des tailles de particules différentes: MCC: cellulose microcristalline ; WP: papier Whatman séché et broyé ; PP-27: pâte à papier extrudée (de bois de conifères - bois tendre) ; PP-31: pâte à papier extrudée (feuillus - bois dur) ; BAG: séché broyé bagasse.

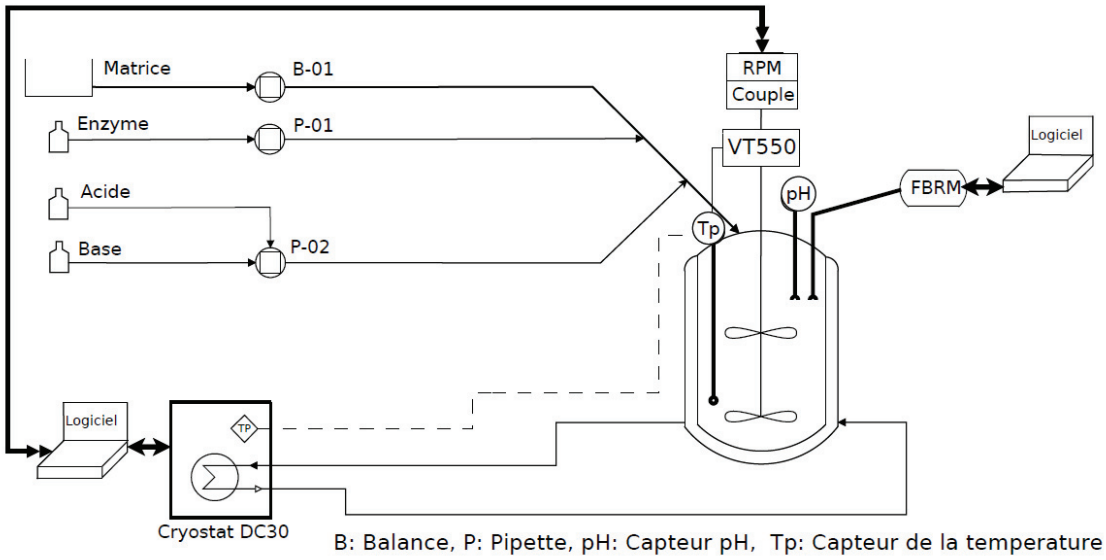

Figure 1: PID de l'outil expérimental.

Tableau 2 : Propriétés physico-chimiques des substrats utilisés.

Matrices	MCC	WP	PP-27	PP-31	BAG
Compositions chimiques					
Cellulose (%)	100	90	82	75	47
Hémicellulose (%)	-	-	8	19	29
Lignine (%)	-	-	2	2	21
Cendre (%)	0.01	0.02	1.50	0.97	1.26
Matière sèche (%)	99	99	28	26	91
Propriétés physiques					
D[4,3] (µm) (DLS)	100±17	363±40	497±77	471±88	230±33
D[4,3] (µm) (Morpho-granulométrie)	105	312	187	222	352
Densité, ρ_{HM} (kg.m^{-3}) at 20°C	1623±28	1200±2	1034±9	1025±8	1100±7
Cristallinité (%)	82.4	90.7	76.8	78.3	57.1

Les substrats modèles, MCC et WP ont été considérés comme des matrices de référence pour l'analyse rhéologique (MCC) et l'hydrolyse (WP). Les substrats industriels (pâtes à papier), PP-27 et PP-31 ont été choisis en raison des prétraitements thermomécaniques et

thermochimiques liés au procédé Kraft, qui conduisent à une matrice prétraitée et délignifiée plus facilement hydrolysable sous condition de haute teneur en matière sèche. Ce point argumente d'une transposition réaliste de ces travaux dans la filière papetière. Le dernier substrat brut, BAG, est sélectionné à la recommandation de notre partenaire EBTA (Hanoi, Vietnam) car il présente la complexité biochimique et structurale la plus élevée. L'influence de cette complexité sur l'efficacité de l'hydrolyse présente un intérêt pour analyser et comprendre l'attaque enzymatique et ses limitations.

Un seul cocktail enzymatique commercial, Accellerase 1500, est utilisé. Son activité cellulosique est rapportée entre 50 et 60FPU.mL^{-1} (Alvira et al., 2011; Govumoni et al., 2013; Pessani, 2011; Wilson, 2013).

Ce travail de thèse s'articule autour d'une approche multi-échelles utilisant différentes mesures *in-situ* et *ex-situ*. La **Figure 2** illustre les blocs correspondant aux trois niveaux d'observation : macro-échelle pour la viscosimétrie et la rhéométrie, micro-échelle pour la granulométrie (DLS, PSD, CLD, d_s) et échelle moléculaire pour les analyses biochimiques (analyse chimique de la fraction soluble et quantification de la fraction insoluble). Le cadre de cette tripode offre de multiples angles d'analyse et de discussion **(Tableau 1)**. Il permet de comparer les analyses *in-situ* et *ex-situ*. Il autorise l'établissement de modèles phénoménologiques (propriétés d'écoulement, granulométrie, cinétique réactionnelle). Enfin, le recoupement des trois niveaux d'observation permet d'embrasser les phénomènes physiques et biochimique pour fournir un aperçu complet des mécanismes impliqués. À cet égard, les modèles phénoménologiques doivent répondre à des critères tels que la fiabilité, la simplicité et l'homogénéité des informations expérimentales.

- pour le rhéométrie : modèle phénoménologique de comportement rhéologique considérant la fraction volumique des substrats, la taille et la forme des particules;
- pour la granulométrie : les fonctions de distribution associées (bilans massique et bilan de population);
- pour la biochimie : modèles cinétiques biochimiques.

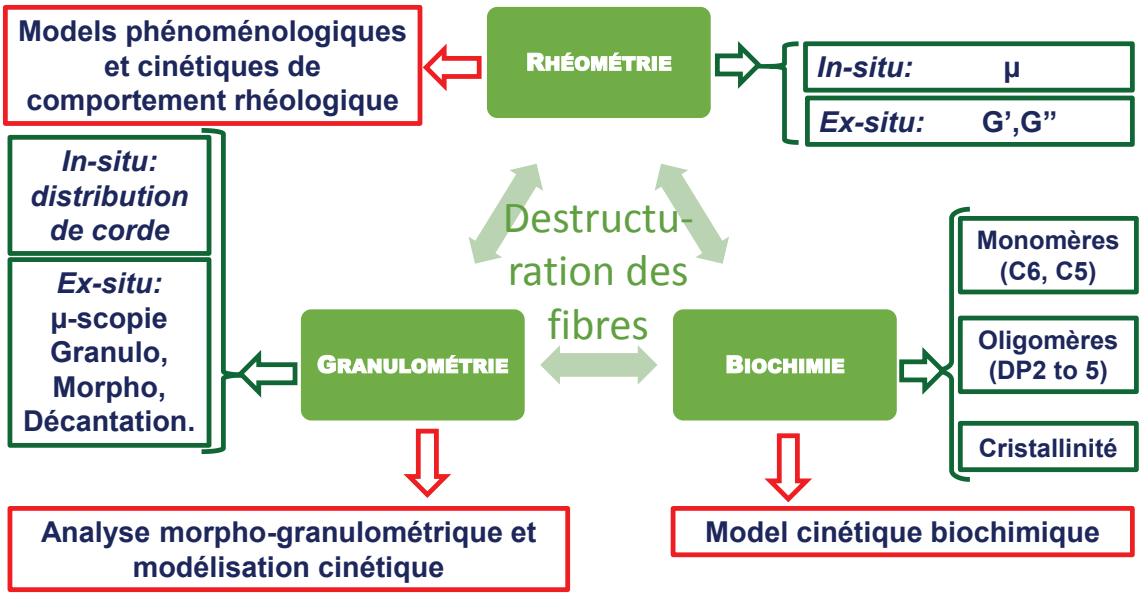

Figure 2: Méthodologie expérimentale et stratégies d'étude.

Tableau 3 : Cartographie de la stratégie expérimentale en relation avec les objectifs industriels et de connaissance.

Echelle	In-situ	Ex-situ	
Macro	Viscosimétrie	Oscillation (G', G'')	⇨ Comportement rhéologique
Micro	Distribution de corde	DLS Morpho-granulométrie Diamètre de chute	⇨ Morphologie et granulométrie
Micro et moléculaire	∅	Matière sèche, Profil de concentration Monomères (C6, C5) Oligomères (DP<6)	⇨ Bilan de matière et analyse biochimique
		↓	
		Intégration des blocs de connaissances pour décrire la dynamique des nouveaux bioprocédés consolidés et intensifiés.	

Une synthèse de ces trois blocs constitue un «bloc de connaissances» pour avancer dans la compréhension de certains verrous scientifiques et conduire à la mise en œuvre de nouveaux bioprocédés. Pour répondre à ces objectifs scientifiques, notre démarche expérimentale est structurée par trois actions principales:

- Mise en suspension et caractérisation rhéologique des suspensions,
- Hydrolyse dans des conditions favorables (1% et 3%dm w/v; 0.1 et 0.5mL enzyme/g cellulose),
- Hydrolyse à haute teneur en matière sèche avec une stratégie basée sur l'ajout cumulé de substrat (concentration finale ≈ 10%dm w/v; 0.5mL enzyme/g cellulose).

Initialement, les cinq matrices sont caractérisées par différentes analyses physico-chimiques: teneur en eau et en cendres, composition biochimique, cristallinité, morpho-granulométrie (distribution de taille), densité, tension de surface, chaleur spécifique, analyse thermogravimétrique, cinétique de décantation et rhéométrie des suspensions. Ensuite, les hydrolyses enzymatiques sont effectuées sur une durée de 24h (période pertinente pour étudier les limitations des transferts physiques et/ou biochimiques) à 40°C (compatible avec des activités microbiennes), pH 4.8 avec le cocktail enzymatique Accellerase 1500 sous une vitesse d'agitation de 100 RPM. Deux stratégies d'hydrolyse sont appliquées : (i) en condition favorable (concentration diluée) et en condition concentrée (stratégie d'ajouts dosés cumulés). La première est réalisée pour deux concentrations de substrat (1 et 3%w/v) et avec deux ratios enzyme/cellulose (0.1 et 0.5mL enzyme/g cellulose correspondant respectivement à 5 et 25 FPU/g cellulose). Ces concentrations en substrat et enzymes assurent des conditions favorables pour l'attaque enzymatique. Avant hydrolyse, les régimes d'écoulement sont laminaires pour WP et PP, et transitoires pour MCC et BAG.

Sur la base des résultats obtenus lors de cette première phase, une seconde stratégie est développée pour atteindre une concentration plus élevée (alimentation dosée et cumulative) avec les matrices PP-27 et WP. Les ajouts des enzymes et du substrat sont réalisées simultanément chaque ½ heure (pour WP) ou chaque heure (pour PP) avec trois débits différents, un seul ratio enzymatique (0.5 ml d'enzyme/g cellulose soit 5 FPU/g cellulose) jusqu'à atteindre une concentration finale de 10%m/m. En complément, une expérience complémentaire où la totalité de l'enzyme est ajoutée à t=0 heure est faite avec la matrice PP-27. La finalité de ces expérimentations est l'augmentation de la concentration en substrat au cours de l'hydrolyse, l'optimisation du temps d'hydrolyse (absence ou réduction de la limitation des transferts) et la réduction des consommations d'énergie. Enfin, un dernier objectif est de valider la transposition des phénomènes modélisés à faible concentration

(couplage des cinétiques et des bilans) et confirmer l'interdépendance entre les trois blocs: rhéologie, morpho-granulométrie et biochimie pour l'hydrolyse à haute teneur en matière sèche.

Résultats et Discussion :

Les objectifs, les défis, la stratégie proposée et la méthodologie utilisée dans ces travaux sont rappelés dans le **Tableau 3**. L'approche pluridisciplinaire et la complexité scientifique de cette problématique est associée à deux degrés de liberté : (i) les matrices (la nature, la structure et les compositions) et (ii) les conditions opératoires d'hydrolyse (ratio enzyme/substrat, haute teneur en matière sèche) associées à la limitation des transferts et l'apparition d'inhibitions.

Les principales contributions de ce travail concernent d'une part les avancées relatives aux matériels & méthodes et, d'autre part, aux résultats obtenus dans chacun de nos trois axes majeurs d'analyse : rhéométrie (échelle macroscopique), morpho-granulométrie (échelle microscopique) et cinétique biochimique (échelle moléculaire). Ces résultats sont présentés en cinq parties : (i) Développements méthodologiques ; (ii) Etude des suspensions initiales ; (iii) Etude des hydrolyses en mode batch ; (iv) Modélisation des cinétiques réactionnelles et (v) Etude des hydrolyses en mode fed-batch.

- **Développements méthodologiques** :

L'un des aspects pouvant être souligné dans les méthodologies mises en œuvre est la caractérisation multi-échelle des phénomènes physiques et biochimiques. A l'échelle macroscopique, traditionnellement, les comportements rhéologiques sont décrits par des mesures ex-situ. Ces dernières sont limitées par le nombre des échantillons prélevés ainsi que par les difficultés inhérentes aux substrats, essentiellement la décantation et la floculation. Pour résoudre ces problèmes, nous avons proposé et validé la mesure *in-situ* de la viscosité d'une suspension en appliquant le concept de Metzner et Otto (Metzner & Otto, 1957). La viscosité de suspensions newtonienne et non-newtonienne est déduite de la courbe de consommation de puissance Np-Re en utilisant la vitesse de rotation et la puissance consommée. Dans le cas de comportement non newtonien, l'approche de Rieger et Novak (Rieger & Novak, 1973) a été appliquée pour déterminer le coefficient Ks traduisant la proportionnalité entre la vitesse de cisaillement équivalente et la vitesse de rotation en régime laminaire et ainsi estimer une viscosité équivalente. Les équations pour calculer la viscosité ainsi que la vitesse de cisaillement sont présentées ci-dessous :

$$Np = \left(\left(\frac{Kp}{\mathrm{Re}_{Ag}} \right)^{q} + N_{p0}^{q} \right)^{1/q} \quad with: Kp = 97.9; N_{p0} = 0.13; q = 0.784 \quad \textit{(Eq. 1)}$$

$$\dot{\gamma} = K_s \cdot N \quad \text{avec Ks} \approx 32$$

où *Np* et *Re* sont respectivement le nombre de puissance et le Reynolds d'agitation et *Kp* une constante du système.

A l'échelle microscopique, et ne ce qui concerne la caractérisation de taille des particules, parallèlement avec l'utilisation des mesures classiques ex-situ (DLS, morpho-granulométrie) nous avons également utilisé et validé la mesure *in-situ* des distributions en nombre des longueurs de corde puis validé une méthode de conversion de distribution en nombre de corde en distribution en nombre et en volume des diamètres de sphère équivalente. Un programme écrit sous Matlab nous permet d'effectuer cette conversion de manière automatique.

Dans ce travail, un nombre important de techniques analytiques a été mis en oeuvre qui ont été associées au traitement et à l'analyse des données brutes obtenues. Le **Tableau 4** présente un récapitulatif des techniques analytiques utilisées avec, pour chacune, les données

brutes, les résultats ainsi que les analyses pouvant effectuées. En particulier, les conversions de (i) la distribution en nombre de l_c, d_{CE}, d_{ES} en distribution en volume ; (ii) du signal transmis et rétrodiffusé en profil de concentration du substrat et (iii) de la vitesse limite de chute en distribution de diamètres de Stokes ont été réalisées avec succès.

Nous avons caractérisé, d'un point de vue thermique, physico-chimique et biochimique, les cinq matrices et établi une classification par rapport à leur potentialité d'hydrolyse sous conditions de haute teneur en matière sèche **(Tableau 5)**. Les pâtes à papier apparaissent comme les matrices les plus adaptées pour la mise en œuvre de l'hydrolyse et sa transposition industrielle.

Tableau 4 : Données brutes, résultats et analyses effectués pour les techniques analytiques mises en œuvre.

	Données brutes	Résultats	Analyses
Rhéométrie in-situ	Viscosimétrie (C, N)	τ vs $\dot{\gamma}$; μ vs $\dot{\gamma}$	Comportements rhéologiques
Rhéométrie ex-situ	Oscillation (C, γ, f)	G' et G" vs $\dot{\gamma}$ et f.	μ, τ_0, comportements rhéologiques
Cinétiques de décantation	T et BS vs h et t	Profil de concentration vs t, h, d_s	d_s, Ev(d_s), bilan de matière, concentration critique de culot.
Mesure in-situ de cordes de particule	En(l_c) vs t	En(l_c), N(l_c), valeurs spécifiques de l_c vs t ; conversion de CLD à PSD: Ev(d_{SE})	Evolution de En(l_c), N(l_c), Ev(d_{SE}); impact de l'hydrolyse, de substrat et de la dose d'enzyme.
DLS	Signal brut en fonction des détecteurs angulaires	Ev(d_{SE}), obscuration vs concentrations des échantillons	Evolution de Ev(d_{SE}); impact de l'hydrolyse, de substrat, de la dose d'enzyme.; évolution des propriétés optiques.
Morpho-granulométrie	Images composées	Identification et caractérisation des particules basées sur le traitement d'image, Ev(d_{CE})	Evolution de Ev(d_{CE}), propriétés morphologiques (intensité, élongation); impact de l'hydrolyse, de substrat, et de concentration d'enzyme
YSI	Concentration de glucose	Taux de bioconversion	Efficacité de l'hydrolyse
HPLC	Concentration des monomères et oligosaccharides	Taux de bioconversion	Efficacité de l'hydrolyse, estimation de teneur en matière sèche
Humidité	Matière sèche vs t	-	Bilan de matière

- **Etude des suspensions initiales**

Dans le procédé de la conversion des matières lignocellulosiques en sucres fermentescibles, la connaissance des comportements rhéologiques des suspensions joue un rôle fondamental dans le design des équipements et des processus. Le comportement rhéologique impacte l'hydrodynamique se développant dans les suspensions et donc également la dynamique des phénomènes de transfert (masse et/ou chaleur). Dans ce travail, il

est caractérisé par trois grandeurs : la viscosité, la viscoélasticité et le seuil d'écoulement. Cinq substrats ont été mis en suspension à différentes concentrations. Les résultats ont montré que le comportement rhéo-fluidifiant apparait pour toutes les suspensions lignocellulosiques. De même, un seuil d'écoulement est trouvé pour les suspensions de PP et de WP quel que soit la concentration, illustrant ainsi un comportement viscoplastique. Le module élastique se trouve toujours plus important que le module visqueux.

Le comportement rhéologique des suspensions étant de type rhéo-fluidifiant, nous partons d'un modèle classique de type loi puissance pour établir un modèle phénoménologique décrivant le comportement rhéologique des suspensions initiales ($\mu = k \cdot \dot{\gamma}^{n-1}; k = f(C_m); n = f(C_m)$). Les relations entre l'indice de consistance k, et l'indice de comportement n avec la concentration de substrat sont traduites respectivement par une relation exponentielle et une relation linéaire. Nous avons, pour WP: $k=0.724e^{0.075Cm}$, $n= -6.10^{-3}Cm + 0.701$; pour PP : $k= 0.017e^{0.175Cm}$, $n= -9.10^{-3}Cm + 0.555$. Ce modèle nous aide à prédire la viscosité d'une suspension de concentration donnée dans la gamme de travail.

Les résultats de la mise en suspension nous amènent à déterminer une concentration critique (ou technique), C* indiquant le passage du régime dilué/semi-dilué au régime concentré pour toutes les matrices. Ses valeurs sont respectivement >396 ; 35 ; 29 ; >200g $ms.L^{-1}$ pour MCC, WP, PP (27 et 31) et BAG. Ces concentrations techniques indiquent qu'au-delà de ces valeurs, la viscosité ou les propriétés rhéologiques en général deviennent un facteur limitant.

Tableau 5 : Classification des matrices cellulosiques en fonction des critères physiques, thermiques et biochimiques en relation avec les procédés d'hydrolyse (rouge: défavorable, vert: favorable).

Propriétés			MCC	WP	PP-27	PP-31	BAG
Réalisabilité industrielles							
Propriétés physiques	Densité intrinsèque						
	Cristallinité						
	Diamètre	Surface spécifique					
		Suspension					
	Forme	Surface spécifique					
		Suspension					
	Energie surfacique						
Propriétés thermiques	Chaleur spécifique						
	Thermogravimétrie						
Propriétés biochimiques	Compositions						
	Humidité						

- **Etude des hydrolyses en mode batch**

Comme présenté dans la partie Matériels et Méthodes, nous avons réalisé dans un premier temps les hydrolyses en mode batch pour tous les substrats avec des concentrations allant de diluée (1-3%) à concentrée (≥10%) sous 2 doses enzymatiques (5-6 FPU/g cellulose et 25-30 FPU/g cellulose).

D'un point de vue macroscopique, le comportement rhéo-fluidifiant est conservé durant l'attaque enzymatique mais apparait de moins en moins prononcé. Le seuil d'écoulement diminue au cours de l'hydrolyse avant de disparaitre au-delà de 10 heures d'hydrolyse dans nos conditions (**Figure 3-B**). Les mesures in et ex-situ présentent le même ordre de grandeur

pour la viscosité de ces suspensions. En lien avec les limitations des transferts, la viscosité des suspensions et le diamètre moyen des particules diminuent régulièrement avec l'avancement de l'hydrolyse et atteignent des valeurs quasi-stationnaires au-delà de 10 heures. Cependant, la cinétique associée dépend intrinsèquement du ratio enzyme/substrat utilisée.

D'un point de vue microscopique, nous avons montré la réduction de la taille de particule (sauf pour BAG) quelles que soient la matrice et les conditions opératoires : la disparition des grosses particules est synchrone avec l'augmentation de la proportion des fines (**Figure 4**). Les résultats des analyses morpho-granulométriques démontrent la cohérence entre les différentes techniques *in et ex-situ* (**Table 6**). Toutes les techniques de mesure montrent la même tendance pour l'évolution de taille des particules. Le diamètre moyen réduit est réduit dans un facteur 2-3 après 24h d'attaque enzymatique. Cependant, les valeurs absolues obtenues présentent un grand écart selon les techniques utilisées. Il baisse de DLS à morpho-granulométrie à FBRM. Cette hétérogénéité peut être liée au principe de mesure, à la quantité mesurée et à la base théorique utilisée pour traiter les données. Les évolutions de taille des particules peuvent être corrélées avec les changements de viscosité pendant l'hydrolyse.

Comme cela a été rapporté dans la littérature, nous retrouvons nettement l'impact de la nature et de la concentration en substrat et des ratios enzyme/substrat sur les évolutions des paramètres physiques et biochimiques lors de l'hydrolyse (**Figure 3-A, 3-B ; Figure 4 ; Tableau 6**).

Pendant l'hydrolyse, la matière solide est dégradée en donnant les matières hydrosolubles. Les propriétés d'écoulement sont les résultats de la concentration de substrat, de la structure des fibres et de la taille des particules. Les relations entre ces variables sont complexes et difficiles à décrire. Dans le cadre de ce travail, nous nous sommes attachés à quantifier les contributions relatives (i) de la solubilisation des matières sèches et (ii) de la modification morphologique des fibres lignocellulosiques (**Figure 3-C**) sur l'évolution de la viscosité des suspensions. En général, le poids de ces contributions varie pendant l'hydrolyse. L'effet de la solubilisation des matières sèches devient de plus en plus important par rapport à la modification morphologique des fibres.

Soulignant encore une fois la complexité des matrices lignocellulosiques, nos observations microscopiques indiquent une hétérogénéité des vitesses de décantation liée à la nature des substrats et aussi à la dose des enzymes utilisées. Après 24 heures d'hydrolyse enzymatique la vitesse de décantation des particules de substrat a lieu plus rapidement pour les substrats MCC, BAG et WP. Comparativement aux particules non hydrolysées, la vitesse de décantation des particules de PP semble peu impactée avec une dose de cellulase faible alors qu'elle est augmentée avec une dose d'enzyme 5 fois plus importante. Dans ce dernier cas, une explication possible serait que les particules plus petites générées par l'action enzymatique sont plus compactes.

D'un point de vue moléculaire, nous avons confirmé des résultats connus et rapportés dans la littérature en soulignant, par exemple, l'impact de la concentration enzymatique sur l'efficacité de l'hydrolyse. Le taux de bioconversion (équivalent glucose) est proportionnel aux ratios enzymes/substrats (sauf BAG). Ce taux de bioconversion atteint environ 80% pour la concentration diluée (1-3%w/v ; 25FPU/g cellulose) pour WP et PP. En revanche et de façon prévisible, les rendements sont beaucoup moins importants pour la cellulose microcristalline (14 à 62% selon la dose de cellulase et la charge en substrat) et la bagasse (10 à 15% selon la dose de cellulase et la charge en substrat). En cohérence avec les activités présentes dans le cocktail, aucune accumulation significative des intermédiaires de dégradation (DP≥2) n'est observée durant les 24 heures d'hydrolyse.

L'indice de cristallinité de la biomasse est supposé correspondre à la conversion enzymatique de biomasse en glucose. Cependant, il y a toujours des recherches contradictoires concernant le rôle de cet indice dans l'efficacité de l'hydrolyse ainsi que son

évolution lors de l'hydrolyse. Dans notre cas, nous avons montré que l'impact de l'attaque enzymatique sur l'évolution de la cristallinité des substrats n'exhibe pas de tendance claire et unique.

- **Modélisation des cinétiques réactionnelles**

Afin d'explorer l'évolution de la viscosité lors de l'hydrolyse enzymatique et de comparer les cinétiques entre les différentes conditions expérimentales et les différents substrats, la viscosité et le temps d'hydrolyse sont adimensionalisés. Nous avons obtenu une courbe unique traduisant la relation entre la viscosité adimensionnelle, $\mu^* = \frac{\mu_0 - \mu_t}{\mu_0 - \mu_\infty}$ et le temps d'hydrolyse adimensionnel, $t^* = \frac{t}{t(\mu^* = 0.1)}$ pour WP et PP quelles que soient les conditions opératoires (**Figure 3-D**). Ces résultats signifient que pendant la période de réduction de 90% de la viscosité initiale, un mécanisme similaire de dégradation pourrait être supposé pour chaque substrat.

Nous avons proposé un modèle cinétique au même l'ordre (deuxième ordre) pour toutes les cinétiques macroscopiques (viscosité), microscopiques (diamètre de particule) et moléculaires (glucose produit et substrat consommé). Ce modèle est applicable en fonction de la fraction potentiellement hydrolysable : pour la bio-cinétique : $S = \frac{S_0}{S_0 \cdot k_{bio} \cdot t + 1}$; pour la granulo-cinétique : $D[4,3] = \frac{D[4,3]_0 - D[4,3]_\infty}{(D[4,3]_0 - D[4,3]_\infty) \cdot k_{granulo} \cdot t + 1} + D[4,3]_\infty$ et pour la visco-cinétique : $\mu = \frac{\mu_0}{\mu_0 \cdot k_{visco} \cdot t + 1}$. Par conséquent, la capacité d'interprétation des variables physiques et biochimiques ainsi que des taux de bioconversions est réalisable et à affiner plus profondément.

- **Etude des hydrolyses en mode fed-batch**

Afin d'avoir les résultats en mode batch et de rester dans l'objectif de maîtriser la limitation des transferts à travers l'évolution de la viscosité en fonction de la cinétique de libération de glucose et aussi d'apprécier la cohérence des modèles établis dans des conditions diluées appliqués dans un mode fed-batch, une stratégie d'ajouts cumulés (enzyme et substrat) avec quantité et temps d'hydrolyse définis est réalisée.

Le temps critique t(μ*=0.1) qui correspond à une réduction de 90% de la viscosité initiale, est utilisé pour définir un débit critique (ou de référence) pour l'ajout de substrat, Qs. Ce paramètre opérationnel est calculé par le ratio C*/t(μ*=0.1) (avec la concentration critique C* présentée dans la partie de l'étude des suspensions initiales). Les expérimentations en mode fed-batch montrent une évolution du comportement rhéologique analogue aux essais conduits en mode discontinu, à savoir une chute de viscosité du milieu consécutive à l'hydrolyse enzymatique. L'évolution de taille des particules est en accord avec celle d mode batch et reste indépendante du débit de substrat utilisé. Les expérimentations réalisées avec des débits d'alimentation de 0.5x, 1x et 1.5x le débit critique Qs montrent la pertinence et l'importance de ce débit critique d'alimentation pour contrôler le comportement rhéologique des suspensions lignocellulosiques (**Figure 3-D-E**) et donc la viscosité apparente du moût.

Pour ces hydrolyses à haute teneur en matière sèche, nous avons donc montré que nous pouvons réduire considérablement la limitation des transferts liée aux hautes concentrations et contrôler la cinétique de production de glucose par une stratégie d'ajouts dosés cumulés de substrat.

Dans nos conditions aucune limitation de transfert n'est observable à partir des cinétiques de production du glucose. Le rendement final est identique (environ 40%) pour tous les débits d'ajout de substrats. Comme escompté, l'ajout initial total d'enzyme initial favorise la biocatalyse en réduisant la viscosité des suspensions et en augmentant le taux de bioconversion de la biomasse en glucose (environ 8% d'amélioration du rendement).

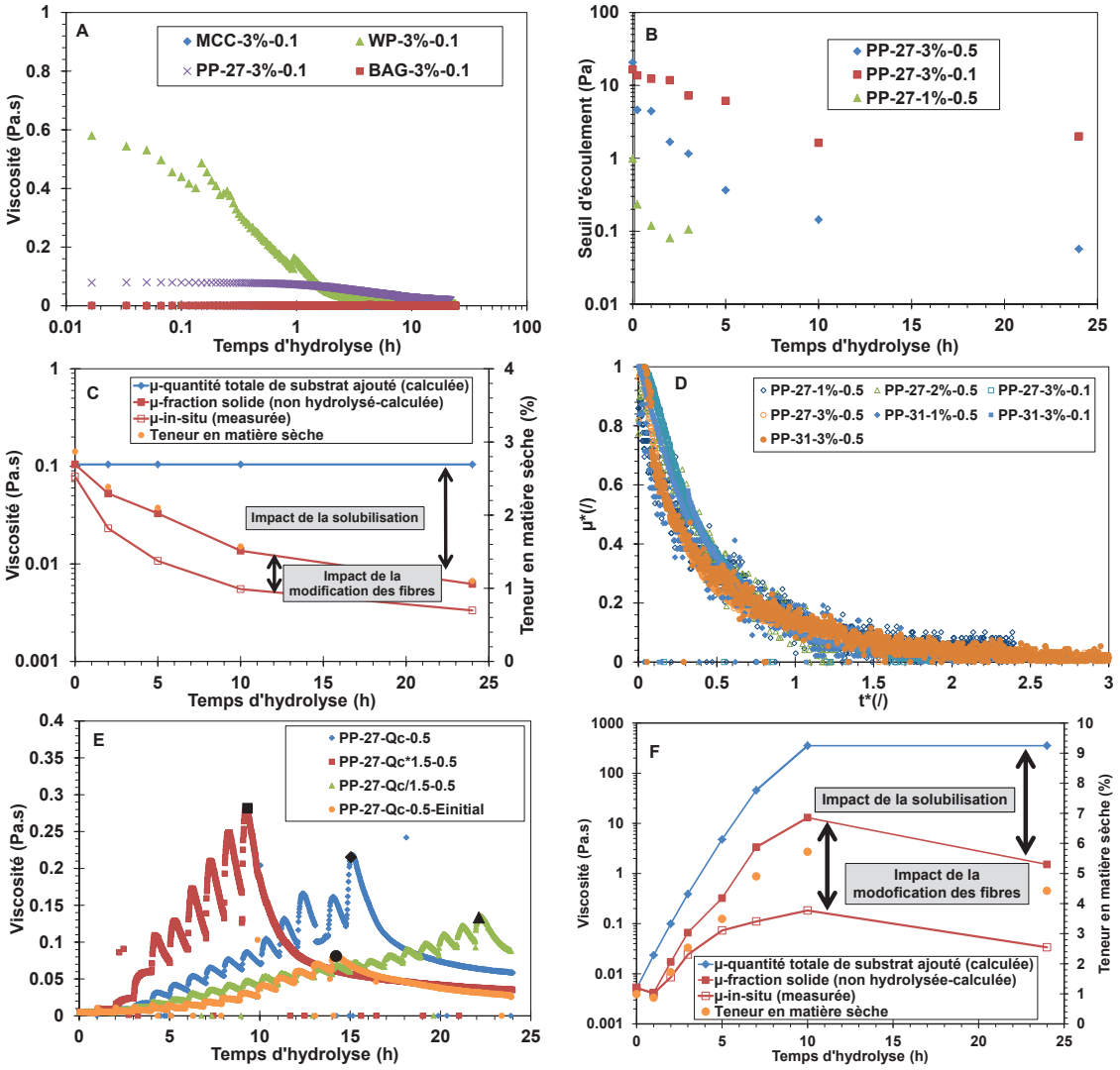

Figure 3: A- Impact de la nature des substrats sur l'évolution de la viscosité (MCC, WP, PP et BAG à 3%w/v ; 0.5mL enzyme/g cellulose) ; B- Evolution du seuil d'écoulement pour PP-27 (1 et 3%w/v ; 0.1 et 0.5 mL enzyme/g cellulose) ; C- Impact de l'hydrolyse sur la viscosité de la suspension – Mise en évidence des contribution des phénomènes de solubilisation et de déstructuration/fractionnement (PP-27-3%w/v, 0.5mL enzyme/g cellulose) ; D- Unicité de la courbe liant la viscosité et le temps d'hydrolyse adimensionnalisés pour PP ; E- Evolution de la viscosité des suspensions au cours de l'attaque enzymatique suivant une stratégie d'ajouts dosés cumulés (mode semi-continu aux différents débits équivalents : Qc/1.5 ; Qc ; Qc*1.5 avec Qc=8.67gms/h) ; F- Contributions relatives de la solubilisation des matières sèches et de la modification morphologique des fibres sur la viscosité de suspension lors d'une stratégie d'ajouts dosés cumulés (mode semi-continu, PP-27-Qc-0.5mL enzyme/g cellulose avec Qc=8.67gms/h)

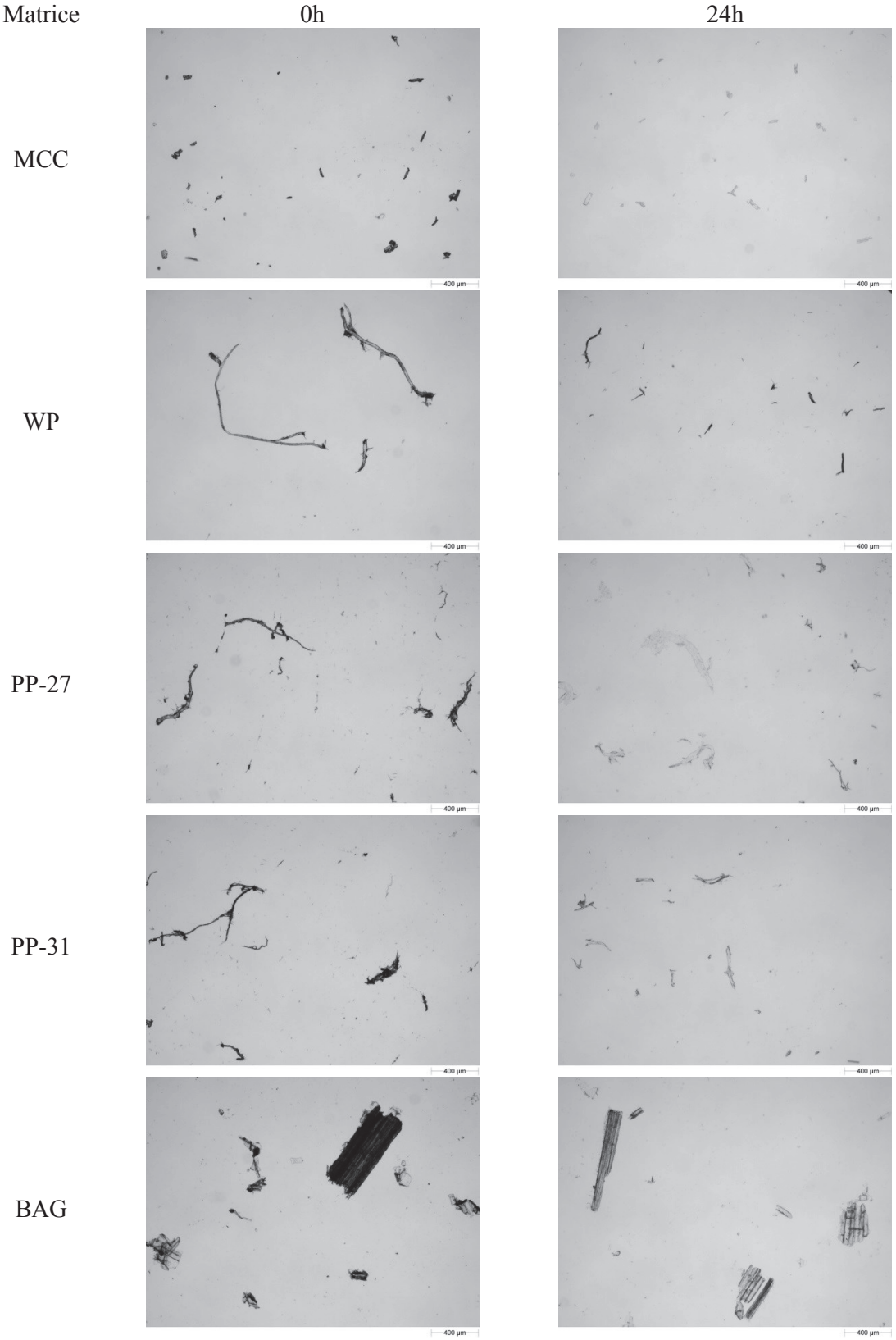

Figure 4: Morphologie des fibres avant (0h) et après (24h) l'hydrolyse (pour MCC, WP, PP-27, PP-31 et BAG à 1%w/v; 0.5mL enzyme/g cellulose; objective x2.5)

Tableau 6 : Comparaison des diamètres moyens D[4,3] obtenus par différentes techniques de mesure pour cinq matrices (3%w/v, 0.5mL enzyme/g cellulose; sauf MCC-1%w/v)

Substrat	Technique	0h	2h	5h	10h	24h
MCC	FBRM	95	64	41	37	36
	DLS	108	41	39	36	34
	Morpho	105	-	72	63	62
WP	FBRM	53	53	52	51	51
	DLS	351	162	136	124	114
	Morpho	312	194	184	144	130
PP-27	FBRM	52	46	44	43	39
	DLS	497	-	201	130	103
	Morpho	187	155	126	97	70
PP-31	FBRM	53	46	42	40	38
	DLS	471	295	216	136	126
	Morpho	222	157	154	140	91
BAG	FBRM	51	51	45	45	44
	DLS	227	-	-	229	221
	Morpho	171	-	-	168	161

Conclusion & Perspectives :

Ce travail étudie la dynamique des phénomènes de transfert et la limitation des réactions biocatalytiques pour les biomasses lignocellulosiques à haute teneur en matière sèche. Il est centré sur le développement des analyses physiques et biochimiques in et ex-situ pour mieux comprendre les mécanismes de déstructuration des fibres et caractériser la cinétique de la production de glucose afin de contrôler des activités microbiennes. Nous avons proposé un banc expérimental spécifique couplé avec différentes techniques analytiques pour apporter une vue générale multi échelle sur l'hydrolyse enzymatique. Les évolutions des grandeurs physiques et biochimiques ont été suivies et modélisées par différents modèles phénoménologiques et cinétiques. Le contrôle de la limitation des transferts physiques par une stratégie d'apport des matières premières est proposé et validé. Les connaissances acquises permettent d'envisager une transposition à l'échelle industrielle.

L'analyse des travaux réalisés permet de proposer plusieurs perspectives. Trois principaux axes (technologie, expérimentation et modélisation) peuvent contribuer à renforcer, approfondir et élargir nos axes de recherches :

- **D'un point de vue technologique** : l'implémentation du dispositif expérimental peut être envisagée sur la base :

(i) De l'intégration et du développement d'instrumentations *in-situ* (ex : mesure optique in-situ avec multi-longueurs d'ondes pour discriminer les particules)

(ii) De l'élargissement des performances incluant les conditions opératoires accessibles (ex : valeurs min et max des couples mesurés, précision améliorée)

(iii) Du développement d'un contrôle/commande adapté et flexible des intrants (substrat, enzyme, microorganisme) pour une conduite optimale de la biocatalyse (ex : stratégie d'ajout des substrats, régulation des ajouts par le contrôle de la viscosité)

(iv) De l''intégration et de la prise en considération des spécifications des cultures microbiennes (ex : assurer la stérilité et la stérilisation du bioréacteur et de son instrumentation *in-situ*)

- **D'un point de vue expérimental** :

(i) La caractérisation élargie des substrats lignocellulosiques complexes (ex : mesure de la porosité et de la surface spécifique par tomographie, évolution des tensions de surface (hydrophilicité) au cours de l'hydrolyse)

(ii) L'identification et la quantification des fractions solubles (DP<16) pour construire un profil des intermédiaires de dégradation des fibres lignocellulosiques et étudier leur impact sur la viscosité des suspensions.

(iii) La quantification de l'efficacité des enzymes par le dosage des activités résiduelles,

(iv) L'étude de l'impact de l'activité enzymatique seule (ex : endo-glucanases, β-glucosidases, xylanases…) sur les paramètres physiques,

(v) La réalisation des hydrolyses jusqu'à 30%w/v avec la stratégie d'ajouts cumulés (semi-continu),

(vi) La conduite de tests de fermentescibilité des surnageants (ex : identification des inhibiteurs) et la consolidation avec l'extrusion-réaction enzymatique et procédé de fermentation

- **D'un point de vue modélisation cinétique** :

(i) L'interprétation des variables physiques et biochimiques et le rendement associé

(ii) L'analyse et la comparaison des constantes réactionnelles identifiées,

(iii) L'établissement d'un « bloc de connaissances »intégrant des modèles rhéométriques, morpho-granulométriques et biochimiques,

(iv) La simulation et la validation des modèles phénoménologiques pour le mode semi-continu à partir des paramètres établis en mode discontinu. .

REFERENCES

Alvira, P., Negro, M.J., Ballesteros, M. 2011. Effect of endoxylanase and alpha-L-arabinofuranosidase supplementation on the enzymatic hydrolysis of steam exploded wheat straw. *Bioresource Technology*, **102**(6), 4552-4558.

Bennington, C.P.J., Kerekes, R.J., Grace, J.R. 1990. THE YIELD STRESS OF FIBER SUSPENSIONS. *Canadian Journal of Chemical Engineering*, **68**(5), 748-757.

Blanco, A., Negro, C., Fuente, E., Tijero, J. 2006. Rotor selection for a Searle-type device to study the rheology of paper pulp suspensions. *Chemical Engineering and Processing*, **46**, 37-44.

Bommarius, A.S., Katona, A., Cheben, S.E., Patel, A.S., Ragauskas, A.J., Knudson, K., Pu, Y. 2008. Cellulase kinetics as a function of cellulose pretreatment. *Metabolic Engineering*, **10**(6), 370-381.

Derakhshandeh, B., Kerekes, R.J., Hatzikiriakos, S.G., Bennington, C.P.J. 2011. Rheology of pulp fibre suspensions: A critical review. *Chemical Engineering Science*, **66**(15), 3460-3470.

Ferreira, A.G.M., Silveira, M.T., Lobo, L.Q. 2003. The viscosity of aqueous suspensions of cellulose fibres. Part 2: influence of temperature and mix fibres. *Silva Lusitana*, **11**(1), 61-66.

Govumoni, S.P., Koti, S., Kothagouni, S.Y., S, V., Linga, V.R. 2013. Evaluation of pretreatment methods for enzymatic saccharification of wheat straw for bioethanol production. *Carbohydrate Polymers*, **91**(2), 646-650.

Lapierre, L., Bouchard, J., Berry, R. 2006. On the relationship between fibre length, cellulose chain length and pulp viscosity of a softwood sulfite pulp. *Holzforschung*, **60**(4), 372-377.

Metzner, A.B., Otto, R.E. 1957. Agitation of non-Newtonian fluids. *AIChE Journal*, **3**(1), 3-10.

Ogier, J.C., Ballerini, D., Leygue, J.P., Rigal, L., Pourquie, J. 1999. Ethanol production from lignocellulosic biomass. *Oil & Gas Science and Technology-Revue D Ifp Energies Nouvelles*, **54**(1), 67-94.

Pereira, L.T.C., Pereira, L.T.C., Teixeira, R.S.S., Bon, E.P.D., Freitas, S.P. 2011. Sugarcane bagasse enzymatic hydrolysis: rheological data as criteria for impeller selection. *Journal Of Industrial Microbiology & Biotechnology*, **38**(8), 901-907.

Pessani, N.K. 2011. Simultaneous saccharification and fermentation of switchgrass by thermotolerant Kluyveromyces marxianus IMB3: Effect of enzyme loading, temperature and operating mode. in: *Biosystems & Agricultural Engineering*, Oklahoma State Universit. Oklahoma.

Rieger, F., Novak, V. 1973. Power Consumption of Agitators in Highly Viscous non-Newtonian Liquids. *Trans. Instn. Chem. Engrs*, **51**, 105-111.

Um, B.-H. 2007. Optimization of Ethanol Production from Concentrated Substrate, Auburn University, pp. 268.

Wilson, C.A. 2013. Effect of endoxylanase and alpha-L-arabinofuranosidase supplementation on the enzymatic hydrolysis of steam exploded wheat straw. in: *Chemical & Biomedical Engineering*, Florida State University. Florida, pp. 170.

Wiman, M., Palmqvist, B., Tornberg, E., Liden, G. 2010. Rheological Characterization of Dilute Acid Pretreated Softwood. *Biotechnology And Bioengineering*, **108**(5), 1031-1041.

Zhang, X., Qin, W., Paice, M.G., Saddler, J.N. 2009. High consistency enzymatic hydrolysis of hardwood substrates. *Bioresource Technology*, **100**(23), 5890-5897.